Head Office: Università degli Studi di Padova

Department: Industrial Engineering

_____

Ph.D. COURSE IN: Electrical Energy Engineering

THESIS TITLE

Power system assessment of HVDC-VSC in the future high voltage transmission grids

Coordinator: Ch.mo Prof. Giulio ROSATI
Supervisor: Ch.mo Prof. Roberto BENATO

Ph.D. student: Antonio CHIARELLI

Summary

The study of high voltage direct current (HVDC) connections arises from careful observation of the continuous evolution of the electrical system from the 1960s to today. Over the years, HVDC inter-connections have emerged to become increasingly important infrastructures, nowadays playing a fundamental role in the world panorama of electrical systems. The advent of increasingly advanced technologies has made this type of solution not only sustainable from a technical-economic point of view, but necessary for the optimization and efficiency of the stability of national and international networks.

The thesis aims to analyze HVDC systems in all their configurations and applications, in particular, it is divided as in the following:

Firstly, an in-depth analysis of the scientific literature of HVDC systems has been carried out, taking into account all HVDC components, starting from the typical configurations of HVDC systems, towards the study of the various operating modes that these systems can assume.

Then, the issue related to the dynamic operation of HVDC systems with multi-level converters in the event of a fault has been addressed. An electromagnetic study has been also carried out to identify the various problems that may arise on the components of the HVDC system, paying greater attention to the transient overvoltages that are generated on the DC (Direct Current) bus of the connection itself.

In particular, several electromagnetic studies have been carried out to evaluate the transient overvoltages of higher value. Therefore, it has been proceeded to limit this phenomenon by adopting surge arresters, subsequently evaluating in quantitative terms the reduction in overvoltage obtained. In addition, the recent multi-infeed HVDC systems have been analyzed. In particular, the interactions between the Line-Commutated Converter (LCC) HVDC type and the Voltage Source Converter (VSC) HVDC type have been evaluated when a transient overvoltage occurs on the VSC terminal.

The HVDC connections present today are systems that consist of numerous components that have to cooperate and work continuously and without interruptions. Therefore, the study of the reliability and availability of HVDC systems is an integral part of what encompasses the set of assessments necessary for the analysis of the resilience of the electrical system. For these reasons, this research thesis pays great attention to the reliability and availability studies of HVDC systems based, in particular, on voltage source converters (VSC).

For these reasons, this research thesis pays great attention to the reliability and availability studies of HVDC systems and, in particular, to voltage source converters based systems. The reliability and availability analysis lays its foundations on in-depth studies of probability and statistics. For this reason, the main notions and definitions used throughout the thesis are subsequently given. In particular, the study of the reliability of multi-level converters is addressed, taking into account the different ways of managing the converters' redundancies.

A thorough study of Markov chains with an investigation on how the Markov chains could be used to model symmetrical monopolar configurations is also presented. In particular, Markov chains are used to highlight how the management of spare parts of HVDC system components affects the availability of the overall system.

Subsequently, the analysis of reliability and availability has been also extended to the multi-terminal direct current systems (MTDC). These very complex systems, both in terms of topology and in the number of possible states, have been analyzed by adopting a matrix-based method called the "Multi-State Reliability" method (MSR). With this method, different multi-terminal systems have been compared using different HVDC converter technologies.

Finally, the Multi-State Reliability and the Markov chain methods have been combined to analyze different configurations of multi-terminal HVDC systems. In particular, it has been highlighted how, for a correct analysis of the reliability of HVDC systems, the real installation and spares management of each component must be taken into account.

Sommario

Lo studio dei collegamenti in alta tensione in corrente continua (HVDC) nasce da un'attenta osservazione della continua evoluzione del sistema elettrico a partire dagl'anni '60 ad oggi. I collegamenti HVDC hanno rivestito nel corso degl'anni sempre più importanza, rivestendo al giorno d'oggi, un ruolo fondamentale nel panorama mondiale dei sistemi elettrici.

L'avvento di tecnologie sempre più avanzate ha reso questo tipo di soluzione, non solo sostenibile da un punto di vista tecnico-economico, ma necessario per l'ottimizzazione e l'efficientamento della stabilità delle reti nazionali e internazionali.

La tesi si pone come obiettivo l'analisi dei sistemi HVDC in tutte le loro configurazioni e applicazioni, in particolare, si articola come segue: è stata eseguita un'approfondita analisi della letteratura scientifica dei sistemi HVDC, tenendo conto di tutti i suoi componenti, partendo dalle configurazioni tipiche di questa tipologia di impianti arrivando allo studio delle varie modalità di funzionamento che questi sistemi possono assumere.

Viene inoltre affrontata la tematica relativa al funzionamento dinamico dei sistemi HVDC con convertitori multi-livello nel caso di guasto. Viene quindi effettuato uno studio elettromagnetico per individuare i diversi problemi che possono insorgere sui componenti del sistema HVDC, ponendo maggiore attenzione alle sovratensioni di origine transitoria che si generano sul bus DC del collegamento stesso.

In particolare, sono stati effettuati diversi studi elettromagnetici al fine di valutare quali fossero le sovratensioni transitorie di valore maggiore. Si è quindi provveduto a limitare questo fenomeno adottando scaricatori di sovratensione, valutando successivamente quanto fosse la riduzione di sovratensione ottenuta.

Inoltre, sono stati analizzati i recenti sistemi HVDC multi-infeed. In particolare, sono state valutate le interazioni tra il convertitore LCC e il convertitore VSC quando si verifica una sovratensione transitoria sul terminale VSC.

I collegamenti HVDC presenti oggigiorno, sono sistemi composti da numerosi

componenti che necessariamente hanno bisogno di cooperare e lavorare in maniera continuativa e senza interruzioni. Lo studio, dunque, dell'affidabilità e della disponibilità dei sistemi HVDC sono parte integrante di quello che racchiude l'insieme delle valutazioni necessaria all'analisi della resilienza del sistema elettrico.

Per questi motivi, questa tesi di ricerca presta grande attenzione agli studi di affidabilità e disponibilità dei sistemi HVDC e, in particolare, dei sistemi basati su convertitori a tensione impressa (VSC). Gli studi sull'analisi dell'attendibilità e della disponibilità pongono le loro basi, come è facile immaginare, su approfondimenti di probabilità e statistica, per questo, sono state fornite le principali ed utili nozioni per l'utilizzo dei metodi presentati successivamente. In particolare, viene affrontato lo studio dell'affidabilità dei convertitori multilivello, tenendo conto delle diverse modalità di gestione delle ridondanze dei convertitori.

Si è quindi passati allo studio dettagliato delle catene di Markov e di come potrebbero essere utilizzate per modellare in modo appropriato un sistema HVDC di tipo monopolare simmetrico. In particolare, le catene di Markov vengono utilizzate per evidenziare come la gestione delle parti di ricambio dei componenti del sistema HVDC influisca sulla disponibilità dell'intero sistema.

Successivamente, l'analisi di affidabilità e disponibilità è stata estesa anche ai cosiddetti sistemi in corrente continua "multiterminale" (MTDC). Questi sistemi essendo molto complessi, sia in termini di topologia che di numero di stati che il sistema complessivo può assumere, sono stati analizzati adottando un metodo matriciale denominato metodo "Multi-State Reliability" (MSR). Con questo metodo, sono stati confrontati diversi sistemi multi-terminale utilizzando diverse tecnologie di conversione HVDC.

Infine, i metodi Multi-State Reliability e quello delle catene di Markov sono stati combinati per analizzare diverse configurazioni di sistemi HVDC multi-terminale. In particolare, è stato evidenziato come, per una corretta analisi dell'affidabilità dei sistemi HVDC, si debba tener conto della reale gestione di ogni componente e di ogni sua riserva.

"Ut sementem feceris ita metes"
Cicerone

Table of Contents

List of Tables

List of Figures

Acronyms

HVDC	High voltage direct current
MMC	Modular multilevel converters
MTDC	Multi-terminal direct current
LCC	Line-commutated converter
VSC	Voltage-source converter
SMs	Sub-modules
ACFs	AC filters
CAPs	Shunt capacitor banks
VSC CAPs	Shunt capacitor banks for VSC technology
Brks	AC breakers
Trns	Converter transformers
Vlvs	Valves
SRs	Smoothing reactors
PRs	Phase reactors
DCSWs	DC switches
DCFs	DC filters
VSC DCFs	DC filters for VSC technology
MSR	Matrix-based system reliability
I-SM	single IGBT valve sub-module
SP	Stack pack
S-SM	Multiple IGBT valve sub-module
RBD	reliability block diagram
SCFM	short circuit failure mode
CDF	cumulative distribution function
PDF	probability density function
MTTF	mean time to failure
MTTR	mean time to repair
CCF	Common cause failure

Symbols

Sign	Description	Unit
τ_x	Time rate to resupply the component x	[h/year]
λ_x	Failure rate of the component x	[h/year]
μ_x	Mean time rate to repair of component x	[h/year]
η	De-rating factor	
V_i	Sub-module actual operating voltage	[V]
V_w	Sub-module withstanding voltage	[V]
V_{SM}	Sub-module nominal voltage	[V]
$R_x(t)$	Reliability function of the item x	
k	Minimum number of sub-modules per arm	
m	Number of redundant sub-modules per arm	
n	Total number of sub-modules per arm	
r	Percentage of redundant SMs	[%]
V_{DC}	Converter phase leg voltage	[V]
V_{arm}	Converter arm voltage	[V]
A_x	Availability of the item x	
A_∞	Steady-state availability	
v_s	V_i/V_{SM}	
T_{va}	Valve arm lifetime	[t]
β	Common cause failure parameter	
Ω	Markov state space	
$X(t)$	Time-homogeneous Markov process	
p_{ij}	Time-independent transition probability	
$P(s)$	Transitional probability matrix	
$P(0)$	Identity matrix	
$\pi(t)$	Probability distribution X(t), t≥0 at time t	
Q	Transitional matrix	
$\pi*$	Steady-state probability distribution $\pi(t)$	
T	One spare cable termination	
CS	One spare cable span	

Sign	Description	Unit
L	Length Of Each Cable	[km]
L_{span}	Length Of One Cable Span	[km]
N_{jtot}	Total Number Of Joints	
N_t	Total Number Of Terminations	
s	Number of IGBTs in series inside the S-SM valve	
z	Minimal Number of IGBTs in series inside the S-SM valve	

Chapter 1

HVDC power system overview

The aim of this chapter is to provide an overview of the high voltage direct current power transmission systems, based on the voltage source conversion technology.

In order to fully understand the characteristics and technical implications related to the use of VSC technology compared to more traditional systems, it is also useful to describe the operation of direct current transmission systems based on the technology of LCC conversion or "Line Commuted Converter". The latter has been the first conversion configuration used for direct current power transmission, and for this reason it is the most widespread.

Therefore, the key aspects of the two technologies are first identified, analyzing the main differences, then the HVDC-VSC systems are investigated. In particular, starting from the basic structure of an elementary VSC system, the purpose has been to describe a "multi-level" type impressed voltage converter.

1.1 Introduction

In the last fifteen years, the management of electricity systems has undergone the changes encountered by the liberalization of the energy market. This has led to a reconsideration of the electrical system with a vertical structure, consisting of the generation, transmission, and distribution, to an integrated horizontal structure in which the actors refer to the transmission/distribution network and can participate in the generation, exchange, and sale of energy.

Today, the continuous rise of the distributed generation and the increase of power

demand result in increasingly less predictable power flows. Adapting the system according to the new structure, therefore, requires not only a "robust" network but also more flexible, intelligent, and efficient system than the current one.

Thanks to the recent development of solid-state power devices, it was possible to create innovative solutions to meet the new demands of the transmission network both in the field of FACTS (Flexible Alternated Current Transmission Systems) and of HVDC (High-Voltage Direct current)[1].

1.2   Advantages and costs of HVDC

The original motivation behind the development of direct current (DC) transmission was its efficiency. However, this requires the use of high DC voltages and consequently the use of electrical and electronic components that can withstand this kind of stress.

The achievements about the performance and reliability of solid-state devices, to date, allow the adoption of new installations of HVDC converters that are more competitive than the previous ones.

Thus, in addition to transmission efficiency, other advantages can be decisive in the adoption of an HVDC system.

Thanks to the reactivity of the power electronics, it is possible to have full control of the transmitted power and to improve fault management. In addition, the DC transmission exceeds some limitations of the AC transmission stated below.

1.2.1   Technical-economic overview of HVDC systems

The total cost of an HVDC transmission system is given by the sum of two main cost items. The first relates to the conversion station which includes, in addition to the converters, all the equipment that helps to ensure safe and reliable operation of the station such as transformers, filters, protections, the cooling system and the AC side protection switches. The second relates to the cost of the transmission line, which is affected of labor costs. By way of indication, the values commonly found in literature relating to the aforementioned cost items are reported in Table 1.1 and 1.2 [2].

Due to the modular configurations of the conversion stations, the cost as a function of the installed power presents an approximately linear trend. However, it must be considered that increasing the transmissible power from the system does not

always reduce the specific costs since higher voltages and currents require more complex conversion devices with a higher cost.

It should also be considered that a correct assessment of the cost of an HVDC transmission line must also take into account the environmental conditions and in particular the geographical conformation of the transmission line path.

Table 1.1: HVDC converter station costs

Power [MW]	HVDC-LCC [M€]	HVDC-VSC [M€]
500	40	51
1000	90	110
1500	120	153

Table 1.2: HVDC transmission line costs

Power [MW]	Cable $\left[\frac{M€}{km}\right]$	Over-head line $\left[\frac{M€}{km}\right]$
500	0.8	0.26
1000	1.6	0.25
1500	2.4	0.34

For instance, the cost per kilometer of a transmission line installed in the Swiss Alps could reach 4 times that of an equivalent line in Finland or Sweden. In the assessments shown in Table 1.2, therefore, only the costs of building the line were considered, without including the environmental impact, the necessary permits and other legal costs. From the Figure 1.1, which compares the trend in costs for AC and DC transmissions, it can be seen that an HVDC system is only convenient for long distances, thanks to the reduced losses and the lower investment required by the DC transmission lines. However, in some cases, the higher outlay is justified by the advantages offered by the technology and by overcoming the limits of AC connections.

For this, HVDC systems can be used in:

- submarine connections, in which the electrical return of the circuit can be carried out by sea (less and less frequent because it is not allowed by the authorities) or by means of a dedicated metal return (DMR);

- underground connections, if the distance exceeds 50 km and the reactive
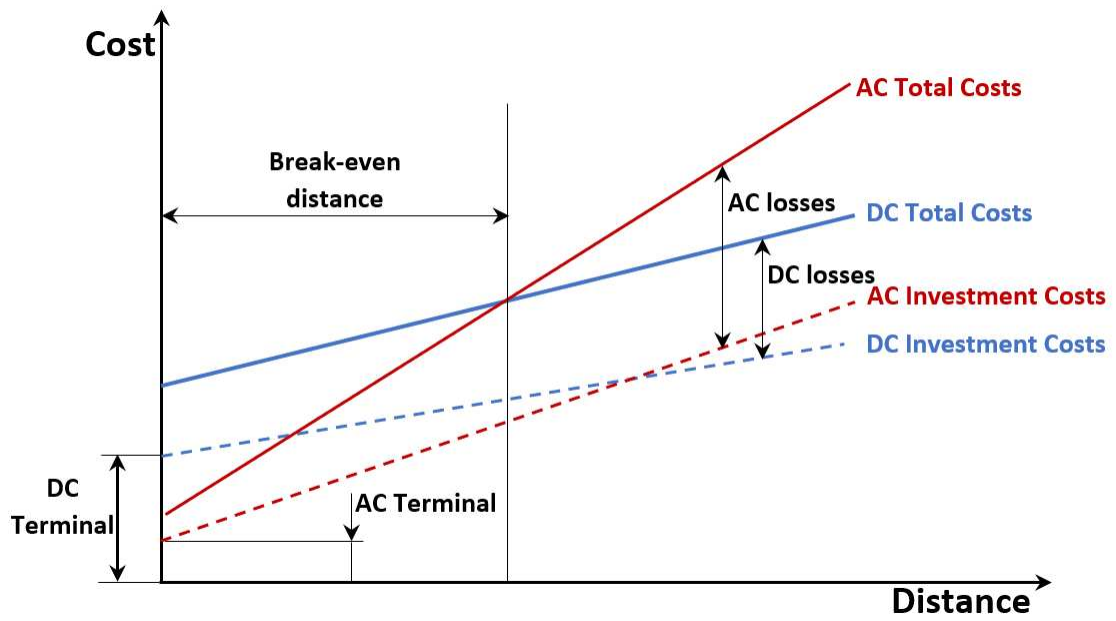
Figure 1.1: Cost comparison between the two transmission technologies

compensation of the AC cable is inconvenient;

- connections between two systems with different frequencies or with too large a phase angle;

- regulators of power flows between two interconnected systems.

1.3 HVDC Configurations

In this chapter, a close examination of the possible topologies for HVDC transmission systems is conducted[3].

1.3.1 Symmetrical monopolar system

The symmetrical monopolar configuration shown in Figure 1.2 is the simplest in HVDC-VSC systems, where the DC terminals of the converters are symmetrical, with the same voltage and opposite polarity.
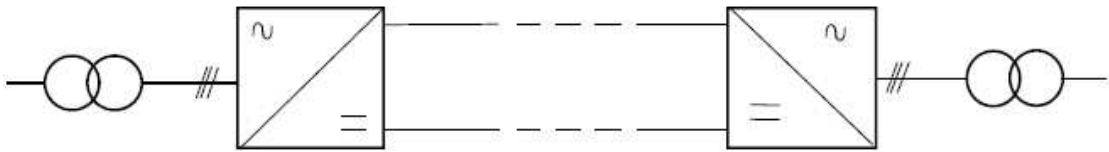
Figure 1.2: Symmetrical monopolar configuration

The failure of a part of the system or the DC conductor or converters results in a total loss of transmission capacity.

1.3.2 Monopolar asymmetric system with metallic or ground return

The asymmetrical monopolar configuration schematized in Figure 1.3 has, on the DC side, a physical connection to ground of a converter; the DC side of the converters is asymmetrical, as one terminal is at the potential of the HVDC, the other is at the ground potential.
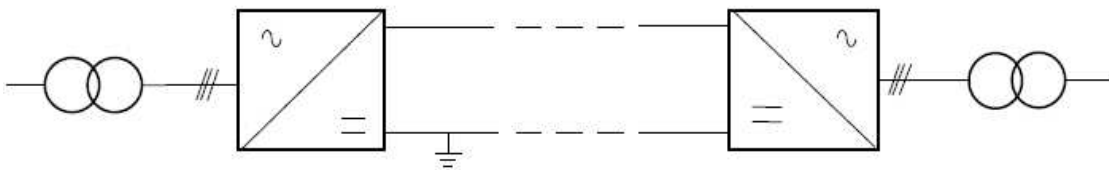
Figure 1.3: Asymmetrical monopolar configuration

The failure of a part of the system or the DC conductor or converters results in a total loss of transmission capacity.

1.3.3 Bipolar system grounded via neutral point of one or both terminals
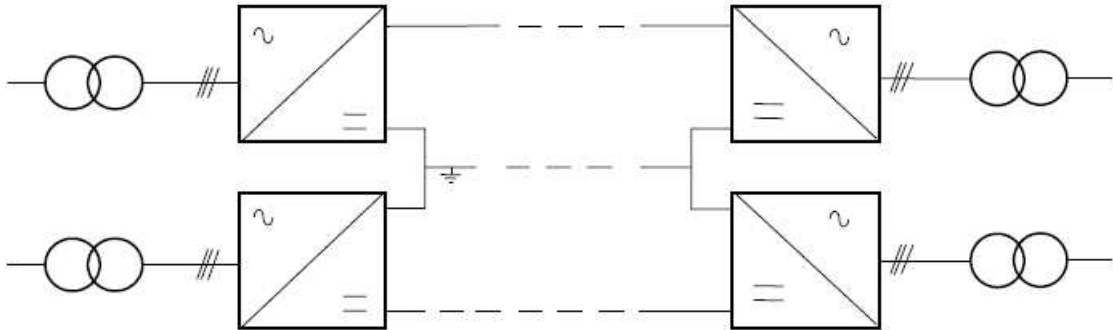
Figure 1.4: Asymmetrical bipolar configuration with earthed or dedicated metallic return
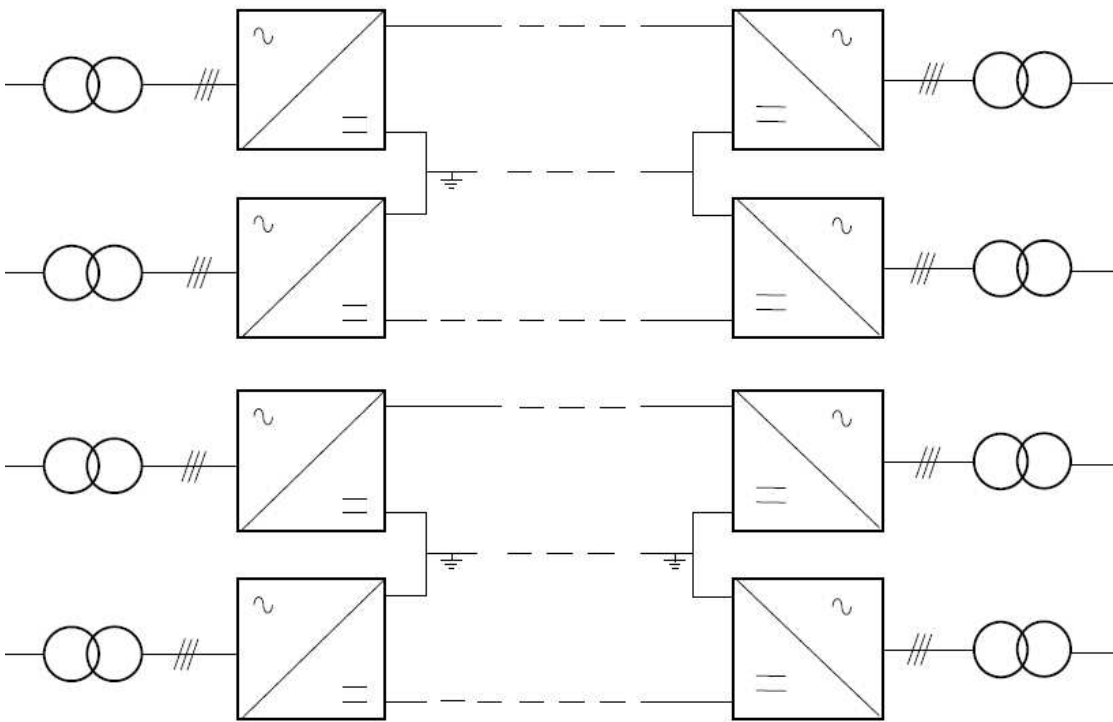
Figure 1.5: Bipolar system grounded at one or both the terminals

In Figures 1.4 and 1.5 two independent asymmetrical monopoles are used and the presence of two or three conduction paths is required, one for each HVDC pole of the converter and one for the common connection of the two converters. The

transmitted power is shared equally between the two poles of the converters, this means that the current flowing in the shared conductor is close to zero. If the power is not shared equally, current flows in the common conductor.

If a pole goes out of service, due to maintenance or a fault, the remaining converter will continue to transmit, but with capacity reduced to 50 % of the nominal transmissible power capacity. This is the main reason why this configuration is widely used in HVDC systems.

1.3.4 Bipolar system with earthing via dedicated metal return

In this configuration, the two conductors can operate with metal return, thus presenting the advantage of a reduced insulation cost and a redundancy of 50 % of the total power. However, the overall cost, compared with a monopolar system of similar power, is higher. An example of this variant is shown in Figure 1.6.
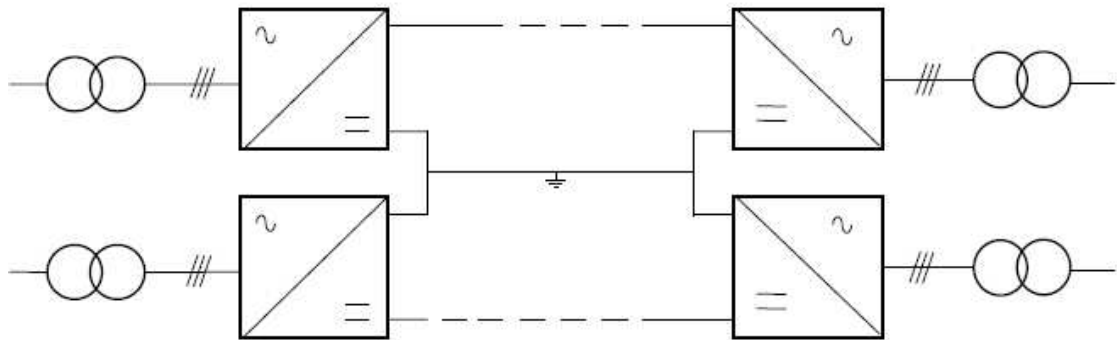
Figure 1.6: Bipolar system grounded with dedicated metallic return

1.3.5 Multi-terminal system

This type of HVDC system, shown schematically in Figure 1.7, consists of a minimum of three conversion stations with the connections arranged in series or in parallel. Its configuration is more complex when compared with previous systems, especially as regards the control and communications between the various transformer stations. This type of system is preferred when the transmission line crosses different geographical areas, interconnecting with other countries.
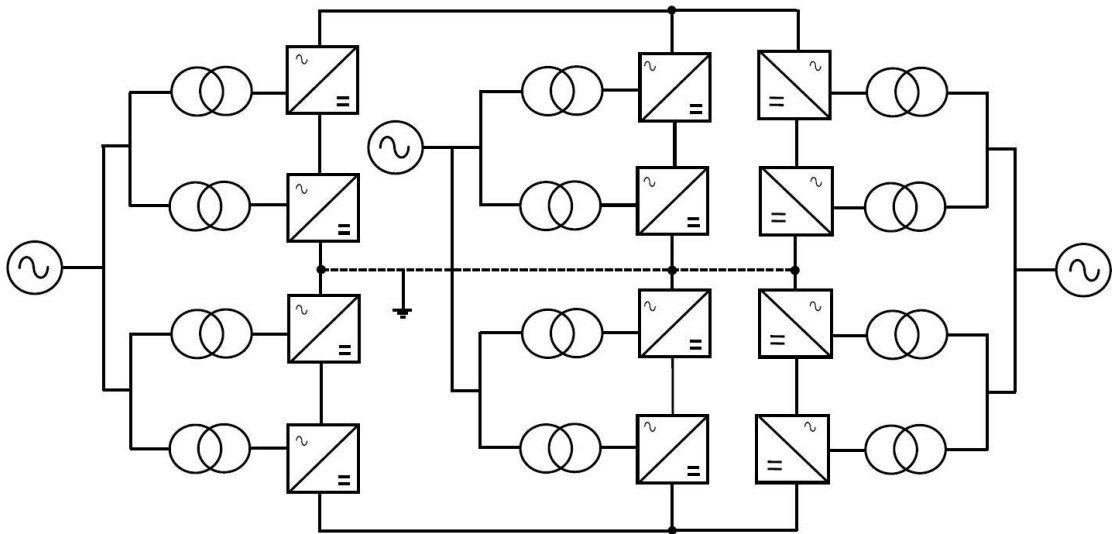
Figure 1.7: Multi-terminal system

1.3.6   Back-to-Back system

As the name suggests, the expression Back-to-back indicates that the rectifier and the inverter are placed in the same location. The main purpose of this system is to control the power flow between two AC networks at different frequencies, even in conditions of variable voltage on the DC side. Another benefit is using a back-to-back for splitting up a too strong network to reduce short circuit current. A typical example of this system is shown in Figure 1.8.
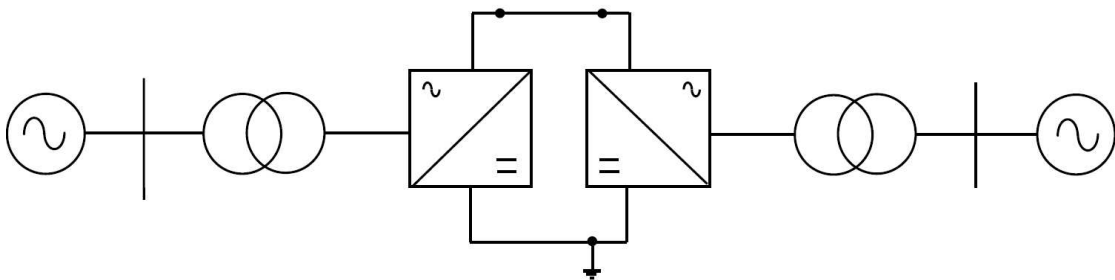
Figure 1.8: Back-to-Back system

8

1.4 HVDC switches

Some traditional equipment with low and medium voltage AC using the atmospheric air as an extinguisher, have a certain, often very large, DC breaking capacity. Hence, these can be used for low DC voltage values typically seen in traction applications and industrial applications with voltages up to about 10 kV.

Load changeover switches, such as MRTS (Metallic Return Transfer Switches), are readily available for HVDC applications. However, the energy leakage, the extinguishing current and the operating speed required for the circuit breakers make the opening circuit very expensive. It is important to note that switching the current is much less burdensome than interrupting. It can be shown that the voltage drop across the switches and the power dissipation become much lower when redirecting the current flow from one branch to the other (Figure 1.9 - right circuit) than when interrupting it (Figure 1.9 - left circuit). The energy to be absorbed, the overvoltage during absorption and the absorption time are interdependent[4].
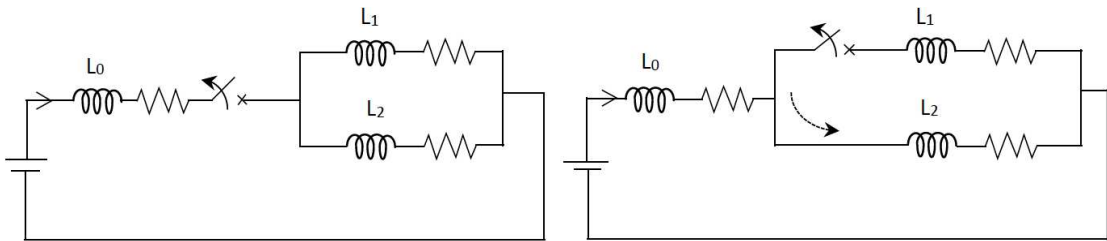
Figure 1.9: Current readdressing

Some methods and technologies for switching and interrupting the current in HVDC have been developed and can be divided into three categories:

1. those that use mechanical switches;

2. those that use semiconductor devices;

3. those that use a combination of mechanical and semiconductor switches.

HVDC systems that use semiconductor switches are significantly faster than those that use mechanical switches. However, the use of semiconductor devices in the main current path is very expensive and causes high conduction losses (0.1% - 0.4% of the value of the transferred power). Mechanical switches, on the other hand, have significantly lower losses, but their break time is considerably longer than that of semiconductor switches. A combination of mechanical and semiconductor switches can be used to achieve high-speed switching with acceptable losses, but still at an higher cost compared to mechanical solutions, as they involve semiconductor materials.

9

1.4.1 Classifications

In the following, it is presented a classification of the switching[4], interruption and sectioning devices used in the HVDC, grouping them into four categories according to their function:

- sectioning (see Table 1.3);

- grounding(see Table 1.4);

- current transfer (or switching) (see Table 1.5);

- current break (see Table 1.6).

Table 1.3: Classification of disconnector devices

	DISCONNECTORS	
CD	Converter Disconnecting switch	
BPD	Bypass Disconnecting switch	
FD	Filter Disconnecting switch	
SD	Substation Disconnecting switch	
LD	Line Disconnecting switch	Interrupt residual current withstand voltage
PLD	Pole Line Disconnecting switch	
LND	Line to Neutral Disconnecting switch	
NBD	Neutral Bus Disconnecting switch	
NBED	Neutral Bus Earthing Disconnecting switch	
ELD	Electrode Line Disconnecting switch	
SPPD	Substation Pole Paralleling Disconnecting switch	

Table 1.4: Classification of earthing devices

	EARTHING SWITCHES	
PLES	Pole Line Earthing switch	
NBES	Neutral Bus Earthing switch	
FES	Filter Earthing switch	Earthing withstand voltage
CES	Converter Earthing switch	
SES	Substation Earthing switch	
PPES	Pole Paralleling Earthing switch	

Table 1.5: Classification of switching devices

	SWITCHES	
NBS	Neutral Bus switch	
MRTS	Metallic Return Transfer switch	Commutate current
ERTS	Earth Return Transfer switch	Making current
BPS	Bypass switch	Withstand voltage
HSES	High Speed Earthing switch	
PS	Paralleling switch	

Table 1.6: Classification of circuit breaker devices

	SWITCHES	
		Interrupt Current
CB	Circuit Breaker	Dissipate energy
		Withstand voltage

1.4.2 General specifications on each specific device

General specifications are given in the following on the devices listed in Table 1.3 in order to highlight their main characteristics:

- **Converter disconnecting switch (CD) and bypass disconnecting switch (BPD)**

  The CDs are set up one on each side of each series-connected converter and the BPD is installed for bypassing the converter unit, allowing the disconnection and isolation of a series-connected converter unit, including the associated BPS, without blocking the entire pole of substation.

- **Filter disconnecting switch (FD)**

  The FD allows maintenance of the HVDC filter during normal operation of a substation pole.

- **Substation disconnecting switch (SD)**

  The SD isolates the high voltage side of a substation pole from the line to allow maintenance of the equipment of a substation pole or repair following a fault when the line of a pole is energized or operating in metallic return mode.

- **Line disconnecting switch (LD) and pole line disconnecting switch (PLD)**

  The LD and PLD are connected in parallel of the substation poles in the event of a line fault. While the PLD only disconnects the line, LD also deactivates the switch. If this operating mode is not required, LD and PLD are not normally installed.

- **Line to neutral disconnecting switch (LND)**

  The LND is used in conjunction with the ERTS for metallic return. These disconnect switches also allow maintenance of the ERTS.

- **Neutral bus disconnecting switch (NBD)**

  The NBD is used to isolate the neutral end of a substation pole.

- **Neutral bus earthing disconnecting switch (NBED)**

  The purpose of the disconnect switch is to isolate the high-speed earth switch (HSES) for maintenance.

- **Electrode line disconnecting switch (ELD)**

The ELD is used to isolate the electrode from the metallic return transfer switch (MRTS).

- **Substation pole paralleling disconnecting switch (SPPD)**

In the event of a fault on a bipole HVDC line, the parallel SPPD can be used to parallelize the substation poles after a polarity reversal has been performed in one of the poles and the LND and PPES have been opened.

- **Pole line earthing switch (PLES)**

This switch is for grounding one pole, e.g. for maintenance.

- **Neutral bus earthing switch (NBES)**

This switch is for grounding the neutral bus, eg. for the maintenance of the NBS and the HSES. There are possible schemes in which grounding is not performed on the neutral bar, but on the electrode line.

- **Filter earthing switch (FES)**

This switch is for filter grounding, e.g. for maintenance.

- **Converter earthing switch (CES)**

This switch is for grounding the converter.

- **Substation earthing switch (SES)**

This switch is for grounding the substation.

- **Pole paralleling earthing switch (PPES)**

This switch is for grounding one or both of the HVDC poles, e.g. for the maintenance of downstream equipment.

- **Bus neutral switch (NBS)**

In normal operation, the NBS is closed and normally is subjected to the nominal pole current. If a substation pole needs to be blocked, the purpose of the NBS is to isolate the blocked pole permanently and to switch the pole current to the electrode line. Normally, the NBS is operated under no-load conditions. However, there are some failure cases where it must be possible to operate under load. The NBS should be able to switch a fault current on the electrode line. The voltage it withstand with open contacts is modest, about four times the maximum arc voltage if the electrode line is not too long.

- **Earth return transfer switch (ERTS) and metallic return transfer switch (MRTS)**

  ERTS is only installed in bipolar HVDC systems without a dedicated metal return line. In many areas, it is not allowed to continuously use HVDC systems with a large earth current. If a substation pole is not available, the system can be operated in metal return, i.e. the HVDC transmission line belonging to the unavailable pole is used as a metal return conductor. The ERTS is used in conjunction with the MRTS to switch back and forth between metal return mode and ground return. In point-to-point links, these two switches are installed only in one station. The ERTS and MRTS must be able to switch the load current. The voltage they withstand with open contacts is modest. In some applications, the MRTS is closed to eliminate ground faults that occur in overhead lines to continue the HVDC broadcast.

- **Converter bypass switch (BPS)**

  The purpose of the BPS is to allow the conversion units connected in series to be put into service or taken out of service without affecting the operation of the other converter unit in the bipole. The BPS is used to bypass the converter unit, which is deactivated, and vice versa by switching the current in the converter unit when it is put back into service. The BPS can be omitted when there is only one converter per pole. The BPS can be a single circuit breaker or consist of two units, a breaking unit, and an isolation unit. The BPS must be able to switch the load current and withstand the voltage of the converter on its open contacts during the normal operation of the converter unit.

- **High-speed earthing switch (HSES)**

  In normal operation, HSES is in the open position and therefore is not affected by any current. If the electrode line is disconnected during operation in bipolar configuration, due to maintenance or fault, the HSES is closed and thus carries the unbalance current between the poles. Using this procedure, the ground connection is re-established and the bipolar configuration is continues. This switch is also sometimes called the neutral bus ground switch, not to be confused with the NBES.

- **Paralleling switch (PS)**

  The parallel switch is used to couple or uncouple two bipolar schemes in or from parallel operations.

- **Circuit breaker (CB)**

HVDC switches are required to interrupt the fault current at a specified value on the rising edge below the rated extinction current. These devices were not put into service in MV HVDC networks (at least until 2016) for this reason, a complete short circuit must be removed for the time being with the DC command, converter shutdown and / or HVAC side circuit breaker interruption. Depending on the layout of the HVDC system, a CB may not be necessary and may be replaced by a parallel switch or a high-speed switch.

1.5 Converters types

As previously mentioned, an HVDC system requires an electronic converter to convert the electricity from the alternating form to direct and vice versa. Basically, there are two main HVDC converter typology :

a) Line Commutated Converter (LCC);

b) Voltage Source Converter (VSC).

The first converters used in HVDC direct current transmission were the Current-Sourced Converters (CSCs) which used mercury vapor valves, replaced in 1972 by thyristor valves as a switching device. Starting in 1990, the HVDC-VSC technology also began to be used as an economically viable alternative to the CSC one, thanks above all to a new type of valve, the IGBTs (Insulated-Gate Bipolar Transistor)[5].

1.5.1 Line Commutated Converters

Impressed current converters, also known as Line Commutated Converters (LCC), are composed of two conversion stations at the ends and a connecting line between the two, as shown in Figure 1.10. They require a relatively strong network upstream in order to run correct switching of the valves, given that the thyristors used are not able to switch off autonomously until the current has zeroed. The short-circuit power of the network must be at least double the converter's power level and the supply voltage must be ahead of the current as the conversion process requires reactive power.

Generally, they base their operation on the 6-pulse bridge, with six commutations per period, where each bridge is made up of six valves divided in turn into a series of more thyristors to reach the desired voltage, thus producing a harmonic voltage ripple on the DC side of six times the fundamental.

Normally, two 6-pulse bridges are connected in series to operate with a 12-pulse configuration, phase-shifting them by 30 electrical degrees and powering a bridge through the secondary of a star-connected transformer while the other with a secondary connected in delta, obtaining a reduction of harmonics of both voltage and current.

Thanks to the thyristors, the control of the HVDC system is able to quickly by-pass transient faults and thanks to the fast reaction of the protection switches the system is isolated if the control system fails. The thyristors are also responsible for regulating the power flow, by controlling the ignition angle of the converters at both terminals of the line. In this case the power inversion is made possible by
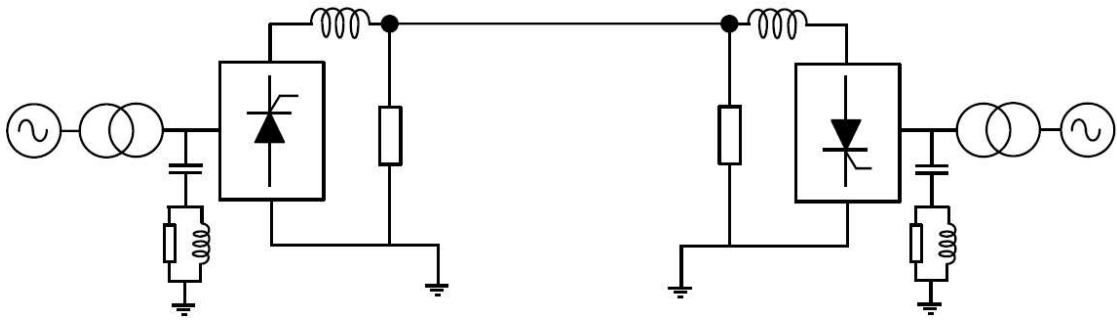
Figure 1.10: Example of a HVDC-LCC Configuration

keeping the direction of the current flow constant and reversing the polarity of the voltage in both stations.

The configurations with which this system is mostly used are the monopolar and the bipolar. In the first, the return current can pass through the land (or the sea) or through a metal return and is often used for small systems. With a bipolar system, on the other hand, there are two lines (with positive and negative polarity) which can operate independently and therefore allow operation at half power in case of failure of one of the two or use the return via earth if one pole is out of service. This configuration is suitable for long distance transmission. Other configurations used are the "Back-to-Back" system scheme, where the two converters are located in the same site and there is no power transmission via a direct current line, and the multi-terminal system, where there are more than two conversion groups.

1.5.2 HVDC-LCC Configuration

In order to describe the main components that make up an HVDC-LCC system, the electrical diagram shown in Figure 1.11[6] is used.

Figure 1.11: HVDC-LCC monopolar configuration

Converter transformer

Converter transformers connect the AC side network with the conversion bridge, transforming the AC side voltage to an adequate level required by the converter and to the transmission line, also ensuring galvanic separation between the AC system and the converter bridge. Unlike traditional transformers, in converter transformers the insulation must be uniform due to the alternation of the voltage levels generated by the valves inside the bridge. Depending on the power of the connection, the converter transformers can be built with two or three windings. In the latter case, the secondary windings are configured so that one is connected in a star while the other in a delta, out of phase by 30 electrical degrees, thus obtaining the elimination of current harmonics of order n = $(6 \cdot k) \pm 1$ (typical of 6-pulse conversion bridges). However, they are designed to work with high harmonic currents, able to withstand continuous voltage fluctuations due to the switching of the switches: for these reasons, they have higher losses and acoustic noise than traditional transformers. They can be equipped with switches to optimize operations.

Smoothing reactor

This component is inserted on the DC side downstream of the converter, preventing its discontinuous operation due to current ripple that could cause high overvoltages in the transformer and in the reactor itself, also preventing power interruptions in situations of low load. It limits the peak current in the event of a short circuit, limiting the speed with which it increases in transient situations. Considering that it is inserted in series with the circuit, together with the DC filter, it manages to break down the harmonic content and prevent resonance in the DC side circuit at low order harmonic frequencies.

AC Filters

They are located on the alternating side and have the main purpose of absorbing the harmonics of current and voltage generated by the converter and therefore, of reducing the impact they would have on interconnected alternating current systems. They also have a second purpose, which is to compensate for the inductive reactive power absorbed by the HVDC system. Filters tuned to different frequencies are usually inserted for the attenuation of the most significant harmonics. In the specific case of a 12-pulse converter, filters tuned on the harmonics of order n = $(12 \cdot k) \pm 1$ (k = 1,2,3...) and one for the third harmonic are inserted if required. For all frequencies above those characteristics, normal high-pass filters can be used.

DC Filters

DC side filters are also installed in the converter stations, eliminating the voltage harmonics characteristic of an AC / DC converter which cause alternating currents that overlap the direct current in the transmission line, thus generating interference in neighboring telephone lines. In this case the filters are connected in parallel, between the two then of the transmission line.

Active Filters

They can be inserted to support passive filters on both the AC and DC sides. Thanks to their superior performance, it is possible to overcome the stress limits due to transients on the active parts of the system. When coupled with passive filters, it is possible to have a filtering action also during maintenance operations of one or the other.

Electrodes

If present in a monopolar configuration, they allow to avoid the use of a second conductor for the return of the current, thus reducing costs. For some bipolar systems, ground return operation with half power is allowed for a short time in the event of a pole failure, however the electrodes are sized for full power even if they are not crossed by current during normal conditions. However, these electrodes require continuous maintenance.

DC transmission line

It can be an overhead line, cable or a mix of the two. For the overhead lines, towers with geometries appropriate to the environmental conditions will be prepared while for the cable lines the coordination of the insulation is to be assessed in conjunction with the magnitude of the overvoltages of internal origin (and also of atmospheric origin, if the line is of mixed type). An important factor for the cable is the insulation to be used: among the most important is the insulation with paper

impregnated in oil and extruded insulation (XLPE). The choice also falls on the type of converters that will be installed.

1.5.3 Voltage Source Converter

The HVDC-VSC system has seen its commercial diffusion thanks to the development and maturation of IGBT technology. Typical of these particular transistors is the ability to switch off and on without the voltage having previously canceled, as is usually the case for LCCs, thus eliminating the need for an external power supply for valve control.

The HVDC VSC is based on impressed voltage converters that extend in the transmission field with powers of a few MW up to 1000 MW with voltages that do can exceed 320 kV. The development of power electronics has made it possible to improve the switching valves, in particular the development of IGBTs (see Figure 1.12) (Insulate Gate Bipolar Transistor) that allow them to be controlled in voltage both on and off[6].
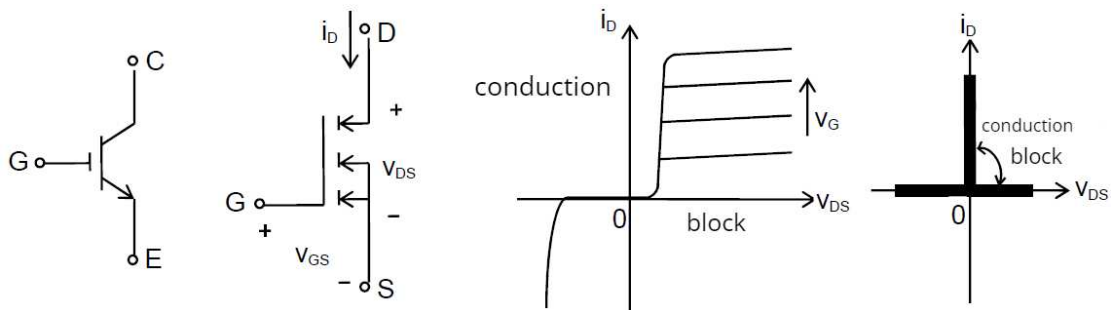
Figure 1.12: IGBTs characteristics

IGBTs are capable of switching at high frequencies (100 kHz), withstanding high voltages (both direct and inverse), and allow the passage of high current values (from $1000 \div 1500A$). It has to be highlighted that, as the switching frequency increases, the values of voltage and current supported decrease. The high switching frequency allows the generation of harmonics with frequencies that are far from the industrial frequency and therefore less burdensome for the use of the AC side filters. These valves allowed the development of VSC systems.

21

Figure 1.13 shows the HVDC (VSC and LCC) connections which are either in the study phase (feasibility) or under construction[7].
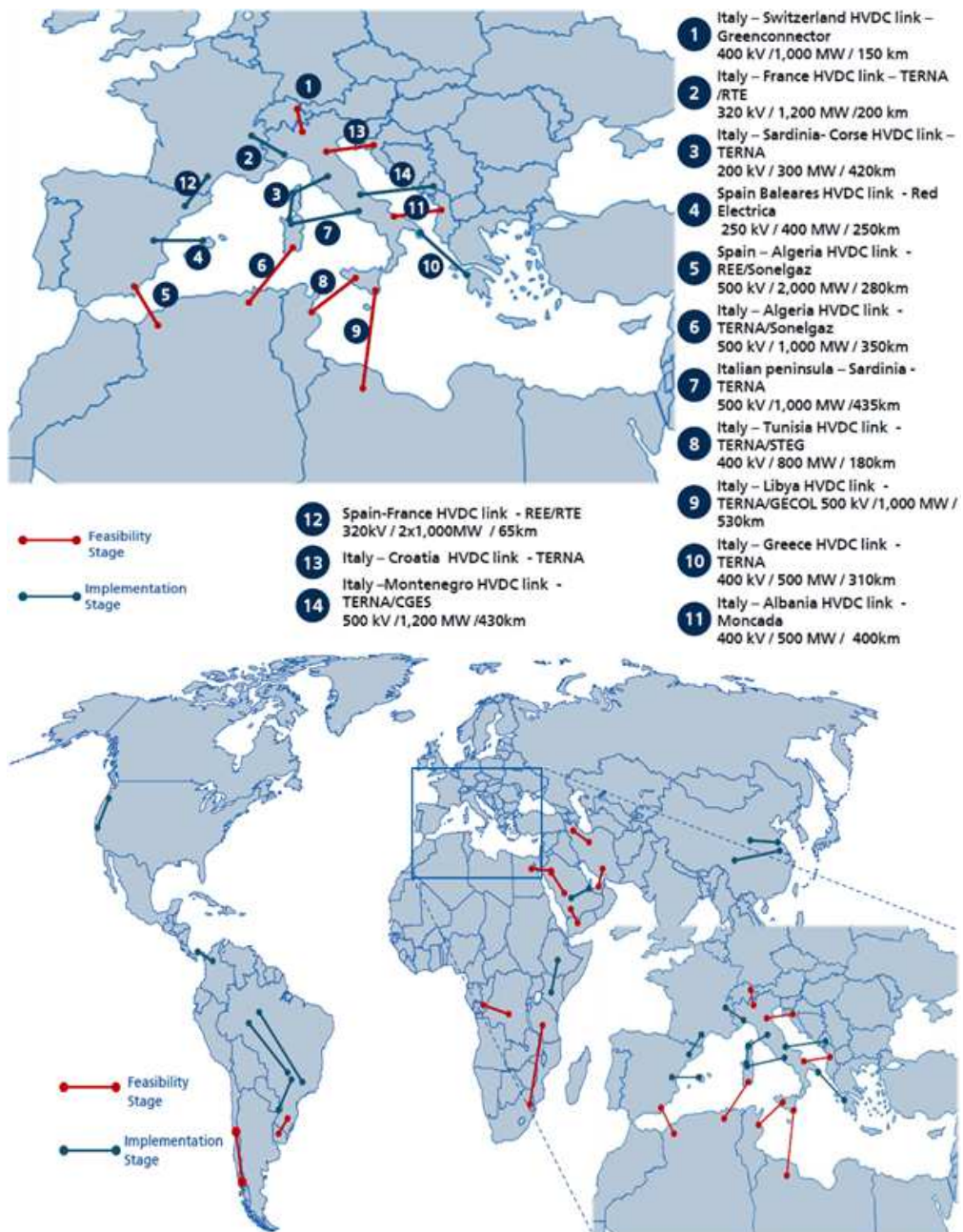
Figure 1.13: Example of HVDC link in Italy and worlwide

A general scheme of HVDC-VSC system is shown as follows:
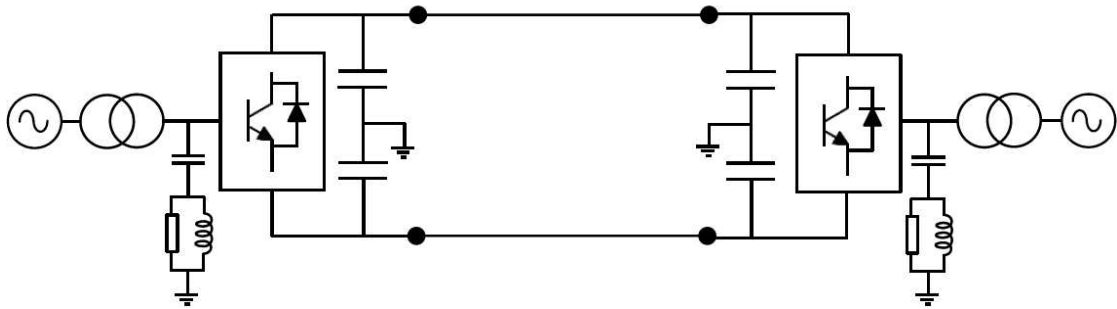
Figure 1.14: HVDC-VSC configuration

As can be seen from Figure 1.14, one or more capacitors are inserted in the DC side, to store energy, control the power flow and in particular reverse the current flow while keeping constant the voltage polarity. They also act as filters for the DC side harmonics. Similarly, as happens for the LCC technology, also in the VSC technology more IGBTs are connected in series in order to withstand and therefore reproduce a higher output voltage. Anti-parallel "free circulation" diodes are also added which ensure operation in the four quadrants of the converter. A system based on VSC technology is considered the equivalent of a synchronous generator with no moment of inertia, therefore able to control the active and reactive power absorbed and supplied by both converters connected to the ends of the line, regardless of the flow of active power but with only the maximum limit of apparent power and output voltage. The exchange of active and reactive power between the VSC converter and the AC network is determined by the phase shift angle between the output voltage of the converter and that of the network, taking into account the relative amplitudes. Usually, the control of the IGBTs is carried out using the PWM (Pulse-Width Modulation) modulation technique, which involves high losses due to the high switching frequency of the switches, a factor that limits the performance of VSC technology.

1.5.4 HVDC-VSC Configuration

An HVDC-VSC system consists mainly of the typical components of a classic HVDC system, with the addition of other elements suitable for the operation and protection of this particular technology. The components that make up a typical HVDC-VSC conversion station are initially described below[8]. Hereafter some of the features of the VSC components are reported as following:

a) **Power transformer**

It can be single-phase or three-phase with step switch and allows to adapt the voltage level of the network to an adequate level for the impressed voltage converter; it also provides galvanic isolation between the AC and DC systems. Depending on the type of converter that will power and therefore the switching speed of the valves, this transformer must be designed to withstand certain voltage stresses in the insulation.

b) **Capacitor bank**

They are located on the DC side and are usually of the dry type, they serve the energy storage function, charging and discharging according to the direction of the current. They stabilize the voltage and filter the high frequency harmonic currents. The size is chosen on the basis of the energy it can store at the rated voltage and the voltage ripple allowed on the DC side.

c) **Phase reactors**

They mainly filter the high frequency harmonics of the converter output voltage, they also allow the control of active and reactive power and limit the short-circuit currents in the valves. There are two reactors per phase or per leg of the converter to interface with the AC system.

d) **AC harmonic filter**

they have the purpose of limiting the harmonic content but above all improving the filtering performance in case of voltage distortion. Two converters, in the role of rectifier and inverter that can be interchanged between the two stations when required without the need to reverse the polarity of the voltage.

e) **Valve**

The modules containing the valves suitable for switching are installed, controlled and protected inside them.

f) **Valve reactor**

They are connected in series to the converter valves and have the function of

24

limiting the circulation currents between the phase units due to the inequality of the three DC voltages during operation and limit the short-circuit current in the valve.

g) **Smoothing reactor** it is located at the ends of the transmission line, it reduces the current harmonics. It can influence the dynamics of stress during faults or disturbances.

h) **Direct current transmission line** it can be of the underground or submarine type, of the aerial type or a mixture of the two. The difference with a line of a classic HVDC system is that it is not subjected to voltage inversion issues.
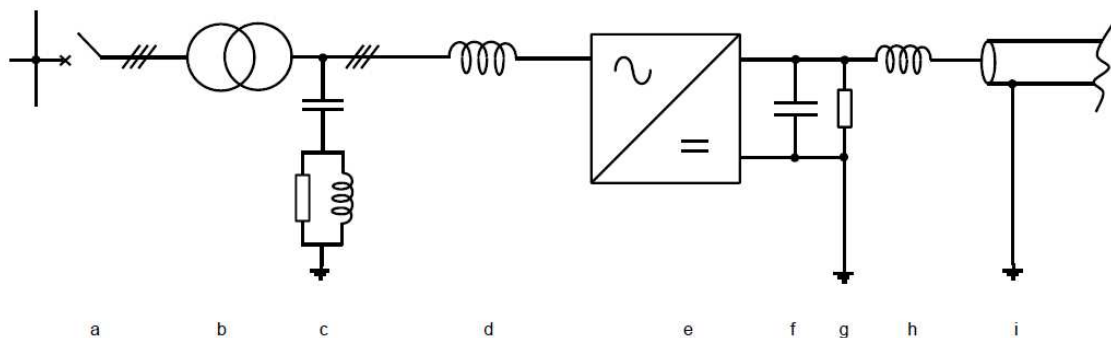
Figure 1.15: HVDC-VSC configuration

A typical single-line diagram of an HVDC-VSC conversion station is shown in Figure 1.15, where the various areas making up the entire plant are highlighted:

a) Circuit breaker of the VSC substation;

b) Converter transformer;

c) Harmonic filter on the AC side;

d) Phase reactance;

e) VSC converter;

f) DC capacitor of the VSC converter;

g) harmonic filter on the DC side (if necessary);

h) smoothing reactance (if necessary);

i) cable or OHL of the DC transmission line.

1.6 HVDC Multilevel Modular Converter

Today's HVDC VSC technology preferably uses IGBT forced switching switches as they can withstand the high switching frequencies imposed by control techniques. There are various types of converters that can be operated[10], depending on the output voltage waveform and therefore the voltage level that can be reached. Among the most common there are these types:

a) 2-level Converter;

b) 3-level Converter;

c) Multi-level Modular Converter (MMC).

1.6.1 Two-level converter

Consisting of two-level phase units connected in parallel, each of which with the series connection of two groups of valves, formed by the series of several IGBTs. Each of them has an antiparallel diode to allow current flow in both directions since IGBTs do not allow bidirectional current flow, while the voltage is maintained at the same polarity by locking the gate.

This converter has the simplest and cheapest scheme to output a square wave voltage. A typical diagram is shown in Figure 1.16 with the relative waveform of the output voltage of a phase, representing the alternating voltage.

The AC terminals are formed by the intermediate points of each leg and an inductance is inserted in series to keep the output current as uniform as possible during switching from one phase to another. The control of this converter is based on the PWM system, i.e. through the control of the amplitude of the fundamental of the output voltage based on a high switching frequency which consequently increases the losses in the converter and the stresses on the windings. The two-level converter is the basis of a multi-level configuration and a modular structure.

1.6.2 Three-level converter

An example of a three-phase converter with a three-level phase unit is shown in Figure 1.17 together with the output waveform of the inverted voltage, being in this case an inverter. It has three DC terminals connected via diodes to a central socket, which represents the reference of the zero potential, and it can be seen that there are twice as many valves as one at two levels. The waveform consists of three voltage levels that can be controlled by PWM technique to reach a shape closer to the ideal sinusoidal one; by increasing the switching frequency, this converter has a cleaner and less distorted harmonic content.
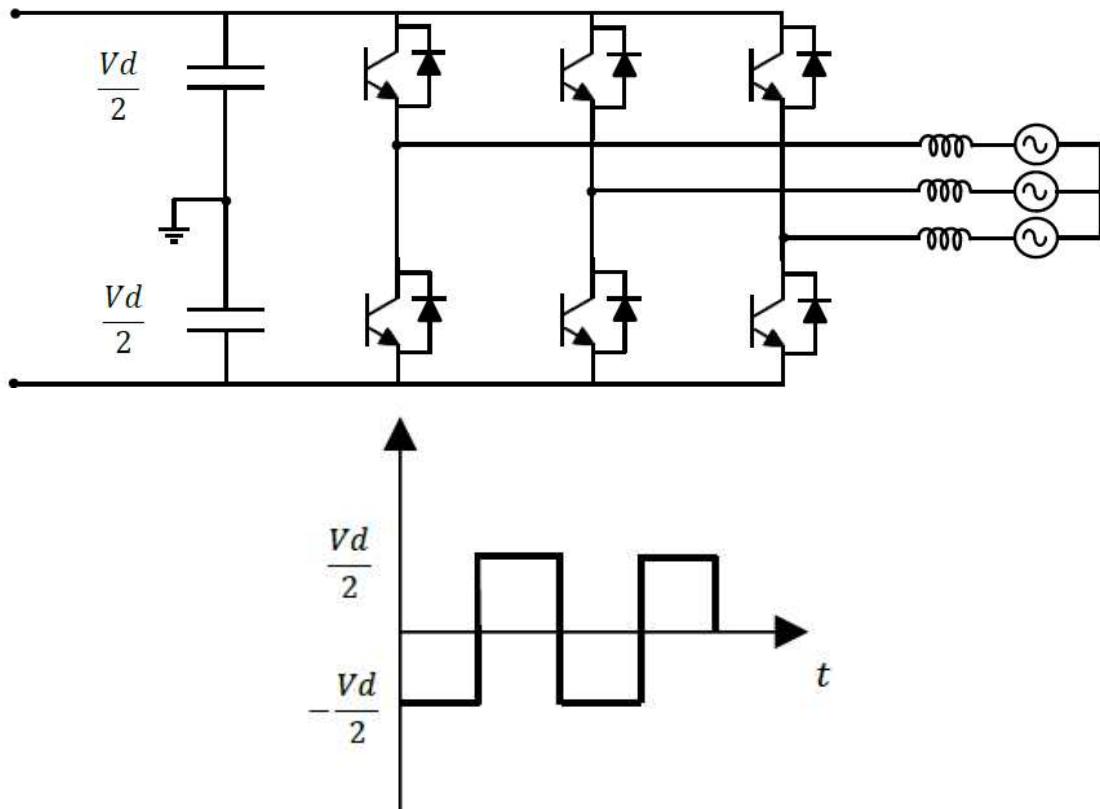
Figure 1.16: HVDC-VSC 2-level Converter

1.6.3 Multi-level Modular Converter

In the case of high voltage applications the number of levels to be added increases further. Solutions of sub-modules in cascade are therefore adopted, obtaining multi-level modular converters[9]. They can be divided mainly into two categories:

- Half Bridge (HB);

- Full Bridge (FB);

The former consists of a single leg, consisting of two IGBTs with diode in anti-parallel, in turn connected in parallel with a capacitor that keeps the voltage at its ends constant. The voltage that can be obtained is unidirectional and is taken through the mid-point of the half-bridge. A diagram of it is represented in Figure 1.18 together with the waveform of the output voltage that can be obtained by

27
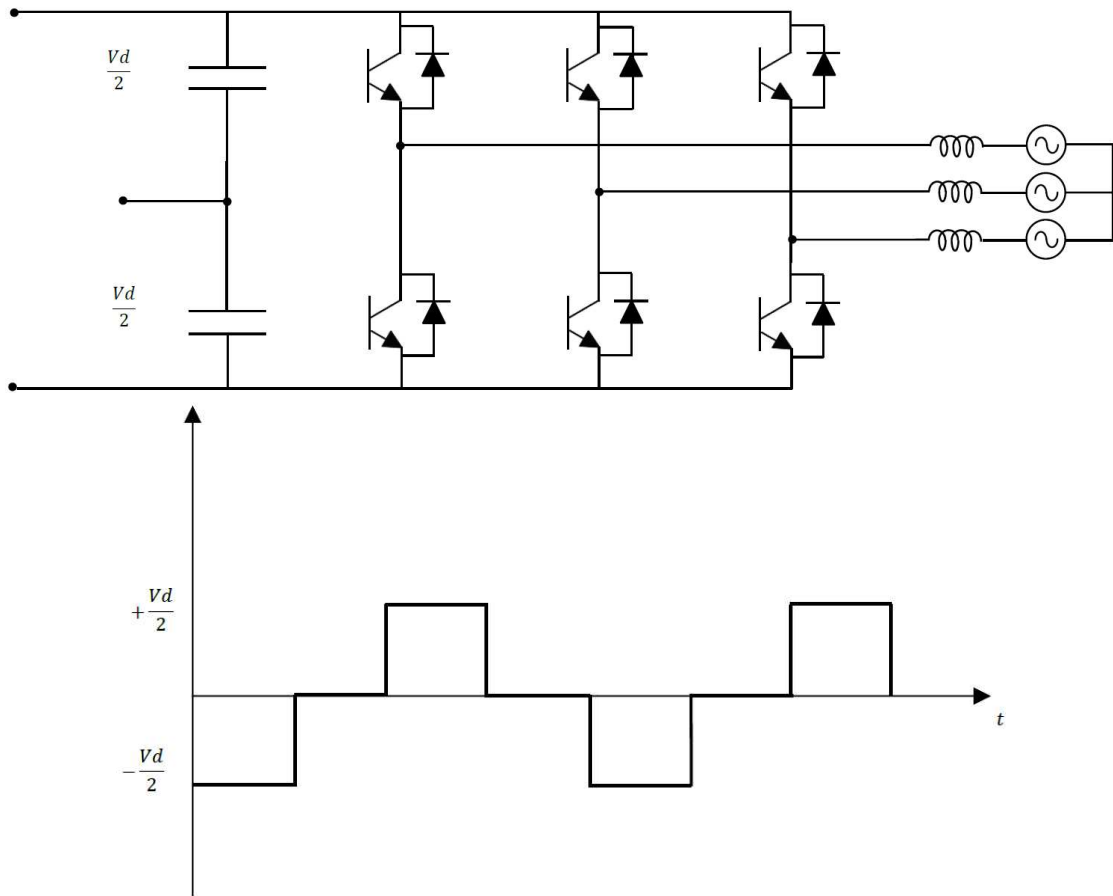
Figure 1.17: HVDC-VSC 3-level Converter

cyclically switching the switches. This structure has the advantage of having lower losses due to the reduced number of components, however, it is not able to limit the overcurrents coming from the DC side.

The full-bridge sub-modules, on the other hand, are made up of two legs and therefore double valves compared to the half-bridge and allow for a bipolar output voltage, which is taken from the intermediate points of the two legs. A typical diagram is shown in Figure 1.19 together with the waveform of the output voltage that can be obtained by cyclically switching the switches. This structure can produce a reverse voltage that opposes the driving voltage of the switches thus generating a negative electromotive force that opposes the flow of currents produced by faults in the DC side.

In both cases, the capacitor must be sufficiently large to be able to maintain the
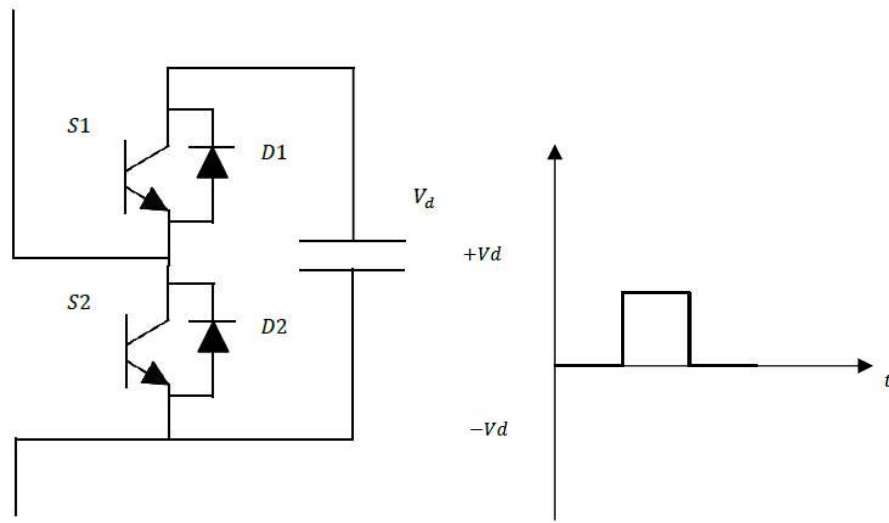
Figure 1.18: Half Bridge Sub-module

voltage almost constant despite the harmonic currents that pass through it, and therefore the sub-modules behave as a controllable voltage source. The above refers only to a sub-module, with which it is possible to obtain a low voltage level with a non-sinusoidal waveform. To extend the number of generated voltage levels, multiple sub-modules can be connected in series, increasing the number of semiconductors present, including sharing the total voltage as long as the energy between the various sub-modules is kept balanced. An example of a multilevel modular converter is presented in Figure 1.20.

Basically, an MMC converter consists of three legs per phase, each of which is composed of an upper and a lower "arm". Each of these "arms" includes a large number of sub-modules, which in turn consist of a valve (single valve configuration) or multiple valves (multiple valve configuration). The sub-modules are connected in series to reactors to reduce the overcurrents that can arise following a fault and reduce the circulation currents between the phases to minimum values.

Unlike the previous converters, this reactance has relatively lower values, as the switching of the switches takes place within the sub-modules and therefore there are no major variations in the phase leg. Having more sub-modules available it is possible to reach more voltage levels without having to increase the frequency too much, but simply by acting on the control of the various switches present inside them, always maintaining a tolerable voltage from each sub-module. This does not involve an increase in the harmonic content since the switching process in an MMC involves one sub-module at a time, changing only one voltage level and not the entire voltage of a leg.
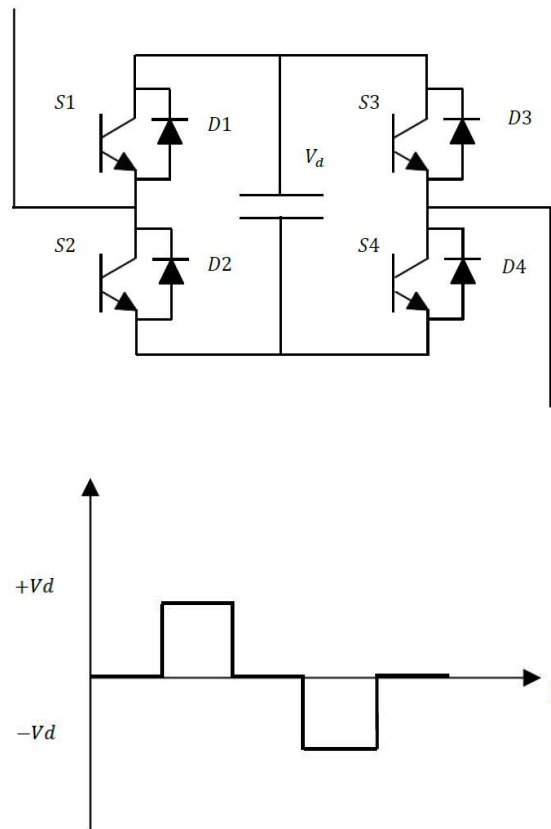
Figure 1.19: Full Bridge Sub-module

A multi-level converter generates a multi-step waveform with small voltage increases from one level to another without incurring stress due to voltage transients. Thus, any voltage level can be reached by simply changing the number of submodules. An example can be seen in Figure 1.21.

Multi modular technology has evolved to become one of the primary choices to be adopted in HVDC system converters. Table 1.7 lists some projects made with the different types of converters just seen.

It can be concluded by stating that the evaluation of the reliability and availability of HVDC connections will continue to be the subject of study for the development of electricity transmission systems, thanks above all to their strong growth and their implementation according to their characteristics and the advantages they present for future super-grid applications.
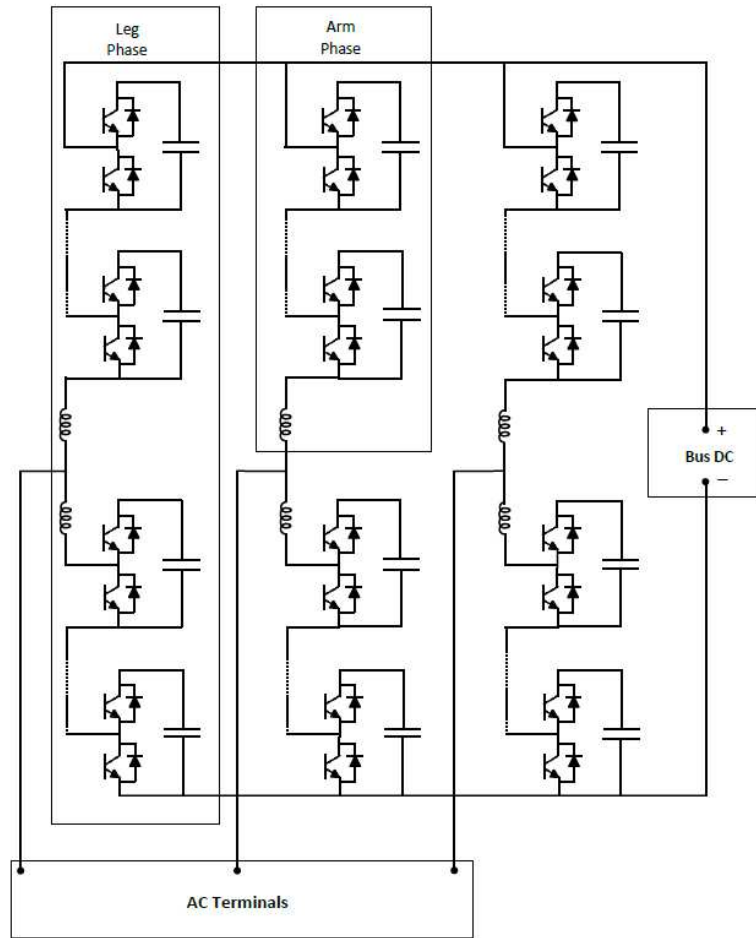
Figure 1.20: HVDC-MMC with Half Bridge sub-modules configuration

Table 1.7: HVDC-VSC technlogy evolution

Commissioning year	Converter Type	HVDC Project
1997	2 Levels	Gotland
2000	3 Levels	Eagle Pass
2002	3 Levels	Murraylink
2006	3 Levels	Estlink
2010	MMC	Trans Bay Cable
2014	VSC	Tres Amigas SuperStation
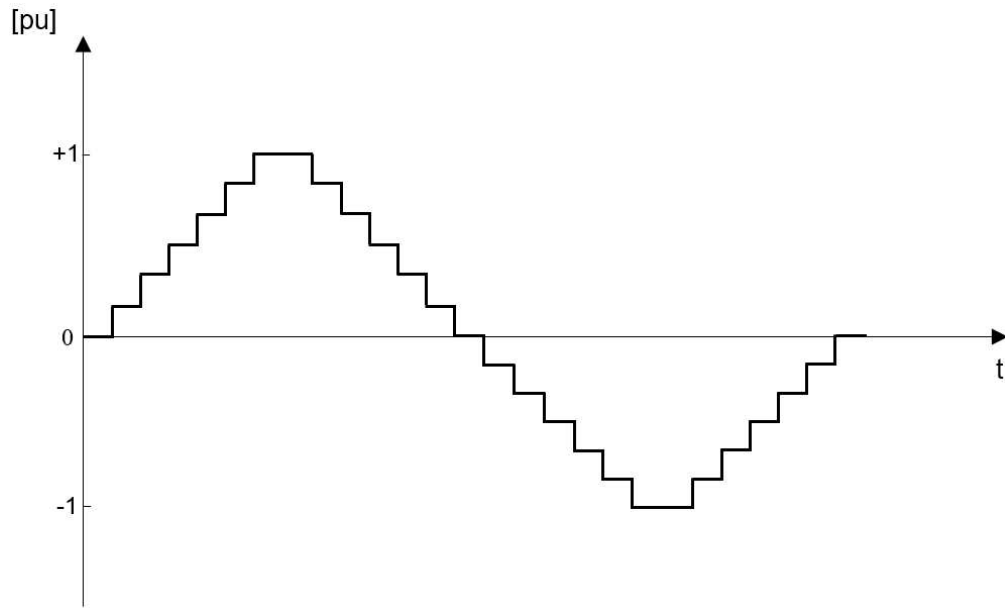
Figure 1.21: Example of output waveform from the MMC converter

1.6.4   Importance of the MMC FB configuration

Multi-level converters allow a significant increase in transmitted power, combined with a reduction in losses. Generally, they are defined as VSCs with three or more levels. The modular approach using a large number of submodules allows for a higher voltage range, easy modularity, and greater reliability. With a greater number of output voltage levels, harmonics generated by switching decrease, and less filtering is required.

There are several multilevel converter topologies, each with associated functionality. VSCs are prone to DC side faults and, depending on the MMC topology, there will be a different type of fault response. It is interesting to observe the behavior of the converter in the case of MMC with half-bridge or full-bridge SM.

Half-Bridge MMC (HB-MMC) and its variants are considered the main contenders for future multi-terminal HVDC applications. Instead of a series of devices, the MMC is constructed from a series connection of cells or "sub-modules" (SM). The modular design consists of three stages, each of which includes an upper and a lower half-branch. Each half-branch contains an inductor (arm reactor) and a series of submodules, each with a capacitor adjusted to an average voltage. The number of SMs varies based on the required converter rating. In this case, the submodule consists of a valve HB, shown in Figure 1.22(B). In the ON state, the capacitor voltage is projected between the power terminals of the submodule; in the OFF
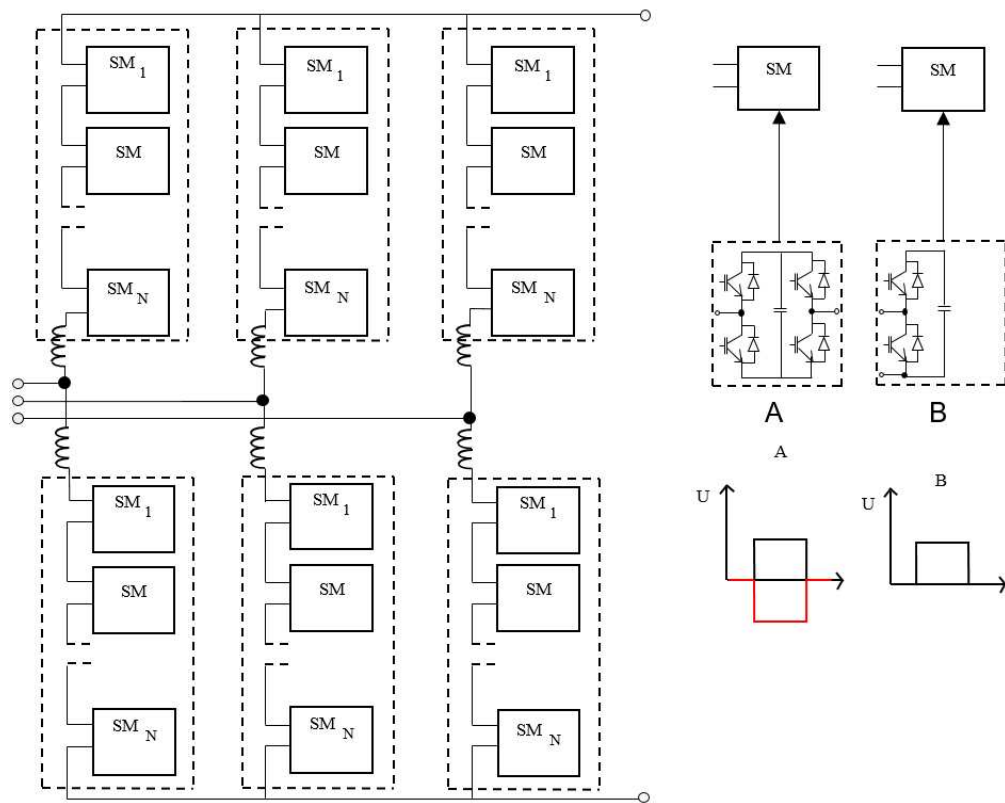
Figure 1.22: MMC topologies (A) Full-Bridge (B) Half-Bridge

state, the submodule is bypassed. By varying the number of submodules in the upper and lower arms of a phase, it is possible to control the voltage of AC output of the converter. The full-bridge submodule (FB-SM) is a mirror arrangement of the half-bridge configuration (HF-MMC) and therefore contains two pairs of switches (IGBT and diodes) and a capacitor, as shown in Figure 1.22(A).

In the event of a DC fault in the network, the VSC FB-MMC is capable of producing the nominal AC waveform up to full voltage reversal on the DC-Link, thereby providing a DC fault blocking response. A full-bridge MMC is designed primarily with a focus on reliability. In normal operation, the full-bridge submodules are modulated as half-bridge submodules, with only two of the switching valves operating at all times. The main difference in operation appears in case of a DC failure. During a DC fault, a high overcurrent occurs on the DC network. As soon as a DC fault is detected, the AC side can be isolated from the DC side by inhibiting the submodule control operation. Once the control operation is blocked unlike the half-bridge submodules, which are bypassed by the diodes or thyristors in antiparallel to the IGBTs continuing to supply the fault, the full-bridge submodules

33

are connected as shown in Figure 1.23.
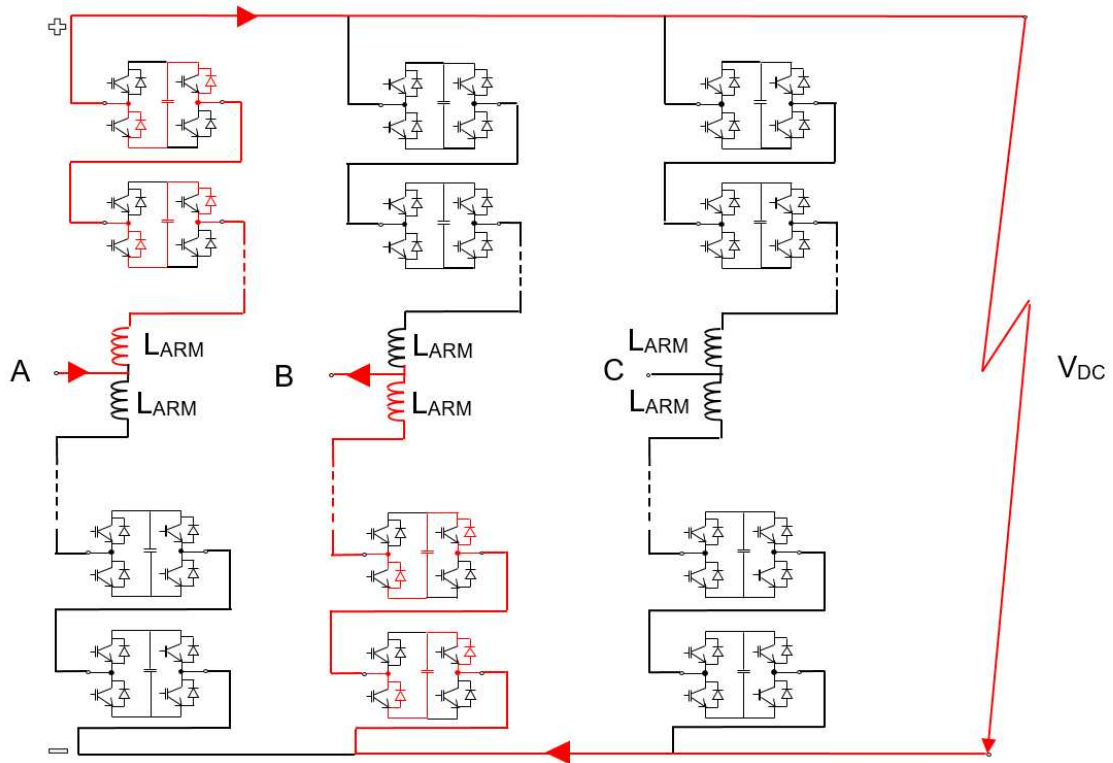
Figure 1.23: Full-Bridge DC fault through

In this case, the DC fault current cannot flow, since it is directed through the capacitors of the sub-modules, which are connected in series and opposition of polarity to the direction of the current. Since the total voltage of the series capacitor is higher than the peak AC grid voltage V_{LL}, the current drops to zero. However, the disadvantage of this method is that controllability is lost and therefore the MMC station cannot provide support to the AC side[10].

The FB option offers greater reliability at higher costs and higher conduction losses. However, in point-to-point schemes using overhead lines for transmission, most failures are of a temporary nature. Consequently, it is normally required to attempt several re-closing operations before shutting down the system. Within a multi-terminal system, the failing part of the network should be isolated so that healthy sections can continue to exchange energy. The application of the full-bridge converter, capable of blocking the contribution from the AC side, can limit the development of the fault current within the transient phase. For this reason, the full-bridge configuration is heavily used in overhead transmission lines, as it favors greater reliability and compensates for the need to control the fault current, thus

avoiding interruption.

On the other hand, when the cable lines are managed, the use of the full-bridge becomes useless and therefore the use of the half-bridge, which is not able to block the fault, is sufficient since in this case the insulation is not air and maintenance work is required. The need to interrupt the service is therefore inevitable. Furthermore, it can be observed that in particular for the half-bridge technology the use of DC switches is of fundamental importance for the correct interruption of the fault current.

1.6.5   Possible typologies of the sub-modules used in MMC converters

Mainly there are four topologies used in industrial field[11] that rely on modular multilevel converters (MMC) and they are:

- **Modular Multilevel Converter with half-bridge modules (MMC half-bridge)**

  As shown in Figure 1.24, the cells consist of individual IGBT modules with integrated free-wheeling diodes, DC capacitance, bypass thyristors, and electromechanical switch relay for cell protection.

- **Cascaded Two Level Converter with half-bridge modules (half-bridge CTL)**

  As shown in Figure 1.25, this configuration has the main characteristics of an MMC, but has a cell design in which the individual IGBTs are replaced by tubes made up of a series of eight stacks of IGBTs. Due to the short circuit handling of the IGBT modules, no bypass thyristors or mechanical switches are required. In the event of a single IGBT failure, the remaining IGBTs continue to operate but with a slight voltage increase.

- **Modular Multilevel Converter with full-bridge modules**

  As shown in Figure 1.26, they are used in cascade topologies, with an operating principle similar to the previous cases. Individual IGBT modules are used in each cell, equipped with DC capacitance and bypass thyristors, protection switches, and dissipation resistors.

- **Hybrid multilevel converter with full bridge modules** By connecting all the terminals of the full bridge module together with the IGBT switch, a voltage wave can be shaped as desired while allowing zero voltage switching for two-level operation (see Figure 1.27).
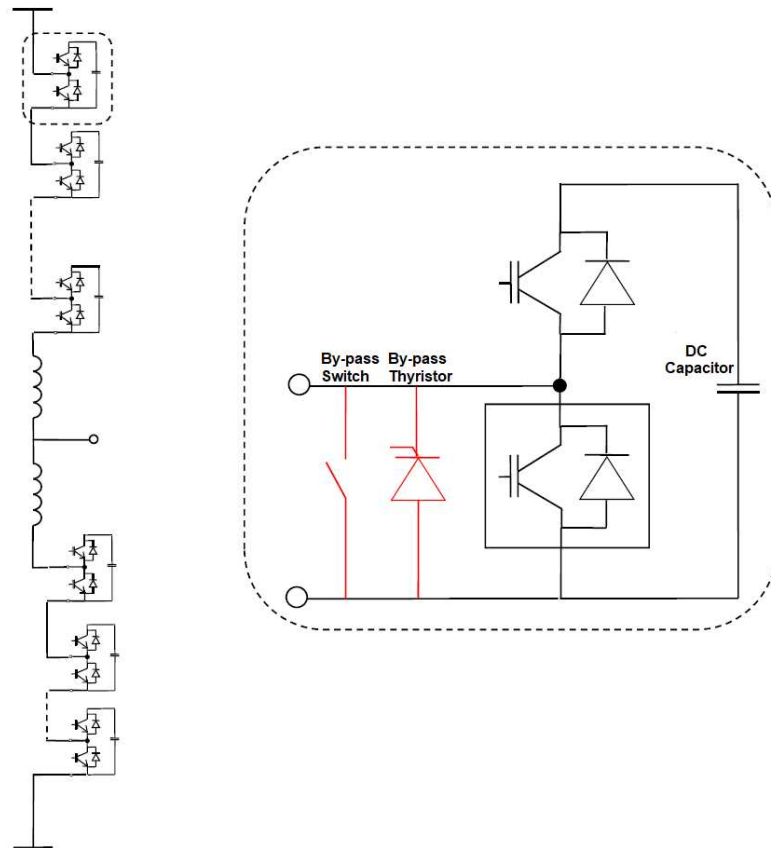
Figure 1.24: Half-Bridge Sub-module
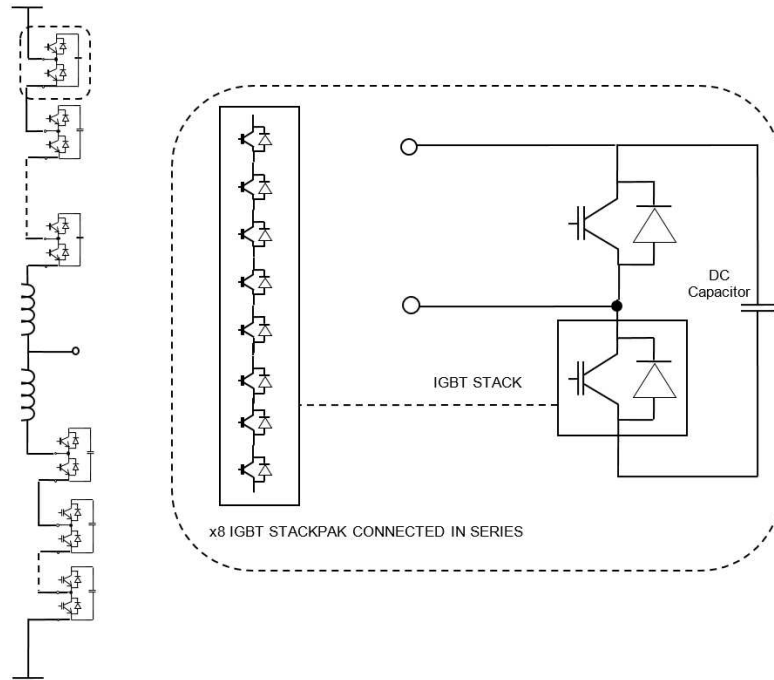
Figure 1.25: Half-Bridge CTL Sub-module
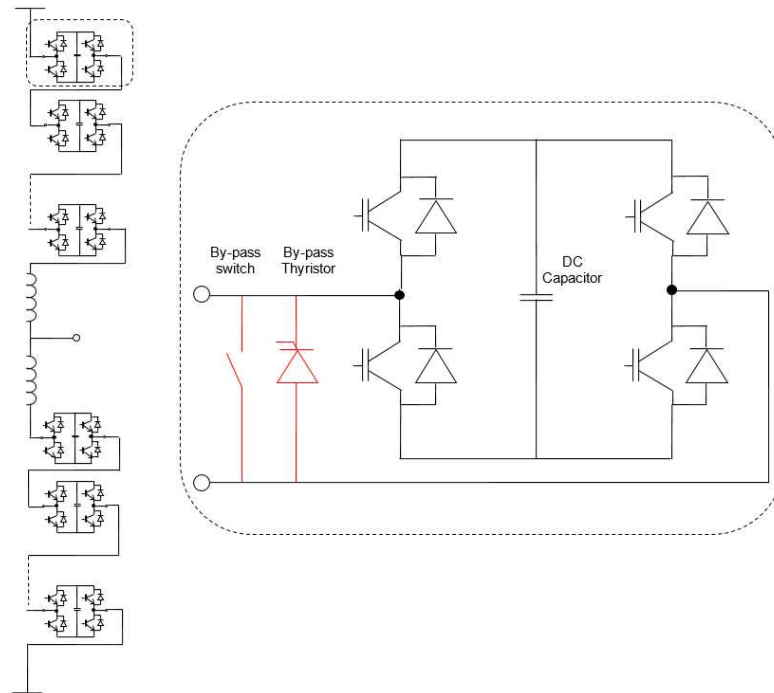
Figure 1.26: Full-Bridge Submodule

37
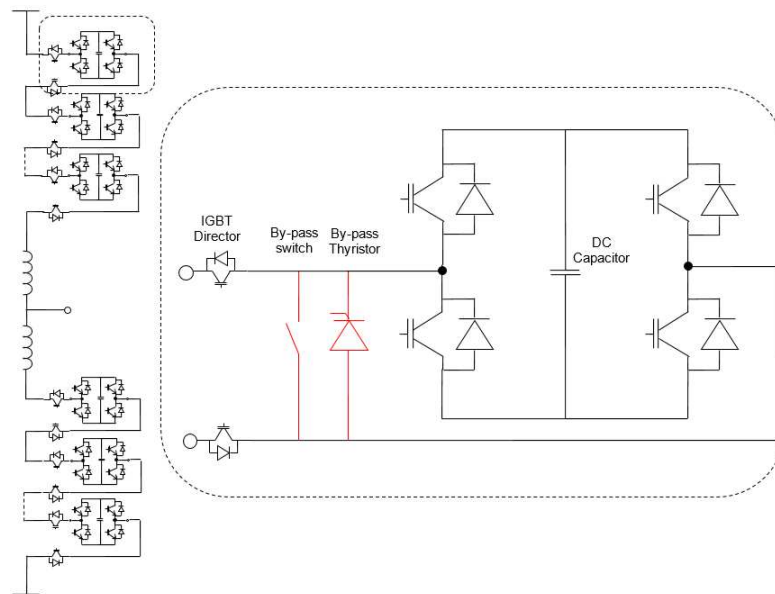
Figure 1.27: Hybrid Submodule

38

1.7   Overview of the main control modes in HVDC-VSC systems

The basic control methods of HVDC-VSC systems[12] are described below, but not in details, as these will be analyzed in depth in the following paragraphs. The voltage control on the AC terminals of the converter is possible thanks to the control of the energy flowing through or from the converter capacity. To illustrate the basic control system of VSC converters, consider the wiring diagram shown in Figure 1.28.
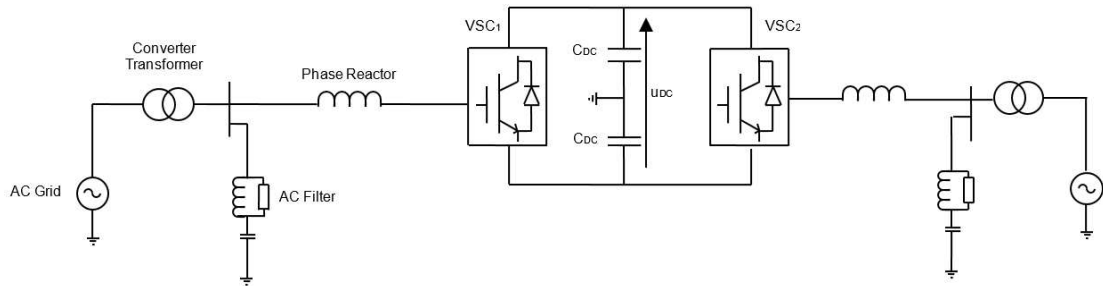
Figure 1.28: HVDC-VSC system

Active power control

By controlling the transmitted active power through the VSC-HVDC, it is possible to enhance the system transient stability, and to improve the low-frequency power oscillations damping. The conversion station does not increase the short-circuit level as the presence of the IGBT valves allows control of the fault current supplied, limiting it to the maximum, transiently by $1.2 \div 1.5$ times the rated current.

Reactive power control

The HVDC-VSC system can absorb or deliver reactive power. This is done regardless of the converters in the scheme and the transferred active power within the limits of the P-Q characteristic. Once the value of Q has been fixed to the set point, the converter will absorb or will deliver the amount of reactive power regardless of the voltage variations in the AC grid.

Power factor control

Another way to regulate reactive power flow is by controlling the power factor (see Figure 1.29). According to this approach, the HVDC converters are coordinated by the C&P HVDC system so that the HVDC converter stations are able to control the power factor at the connection point within the considered power ranges.
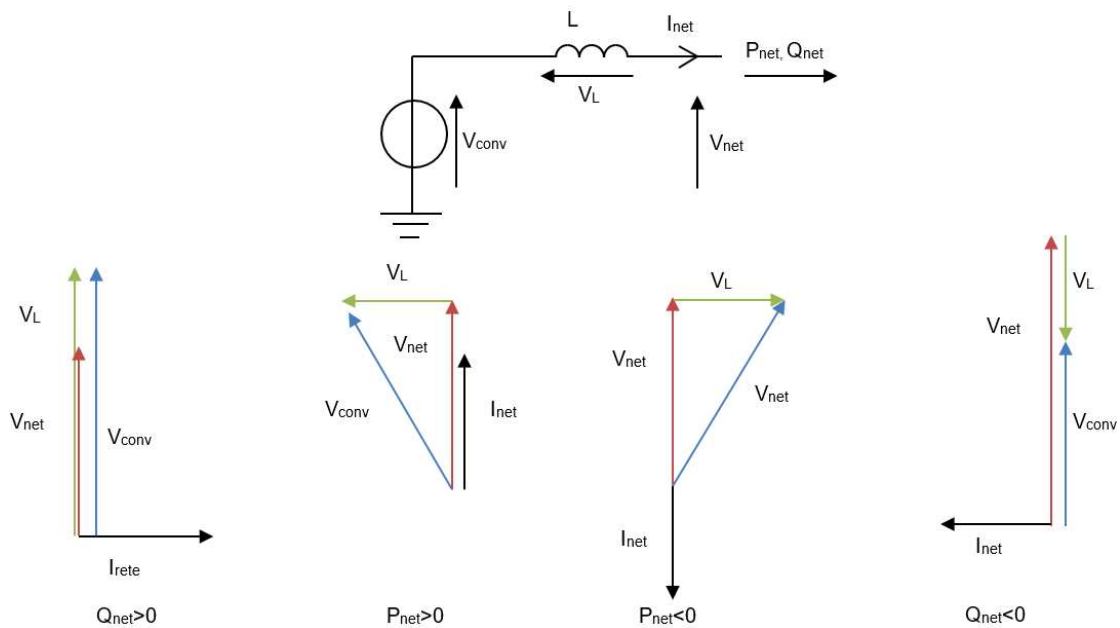
Figure 1.29: P-Q Regulation scheme

DC side voltage control

While one converter controls the active power, the other must operate in "V_{DC} control mode" and set the voltage at a specific level. Once the voltage value is fixed at one end of the line, the converter that is checking the active power makes the power flow on the DC side, adapting its DC voltage with respect to the DC voltage at the other end.

AC side voltage control

The regulation of the AC voltage allows, by regulating the reactive power to or from the converter, to reach the set voltage. By adjusting the amplitude of the fundamental of the AC voltage generated by the interface reactor and/or transformer. If the HVDC-VSC system is feeding an isolated AC system or with no other significant source of active power, the converter will automatically control the power to the load, assuming that another DC side converter independently controls the DC side voltage.

Frequency control

Frequency control in HVDC-VSC systems is normally applied through the use of an internal oscillator or phase locked control (PLL). In AC systems operating in stand-alone or black-start situations, the oscillator in the internal control system is used as the reference frequency and the power flowing through the converter is

dynamically varied to keep the frequency constant as if the load on the AC grid had increased or decreased.

Possible operations / states of the HVDC-VSC system

Grounded mode: the converter is isolated and blocked, grounded on the AC and DC side; this mode is usually adopted for safe maintenance work.

Isolated mode: the converter is isolated on both AC and DC sides with all ground terminals open.

Standby/De-energized mode: the converter is not transmitting power, the auxiliary circuits and secondary systems are all operational, the drive is not yet able to receive control signals, there is no high voltage supply on either AC sides and DC.

Block mode: the converter is fully energized on both sides, but cannot yet receive control commands. In many drives the lock state is only allowed as a temporary condition in the power-up sequence.

Unlock mode: the converter is powered from either the AC or DC side and receives control commands to allow the VSC valves to be switched to allow control of AC or DC voltages at the converter terminals if required.

STATCOM mode: the converter is unlocked and fully energized on the AC side, but the DC side is isolated or configured so that no active power is transmitted.

Island mode: the converter is connected at one end via the DC system to another converter which is in turn connected to an island AC grid. The converter connected to the stand-alone grid is able to control the voltage and frequency of the portion of the stand-alone grid.

Transmission mode: the converter is unlocked and fully energized on the AC side and is joined to one or more converters by a DC interconnect. Active and reactive power and AC and DC side voltages can be controlled.

1.8   Technologies compared

Table 1.8 reports the main differences between VSC (Voltage Source Converter) technology compared to LCC (Line-Commutated Converter) technology for HVDC:

Table 1.8: Main differences between LCC and VSC technlogies

	LCC	VSC (2-3 Levels)	VSC (Multi-level)
Harmonics	low frequence harmonics, hence, big AC filters	low frequence harmonics, hence, big AC filters	sharp harmonic reduction, no filter required (or tiny)
Losses	low	high commutation losses	lower than the previous one
DC Fault	uncontrolled short circuit current	uncontrolled short-circuit current (however there is the presence of re-circulation diodes)	Half Bridge: uncontrolled short circuit current Full Bridge: controlled / extinguishing short circuit current
AC Fault	risk of switching failure for the converter	control operations are possible, in order to improve the stability of the AC network	
Weak AC grid operations	risk of switching failure for the converter	no minimum short circuit power is required; black start operation feasible	

One of the first major differences between these two categories of technologies is the semiconductor device used inside the converter for switching operations. These devices are:

- thyristor for LCC impressed current converters;

- IGBTs for VSC impressed voltage converters.

Thyristors see their advent on a commercial level at the beginning of the 70s and therefore converters based on this technology (i.e., the LCCs) begin to develop very soon compared to VSC converters, which instead will begin to develop only in the 80s[13].

42

Table 1.9: Main IGBT and tyristor characteristics

Characteristics	Thyristor	IGBT
Maximum voltage tolerable [kV]	7÷8	1.7÷2.5
Maximum current tolerable [kA]	3.5÷4	1÷1.2
Conduction voltage losses [V]	1.2	3
Commutation frequencies [kHz]	1	20

As can be seen from Table 1.9, the IGBTs have a high switching frequency which allows reducing the harmonic content produced by the converter, however, substantially increasing the losses, due precisely to the greater number of switching of these switches.

Another parameter that differs substantially is the maximum applicable voltage, which is lower for IGBTs, which implies the need to have a greater number of devices than a thyristor converter to reach the same voltage level. Basically, these two technologies have different operations, which can bring benefits on the one hand and disadvantages on the other, both for the converter itself and for the network to which they are connected.

1.8.1 Power flow control

As already mentioned in the previous paragraph, one of the main features of the HVDC-VSC system is the independent control of the active and reactive power flow, always keeping the power flow both in and out of the converter balanced, net of losses. The balancing occurs without the use of telecommunications between stations but simply by measuring the direct voltage. For an HVDC-LCC system, on the other hand, an active network is required to supply the AC voltage to obtain the switching process, with a power flow control dependent on external sources.

Furthermore, a change in active power causes a change in reactive power, triggering a voltage fluctuation in the network, generating voltage drops, which in turn result in a further consumption of reactive power to further voltage drops. To avoid this voltage instability, it is necessary to connect the converter to a point of the network where the short circuit power is at least double the nominal power of the DC line. However, this problem does not exist for the VSC, since active and reactive power can be controlled separately, in this way it is possible to control the flow of power in the network, reducing the risk of any congestion.

1.8.2   Power flow reversal

Since for an HVDC LCC system it is not possible to change the direction of the current (see Figure 1.30), to invert the power flow it is necessary to invert the polarity of the voltage, as already mentioned previously. However, special mechanical switches are required at the terminals of the DC line. To realize this inversion, the converters must be equipped with complete isolation. The opposite occurs instead in an HVDC-VSC system, where the voltage is kept almost constant by the capacitors located on the DC part. The inversion of the power flow is obtained by changing the direction of the current in times of the order of a millisecond if required. There is no need to change the control mode without using a telecommunication between the stations. Thanks to this ability to avoid the inversion of the voltage polarity for the control of the power flow, cables with extruded insulation (XLPE) can be adopted for the realization of the connection line between the stations, obtaining advantages in economic terms and exploiting the excellent physical and electrical properties of an XLPE cable.
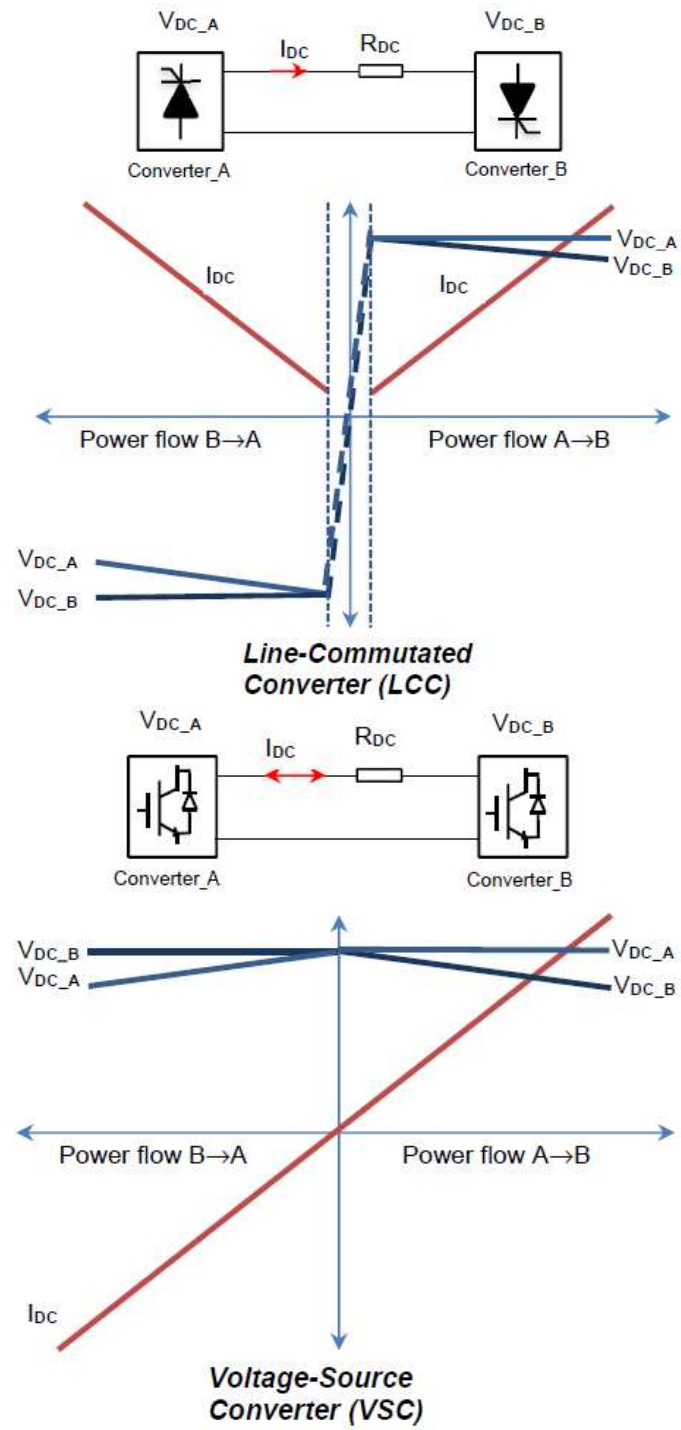
Figure 1.30: Operation areas for HVDC LCC and VSC technologies

1.8.3   Interconnections with multi-terminal system

An interconnection with multi-terminal system is established between different converters via a bipolar DC line, and this reduces costs and increases the reliability of the system. For an HVDC-LCC this represents a problem, as it requires reversing the polarity of the voltage to reverse the flow of power, while with an HVDC-VSC system it is much simpler thanks to the constant voltage polarity. The predominance of the LCC system as a consolidated and best known technology places the latter as the primary choice. However, the advantages VSC boasts over its rival, make it enhanced in many respects. With further developments and a deeper maturation it will be possible to overcome the related problems, leading this type of converters to find a wider space of use in the transmission of electricity and above all in the renewable energy markets, where it is currently experiencing considerable success: an example are the various projects of lines realized through HVDC-VSC system all over the world, shown in Table 1.10.

Table 1.10: Examples of HVDC links with VSC converter

Project	Year	Size [MW]	Voltage [kV]	Length [km]
Gotland, Sweden	1999	50	80	2x70
MurrayLink, Australia	2002	220	150	2x180
CrossSound, USA	2002	330	150	2x40
Valhall, Norway	2009	78	150	292
East West interconnector, UK-Ireland	2012	500	200	261
INELFE, France-Spain	2015	2000	320	364
PiSa, Italy-France	2019	2x600	320	190
FABlink, UK-France	2022	1400	320	220

1.9 Electromagnetic interference

A circuit in which direct current flows generates a magnetic field whose value is constant over time, and therefore does not produce any induced electromotive force. No inductive coupling is generated by perfect direct current. However, harmonic currents flow in the direct current line due to the AC/DC conversion technology; VSC technology with PWM involves a lower content of current harmonics than thyristor technology (LCC). Electromagnetic interference is generated by these harmonics. In addition to the speed of current variation, another fundamental element is the geometry of the coupling circuit. The length of the circuit is a significant quantity, since the longer the circuit, the greater the probability of having circuits susceptible to interference. A critical situation occurs when the earth constitutes a return path. Indeed, a current flowing in the land passes into the deep layers of the soil, thus creating a circuit whose depth is of the order of hundreds of meters or even a few kilometers. The depth of the inducing circuit increases as the resistivity of the ground increases, while it decreases as the frequency increases. A DC system can have an inducing circuit that involves the ground. This occurs in the case of monopolar systems, when the ground is used as a return conductor. In this case, both normal operating and fault conditions must be studied. Overhead line bipolar DC systems produce no interference under normal operating conditions (as the earth is not involved), while under fault conditions, which involve earth as a return path, produce interference and must be analyzed. Even in the case of two-pole DC underground cable systems, the normal operating condition does not produce interference, while in the fault condition the metal screen constitutes the main return path for the fault current; the remaining part flows into the ground. The electromagnetic coupling depends on the distance between the inducing circuit and the induced circuit: the smaller this distance, the greater the coupling. The existence of a metal shield that surrounds the conductor and is suitably connected to earth, has an important shielding effect for the purposes of electromagnetic interference in the event of a fault, since the shield transmits most of the fault current in a direction opposite to the line current. The study of electromagnetic interference was the subject of study in the Italy-France connection conceived as an HVDC connection consisting of two VSC bipoles (4 insulated cables). The link is designed to guarantee a transmission capacity of 1200 MW (2 x 600 MW) and the overall length is approximately 190 km. The cables will mainly be laid along the motorways (A32 in Italy, A43 in France) and will cross the border passing through the future Frejus tunnel (13 km long). The most suitable technical solution for conversion stations and cables is the voltage-Source Converter technology (VSC - 2x600 MW), with two independent bipolar systems, connected by four extruded cables with a nominal voltage of $\pm$ 320 kV. The electromotive force induced by the fault current for the entire length of the cable in the tunnel (13 km) was

evaluated, which is approximately 100 V and the maximum induced voltage to earth is approximately 50 V. Assuming a dwell time of the fault of 50 ms, the standard limit of voltage to earth for the safety of people is 2000 V while that for the safety of telecommunications systems is 1030 V. Therefore, electromagnetic interference in a fault condition is much lower than the normal limits. The harmonic current values in the DC cable line were derived from typical data provided by the manufacturers. The electromotive force induced by the harmonic currents for the entire length of the cable in the tunnel (13 km) was evaluated, which is approximately 16 V and the maximum voltage induced to earth is approximately 8 V. Compared to the limits defined by the standard, the interference associated with harmonic currents is much lower. The induced voltages evaluated both in normal operating conditions and in fault conditions were found to be considerably lower than those allowed by the applicable legislation both for the safety of people and for the correct functioning of the telecommunication systems (signal circuits).

1.10 AC/DC line interactions in parallel

If AC and DC lines were put in parallel, there may be electromagnetic interactions, linked to the fact that the fundamental frequency component on the AC side is induced on the DC line (see Figure 1.31). This implies an increase of the voltage and current to the direct sequence and of the current to the homopolar sequence; on the other hand, the contributions to the inverse sequence of voltage and current and of the voltage to the homopolar sequence are negligible. This causes a necessary oversizing of the DC components, of the conversion transformer, problems in the operation of the converter, increase of non-characteristic harmonics.

Figure 1.31: AC/DC interaction for line in parallel

1.11 Off-shore systems

In recent years, the electrical system industry has recognized that impressed voltage converter (VSC) technology is the most suitable solution for the development of offshore DC connections[14]. The creation of effective DC protection systems, mandatory to ensure that a fault does not cause any damage to the infrastructure or an interruption of the electricity service. In this regard, the DC circuit breaker, i.e. one of the key elements of complex DC networks, is not yet a mature component and currently has no installation. in large scale in operation. The implementation of DC networks requires future specific market rules and regulatory frameworks within the vision of a "single European energy market" (IEM).

1.11.1 Topologies of offshore HVDC networks

The main Off-shore configurations are:

- **Point-to-Point Configuration**
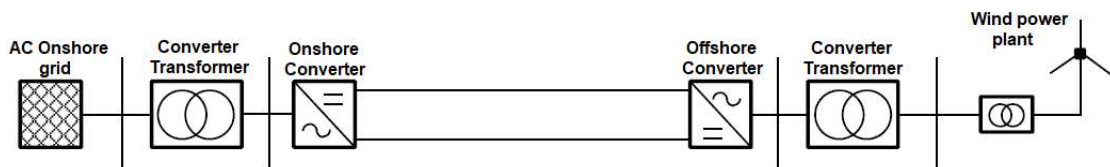
Figure 1.32: Point-to-Point configuration scheme

Features:

- low reliability and flexibility;

- **Backbone configuration**
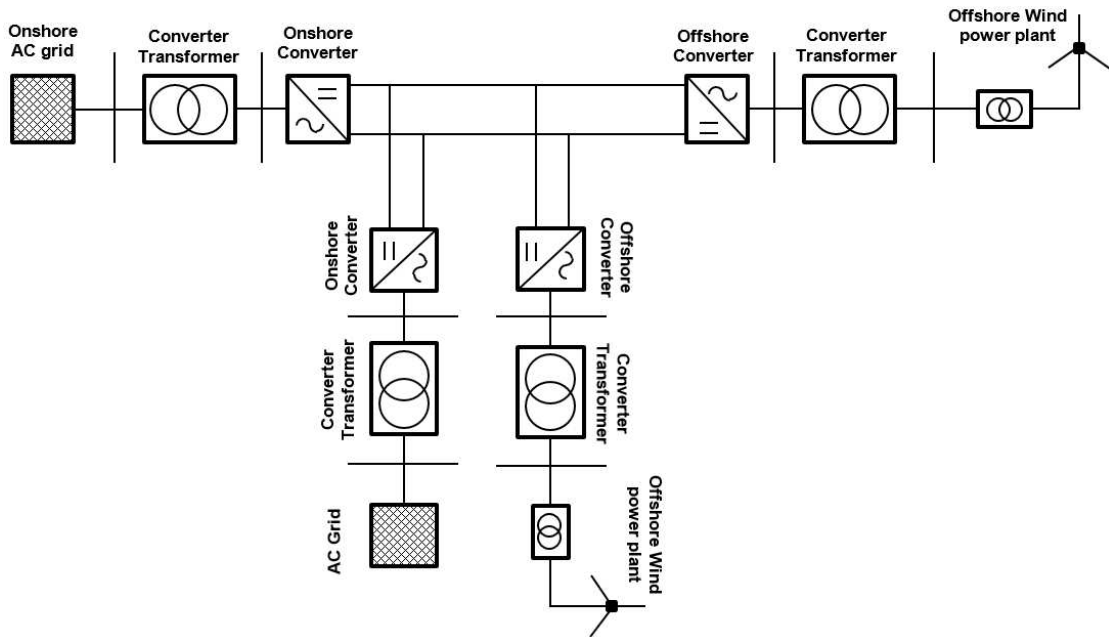
Figure 1.33: Backbone configuration scheme

Features:

- possibility of restarting power flows between off-shore terminals;
- losing the DC cable means losing the entire production park.

- **Meshed configuration**
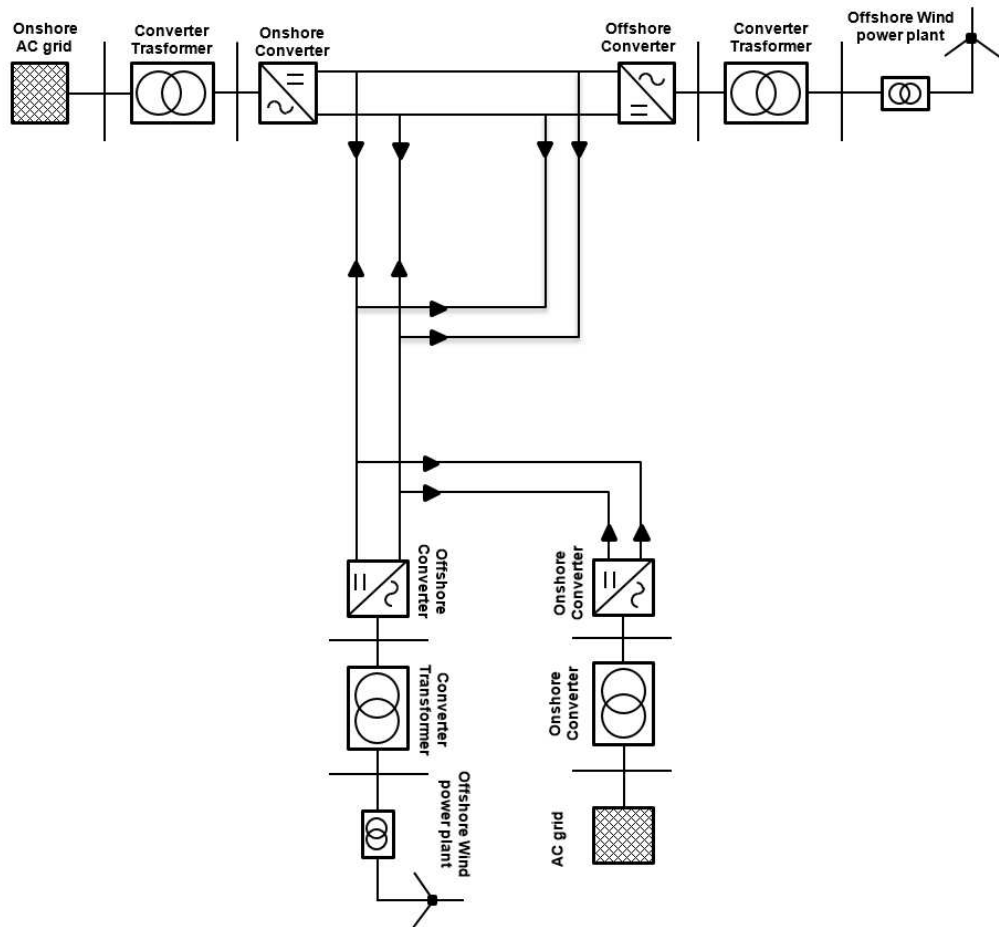
Figure 1.34: Meshed configuration scheme

Features:

– maximum reliability and flexibility: energy can use many paths to go from wind turbines to the shore, and the same for energy exchanges;

– it is based on a meshed DC network configuration with an N-1 degree of failure eventuality (ie, subject to the loss of a converter station or DC line, the rest of the system should maintain operation);

– a meshed network will add flexible interconnection capacity between

51

different countries;

- − a large amount of power can be connected to this network; however, it must be able to handle a failure without losing the entire generation.

The key point in a network is the reliability requirements. This derives from the fact that there is a need to ensure maximum exploitation of the energy delivered to the electricity market so that the economic investment made for the wind farm has an economic return. Reliability means the ability to guarantee the transfer of power from offshore wind farms to the shore even in the event of interruption of some components of the offshore network, thanks to the presence of alternative routes. Reliability refers to the DC transmission lines and the conversion station (e.g., in the case of a point-to-point connection the loss of a conversion station or a DC line would mean losing the entire production. This could be partially solved using a bipolar configuration). The use of a DC network that connects wind farms far from each other can decrease the variability of the power due to the effect of the wind, thus achieving greater stability (mitigating effect), with a positive effect on the efficiency and safety of operations as well as on the environment. This mitigating effect can contribute to the stability of the AC grid frequency. Continuity of power supply could also benefit from offshore networks. A failure of the production park or an onshore converter causes the loss of power injection into the AC grid. In the case of a point-to-point link, stability can be severely affected. In the case of a DC network connected to several AC networks, the disturbance can be redistributed to the individual AC networks, thus reducing the amplitude of the disturbance. Additionally, DC grid injections can be sent to AC grids to improve stability in case of failure. In combination with wind power generation, DC grids could be used to exchange power with AC grids by acting interconnectors. In this way, some onshore DC terminals draw power, others inject it using the VSC's ability to have bidirectional power flow. The interconnection function could be used to provide mutual support between areas of AC grids, to ensure the safety of operations concerning frequency stability to share resources for the power balance. In addition to the above benefits, auxiliary services can be provided from the DC grid to the AC grid. The DC grid with wind generation can be seen from the AC grid as a V_{PP} (Virtual Power Plant) capable of operating in such a way that the overall operation of the DC / AC power system is safe and optimal.

1.12 Piedmont-Savoy: The new interconnection between Italy and France with HVDC-VSC technology. An example of synergy between road infrastructures and power cables

The rationalization of territory resources draws the scientific society attention to the possibilities given by the highway and railway infrastructures (planned or existing) in order to install high voltage direct/alternating current insulated cables. The full compatibility of such synergy "highway/railway transport–electric energy transmission" involves different engineering branches. This topic has been investigated in the last ten years by means of feasibility studies published in scientific papers and technical brochures. These studies have eventually found a real and it is important to highlight that the ± 320 kV High Voltage Direct Current (HVDC) interconnection between France and Italy named "Piedmont-Savoy", based on Voltage Source Converter (VSC) technology, seems the practical transposition of the above mentioned Cigré studies.

1.12.1 Introduction

The use of innovative transmission technologies [15–23] hosted inside railway or highway infrastructures has been investigated in the last ten years by means of feasibility studies published in Cigré plenary session proceedings[24–29]: they usually deal with cross-border interconnections, e.g. a new 380 kV transmission line between Italy and Austria trough the Brenner Pass. Moreover, Cigré has produced two important brochures: N°403 "Cable systems in multi-purpose or shared structures" [30], and N°351 "Application of long high capacity gas-insulated lines in structures" [31]. This work, deals with the ± 320 kV High Voltage Direct Current (HVDC) interconnection between France and Italy named "Piedmont-Savoy", based on Voltage Source Converter (VSC) technology which seems the practical transposition of the above mentioned Cigré studies. In fact, this cross-border intertie will be mostly hosted on the existing highway infrastructures. The line length is considerably long, i.e. about 190 km, and it will include two independent symmetric monopole multilevel VSC systems with overall rated power equal to 1200 MW. The following paragraphs describe the main characteristics of the link (cable insulations, electrical and geometrical characteristics, converter station technologies) and the main drivers for the installation design which allows the power cables to be hosted safely along the highways and inside the new Frejus Gallery (second tube).

1.12.2 Main characteristics of the HVDC interconnection

After the development of the feasibility and preliminary studies and the in-depth analyses of the industrial market and project constraints along the cable route (see Figure 1.35), Voltage-Sourced Converter (VSC) HVDC technology was proved to be the most suitable solution for the Piedmont-Savoy power transmission intertie (see Figure 1.36). The link architecture consists of two HVDC independent symmetrical monopoles, 600 MW each, with a rated voltage of ±320 kV. This configuration assures an increased reliability and availability of the interconnection, and higher operational flexibility and security with respect to a single 1x1200 MW monopole solution. The 320 kV HVDC line is entirely undergrounded: 320 kV - DC-XLPE insulation with one 300 MW 2500 mm2 aluminium conductor. Four cables run together for the whole length of the link, which includes, as already mentioned, 13 km of Frejus tunnel installation. The preliminary project does not have smoothing reactors or DC side capacitors external to the converters, and there is no intentional DC grounding in the converter stations. On the AC network side the neutral of wye-delta converter transformers is solidly grounded; on the converter (delta winding) side of the transformers, neutral is high impedance grounded (at one terminal station of the HVDC link only) via a star point reactor.
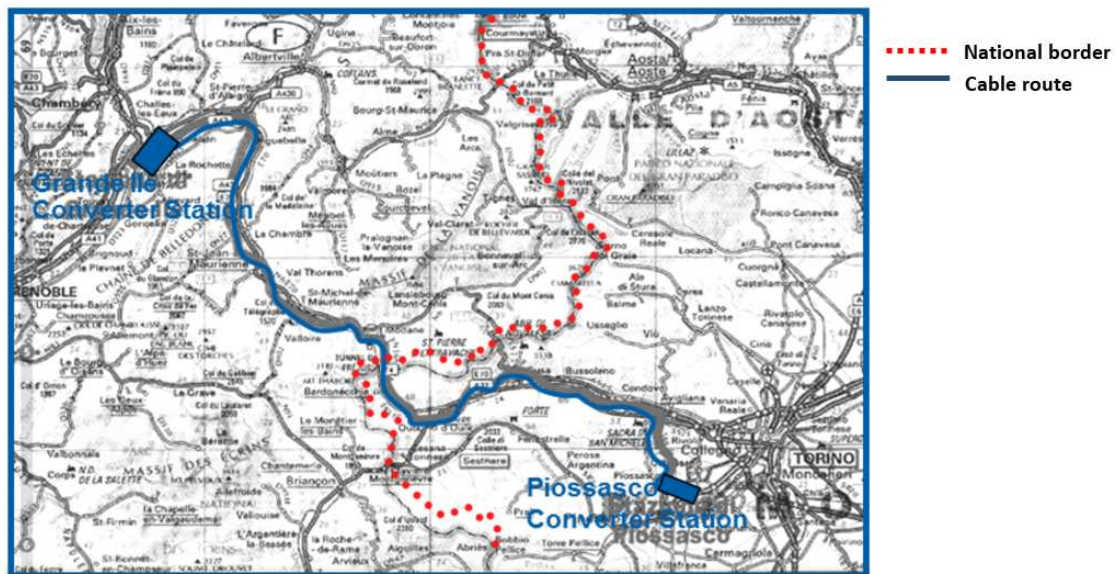
Figure 1.35: Route of the intertie
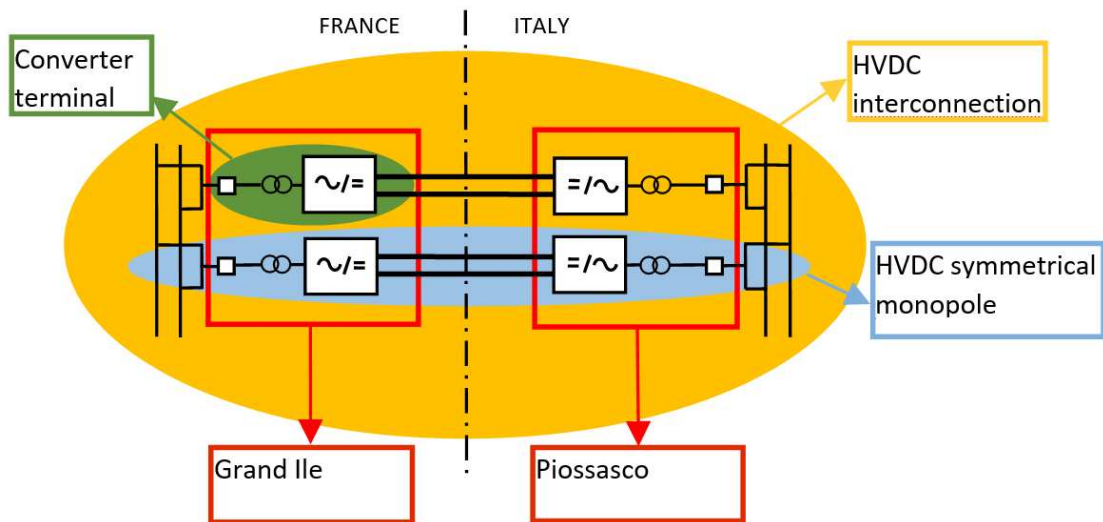
Figure 1.36: Route of the intertie

The four underground cables are XLPE insulated type with 2500 mm$_2$ aluminium conductors, metal aluminium screened, and polyethylene over-sheathed. The chosen cable technology is the only one that guarantees the feasibility of the link, by taking into account the installation difficulties encountered along the highway infrastructures and in the rest of the line route. Indeed, the extruded insulation grants a lower weight per meter of cable and consequently longer elementary cable sections. XLPE cables represent one of the main drivers for the VSC HVDC links, since this power conversion technology does not require the voltage polarity reversal. This is mainly due to the fact that, although research activities are ongoing to make XLPE cable able to support the voltage polarity reversal, they seem not to give sufficient confidence for its use with Line Commutated Converters (LCC) systems in which the polarity reversal is mandatory for the reversal of the power flow [32, 33]. The main characteristics of the HVDC Interconnection are summarized in Table 1.11:

Table 1.11: Main characteristics of the HVDC interconnection

HVDC SCHEME	2 INDEPENDENT BALANCED MONOPOLAR SYSTEMS (VSC TECHNOLOGY)
Rated power of whole interconnection	1200 MW
Rated power of each link	600 MW
Power flow range and direction of each link	bi-directional: from 0 to 600 MW per link
Rated pole voltage [Udn] (pole to ground) of each link	± 320 kV (without polarity reversal)
Maximum continuous pole operating voltage	± 340 kV
Rated pole current	950 A
Cable Technology	XLPE insulation
Length [km/cable]	Around 190 km (13 km inside the Frejus Safety Gallery)
Service Life	At least 40 years

1.12.3 HVDC Cables

The total length of the cable route is about 190 km, split into 95 km on the Italian side and 95 km on the French side. The cable system will be mainly laid along highways (A32 in Italy, A43 in France) and will cross the border inside the new Frejus Gallery, currently under construction (the new 13 km long gallery, half in Italy and half in France is under construction in parallel with the existent Frejus Tunnel - T4).

The entire link has the following characteristics:

- 778 km of 320 kV HVDC cable (see Figure 1.37) ;

- 488 straight joints;

- 140 earthed joints;

- earthing link cables and boxes;

- fibre optic cables and accessories system for TLC and temperature monitoring;

56

- distributed temperature monitoring system (DTS) and other monitoring apparatuses.

Number	Element
1	Conductor
2	Binder
3	Conductor screen
4	Insulation
5	Insulation screen
6	Water barrier
7	Metallic sheath
8	Outer sheath
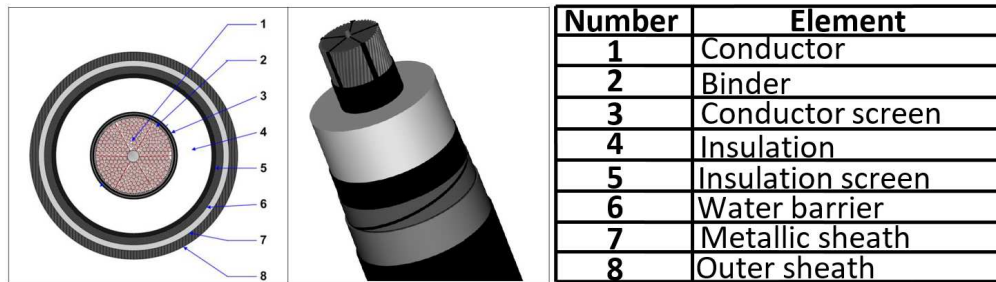
Figure 1.37: Cable characteristics

The cable route on the Italian side has a full length of about 95 km, starting from the substation of Piossasco to the Italian National border sited inside the new Frejus Gallery. Most part of the route runs along A32 highway, for about 51 km. The remaining part is spread over provincial roads (SP 589 and SSP 24), city roads and agricultural terrains. The new Frejus Gallery is 13 km long, the Italian part (from the gallery entrance to the Italian national border) is about 6,5 km long. As mentioned before, one of the main characteristics of the cable path design is definitely linked to the synergy with the existent highways (see figure 1.38and 1.39) on which the cables will be installed. This represents the relevant and innovative peculiarity of the project itself. On the other hand, this introduces a constraint due to the presence of several viaducts to be bypassed (23 only on the Italian side), some of them extremely long and high: this is the main factor constraining the choice of the most flexible and lightest cable technology, i.e. XLPE insulation and aluminium conductors. This choice, compared to copper conductors, results the most cost-effective, and provides several advantages in terms of ease of cable drum transportability and reduction in the number of required joints, thus minimizing both discontinuity points and construction times. Moreover, the selected technology allows an easier localization of the joint pits along the highways and the avoidance of joint installation on viaducts, reducing highway traffic limitations during the construction phase. The cables are typically laid inside trenches in two possible formations:

- square formation (see Figure 1.40);

- flat formation, used on the whole highway pavement and where square formation cannot be used (see Figure 1.41).

During the project design phase and following many survey activities performed along the entire route in several steps, hundreds of services interfering with the power cables (water pipes, MV and LV cables, Telecom cables) have been identified

57

and classified. A specific solution has been designed in order to bypass each one of them: no-dig methods, like horizontal directional drilling (HDD) or pipe jacking, have been adopted to overtake some crossings. Laying depth, type of concrete to be used, filling materials, restoration works and any other detail to define the civil work aspects have been discussed and agreed with the highway operator and the other competent authorities involved for the rest of the route.
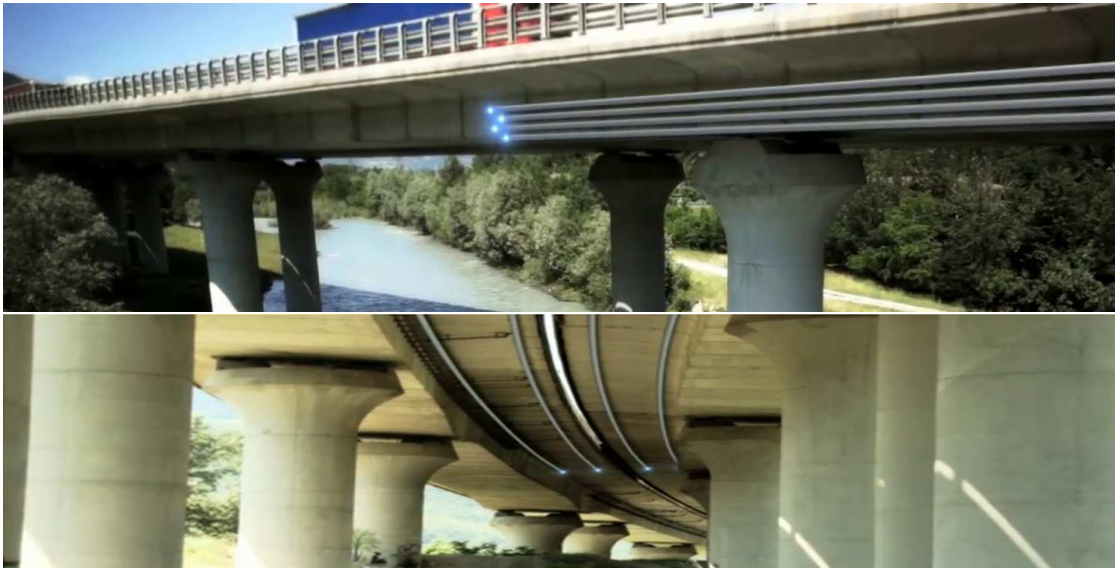
Figure 1.38: Cables route

Figure 1.39: Cable trench close to the highway

Along the A32 highway (see Figure 1.42) it has been necessary to find specific solutions for each of the 23 viaducts existing along the highway route. The most challenging aspect was to build up a singular dedicated installation design for each of them, being each viaduct different from the other, in terms of structural
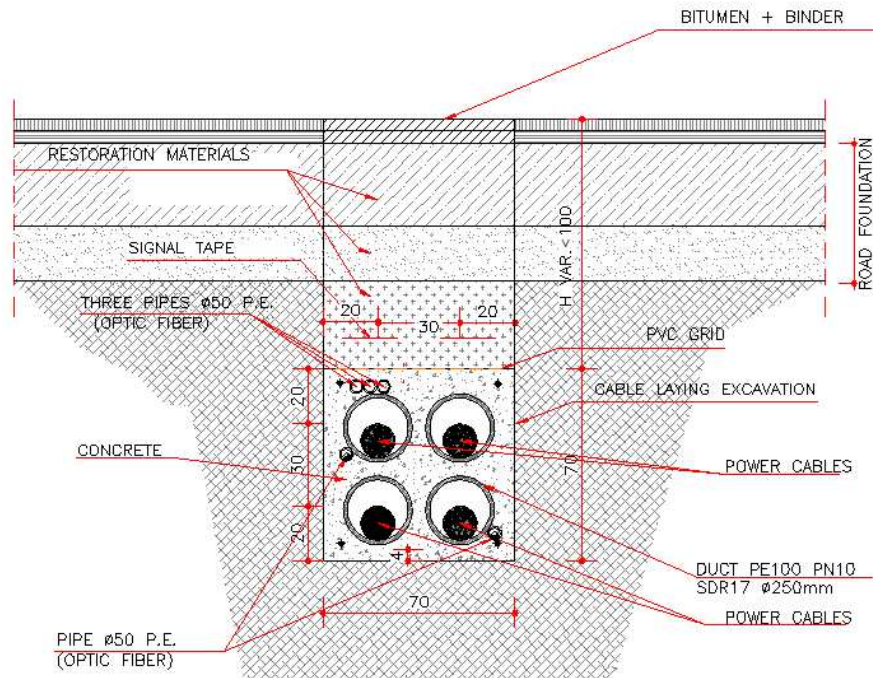
Figure 1.40: Cable laying in square formation
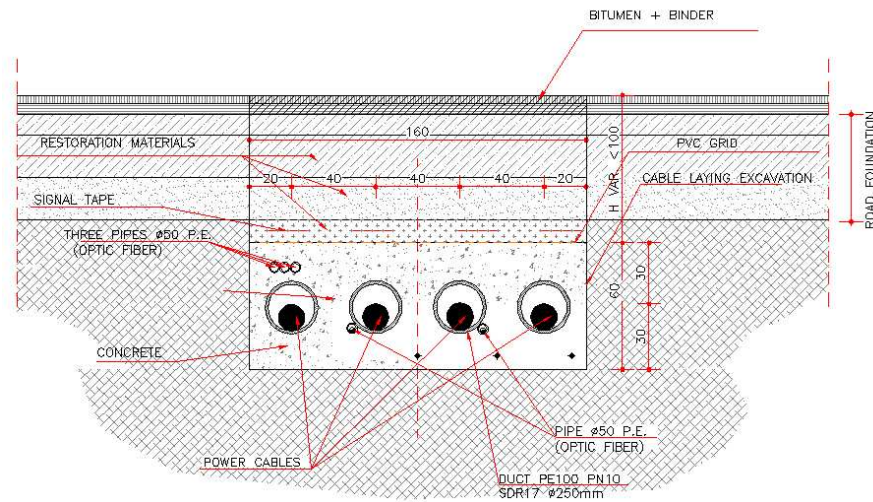
Figure 1.41: Cable laying in flat formation

characteristics, architectural design and thermo-mechanical (movements/expansions) features. For some viaducts it will be possible to install the cables inside

the viaduct structures, where accessible. In case it will be not, the cables and the relative clamps will be installed on the external wall of the viaducts, according to the structural characteristics of the viaduct itself, protected by a steel case.

Figure 1.42: Viaducts of the A32 Highway

During the preliminary phase of the project, the complete drawings and history of each viaduct was received from the highway operators: this information exchange allowed to group the viaducts into 4 different typological categories for which a preliminary installation design was developed. Dedicated carpentries and metallic

structures (see Figure 1.43 and 1.44) have been designed in order to bypass the joints of thermal/seismic expansion and to fulfil the static and dynamic load requirement of the viaduct structures (e.g. pantograph solution of Figure 1.43, increased sag and others). On that preliminary basis, a dedicated constructive design of the installation was than developed for each viaduct of the highway and the structures have been qualified.

The existent Frejus Tunnel crosses the French-Italian border. It is composed of a bidirectional traffic tube (one traffic lane per side) and a new gallery, running in parallel, is under construction at the time of writing. The new gallery will be linked to the Frejus Tunnel through bypasses between the two galleries about every 400 m (ca. 34 bypasses in total). The cross section area of the new Gallery is about 39,7 m² (with a circumference of 23,6 m). The cable system will be installed under the road pavement. The civil work structure of the links will cohabit with many other structures (LV and MV links, drains, multi-pipes, TLC systems, manholes, etc.) for the operation and maintenance of the new Gallery. Consequently, the available area for the cables is relatively small. The Franco-Italian border line is located at the middle of the gallery. The following topics, requested by the Frejus Security Committee, have been analysed on a provisional base by the Italian TSO and the French TSO with the "at that time" available data:

- thermal behaviour of the cables and influence of the thermal losses on the new Gallery air temperature;

- electromagnetic compatibility and interferences with other equipment;

- failure rate and fire risk assessment;

- repair and maintenance procedures.

The joint pits for the power cable junctions will be positioned about every 2000 m and will be 60 m long. Intermediate pulling pits will be also installed with a length of 15 m each, to ease the pulling strength. The power cables will be laid inside high density polyethylene (HDPE) pipes (6 pipes) with a 250 mm outer diameter - SDR 17, directly buried in a concrete bank in flat formation, below the road pavement. The concrete bank will also contain HDPE pipes with a 50 mm outer diameter SDR 11 where FO cables will be laid and a HDPE pipe with a 110 mm outer diameter SDR 13,6 for an eventual grounding cable. Two pipes are considered as spare pipes to be used in case of eventual repairing activities. Figure 1.45 gives the indicative general dimensions of the above-mentioned civil work structure. Inside the new Gallery two FO cables (2x48 fibres) dedicated to the TLC between Piossasco and Grande-Ile and two cables (2x24 fibres) for the distribute temperature monitoring system will be laid. The total number of FO cable splices shall be optimized in order to minimize their number. A FO cubicle

for jointing and pulling the FO cables, with a manhole for the access, has been foreseen around each 4 km inside the Gallery.

All testing activities, including those internal to the manufacturing cycle of the cable supplier, are planned, carried out and reported strictly in accordance with the requirements of UNI EN ISO 9001. The tests to be carried out are listed below:

- qualification tests of the power cable system;

- tests on laying and installation systems and tools;

- special tests – short circuit and analysis of chemical composition of developed gases;

- type tests of the Fibre Optics cables and accessories;

- calibration tests for the Thermal monitoring systems (DTS);

- factory acceptance tests (sample and routine tests) on all supplies;

- partial and final after laying tests;

- tests under load.

1.12.4   HVDC-VSC converter station

HVDC converters based on VSC technology allow the creation of an AC side voltage waveform consisting of small steps, which has an inherently low harmonic content obviating the need, in practice, for AC harmonic filters. The initial studies carried out by the supplier have shown that no ac filters are required for this project. Similar studies have also confirmed that no particular dc filters are needed. As reported in the preliminary layout shown in Figure 1.46, each converter station can be divided in three main parts:

- AC section: it mainly contains the AC switchyard composed by all the equipment required to connect the converter to the AC grid bay. All the apparatuses of this section are for outdoor application.

- Valve Hall: this building contains the valves of the converter and must have a controlled environment, i.e. the temperature and the humidity are controlled and the pollution is filtered.

- DC Hall: this building contains all the equipment in the section between the valves and the DC cables terminals (also to be placed indoor) and must have a controlled environment, i.e. the temperature and the humidity are controlled and the pollution is filtered.

Each converter terminal utilizes 6 half-link IGBT valves, with each valve having about 328 valve submodules, 18 of which are redundant. Each valve sub-module has two 3,3 kV 1500 A IGBTs, a dc capacitor, sub-module electronics and other ancillary equipment. The valve sub-modules are liquid-cooled by a dedicated cooling plant for each Converter Terminal (6 valves). The converter transformer has a sort of conventional AC substation design, consisting of a grounded star primary, a delta secondary and a delta tertiary windings. Each VSC pole is supplied via three 213/208/5 MVA single phase three windings ODAF type transformer. The 21 kV auxiliary winding serves as an alternative source for station auxiliary supplies under temporary conditions (e.g. black start), connected via a 21/15 kV step down medium voltage (MV) transformer.

1.12.5   Conclusions

With its route of about 190 km, mainly installed along highway roads and viaducts, it could represent a reference for the installation of future underground transmission lines, also considering its almost nihil territory impact.These aspects could also play a key role in the reinforcement projects for already developed transmission grids which need new energy corridors but have to face many territory constraints as well. This intertie also boasts another important feature: it is constituted of two independent multilevel HVDC-VSC systems with overall rated power equal to 1200 MW. This section describes the power system choices (type of cables, electrical and geometrical characteristics, converter station technologies) and chiefly the installation solutions (geometrical compatibility between cables and infrastructures) to allow the power cables to be hosted safely along the highways and inside the new Frejus Gallery (second tube). Some features of the converter stations are also presented.
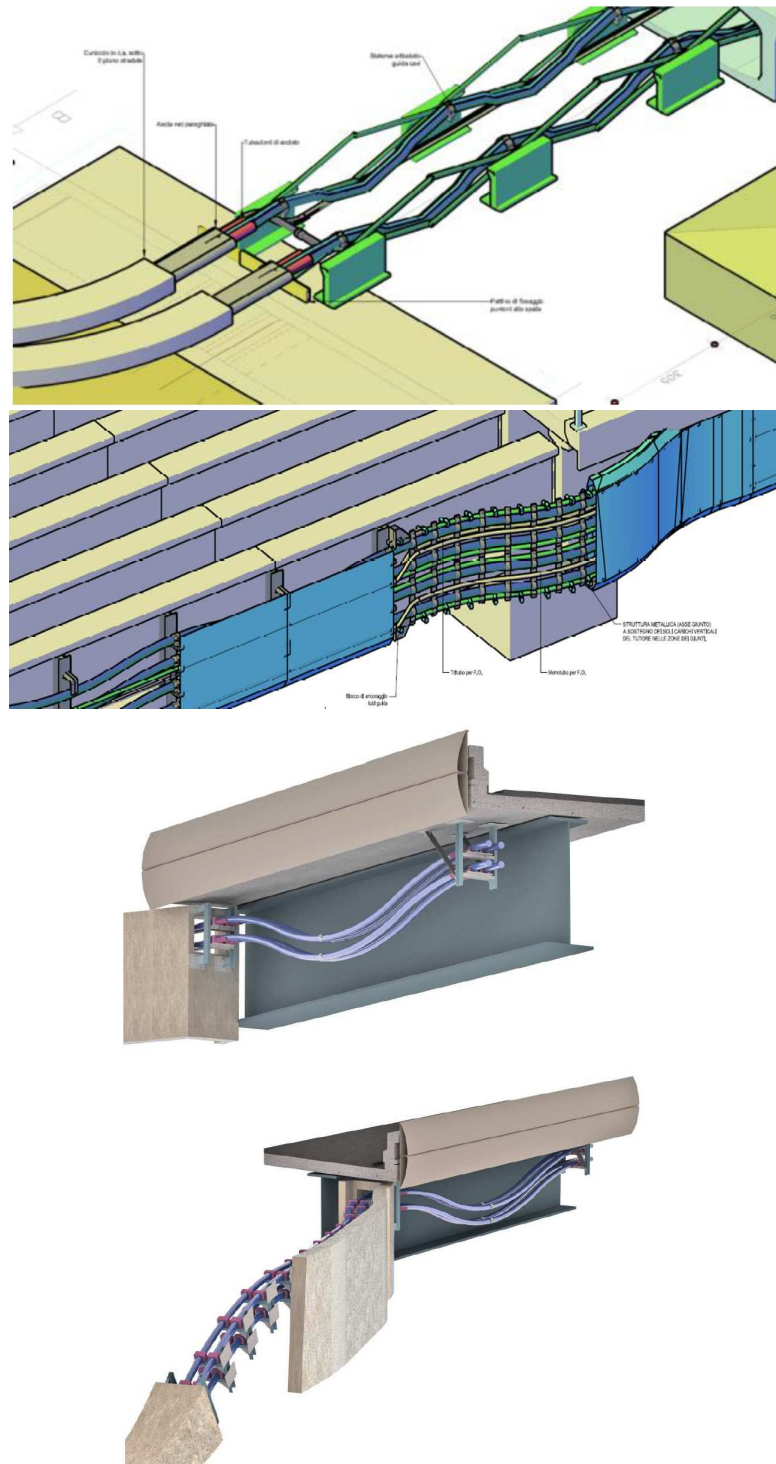
Figure 1.43: Pantograph for bypassing internally the viaducts expansion joints
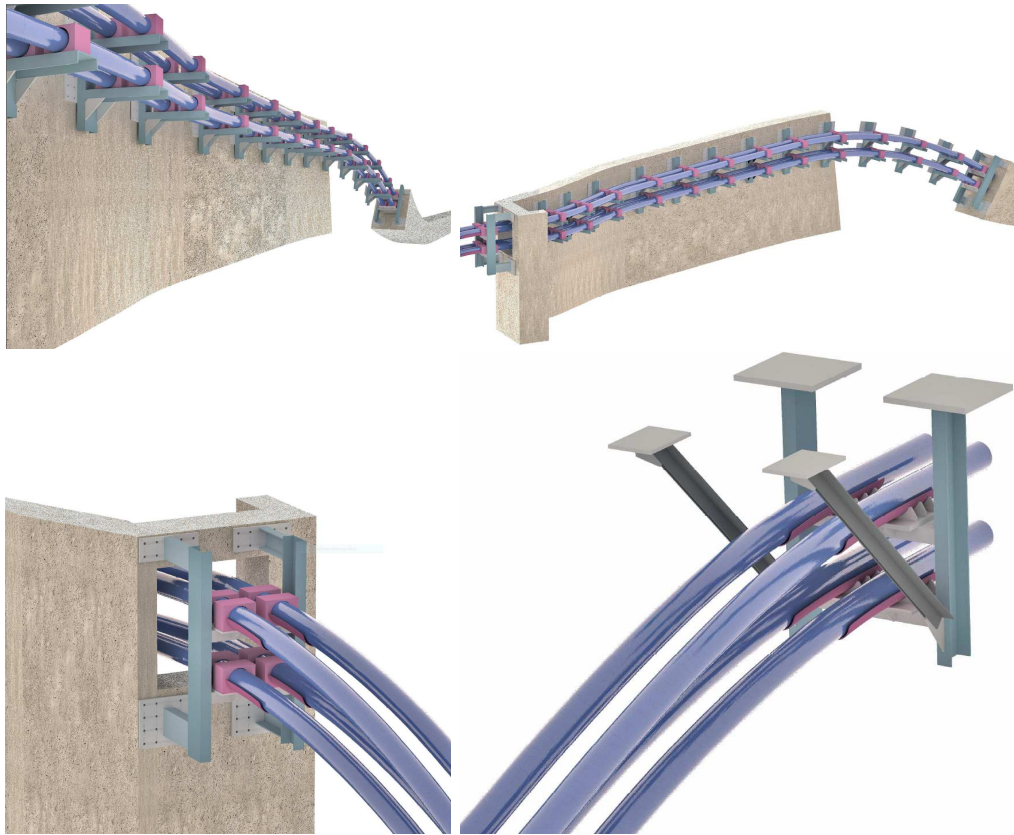
Figure 1.44: Dedicated carpentries and metallic structures
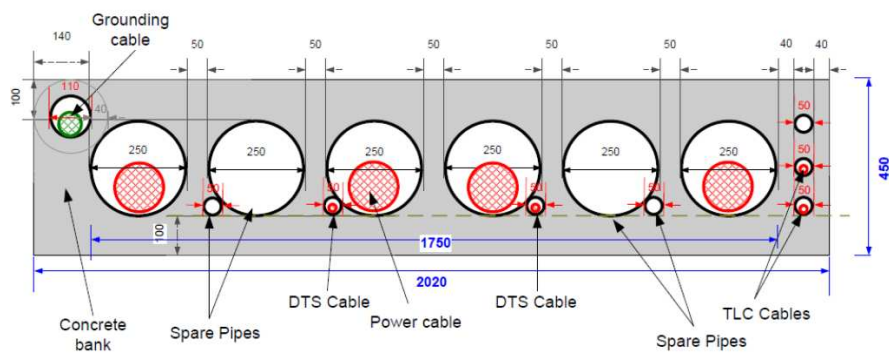
Figure 1.45: Section inside the new Frejus gallery

65
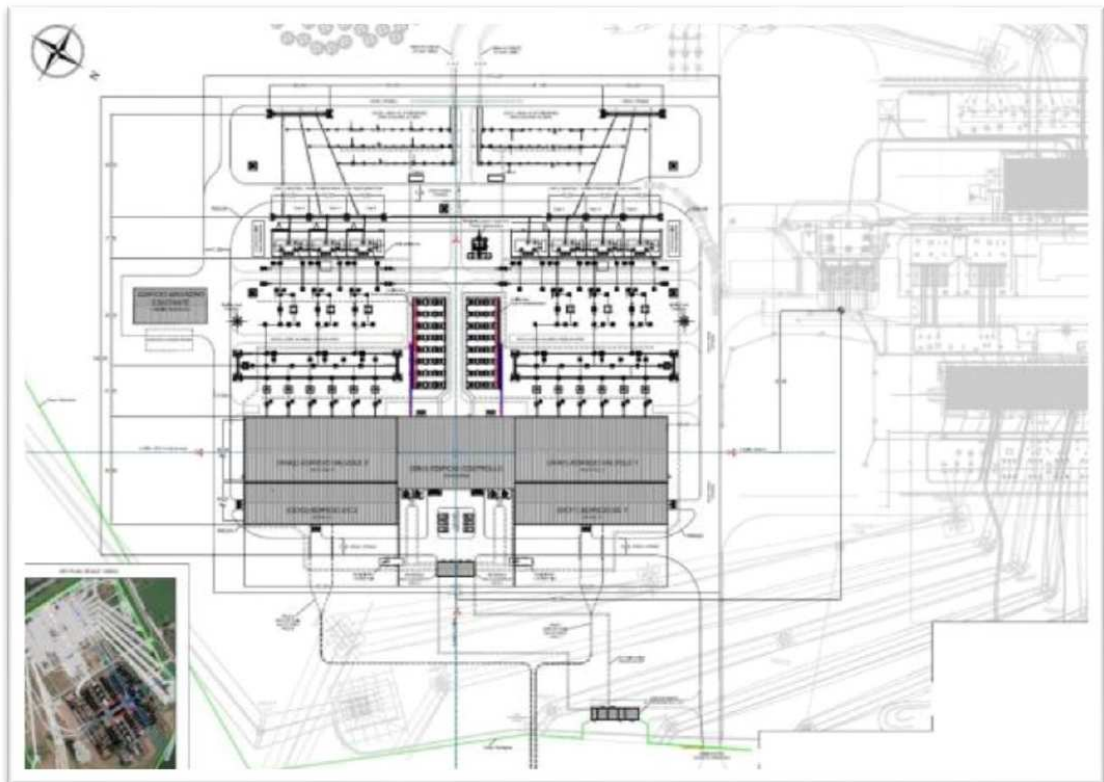
Figure 1.46: Layout of Piossasco converter station

1.13 HVDC Unsolved Issues: a Review

The following subparagraphs aim to be an accurate review of the state of the art of HVDC in order to highlight challenging research fields. With more and more HVDC projects turning into operation several emerging issues deserve strong attention. It is essential to focus on up-to-date problematics related to HVDC technology, in order to improve technical and economical features. The fundamental purpose of this paragraph is to develop a guide capable of giving an overview of main HVDC issues. This work is also a useful basis to steer future researches[10].

1.13.1 Introduction

In modern society, the sustainable development concept is faster growing in importance: the intensification in electrical energy production must comply with environmental issues. For this purpose, renewable energy (RE) power plants are taking off more frequently compared to the past. Furthermore, the increasing lack of territory resources narrows down the sites for power plant and brings the choice towards off-shore ones. In order to connect efficiently such RE power plants to the main grid, power cables are commissioned and two typical technical solutions are feasible: the HVAC connection or the HVDC one. Most of the transmission and distribution systems worldwide work with AC but, in recent years, thanks to the increasing in reliability of AC/DC converters, HVDC power transmission links have strongly increased [34, 35]. HVDC is nowadays used in applications where its technical and economic aspects give an advantage versus the AC solution, i.e. interconnections between asynchronous systems, or lack of reactive power compensation stations, which enable to achieve synergies between different technologies [16, 17, 27, 36]. However, HVDC links are based on relatively young technologies and a certain number of issues restrict installation possibilities (i.e. transient over voltage, fault management, harmonic content, pollution on insulators, etc. . .). Nevertheless, its reliability and technical features can greatly improve if properly supported by a massive research activity. The present paper aims to be an accurate review of the state of the art of HVDC in order to highlight challenging research fields.

1.13.2 Unsolved issues

HVDC interconnection lines are rather young transmission systems. The first plant, by ABB, was installed in Gotland in 1954. That installation worked with mercury-arc converter valves. In any case, the first modern HVDC interconnection is dated 1979 and is the Cahora Bassa one, in Africa. It was the first one with conductor voltage above 500 kV as well as among the first with thyristor converter valves [37, 38]. In these last 50 years a continuous improvement has been made,

but a high number of aspects need to be enhanced. In next sections, the main unsolved issues are described and the state of the art is illustrated, with the aim to set up a useful guide for future researches.

Pollution

An innovative evolution of HVDC transmission system consists in OHLs HVDC (see Figure 1.47). For such application, a main issue is the insulator design process. In fact, unlike the AC transmission systems, DC static fields make flashovers more problematic since a fault current arc does not present zero current states and its extinction becomes more complicate [39, 40]. It is well known that pollution deposit on insulator surfaces affects insulation properties in different ways: pollution degree, surface distribution and constituents can influence insulators withstand voltage. Insulator geometrical characteristics, such as surface layout and materials affect the flashover voltage as well. In recent years, the usage of polymeric composite materials as insulating, become a trend, especially for HVDC applications in areas characterized by heavy pollution conditions because of its higher insulation and mechanical properties compared to porcelain and glass materials [41]. A negative aspect of composite material consists in poor self-cleaning properties, worsened by the easier contaminant adsorption due to the constant electrostatic force: for this reasons, DC insulators are more exposed to contaminants, with a rate of 1.2-1.5 times higher than that of AC insulators under the same condition [42, 43]. An interesting aspect is the pollution deposit ratio T/B between the top surface and the bottom surface, which typically reaches values between 0.1 and 0.2 (0.005 under severe conditions). Works made for glass and porcelain insulators has shown how the withstand voltage reduces proportionally with the T/B ratio or, in other words, with the pollution level [44]. In recent years, Silicon Rubber (SiR) has been widely used because of its resistance against pollution compared to other materials. SiR insulators are typically dimensioned with 75% of the creepage distance normally required for equivalent insulators of other materials. Several studies have been made to improve the insulation characteristics: [45] shows how the influence of non-uniform pollution distribution can affect flashover performance. Despite the pollution flashover voltage gradients of SiR insulators [44] is superior to glass and porcelain insulator under DC conditions, in [46] is showed that DC flashover voltage of an ice covered SiR insulator improves decreasing the ratio between insulator leakage distance and height.

In [47] the SiR properties under fault conditions are calculated, in order to determine the electrical stress on each insulation component. In general, the pollution performance analysis can be evaluate through of an analytical process, by means

Figure 1.47: HVDC insulators

of the following:

$$U_f = a \cdot SDD^{-b} \tag{1.1}$$

where U_f is the flashover voltage, SDD the salt deposit density in mg/cm2, and a and b are respectively the surface pollution coefficient and characteristic exponent. Their values depends on the insulator types, materials, voltage types, etc. Besides, the designing process it is very different between HVAC and HVDC insulation in fact, while for the first case the switching impulse under rain conditions is the main dimensioning parameter, for HVDC case, the pollution deposit is the absolute dominant dimensioning parameter, as it is shown in Figure 1.48 [47]. In recent years, a certain number of goals has been reached, but more in-depth studies have to be done, in order to further improve the performance, i.e. studies on wind effect and non-homogeneous pollution layers characterized by heavy density or studies on insulators profile, to determine the best one could be of great interest for future works.
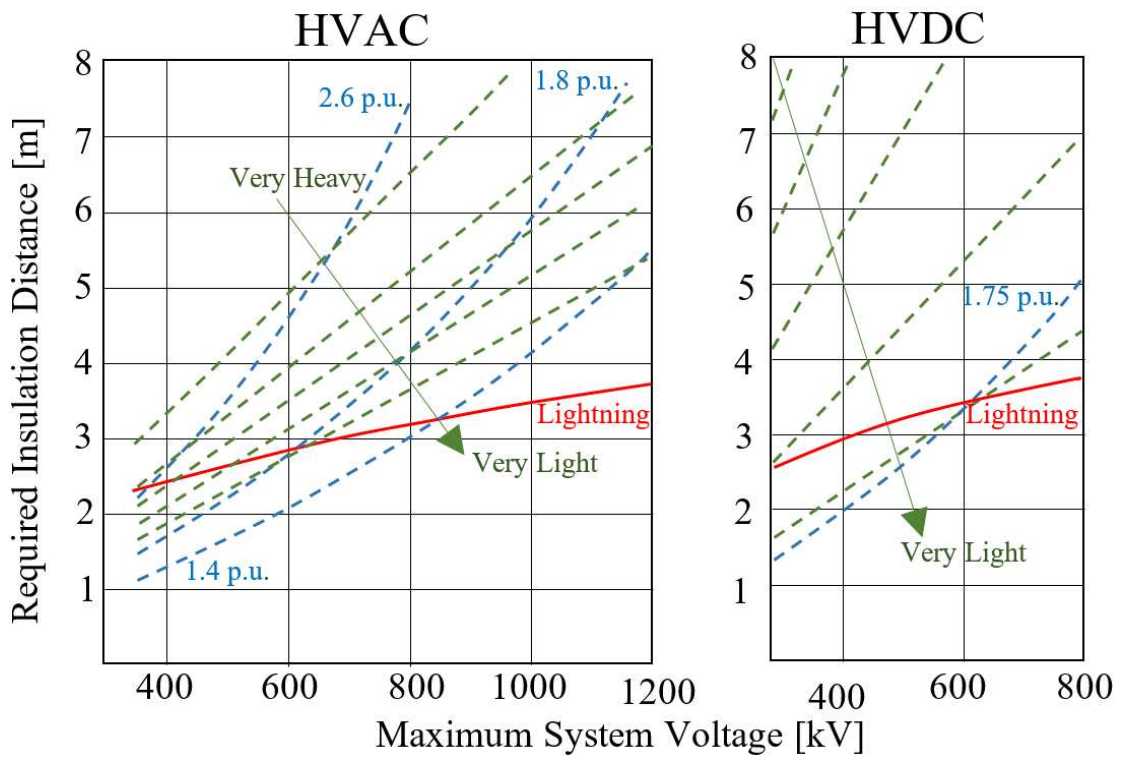
Figure 1.48: Illustration of indicative insulation distance requirements for HVAC and HVDC

Transient OverVoltage

Nowadays, modular multilevel converters (MMCs) are typically built in symmetrical monopole configuration, with no ground connection at any point of the circuit. This unavoidable choice is due to the application of the zero sequence harmonics over modulation of the converter bridge. Furthermore, in case of pole to ground fault, short circuit currents are negligible on converters. The ground reference point is performed by means of a high [48] impedance reactor or by utilizing a high impedance. Obviously, managing the neutral point of the system by means of a high or infinite impedance value has some drawbacks, in particular higher overvoltage are induced on the healthy pole in consequence of a single pole to ground fault and, during the fault occurrence, high and long DC voltage [49] stress arises on both the cable and the converter. The Transient Over Voltage (TOV) problem is of particular interest, because the insulation level of the power cable and the cost of the entire system depends upon such TOV values. However, such problem is known from a long period and it is due to the voltage redistribution along the line, starting from the fault point, and it is generally linked to the travelling waves phenomena. The transient voltages propagate in both directions to the remote end of line with the speed of the related travelling wave at certain characteristic impedance. Once the transient voltage has reached the line terminal, it is reflected backward and the phenomenon repeats itself until complete damping of the wave [50]. It is possible to have an idea of these phenomena by means of the lattice diagram of Figure 1.49
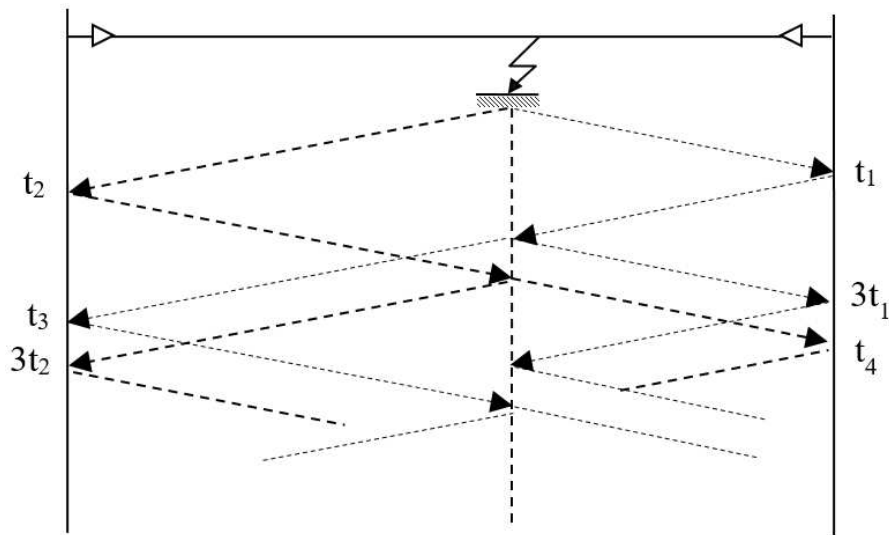
Figure 1.49: Time propagation of transient over voltages through the entire line

Every time the voltage waves reach the remote end of the line, the voltage rises,

until an asymptotic value, which depends chiefly on system characteristic, but typically varies in the range of 1.55 for 320 kV systems to almost 2.0 for 500 kV systems [48]. As a consequence of a single pole to ground fault on a DC line, an overvoltage is induced on the healthy pole [51]. This is undesirable, because a monopolar fault can evolve in a bipolar one, if the withstand insulation voltage is surpassed on the healthy pole. Nowadays, surge arresters (SAs) are used in order to limit ToVs. SA switching impulse protection level (SIPL) is generally higher than the expected TOV value, as a consequence SAs can be designed with an higher energy rating, to cope with temporary overvoltage, leading to an higher cost and footprint. However, the ratio between the SA SIPL and continuous operating voltage Udc, cannot be arbitrarily reduced, so that, SAs can only limit TOV value to about 1.5. The energy rating of the SAs is mainly dictated by the opening time of the AC breakers and the protection relays have to be evaluated in order to avoid thermal runaway [52]. The ToVs are one of the main issue in HVDC cable design because of many aspects that should be taken into account, for example:

- it is not known how TOVs can affect the behavior of DC and AC equipment and their aging;

- there is no agreement on the wave shape among involved parties and it is hard to reproduce them in laboratories, because it needs specific equipment and high cost for the single test.

It is possible to assess that cable systems are for sure the most stressed components by TOVs, insulations in particular due to preexisting space charges. Nevertheless, models describing system properties and aging are not present in literature and it is not possible to know how TOVs will affect different components. Moreover, it is unknown whether standardized wave shapes could be utilized in order to simulate the system behavior.

GIC and Harmonic losses

There is an interaction between space weather and Earth's magnetic field. In case of a solar storm, electro-jets are produced as consequence of coronal mass ejection and passes through the magnetosphere. At the ground level, electro-jets interact with the Earth's magnetic field with the production of an induced geo-electric field as result. The typical frequency of electric power system is 50 or 60 Hz, which is very high compared to geomagnetic variations (in the range of mHz). Whenever there is a flow of Geo-magnetically Induced Current through the converter transformers neutral, it affects the DC current as well [53, 54]. This topic should not be underestimated; in fact, in 1989 a geomagnetic storm caused the blackout of the hydro Quebec transmission system [55]. A certain number of undesired effects could be awarded to GIC current, in particular:

- significant harmonic currents and consequent mal-operation of protective relays;

- system instability;

- intensification in corrosion of pipeline steel;

- occurrence of DC bias and saturation of converter transformer cores to a great extent.

The harmful problem caused by GIC currents is that it generates a DC bias. When the DC bias starts to flow into the AC grid side, it could result in the production of low frequency oscillation due to possible parallel resonance and while the normal operations of converter transformers could change as well. If this phenomenon occurs, it results in the formation of a regenerative feedback between converter transformer and converter bridge. This gives a harmonic content increase; furthermore, the generated harmonics have low order (2nd harmonic) and this cause instability to the HVDC system[56, 57]. Nowadays, to reduce harmonics, the conventional methods consist in the installation of filters between the 3-phase AC source and the converter transformers. Typical filters are:

- active filters, which have the property to control its filtering characteristics;

- passive filters, more economical and effective than active ones;

- hybrid filters, a particular configuration of active filters [58].

Other options [15] could result in the use of current limiting resistors between grounding and converter transformer neutral point or in the connection of neutral series capacitor.

Reliability

At the present state, because of the improvement in the conversion station components, IGBT switching components in MMC are considerably increasing [59]. Furthermore, a high number of SMs is necessary in order to reduce the harmonic losses. While an additional quantity of SMs needs to be installed as redundancies, to guarantee uninterrupted operation between planned maintenances [60]. The main problem of IGBTs based converter station, consists in its high cost and due to this, it is necessary to choose a suitable number of operational and redundant elements, by taking into account the loss energy cost [61]. There are different redundancy schemes, each one ensuring different mean time to failure (see Figure 1.50), several studies on the best configuration have been made and nowadays and others are in progress [62]. The purpose of such studies consists in identifying the best redundancy scheme, which allows minimizing the converter station cost with no drawbacks on the operational lifecycle.
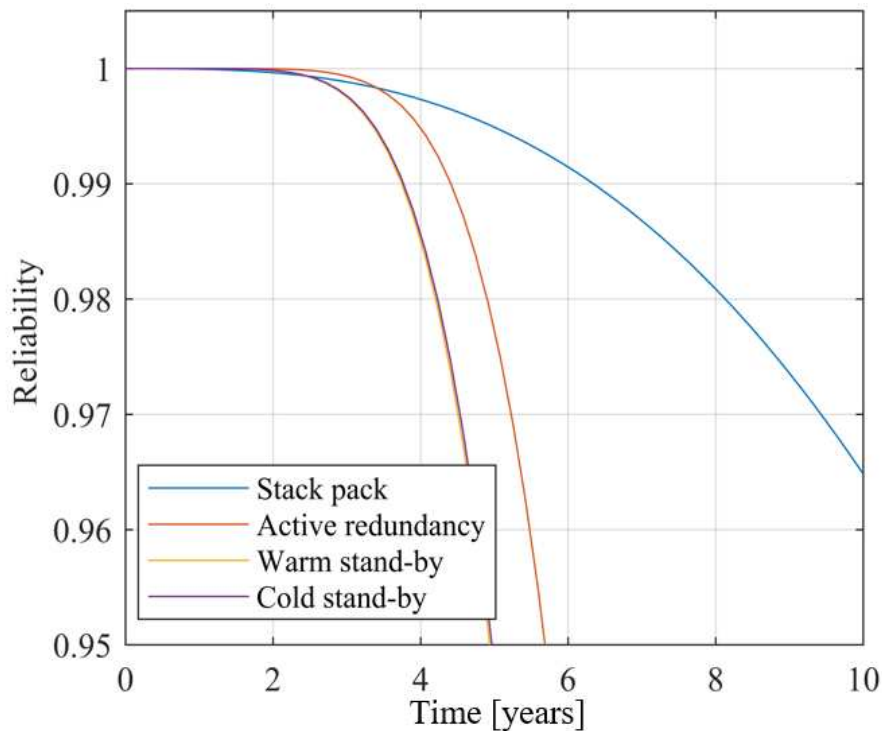
Figure 1.50: Example of how different redundancies schemes can affect the system behavior for a given redundancy rate and components number

DC Faults Management

In case of DC fault [63], VSC MMC FB is able to produce the rated AC waveform up to a complete reversal of the DC-Link voltage, thus providing DC fault blocking response. A full-bridge-based MMC is primarily designed with focus on reliability. In normal operation, the full-bridge submodules are modulated like half-bridge submodules, with only two of the switch valves operating at each moment. The main difference in operation appears in case of a DC fault. During a DC fault, a high overcurrent originates on the DC grid. As soon as a DC fault is detected, the AC side can be insulated from the DC side by inhibiting the control operation of the submodules. Once the control operation is blocked unlike the half-bridge submodules, which are bypassed by the antiparallel diodes of the IGBTs or the thyristors and continue feeding the fault, the full-bridge submodules are connected (see Figure 1.51).

In this case a DC fault current cannot circulate, as it is directed through the capacitors of the submodules, which are connected in series and in opposing polarity to the current direction. As the total series capacitor voltage is higher than
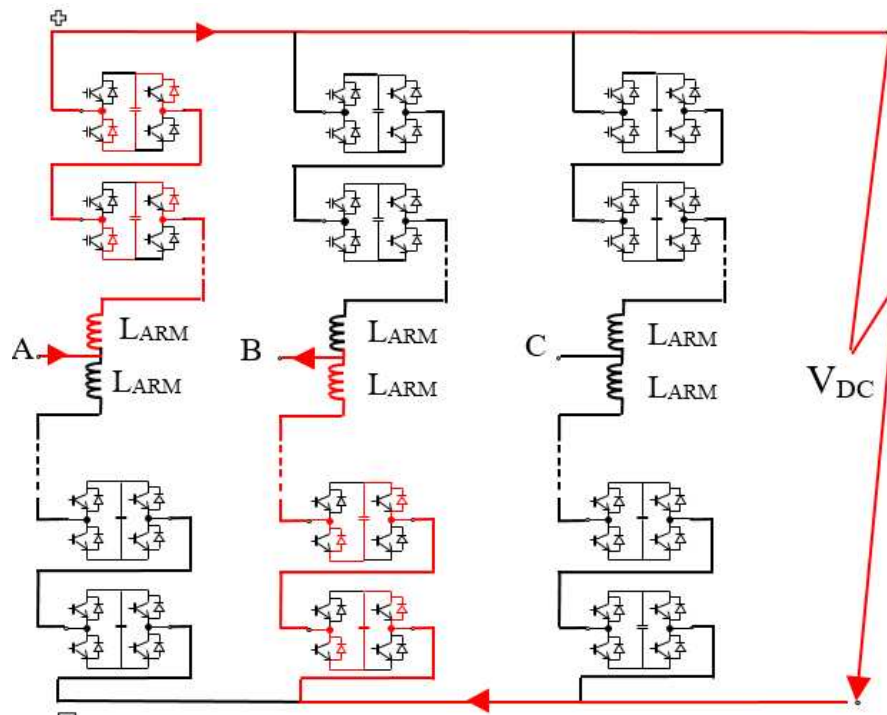
Figure 1.51: Full-bridge MMC in short-circuit DC fault

the peak line-to-line voltage of the AC grid, the current drops to zero. However, the disadvantage of this method is that controllability is lost and therefore, the MMC station cannot provide support to the AC side. It operates like a STATCOM when DC short circuit fault occurs and rides through the fault. The FB option offers a greater reliability at higher costs, larger volumes and higher conduction losses. However, in the point-to-point schemes utilizing overhead lines, the majority of faults is temporary. Hence, it is normally required to attempt several re-close operations before shutting down the scheme. Within a multi-terminal system, the faulted section of the network ought to be isolated so the healthy sections may continue to exchange energy. Application of the full-bridge converter, capable of blocking contribution from the AC side, can limit development of the fault current within the transient phase. For this reason, the use of the full bridge configuration is heavily used in overhead transmission lines, as it favors a higher reliability which is needed to control the fault current, thus avoiding the disruption. On the other hand, when cable lines are managed, full-bridge becomes useless and therefore the use of the half bridge, which is not able to block a fault, is sufficient.

1.13.3 Conclusions

The main characteristics of HVDC transmission systems are described and the main unsolved issues are reviewed in this work. VSC technology can be definitely considered superior to the LCC one in power control, flexibility and efficiency. Since this technology is very young, it is reasonable to expect a future efficiency and reliability enhancement, thanks to improvements in redundancies management. Nowadays, some studies already show great discoveries on insulation material characteristics and SAs. Because of the on-going development of the electric system focused on RE productions, future scenarios foresee a rapid increasing in HVDC interconnections worldwide. These will constitute electric energy corridors linking distant regions or nations. Moreover, it deserves to be mentioned that many wind and photovoltaic farms are connected to the grid onshore via a HVDC transmission system and a battery energy storage system is connected through a DC/DC converter to the DC-link of the HVDC system. Therefore, the development of reliable electrical models [64] of both the HVDC and the stationary storage systems is necessary to be able to analyze and foresee the behavior of the whole system.

Chapter 2

HVDC-VSC: electromagnetic transient analysis

This chapter describes in detail the electrical modeling of a symmetrical monopolar HVDC-VSC system, whose characteristics and topology have been explored in the previous chapter. The model considers an HVDC-VSC system in its entirety and without introducing simplifying hypotheses. In particular, the modeled elements are the conversion system with an attached control system and power transmission. The programming environment chosen is EMTP-RV, whose acronym stands for Electromagnetic Transient Program Restructured Version, widely used both in research and in the design phase of HVDC systems. Several European TSOs/DSOs such as RTE (Réseau de Transport d'Électricité) and EDF (Électricité de France) make extensive use of it. This choice depends on the fact that HVDC-VSC systems are characterized by particularly complex electromagnetic transients that need to be correctly represented. Therefore, it is necessary a programming environment designed to manage and model these transients, in which it is possible to correctly represent the variations as a function of the frequency of the characteristic parameters of the modeled electrical devices, primarily of the power cables. To fully understand the characteristics and potential of the electrical model developed, significant operating conditions were simulated, and the results obtained were included and commented on.

2.1 EMTP model for the Symmetrical Monopolar HVDC-VSC System analysis

This section examines the model developed in the EMTP-RV environment to represent the behavior of a symmetrical monopolar HVDC-VSC system in its totality and for each operating condition. Figure 2.1 shows the basic blocks making up the overall scheme of the model (see Appendix A.1 for the larger scheme with details highlighted).
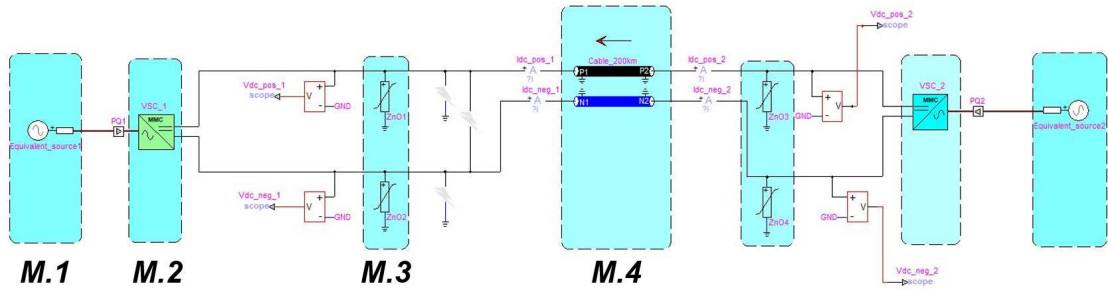
Figure 2.1: General block diagram of the model

The model consists of 4 fundamental macro groups which are repeated specularly with respect to the M4 block and which are:

1. the supply system that represents the network, upstream and downstream, of the HVDC link (M.1);

2. the VSC conversion and control system (M.2);

3. the system of surge arresters for protection against overvoltages (M.3);

4. the cable transmission system (M.4).

2.1.1   M.1 Supply system

The networks upstream and downstream of the HVDC connection are represented as a real equivalent voltage generator (see Figure 2.2, which can be modeled starting from the data shown in Table 2.1.
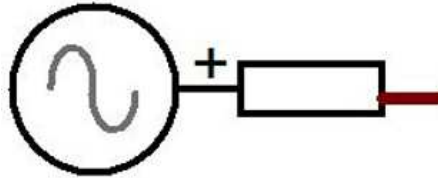
Figure 2.2: Equivalent generation system of the network upstream (or downstream) of the HVDC link

Table 2.1: Main parameters of the M.1 system

Frequency [Hz]	50
RMS Linte-to-Line Voltage [kV]	400
Short-circuit power [GVA]	10
R/L ratio	10

2.1.2 M.2 Converter station

The scheme of the model of a conversion station is shown in Figure 2.3 (see Appendix A.2 for the larger scheme showing the details).
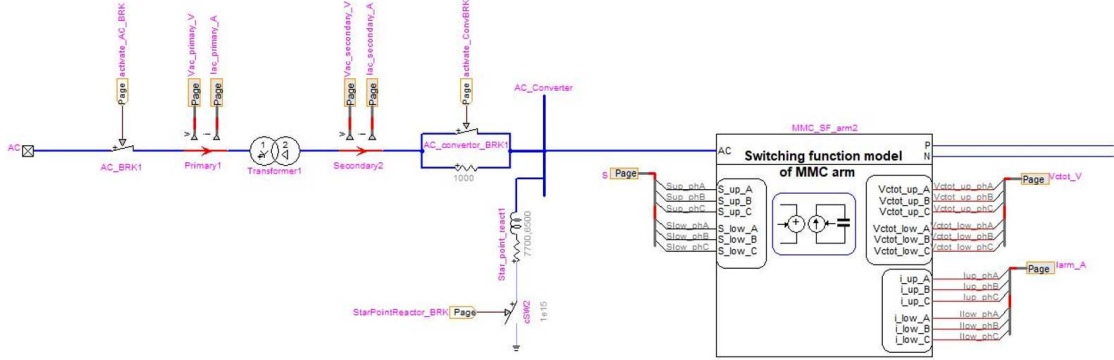
Figure 2.3: Converter station

It consists of the following components:

- a main switch used in case of disconnection of the station from the upstream AC grid;

- a YND conversion transformer;

- a pre-charge resistor necessary for the system start-up sequence;

- star-point reactors necessary for the direct current system reference; these impedances do not make any contribution to the short-circuit current;

- multilevel modular converter (MMC).

Conversion system

The modeling of the conversion system can be diversified on the basis of the type of study to be carried out. In particular, different types of modeling are available in EMTP-RV, illustrated in Figure 2.4, namely:

- Model 1: IGBTs modeled by non-linear resistances;

- Model 2: IGBTs modeled by switchable value resistors;

- Model 3: each converter arm is modeled using controlled voltage and current sources;

- Model 4: it consists of a very simplified model of the average value converter.
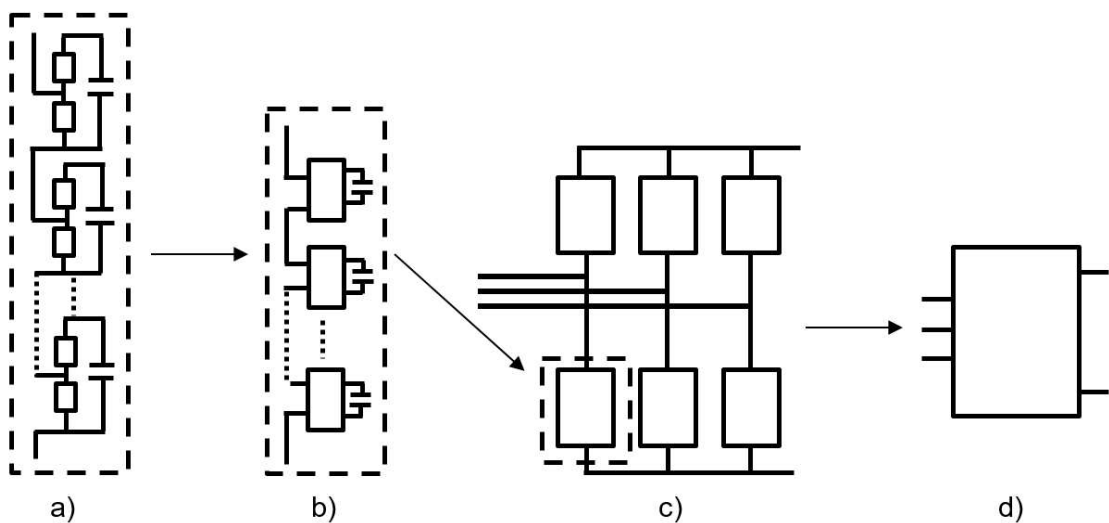
Figure 2.4: MMC converter models a) Model 1, b) Model 2, c) Model 3, d) Model 4

As regards this discussion, Model 3 (see Figure 2.5) was chosen because:

- allows to have a relatively low computational time;

- reduces the electrical connections to three nodes without losing information on the variables of the submodules;

- however, the drawback is the translation into "hard-coded" blocks. They cannot be modified or analyzed since they are written in Fortran code with the .dll extension.

To understand the representation of the conversion system, it is useful to describe the equations that govern its behavior. They can be derived starting from the
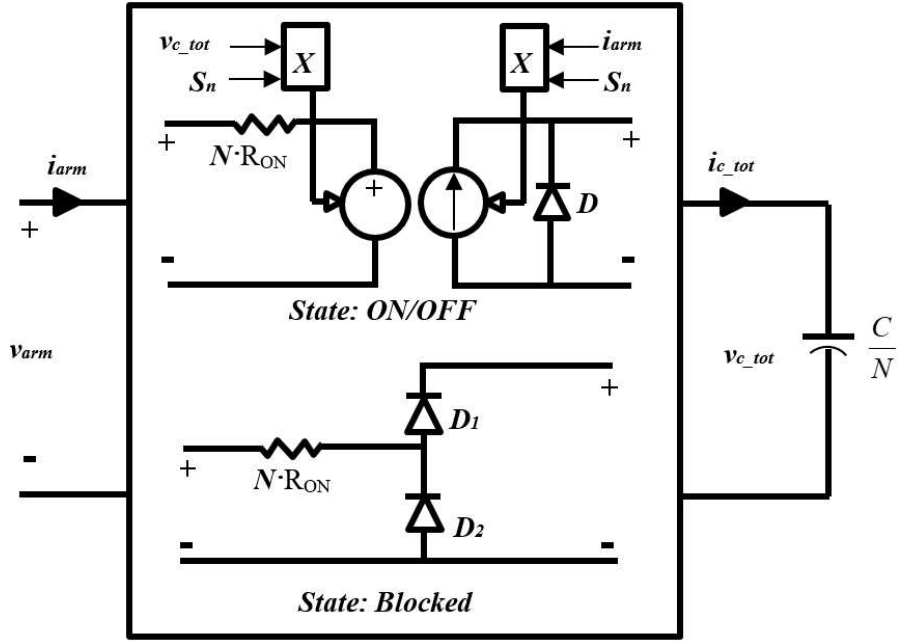
Figure 2.5: MMC converter: model 3

definition of switching function S:

$$
\begin{cases}
S_i = 1, & if \quad State : ON \\
S_i = 0, & if \quad State : OFF
\end{cases}
\tag{2.1}
$$

For each submodule we will therefore assume:

$$
\begin{aligned}
v_{SMi} &= S_i \cdot v_{Ci} \\
i_{Ci} &= S_i \cdot i_{arm}
\end{aligned}
\tag{2.2}
$$

Assuming the voltage of the capacitors on each arm constantly balanced, the average value of the voltage on the capacitors can be considered constant. Therefore the voltage on each capacitor can be defined as:

$$
v_{C1} = v_{C2} = ... = v_{Ci} = \frac{v_{Ctot}}{N}
\tag{2.3}
$$

where v_{Ctot} is the sum of the voltages on each capacitor belonging to a converter arm and N represents the number of submodules present in the arm. Now let's

82

define the sn switching function referred to a converter arm:

$$\frac{1}{N}\sum_{i=1}^{N}S_i = s_n \tag{2.4}$$

It is therefore possible to define, with reference to Figure 2.5, the total voltage to which a converter arm is subjected v_{arm} and the total current flowing through the equivalent capacitor of the converter arm i_{ctot}, taking into account the losses due to conduction through the internal resistance R_{ON}:

$$\begin{aligned} v_{arm} &= S_n \cdot v_{ctot} + (N \cdot R_{ON}) \cdot i_{arm} \\ i_{ctot} &= S_n \cdot i_{arm} \end{aligned} \tag{2.5}$$

The electrical configuration chosen for the submodules is the half bridge one which, as described in the previous chapter, does not allow voltage inversion. Therefore, in order to protect the component from negative voltages, a diode D is inserted in the antiparallel (see Figure 2.5). When all the submodules are in lockout state, each arm of the converter can be seen as a half diode bridge rectifier connected to the equivalent capacitor of the submodules. In Figure 2.6 it can be seen how the converter model is defined through equivalent submodules characterizing the equivalent operation of the N real submodules belonging to each arm of the converter and whose operation, from an electrical point of view, is linked to equations (2.1)-(2.5).
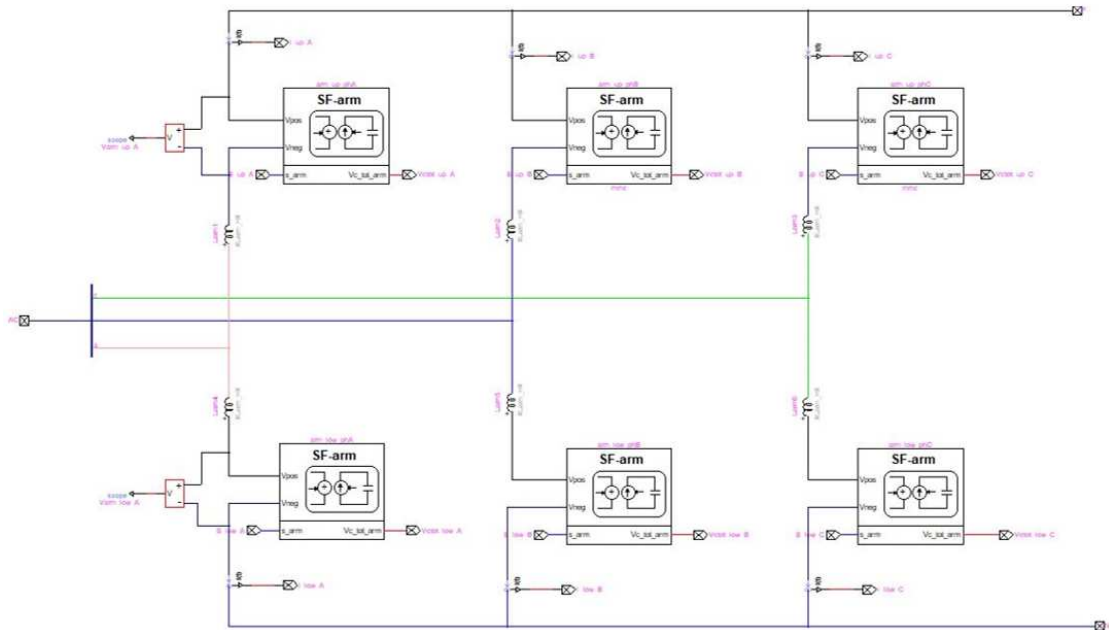
Figure 2.6: Circuit configuration of the modeled MMC converter

Control system

The operating principle of the VSC-MMC control system is based on the same operating principle of the synchronous machine (see Figure 2.7).
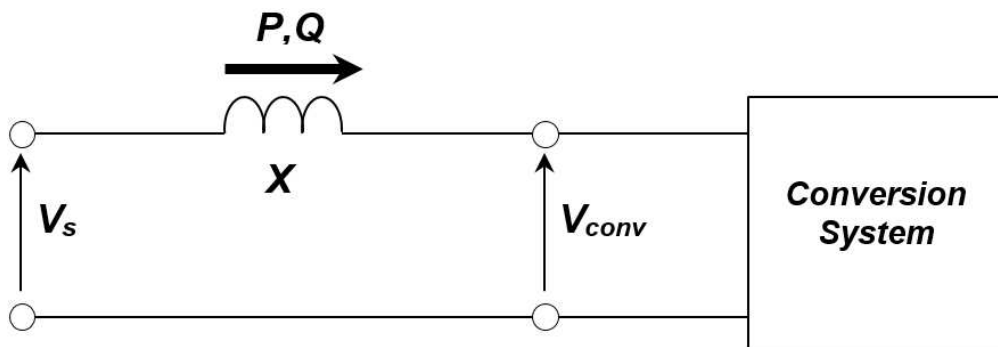
Figure 2.7: Operating principle of VSC converter

Neglecting the active losses, the electrical power transferred (active and reactive)

84

can be expressed as:

$$P = \frac{V_s \cdot V_{conv}}{X} \cdot \sin \delta$$
$$Q = \frac{V_s \cdot V_{conv}}{X} \cdot \cos \delta - \frac{V_{conv}^2}{X}$$

(2.6)

where: V_s is the grid voltage, V_{conv} is the voltage on the AC side of the converter, X is the inductive reactance present between the mains source and the converter, δ the phase shift angle between the voltage V_s and V_{conv}.

For small variations of δ it is permissible to write:

$$P \simeq \frac{V_s \cdot V_{conv}}{X} \cdot \delta \qquad\qquad \Rightarrow \quad P = f(\delta)$$
$$Q \simeq \frac{V_s \cdot V_{conv}}{X} \cdot - \frac{V_{conv}^2}{X} = \frac{V_{conv} \cdot (V_s - V_{conv})}{X} \quad \Rightarrow \quad Q = f(V_{conv})$$

(2.7)

By linearizing the equations relating to the power balance, it can be observed how the control of the active and reactive power can be decoupled, independently controlling the angle δ in the case of the active power and the voltage of the V_{conv} converter for the reactive power. It should be noted that, as it is easy to guess, the actual control adopted by the converter is much more complex, but we wanted to give a first basis that makes us understand the overall logic.

Control logic analysis

The general scheme illustrating the structure of the control system is the following:

The total control is divided into two subgroups:

- low-level control;

- high-level control;

Low-Level control

The low-level control is applied to each arm independently and consists of:

- Circulating Current Suppression Control (CCSC);

- Nearest Level Control (NLC) modulation;

- Capacitor Balancing Algorithm (CBA).
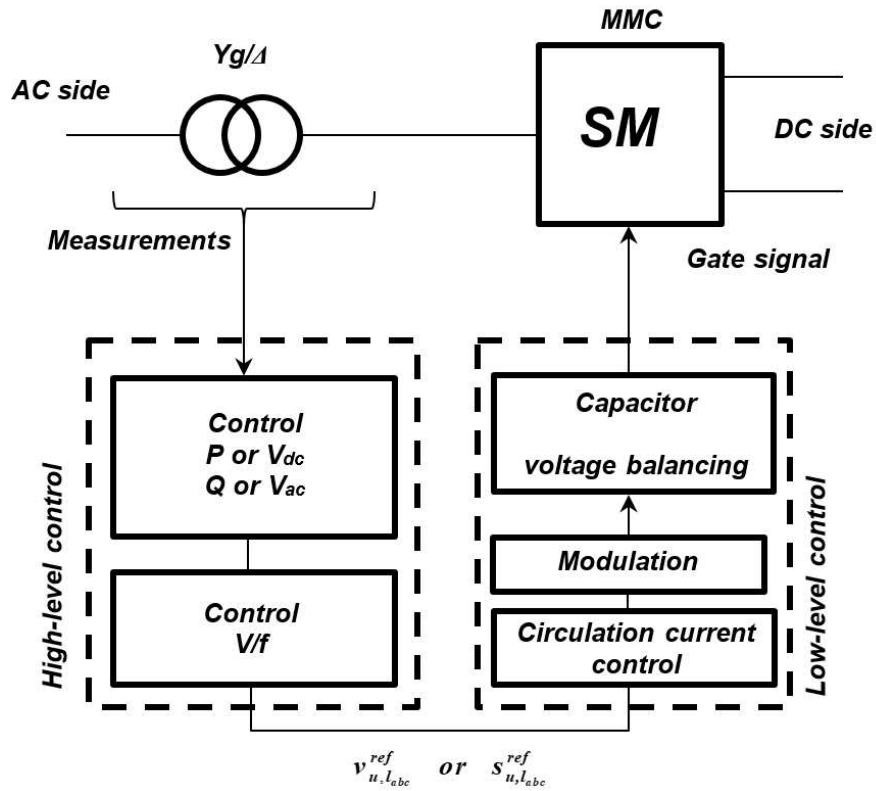
Figure 2.8: Basic structure related to the control logic

Circulating Current Suppression Control
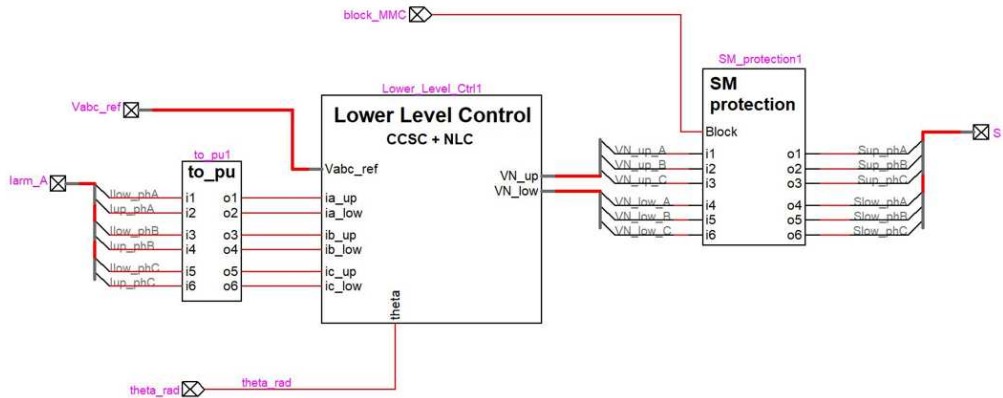
Figure 2.9: Low-level control with sub-module protection

The voltage imbalances between the phases of the MMC converter arms introduce

a circulating current with a 2nd order harmonic component which not only creates a distortion of the current in the arms but increases the voltage ripple on the capacitance of the submodules. This circulation current can be eliminated by introducing resonant filters (capacitance in parallel) in the node present in each phase that divides the inductances of the upper and lower arms or by using an active control on the AC side voltage v_{abc}^{ref}. The system used in the model is the active control as it constantly adapts according to the value of the variables to be controlled.

This active control is derived from the following equations, which express the voltage on the converter side as a function of the voltages on the inductor and on the resistance of the converter arm in relation to the second harmonic (which is the one to be suppressed) in the reference system d-q:

$$\begin{cases} -v_{conv2h,d} = Larm \cdot \frac{di_{2hd}}{dt} - 2\omega L_{arm} i_{2hq} + R_{arm} i_{2hd} \\ -v_{conv2h,q} = Larm \cdot \frac{di_{2hq}}{dt} - 2\omega L_{arm} i_{2hq} + R_{arm} i_{2hd} \end{cases} \tag{2.8}$$

where $C_{1,2}$(s) are the PI controllers mentioned above.
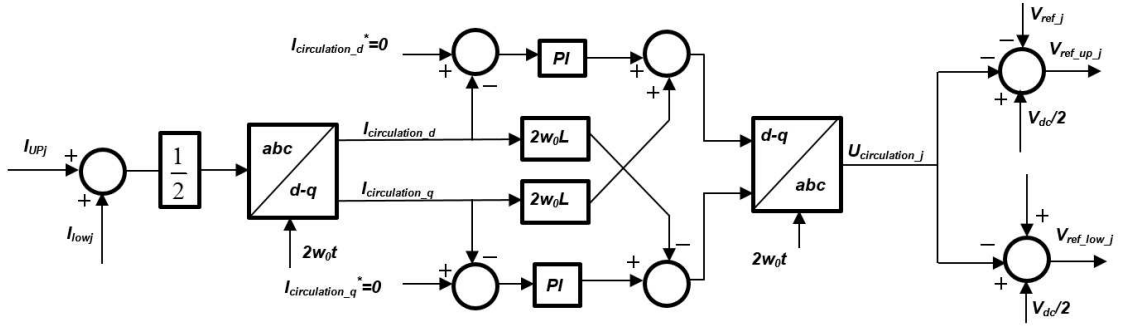
Figure 2.10: "Active" CCSC control system

Modulation

There are several types of modulation techniques that are applicable to the MMC converter, including:

- Nearest Level Control (NLC);

- Phase Disposition PWM (PD-PWM);

- Phase Shift PWM (PS-PWM);

- SHE (Selective Harmonic Elimination method);

- Space-Vector Modulation (SV-PWM);

The model uses the NLC technique.

Capacitor Balancing Control (CBA)

The purpose of this check is to keep the voltage across the capacitors as close as possible to the average value. To achieve this, the voltage across the capacitor must be constantly monitored and adjusted (increasing or decreasing it) based on a balancing voltage algorithm (BCA).

Sub-modules Protection
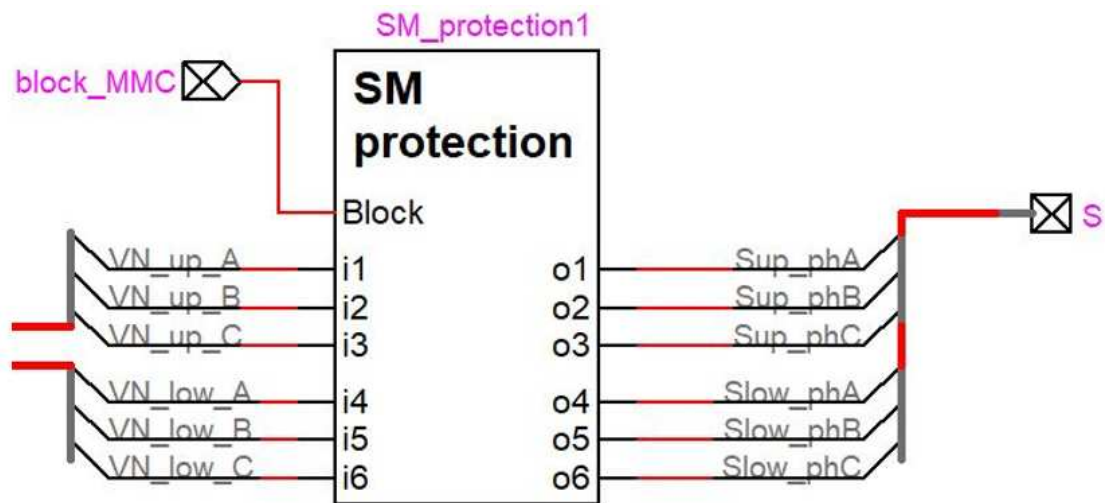
Figure 2.11: Sub-module protection system

The protection system consists of:

- direct current overcurrent detector;

- voltage detector in the event of a deep drop in the same voltage.

When the current, direct side, exceeds the maximum value set in the main settings, the converter station activates the following procedure:

1. the MMC converter is blocked;

2. the main switch, alternating side, is opened.

88
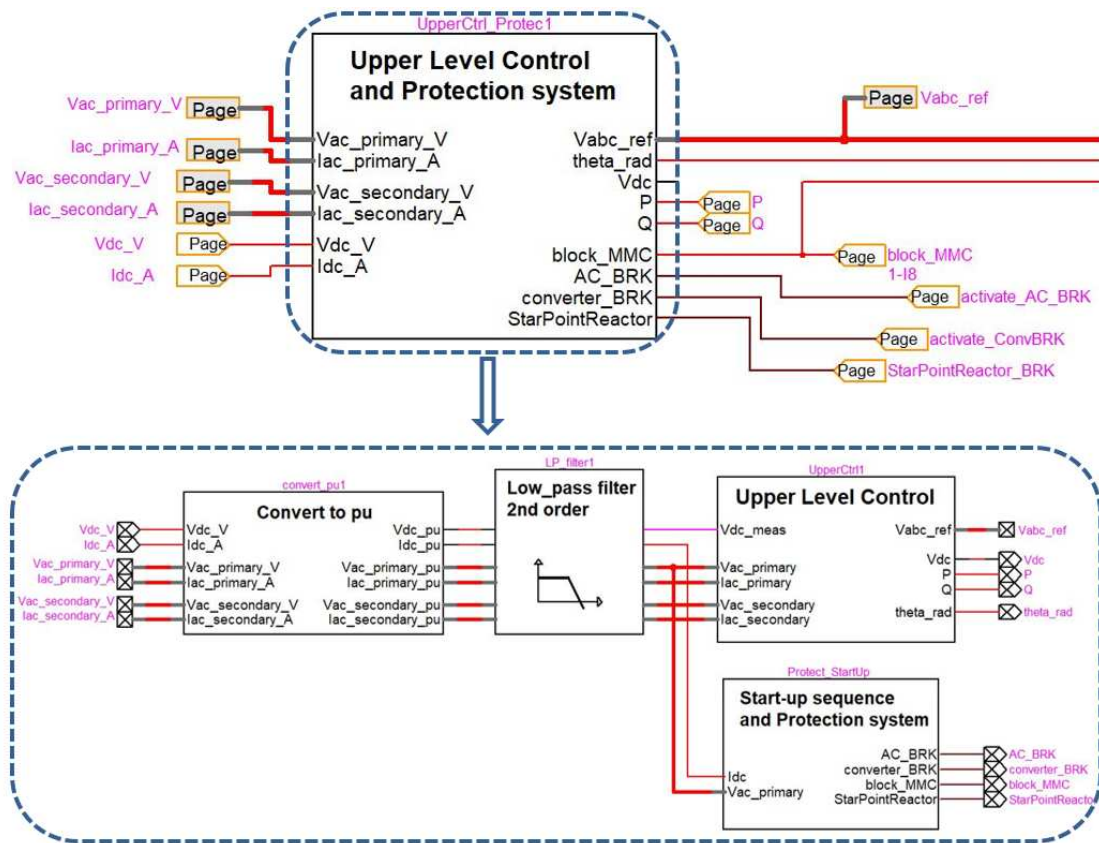
Figure 2.12: High-level control: general scheme

High-Level control

The basic elements that globally represent high-level control (see Figure 2.12) are the following:

- a second order low pass filter, to eliminate the high frequency harmonics coming from the measured inputs;

- the "core" of high-level control whose subsystems provide most of the ancillary services necessary for the correct functioning of the transmission system;

- a system that simulates the start-up sequence of the converter and its protection.

For the understanding of high-level control we must refer to the theory of "space vectors". The fundamental notions of this theory will therefore be highlighted below, without pretending to give an exhaustive treatment but only highlighting the main aspects.

89

In general, the space vector is a symbolic mathematical tool that allow the study of to study the behavior, even dynamic, of three-phase systems by applying a transformation to the quantities involved that allows to significantly simplify the equations that describe the behavior of the system. Therefore, given a generic tern of voltages u_a, u_b, u_c the associated space vector is:

$$\bar{\mathbf{u}} = \frac{2}{3}[u_a(t) + u_b(t) \cdot \exp\left(j\frac{2\pi}{3}\right) + u_c(t) \cdot \exp\left(j\frac{4\pi}{3}\right)] \tag{2.9}$$

that in a complex plane with real axis α and imaginary axis β represents a vector of modulus and phase that are generically variable over time. In the presence of an unbalanced triad of tensions, the homopolar component of non-zero value will be expressed as:

$$u_0(t) = \frac{u_a(t) + u_b(t) + u_c(t)}{3} \tag{2.10}$$

In general it can therefore be stated that any triple $u_a(t)$ $u_b(t)$ $u_c(t)$ can be transformed into the triad $u_0(t)$, $u_\alpha(t)$, $u_\beta(t)$ by means of the transformation:

$$\begin{cases} u_0(t) = \frac{u_a(t) + u_b(t) + u_c(t)}{3} \\ u_\alpha(t) = \frac{2}{3}[u_a(t) - \frac{u_b(t)}{2} - \frac{u_c(t)}{2}] \\ u_\beta(t) = \frac{1}{\sqrt{3}}[u_b(t) - u_c(t)] \end{cases} \tag{2.11}$$

It is therefore possible to compactly express the transformations from a coordinate system abc to $\alpha\beta 0$ through the matrix notation:

$$\bar{\mathbf{u}}_{\alpha\beta\mathbf{0}} = \bar{\mathbf{T}}_{\mathbf{abc}\rightarrow\alpha\beta\mathbf{0}}\bar{\mathbf{u}}_{\mathbf{abc}} \tag{2.12}$$

where the transformation matrix $\bar{\mathbf{T}}_{\mathbf{abc}\rightarrow\alpha\beta\mathbf{0}}$ equals:

$$\bar{\mathbf{T}}_{\mathbf{abc}\rightarrow\alpha\beta\mathbf{0}} = \frac{2}{3}\begin{bmatrix} 1 & -\frac{1}{2} & -\frac{1}{2} \\ 0 & \frac{\sqrt{3}}{2} & -\frac{\sqrt{3}}{2} \\ \frac{1}{2} & \frac{1}{2} & \frac{1}{2} \end{bmatrix} \tag{2.13}$$

The space vector $\bar{\mathbf{u}} = u_a + ju_b$ associated with the generic triad (a b c) can be expressed according to an orthogonal reference system d-q rotating with angular velocity $\omega_{dq}(t)$ with respect to the stationary system $\alpha\beta$ considered. In the

90

new rotating reference d-q we can then define the generic triad expressed in the coordinates $\alpha\beta$ 0 as:

$$\bar{\mathbf{u}}_{\mathbf{dq}} = \bar{\mathbf{u}}_{\alpha\beta\mathbf{0}} \exp\left(-j\omega t\right) \tag{2.14}$$

The transformation matrix from system $(\alpha\beta 0)$ to system (d q 0) assumes the following expression:

$$\bar{\mathbf{T}}_{\alpha\beta\mathbf{0}\to\mathbf{abc}} = \begin{bmatrix} \cos\omega t & -\sin\omega t & 0 \\ \sin\omega t & \cos\omega t & 0 \\ 0 & 0 & 1 \end{bmatrix} \tag{2.15}$$

While the complete transformation matrix from system (a b c) to the rotating system (d q 0) is:

$$\bar{\mathbf{T}}_{\mathbf{abc}\to\mathbf{dq0}} = \begin{bmatrix} \cos\omega t & \cos\omega t - \frac{2\pi}{3} & \cos\omega t - \frac{4\pi}{3} \\ -\sin\omega t & -\sin\omega t - \frac{2\pi}{3} & -\sin\omega t - \frac{4\pi}{3} \\ \frac{1}{2} & \frac{1}{2} & \frac{1}{2} \end{bmatrix} \tag{2.16}$$

If we make the spatial vectors, defined in the rotating reference system dq at the pulsation ω_{dq}, synchronous with the power supply triad, thus setting $\omega_{dq} = \omega_{grid}$, the whole control system will follow some references that in the triad abc would be rotating, but that defined in the new dq system make the signal to be followed practically a constant, with a consequent reduction of problems related to the control itself. as a direct consequence, the use of transformation matrices starts from the knowledge of the phase angle (or pulsation) of the network, this parameter is obtained through the use of a PLL. Ultimately, the use of transformation matrices leads to the definition in the dq coordinates of the following parameters used in the model, for mains currents and voltages:

$$\begin{cases} \bar{\mathbf{i}}_{\mathbf{dq}} = \bar{\mathbf{T}}_{\mathbf{abc}\to\mathbf{dq0}} \cdot \bar{\mathbf{i}}_{\mathbf{abc}} \\ \bar{\mathbf{v}}_{\mathbf{dq}} = \bar{\mathbf{T}}_{\mathbf{abc}\to\mathbf{dq0}} \cdot \bar{\mathbf{v}}_{\mathbf{abc,grid}} \end{cases} \tag{2.17}$$

The active and reactive power and the mains voltage (AC side) are given by:

$$\begin{cases} P = v_d i_d + v_q i_q \\ Q = v_q i_q + v_d i_q \\ v_{grid} = \sqrt{v_d^2 + v_q^2} \end{cases} \tag{2.18}$$

91

To better identify the type of control adopted by the converter, the EMTP-RV interface associates a type of control with the color of the MMC block according to the following scheme:
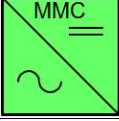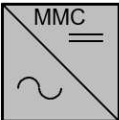
MMC CONTROL	COLORING ASSIGNED
ACTIVE POWER CONTROL **(P-Control)**	
DC VOLTAGE CONTROL **(Vdc-Control)**	
ACTIVE POWER DROOP CONTROL **/ DC VOLTAGE CONTROL** **(P/Vdc Droop Control)**	
AC VOLTAGE AND FREQUENCY **CONTROL** **(V/F Control)**	

Figure 2.13: Control type-color association in the EMTP-RV model

MMC converter control types

The different types of control of the MMC converter listed above will be analyzed below. Assuming that the reference system d q is synchronous with the network, therefore the rotating vector representing the network voltage is aligned to the axis d, there will be $V_q = 0$ and V_d coinciding with the module of the network phasor; in this situation the equations (2.18) are simplified:

$$\begin{cases} P = v_d i_d \\ Q = -v_d i_q \\ v_{grid} = v_d \end{cases} \tag{2.19}$$

The following diagram gives an overview of the controls that will be described:

1. **Power active control (P-Control)**

   With reference to the system of equations (2.19), it is noted that the control of the active power is fundamentally linked to the control of the d-axis current.
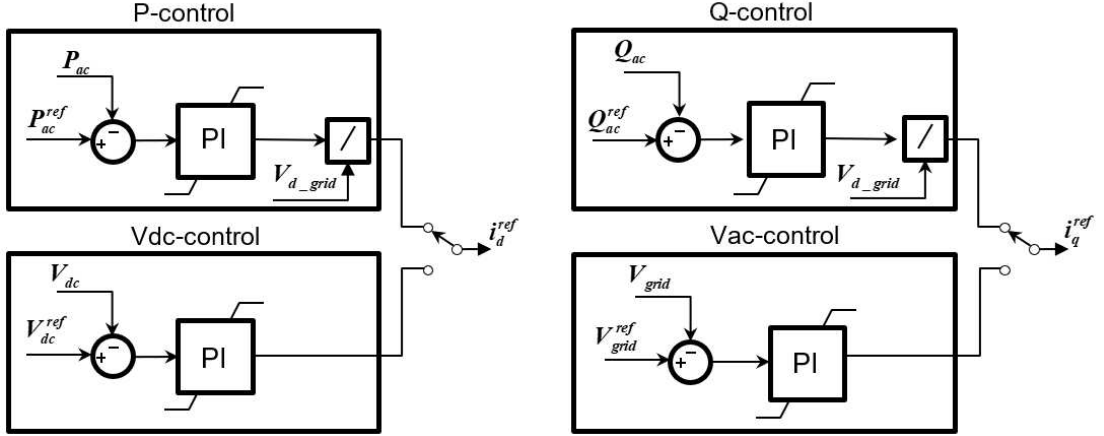
Figure 2.14: General diagram of the different types of MMC control

This control is obtained by using a PI type controller that will follow the active power reference by regulating the d axis current (see Figure 2.14):

$$i_d^{ref} = \frac{1}{v_d}(k_p + \frac{k_i}{s})(P_{ref} - P) \qquad (2.20)$$

2. **DC voltage control (V_{dc}-Control)**

Referring to the average value model of the MMC converter [2-3] and to the equivalent capacitor of Figure 2.5, and also assuming that the energy stored by the L_{arm} inductor, present in each arm of the MMC, is negligible, we can define the current in the equivalent capacitor as:

$$C_{dc}\frac{dV_{dc}}{dt} = i_d - I_{dc} \qquad (2.21)$$

By linearizing the equation and using a PI control it is possible to write:

$$i_d^{ref} = (k_p + \frac{k_i}{s})(V_{dc}^{ref} - V_{dc}) \qquad (2.22)$$

The PI type controller will follow the voltage reference going to regulate the d axis current.

3. **Reactive Power Control (Q-Control)**

With reference to equations (2.19), it is noted that the control of the reactive power is fundamentally linked to the control of the q axis current. This control

is obtained by using a PI-type controller that will follow the active power reference by regulating the q axis current:

$$i_q^{ref} = -(\frac{1}{v_d})(\frac{k_i}{s})(Q_{ref} - Q) \tag{2.23}$$

4. **AC side voltage control (V_{ac}-Control)**

With reference to equations (2.19), it can be seen that the control of the mains voltage is fundamentally linked to the control of the q axis current, by the following equations:

$$\Delta v_s = v_{conv} - v_s \approx \frac{X \cdot Q}{v_s} \tag{2.24}$$

Since the network voltage vs is aligned with the axis d of the reference system dq, this requires that:

$$\begin{cases} v_d = V_s \\ v_q = 0 \end{cases} \tag{2.25}$$

By combining (2.24) with (2.19) and (2.25), it results:

$$i_q^{ref} = (\frac{k_i}{s})(V_{ref} - V_s) \tag{2.26}$$

5. **Active power and DC voltage droop control (P/Vdc Droop Control)**

The DC side voltage droop control is very similar to that used for voltage control, always on the DC side. As regards the AC side, please note that the relationship between frequency and active power is expressed by the coefficient K, the regulating energy of the grid considered:

$$\begin{cases} P_{ref}^{tot} = K(freq, P) \cdot (f_{ref} - f_{station1}) \\ P_{ref}^{tot} = K(freq, P) \cdot (f_{ref} - f_{station2}) \end{cases} \tag{2.27}$$

Differently, for the DC side the relationship is between DC side voltage and active power through the K_{droop} coefficient which takes into account the voltage drop with respect to the active power:

$$K_{droop} = \frac{\Delta V_{dc}}{\Delta P_{ref}} \tag{2.28}$$

6. **Voltage-frequency control (Vac/f Control)**

This control is used when the MMC converter is connected to a passive network (or load) or with asynchronous generation (eg. induction motors) or with connection of wind turbines. From a functional point of view, one of the main differences between this type of control and the non-isolated one is the origin of the angular reference. In non-isolated control, the angular reference comes from the PLL, while in isolated operation the angular reference is generated by an internal oscillator. The mains voltage is regulated through a PI controller according to the law:

$$\Delta v_s = (k_p + \frac{k_i}{s})(v_{ref} - v_s) \qquad (2.29)$$

Assuming again that the voltage vs is aligned with the axis d of the reference system d q we can deduce:

$$\begin{cases} v_d^{ref} = (v_{ref} + \Delta v_s) \\ v_d^{ref} = 0 \end{cases} \qquad (2.30)$$

where v_{ref} is the nominal reference voltage.

2.1.3   M.3 Surge arresters
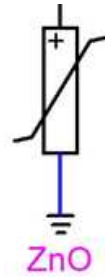
Figure 2.15: Metal oxide surge arrester

Faults occurring on the DC side, on the cable or on the converter, induce overvoltages which can have an impact on the cable. For this reason, it becomes necessary to use surge arresters placed on the departures and arrivals of the continuous transmission system. The arresters consist of a number of metal oxide resistors, in this case zinc oxide, connected in series and/or parallel. These resistors are characterized by a non-linear voltage/current characteristic. This characteristic constitutes a low resistance path for overvoltages while a high resistance path for the industrial frequency voltage. This implies that in normal operation they can be considered as open sides.
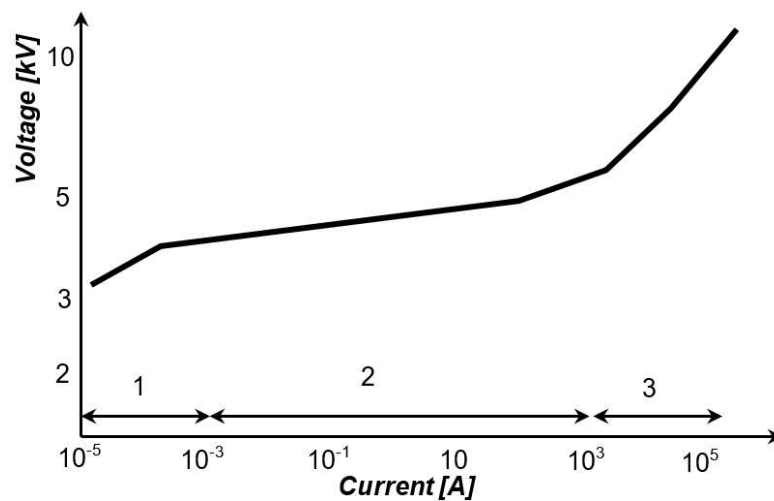
Figure 2.16: Characteristic curve of metal oxide arresters

Typically, metal oxide arresters are characterized by a V-I curve defined in three characteristic regions. The first region is called MCOV (Maximum Continuous Operating Voltage), where the current in the arrester is less than 1 mA. In this region the temperature increases with a corresponding increase in the dissipated

power. The second region is that of transient overvoltages, in which the current in the arrester varies between the range of 1mA and 2kA. The third region relates to lightning strikes with currents ranging from 1 kA to 100 kA. The curve used in the model has been constructed (see Figure 2.17 and 2.18) by reproducing the U-I curve mentioned above focusing on modeling in particular the first and second regions, which for our purpose are the most relevant, assuming a nominal voltage of 320 kV plant.
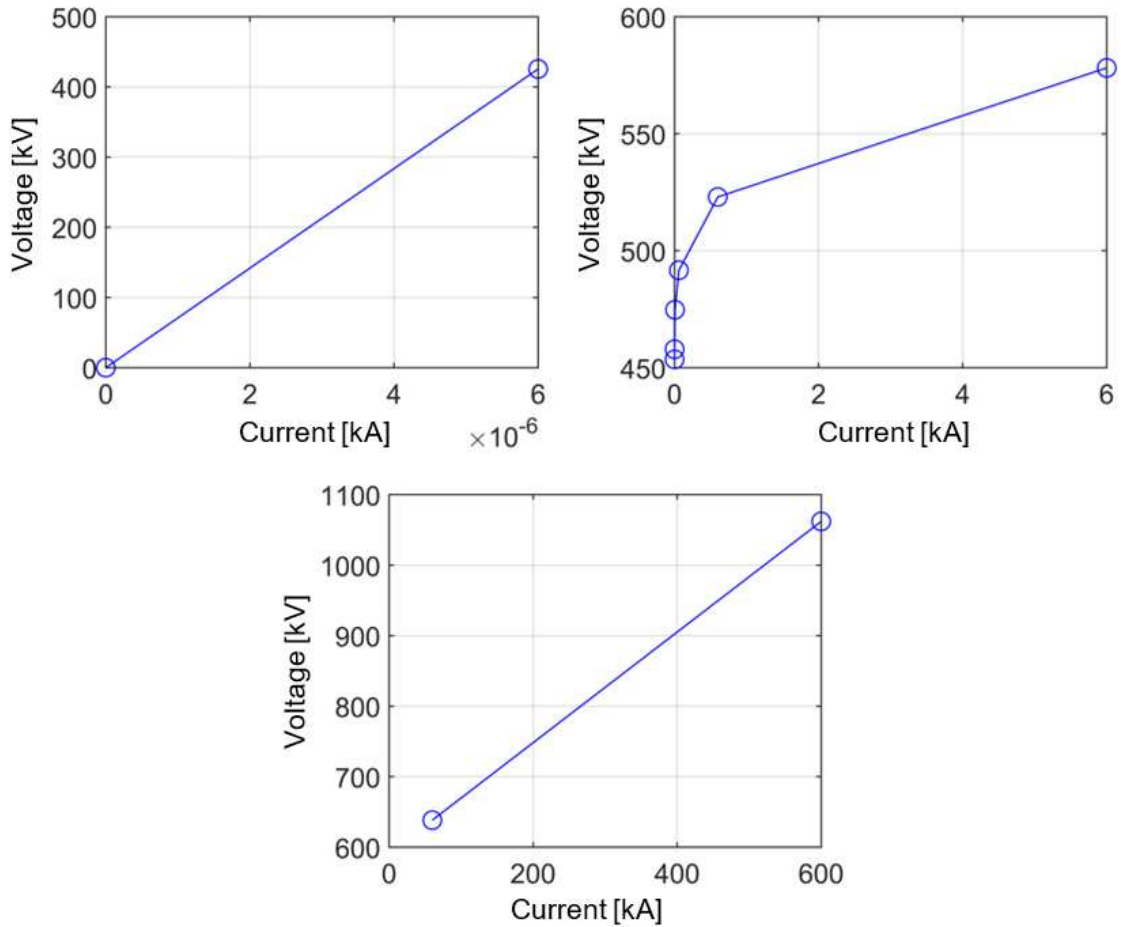
Figure 2.17: Three characteristic regions of the zinc oxide arresters implemented in the model
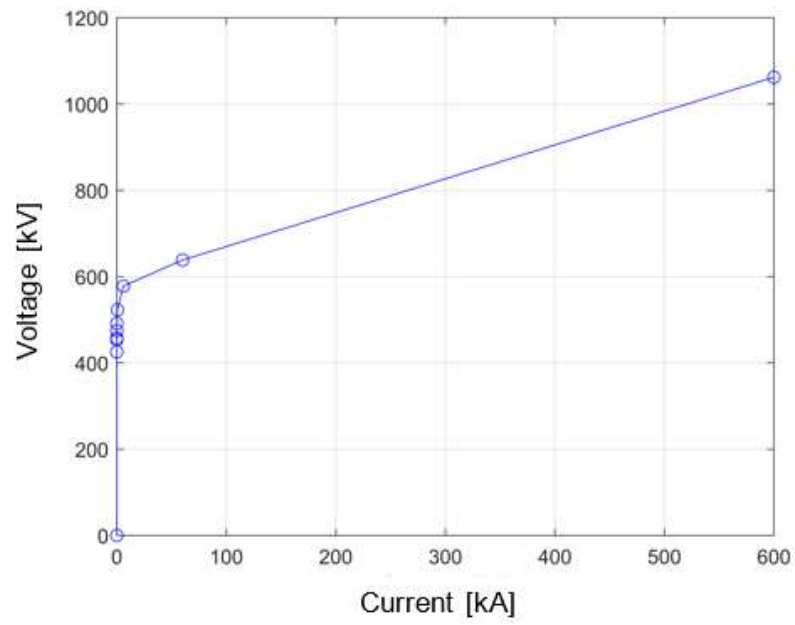
Figure 2.18: Characteristic curve of the zinc oxide arresters implemented in the model

2.1.4 M.4 Power cable system

Figure 2.19: HVDC power cable modeled

The continuous side transmission system was modeled through the use of two cables with the following characteristics:

Table 2.2: Characteristic parameters of the modeled cables

CHARACTERISTICS	CABLE N°1	CABLE N°2
length [km]	200	200
horizontal position [m]	-0.25	0.25
vertical position [m]	1.33	1.33
external sheath radius [mm]	63.9	63.9
SHEATH		
internal radius [mm]	56.9	
external radius [mm]	58.2	
material	aluminum	
resistivity [$\Omega \cdot$ m]	$2.83 \cdot 10^{-8}$	
INSULATOR		
material	XLPE	
dielectric constant ϵ_r	2.5	
loss factor $tan\delta$	0.0004	
screen management	solid bonding	
CONDUCTOR		
internal radius [mm]	0	
external radius [mm]	32	
material	copper	
resistivity [$\Omega \cdot$ m]	$1.72 \cdot 10^{-8}$	

The detail of the modeled HVDC cable is shown in Figure 2.20, while the relative position of the two modeled cables is shown in Figure 2.21.
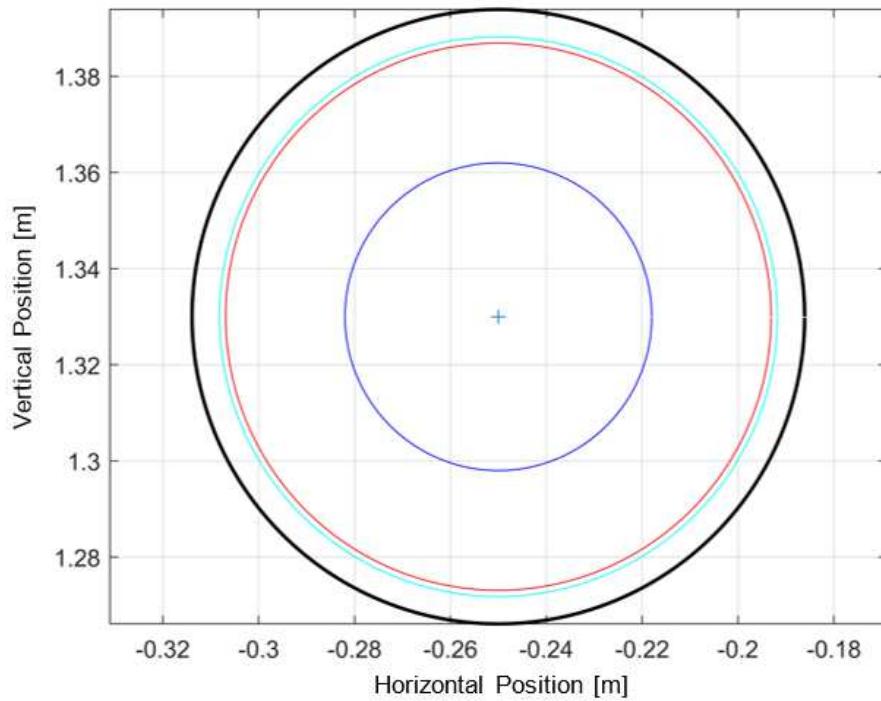
Figure 2.20: Detailed representation of the modeled HVDC cable
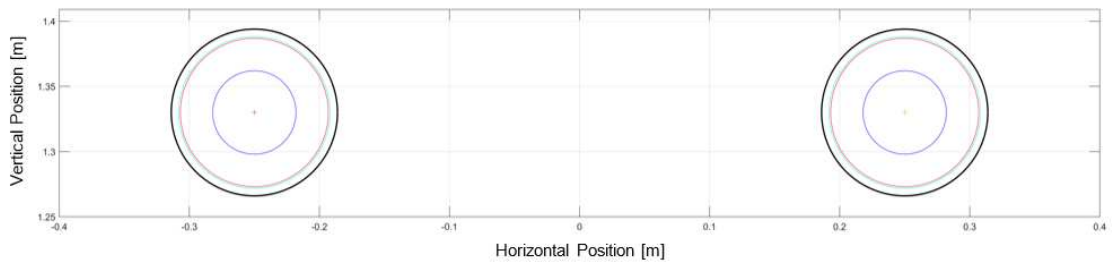
Figure 2.21: Position representation of modeled HVDC cables

100

2.1.5 Behavior of the HVDC system in case of fault on the AC side
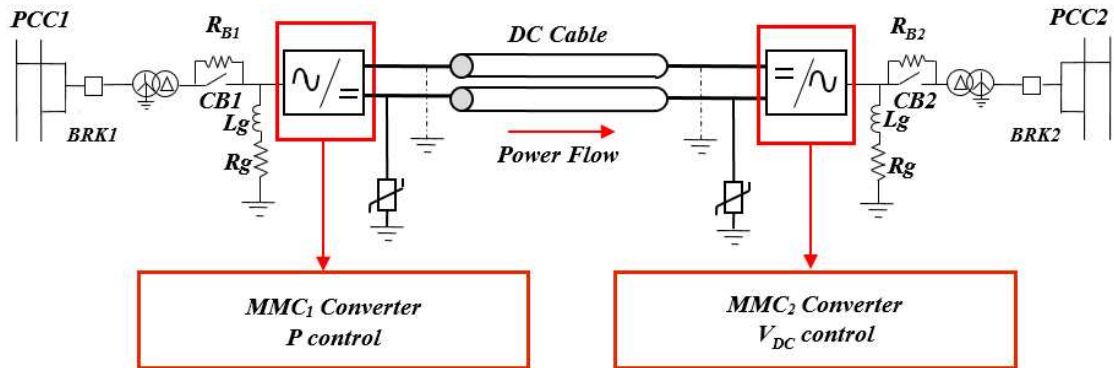
Figure 2.22: General scheme of the analyzed system

Some examples of faults on the HVDC link are shown and commented below. The HVDC transmission system used is modeled as shown in the previous paragraphs, a general scheme of the system under analysis is shown in Figure 2.22 while the characteristic parameters of the system are shown in Table 2.3.

Table 2.3: Main parameters used in the model under analysis

HVDC TRANSMISSION SYSTEM PARAMETERS	
Rated power	1000 MW
MMC Levels	400
Sub-modules technology	Half-Bridge
Rated Voltage	$\pm$ 320 kV
Surge arrester	Metal Oxide
AC Sending - PCC1	50 Hz, 400 kV, 10 GVA, R/L=10
AC Sending - PCC2	50 Hz, 400 kV, 10 GVA, R/L=10
Converter transformer	400/320 kV, 1000 MVA, X= 18 %, YNΔ
Star-point reactors	L_g=5.5 kH, $R_g = 7.7 k\Omega$
MMC Sub-modules characteristics	
Type	Half-Bridge
$\mathbf{L_{arm}}$	50 mH
$\mathbf{C_{arm}}$	10 mF
Cable characteristics	
Conductor	Copper
Section	2500 mm^2
Insulator	XLPE
Length	200 km

1. Three-phase fault on the PCC1 bus with fault resistance Rg = 0.01 Ω at instant t = 1 s with a duration of 100 ms.
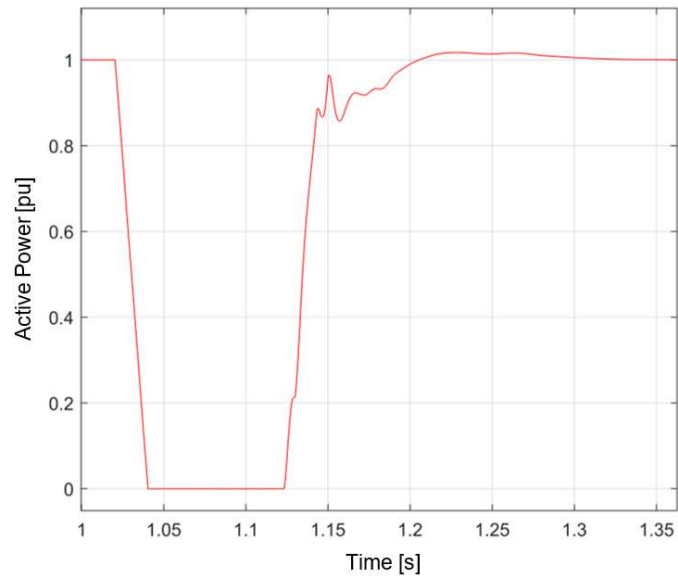
Figure 2.23: Active power profile following a fault on PCC1
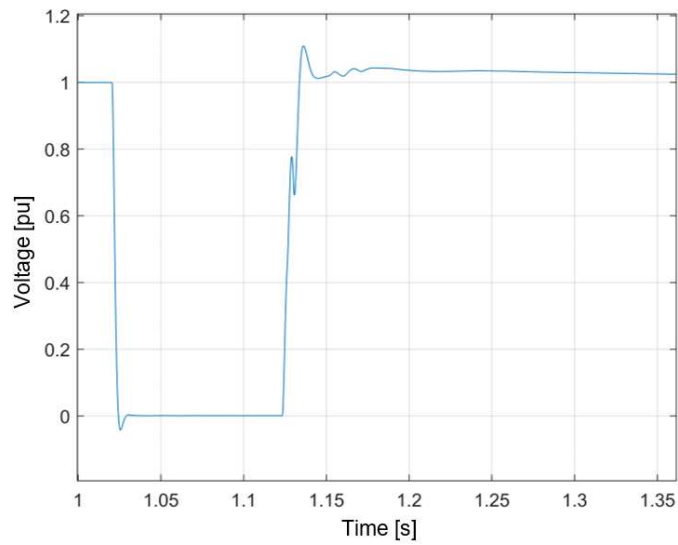
Figure 2.24: AC Voltage profile following a fault on PCC1
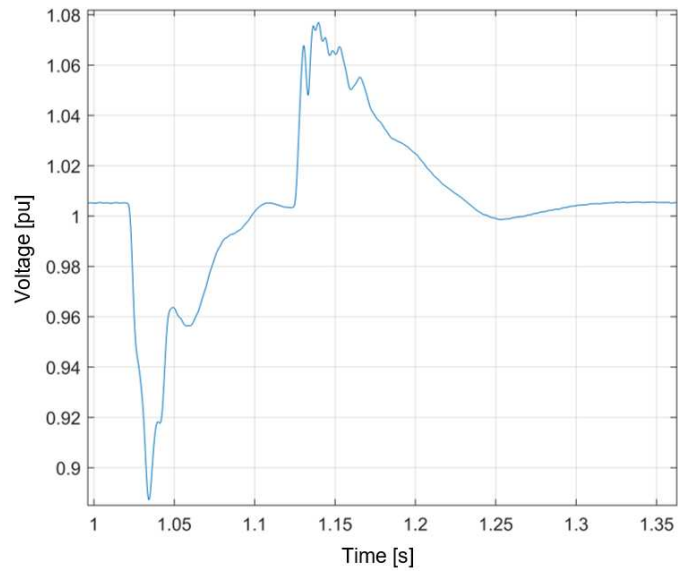
Figure 2.25: DC Voltage profile following a fault on PCC1

2. Three-phase fault on the PCC2 bus with fault resistance Rg = 0.01 Ω at instant t = 3 s with a duration of 100 ms.
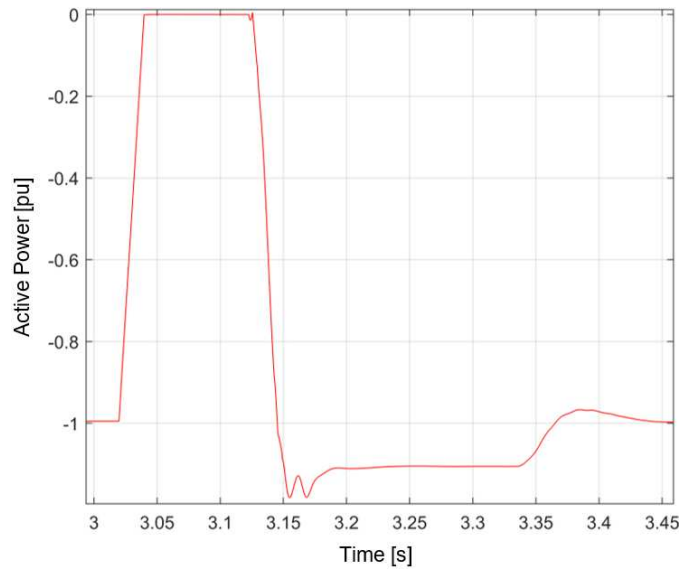
Figure 2.26: Active power profile following a fault on PCC2
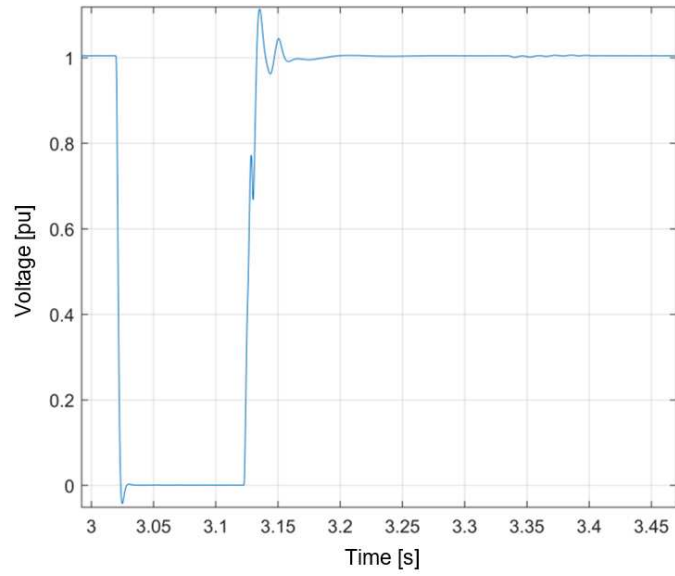
Figure 2.27: AC Voltage profile following a fault on PCC2
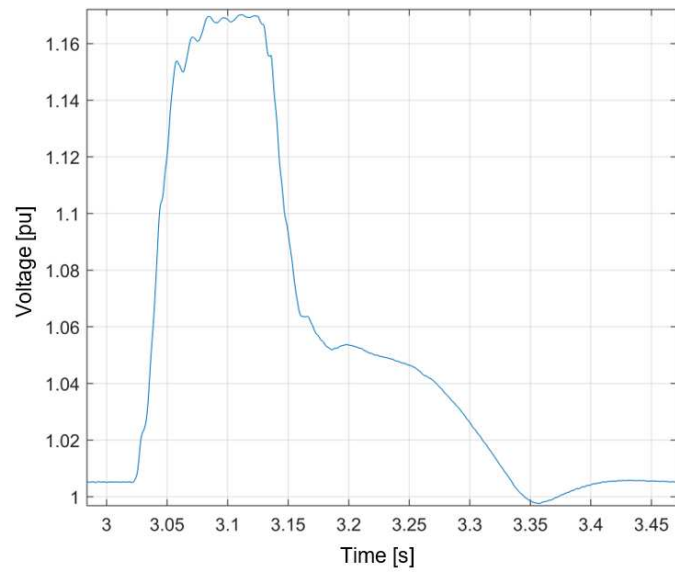
Figure 2.28: DC Voltage profile following a fault on PCC2

105

To correctly understand the PCC1 and PCC2 failure trends, refer again to the synchronous machine:

$$J\frac{d\omega}{dt} = C_{mec} - C_{ele}$$

$$J\omega\frac{d\omega}{dt} = P_{mec} - P_{ele}$$

$$C_{eq}\frac{dV_{dc}}{dt} = P_{PCC1} - P_{PCC2}$$
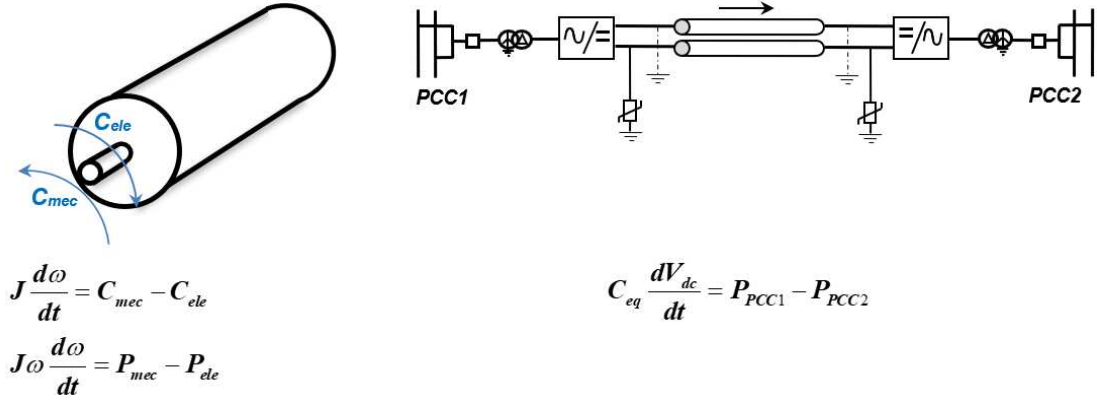
Figure 2.29: Analogy synchronous machine and HVDC-VSC connection

Similarly to the kinetic energy stored in the rotating mass of synchronous machines, the HVDC-VSC connection uses the electrostatic energy stored in the capacitors of the MMC sub-modules and the DC cable to provide an inertial response due to the imbalance of the active power. It is therefore deduced that following a failure in one of the two PCCs, a power imbalance is created which results in a response from the MMC with an increase or decrease in the voltage on the DC bus. In particular, these situations can be expected:

$$P_{PCC1} \approx 0 \Rightarrow C_{eq}\frac{dV_{dc}}{dt} = P_{PCC1} \Rightarrow V_{dc} \searrow \quad Decreases \quad (see \quad Figure \quad 2.25)$$

$$P_{PCC2} \approx 0 \Rightarrow C_{eq}\frac{dV_{dc}}{dt} = P_{PCC2} \Rightarrow V_{dc} \nearrow \quad Increases \quad (see \quad Figure \quad 2.28)$$
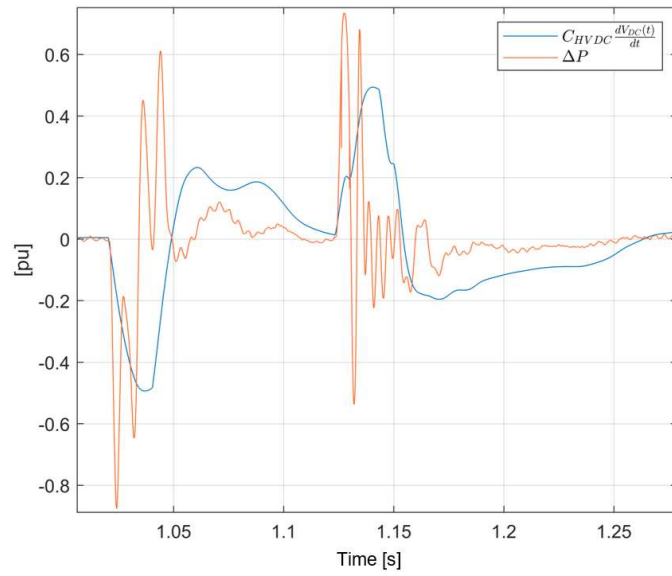
Figure 2.30: Balance between active power variation and DC side voltage variation

From Figure 2.30 it is possible to observe how the variation between the active powers at PCC1 and PCC2 and the derivative of the voltage on the DC bus is always balanced in compliance with what is shown in Figure 2.29.

2.1.6 Start-up sequence

This section shows the start-up sequence related to an HVDC system. The start-up sequence takes place in the following order (the acronyms used all refer to Figure 2.33):

1. the BRK1 AC switch is closed in t = 1s;

2. the CB1 switch is closed in parallel with the precharge resistor RB1 in t = 2s;

3. the sub-modules of the MMC1 converter are released at t = 3s;

4. the voltage reference V_{dc}^{ref} is set and the voltage V_{dc} is increased up to this value, in t = 4s;

5. the BRK2 AC switch is closed in t = 5s;

6. the CB2 switch is closed in parallel with the precharge resistor RB2 in t = 6s;

7. the sub-modules of the MMC2 converter are unlocked at t = 7s;

8. the change of control from V_{dc}-control to P-control is carried out in t = 8s;

9. the power reference P_{ref} is set and the power P is increased up to this value, in t = 9s;

The times set for the start-up sequence are purely indicative and do not reflect the times used in the real application. They have been chosen to better articulate the various steps previously described on a graphic level as well.
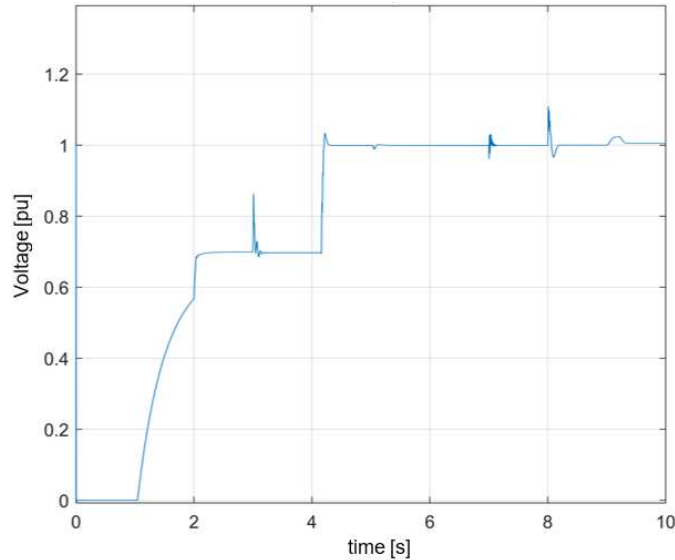
Figure 2.31: Voltage profile on the DC bus
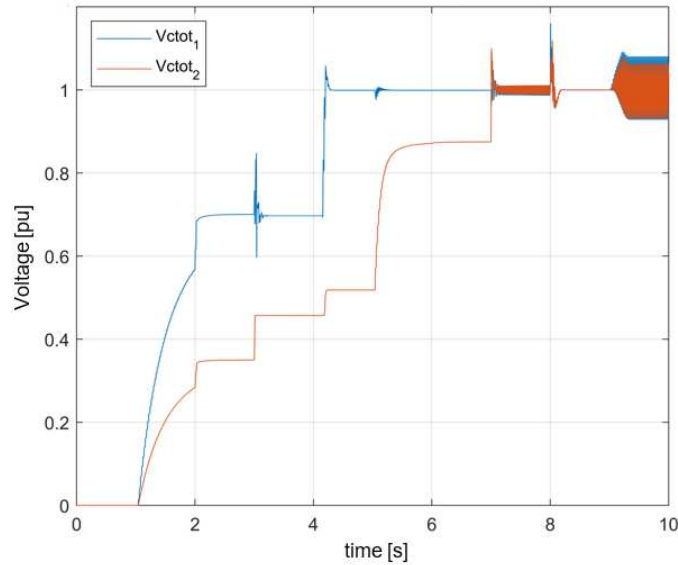
Figure 2.32: Total voltage present on the capacitors of the sub-modules of the converters upstream and downstream of the HVDC connection.

It is worth noting how the displacement of the precharge resistor, upstream or downstream of the conversion transformer, has an impact on the power dissipated by the resistor itself, which justifies the typical choice of the first configuration.
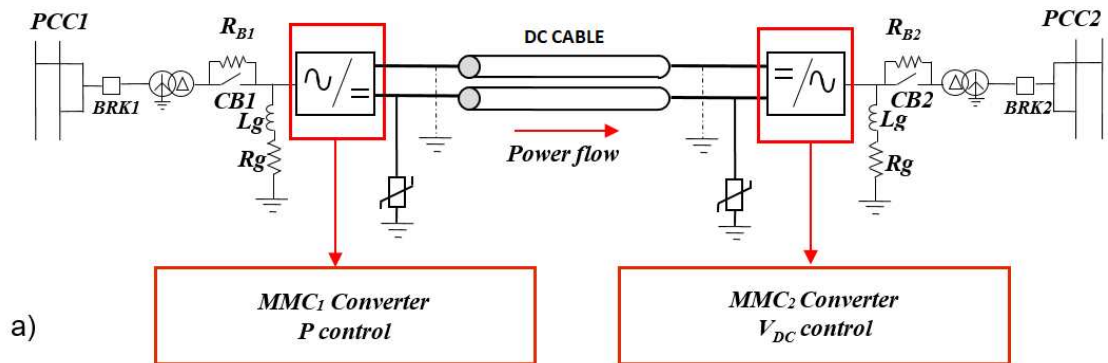
Figure 2.33: Configuration with precharge resistors positioned downstream of the conversion transformer
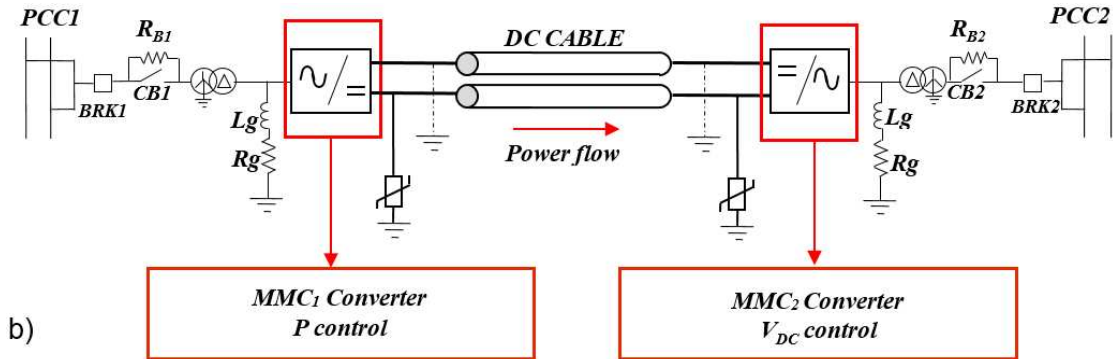
Figure 2.34: Configuration with precharge resistors positioned upstream of the conversion transformer
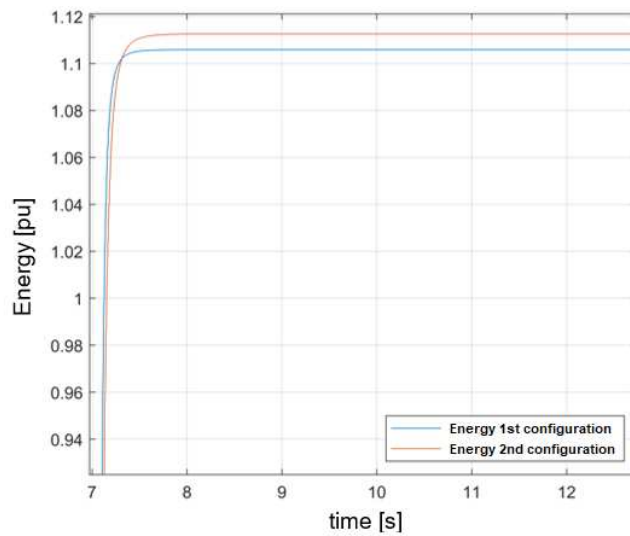
Figure 2.35: Energy dissipated in the precharge resistor in the two configurations

2.1.7 DC Transient analysis

A fundamental and necessary analysis in the design phase is the study of the behavior of the HVDC connection following faults that occur on the continuous side. The following analysis will also justify the adoption of the surge arresters on the DC side. Some specific cases of failure will be examined, which are the worst conditions. Fault conditions will be analyzed first without the use of surge arresters, while later, the reduction of transient overvoltages will be observed by adopting surge arresters.

1. Phase-to-ground fault of the negative arm relating to phase "a" of the converter, without surge arresters:
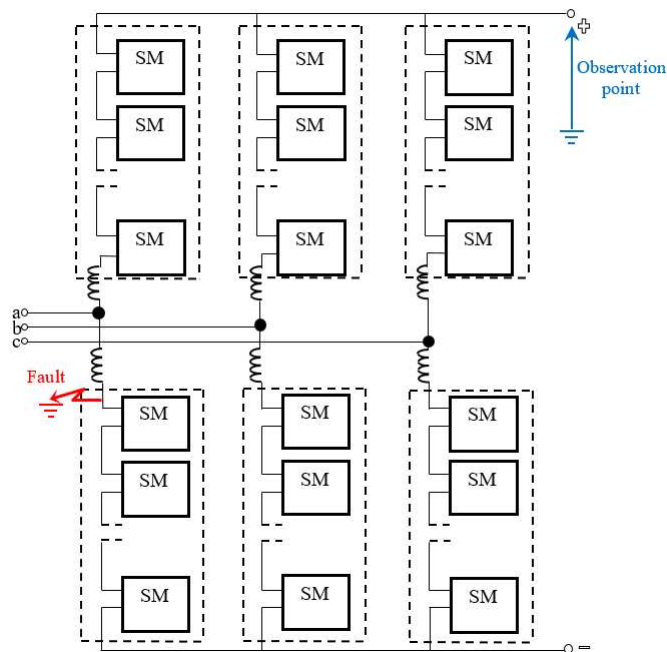
Figure 2.36: Fault location and the point of observation in the first case analyzed
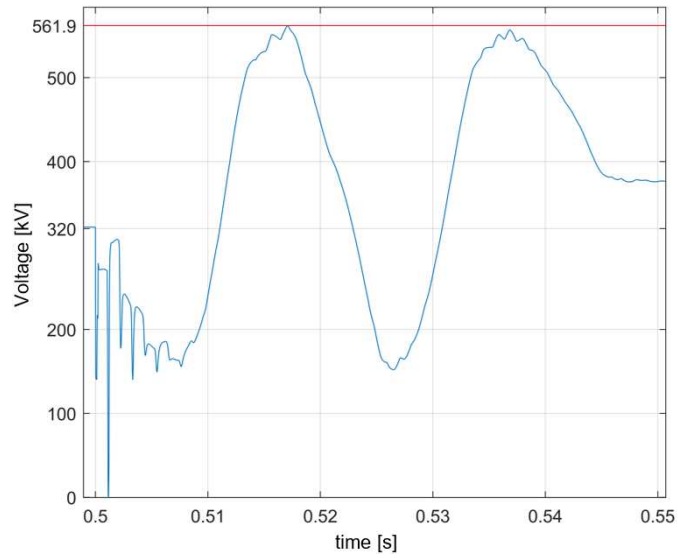
Figure 2.37: Voltage level reached at the observation point

2. Phase-to-ground fault of the positive arm relating to phase "a" of the converter, without surge arresters:
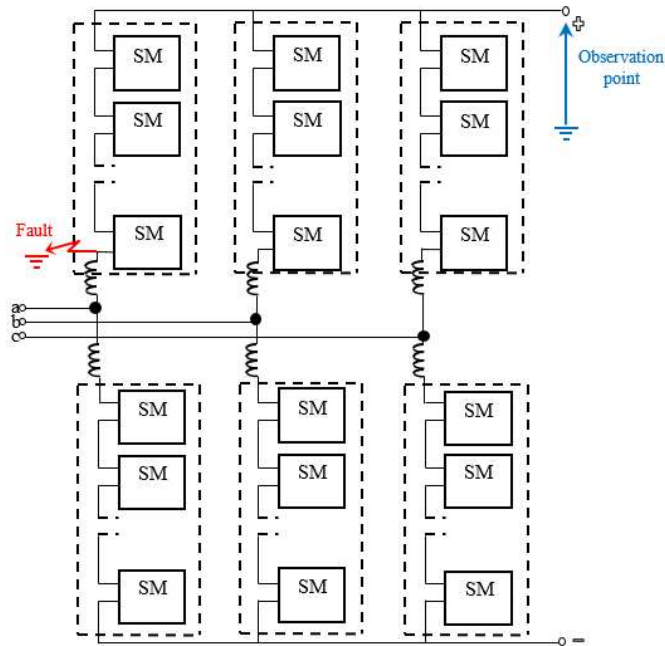
Figure 2.38: Fault location and the point of observation in the second case analyzed
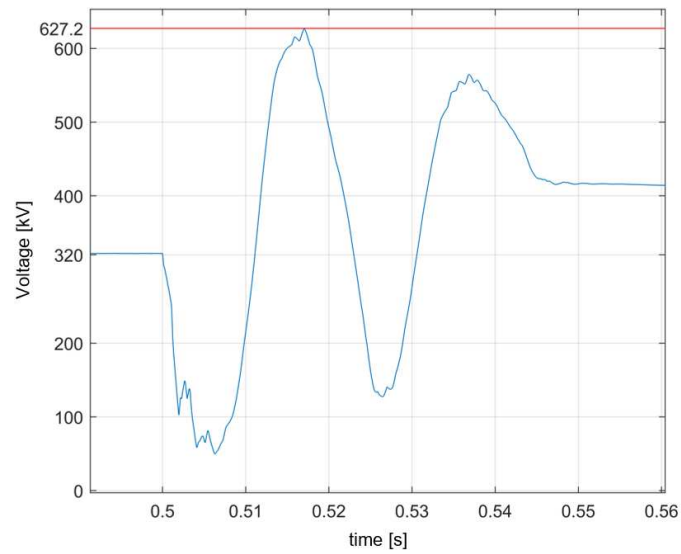
Figure 2.39: Voltage level reached at the observation point

3. Phase-to-ground fault of the positive pole of the transmission cable on the DC side, without surge arresters
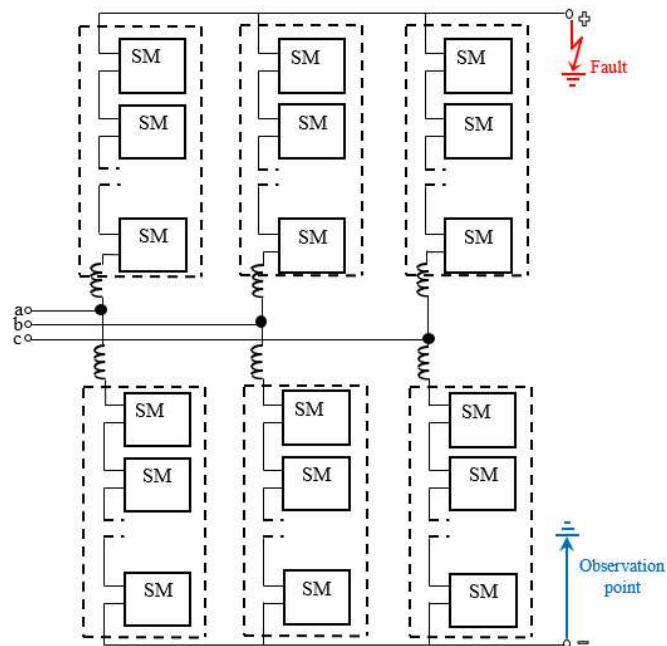
Figure 2.40: Fault location and the point of observation in the third case analyzed

113
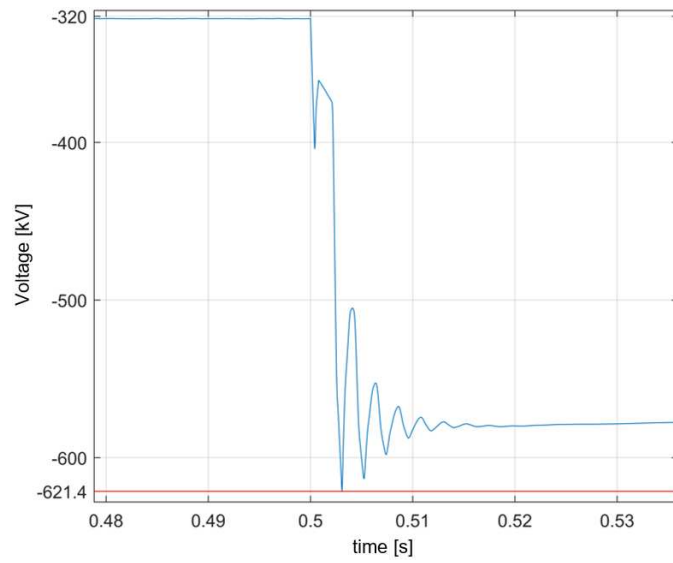
Figure 2.41: Voltage level reached at the observation point

4. Phase-to-ground fault of the negative pole of the transmission cable on the DC side, without surge arresters
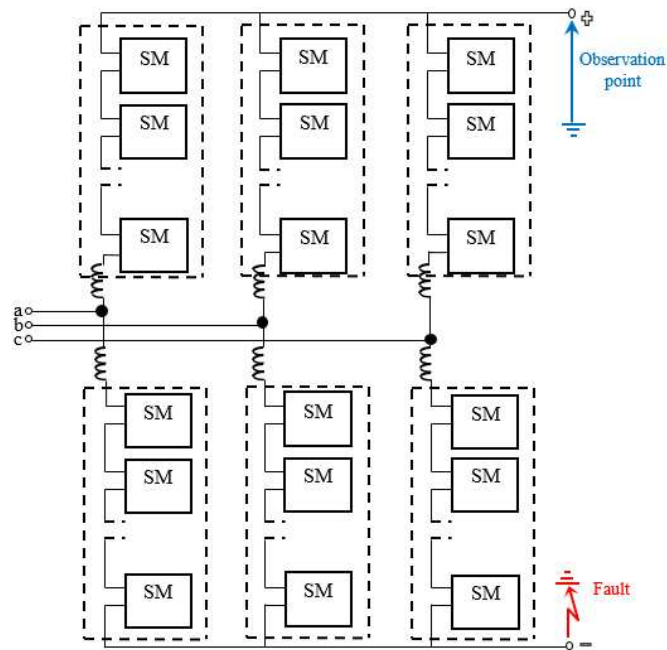
Figure 2.42: Fault location and the point of observation in the fourth case analyzed

114
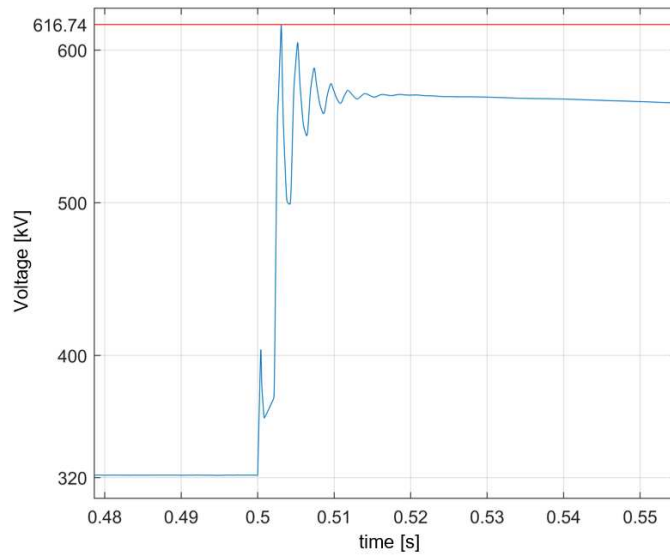
Figure 2.43: Voltage level reached at the observation point

Below, the previous analysis will be shown again but using surge arresters:

1. Phase-to-ground fault of the negative arm relating to phase "a" of the converter, with surge arresters:
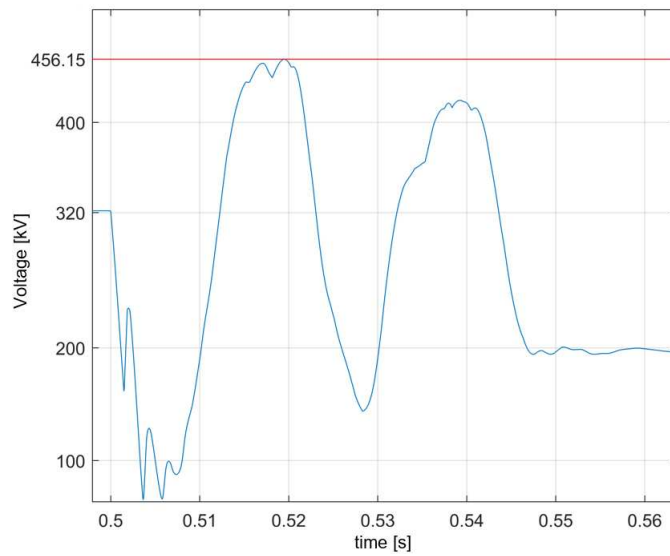
Figure 2.44: Voltage level reached at the observation point

2. Phase-to-ground fault of the positive arm relating to phase "a" of the converter, with surge arresters:

115
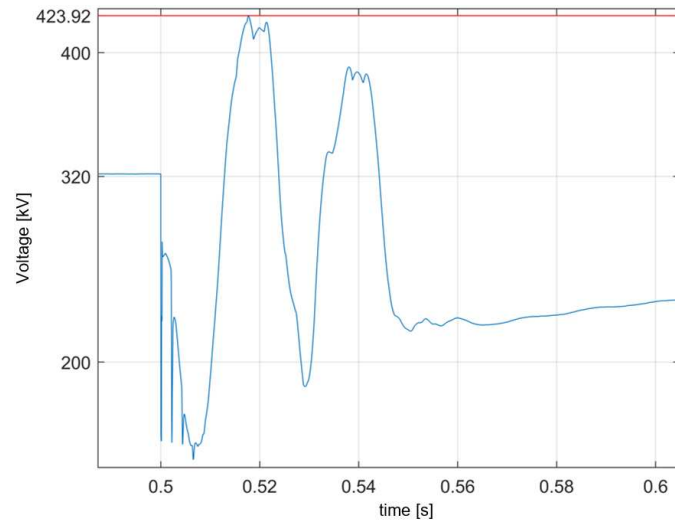
Figure 2.45: Voltage level reached at the observation point

3. Pole-to-ground fault of the positive pole of the transmission cable on the DC side, with surge arresters
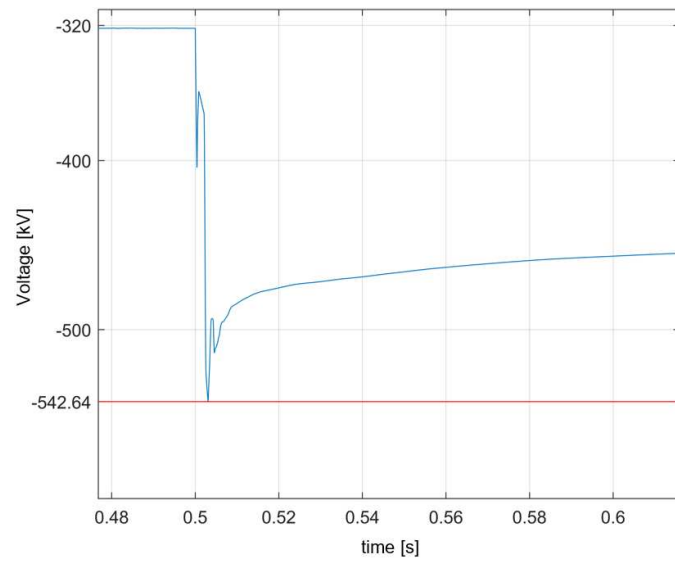
Figure 2.46: Voltage level reached at the observation point

4. Pole-to-ground fault of the negative pole of the transmission cable on the DC side, with surge arresters

116
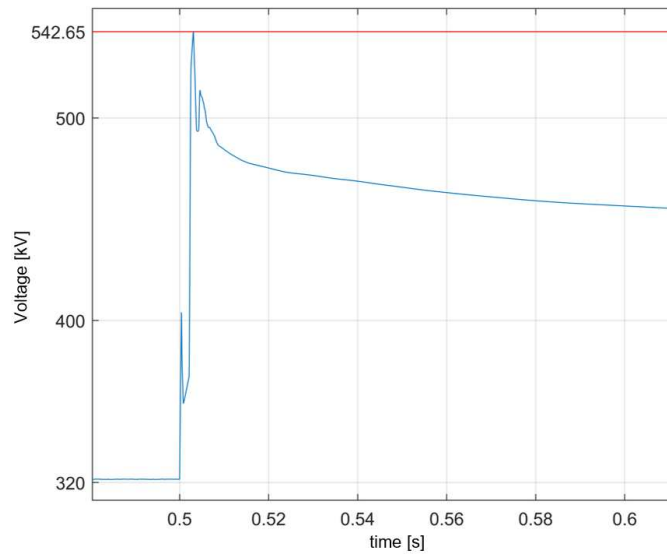
Figure 2.47: Voltage level reached at the observation point

Table 2.4: Results of the EMT analysis

Fault Type	Positive pole voltage [kV]	Positive pole voltage [kV]
	Without surge arrester	With surge arrester
Phase "a" to ground fault of the negative converter arm	561.9	456.15
Phase "a" to ground fault of the positive converter arm	627.2	423.92
Pole-to-ground fault of the negative DC pole	616.74	542.65

117

2.2   Conclusion

This section describes the model of an HVDC-VSC transmission system implemented in an EMTP-RV environment. The chosen configuration was the symmetrical monopolar one and the chosen VSC converter was the multi-level one (MMC). The model was analyzed in all its components, that is:

- generation system, namely, network upstream and downstream of the system;

- conversion station;

- multilevel converter;

- transient overvoltage protection system;

- cable system.

The logic behind the conversion system has also been described in detail. The equations at the base of the control system have been described. A typical geometry of HVDC installation was chosen when the cable system has been modeled. As far as the protection system is concerned, it was modelled with reference to the theoretical characteristics typical of metal oxide arresters. An example of the start-up sequence of the HVDC-MMC system was shown, also analysing the reasons behind some design choices on the positioning of the precharge resistance. Finally, both the behaviour with respect to faults occurring on the alternating side of the converter and those occurring on the continuous side of the transmission system were analysed. Particular attention was paid to the analysis of transient overvoltages that occur on the DC side. On the DC side, an analysis was carried out on the most burdensome faults and therefore of particular interest, observing how the insertion of transient overvoltage protections actually has the required effect.

2.3 PowerFactory DigSilent & EMTP-RV: Transient Overvoltages comparison

In this section the HVDC-VSC monopolar configuration with MMC technology previously modeled is compared with an identical configuration modeled in the DigSilent PowerFactory environment. Figure 2.48 shows the adopted HVDC configuration:
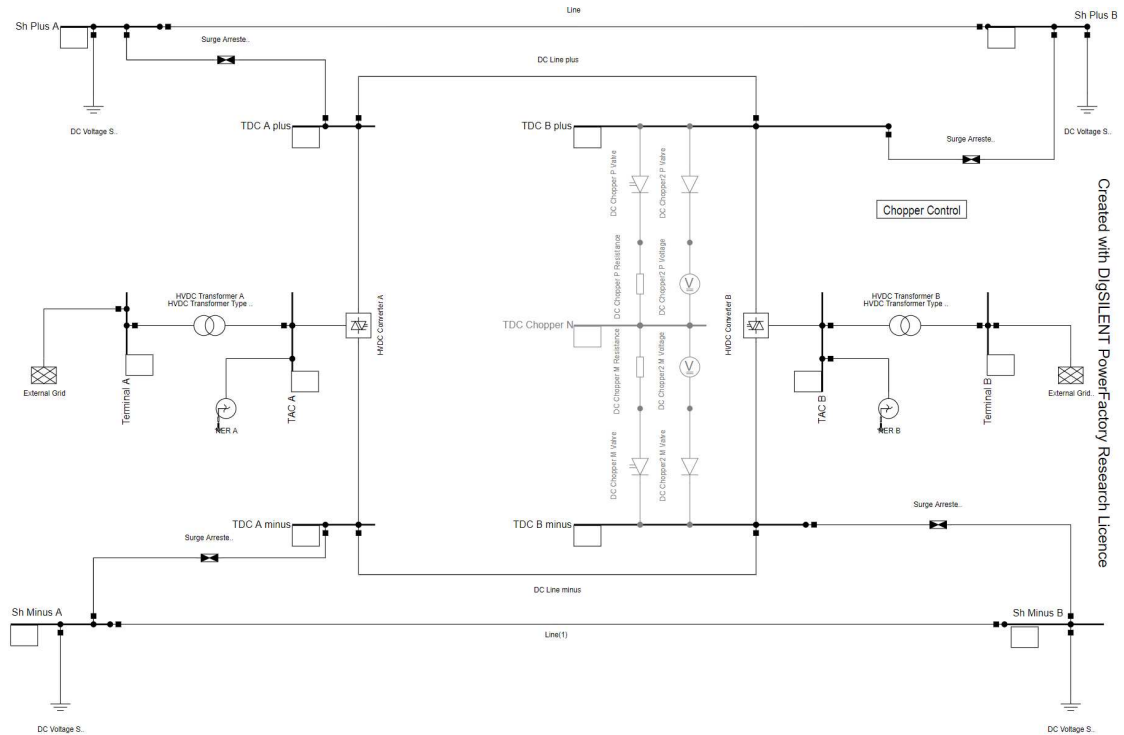
Figure 2.48: HVDC-MMC PowerFactory DigSilent monopolar configuration

All the electrical characteristics of the system refer to those of section 2.1.

In particular, as it is shown in section 2.1, when a polte to ground fault at the DC bus occurs, a transient overvoltage is genereted, causing a sudden voltage rise on the DC bus. It has been seen that the use of arresters is necessary, so they have also been adopted in this system.

The figure shows how at time t=0.5 s a pole-to-ground fault occurs on the DC bus. The blue simulation shows the transient overvoltage trend when using the EMTP-RV software, while the purple simulation shows the transient overvoltage trend when using the PowerFactory DigSilent software. From the two simulations we can observe the following:
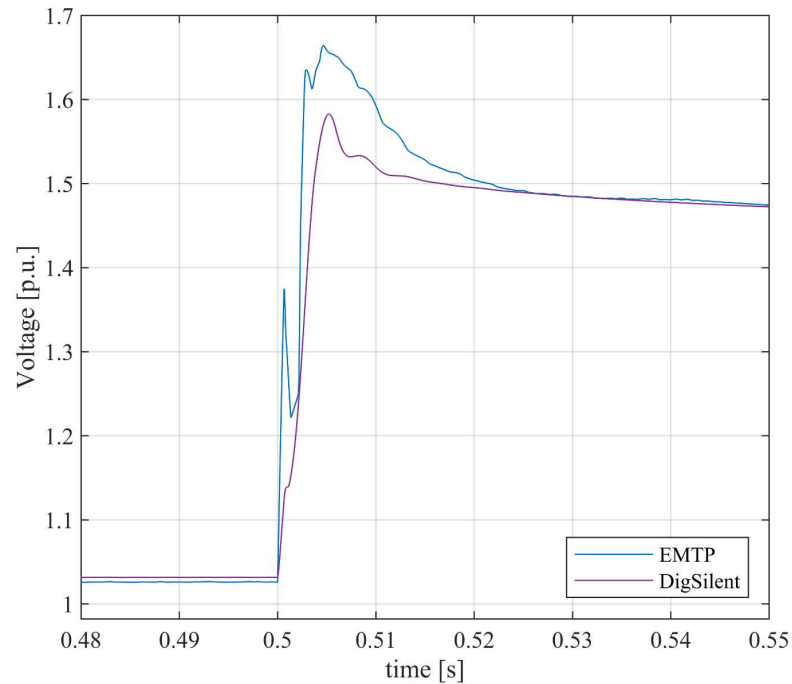
Figure 2.49: HVDC-MMC PowerFactory DigSilent monopolar configuration

- the overvoltage peak when using PowerFactory Digsilent software are lower;

- in the first millisecond after the fault and then near the peak of the overvoltage, there is a very small variation of the voltage derivative in the case of the simulation with the PowerFactory DigSilent software compared to that with the EMTP-RV software.

Conclusions

In this section we aimed to observe the differences in the use of two commercial software for the analysis of transient overvoltages. It was observed that in the case of the PowerFactory DigSilent software there is a reduction in transient overvoltage. This is due to the fact that in combination with the DigSilent arresters it offers the possibility to implement a Chopper Control that once exceeded the threshold value of voltage increase equal to 1.04 p.u. is activated contributing to decrease the maximum value of overvoltage. In addition, the reduction of the voltage derivative is due to the fact that DigSilent implements a Derivative Control in the converter control system.

2.4 A Multi-infeed HVDC System: Assessment of Transient Overvoltages

The section presents an electromagnetic-transient (EMT) analysis of a multi-infeed HVDC cable system to assess the transient overvoltages on the cables due to different fault conditions. It is well known that the HVDC-MMC configuration needs surge arresters to reduce the transient overvoltages on the DC cable system. This work highlights how the voltage perturbations on the HVDC-LCC link due to the faults on the HVDC-MMC link are not negligible and how a reduction of transient overvoltage is necessary for both the HVDC systems. The results of this study can be useful to improve the insulation coordination of the multi-infeed HVDC system and their reliable operation.

2.4.1 Introduction

The use of High Voltage Direct Current transmission systems in ac grids is gaining more and more importance especially with the ever growing penetration of renewable energy sources in the electrical networks, which determines several issues for a reliable operation of the grids[10, 65].

It is also worth noting that the fewer number of power cables required for the DC transmission lines compared with the AC ones and the negligible electromagnetic field emissions [10] make the HVDC systems fully compatible with the installation in railway/highway infrastructures [15–17, 66–68].

The HVDC technologies can be summarized in two main typologies: LCC and VSC. In particular, VSC-based systems are becoming increasingly important, due to their flexibility. The key point of VSC technology concerns the use of the modular multilevel converter (MMC). Each leg of the MMC converter has a number of sub-modules (SMs) in cascade proportional to the number of needed voltage levels. The main benefits of this technology are the lower switching frequency, which allows a converter power losses reduction, and the possibility to avoid the filter devices if a suitable number of levels per leg is used [69]. Moreover, since the VSC technology allows the reverse of the power flow without reversing the polarity of the voltage, cross-linked-polyethylene-extruded (XLPE) cables can be used with this converter typology [32].

There are three basic submodule configurations, Half-Bridge (HB), Full-Bridge (FB), Hybrid-Bridge. Each configuration offers pros and cons, depending on the type of application [10]. A converter reactor is located in series with the SMs in order to limit short-circuit currents through the valves in a fault occurrence and to reduce the balancing currents between individual phases to very low values.

One of the major challenges concerning the HVDC power cables is related to the transient overvoltages (TOVs). During the design phase of a HVDC project, the study of the insulation coordination is very important because it allows knowing the maximum overvoltage value which the equipment shall withstand. It has to be noted that an equipment over-sizing can result in design issues and too high cost, while an equipment under-sizing could cause a failure of the HVDC link. A widely used guide concerning the recommendations for carrying out tests on extruded transmission cables for HVDC applications is the Cigrè TB496 [70]. Nowadays, the usage of several HVDC transmission systems connected to the same ac grid is becoming increasingly common. The converters, which can be of different technologies, share the same ac bus or are connected to an electrically close ac bus. This type of HVDC configuration is called "Multi-infeed HVDC system" (MIHVDC) [71–80]. Hybrid HVDC transmission systems exploit the advantages offered by the VSC converter of a flexible reactive power control, which can improve the voltage stability of the AC system and can also prevent commutation failures in the LCC system when the AC bus voltage drops and supplies power to a passive network. Hence, an EMT analysis is required in order to evaluate the worst overvoltage value, both in the case of a single HVDC-MMC link and a MIHVDC link. There are some meaningful contributions in literature in this filed. Saad et al. [81] and Iravani et al. [82] highlight the main aspects of the transient overvoltages, showing the worst TOV cases for a HVDC-MMC monopolar configuration and the crucial importance of surge arresters in order to limit the overvoltage. Goertz et al. [83] and Freye et al. [84] carry out an electromagnetic transients (EMT) study by varying the fault position and the fault impedance for monopolar and bipolar HVDC configurations.

In [85] a DC TOV investigation is performed by analysing the critical points of power cables with different fault positions along the cable and by observing the most stressed point for each failure condition. Xu et al. [86] analyse the overvoltage phenomenon of hybrid LCC-VSC-HVDC and provide the recommended surge arrester configuration in the converter station of hybrid HVDC LCC-VSC systems.

Differently, in this paper, an EMT analysis is performed in EMTP-RV environment for a Multi-infeed HVDC system to evaluate the transient overvoltages given from faults located in the HVDC-VSC link. The EMT investigation aims at analysing the HVDC-LCC response when the worst fault conditions occur on the HVDC-VSC link. The worst fault conditions for the MMC system are shown in [81] by considering both converter and DC cable faults. It is worth nothing that surge arresters are typically applied to the DC power cables for the HVDC-MMC systems [72] to reduce the transient overvoltage effects but are not commonly applied to the HVDC-LCC monopole configurations [69]. Hence, in this paper the EMT assessment is performed without surge arresters on the LCC side. Subsequently, since the DC power cable has a limited capability to withstand transient overvoltages, metal–oxide varistor

122

(MOV) surge arresters are adopted for the LCC HVDC link.

2.4.2   Case study
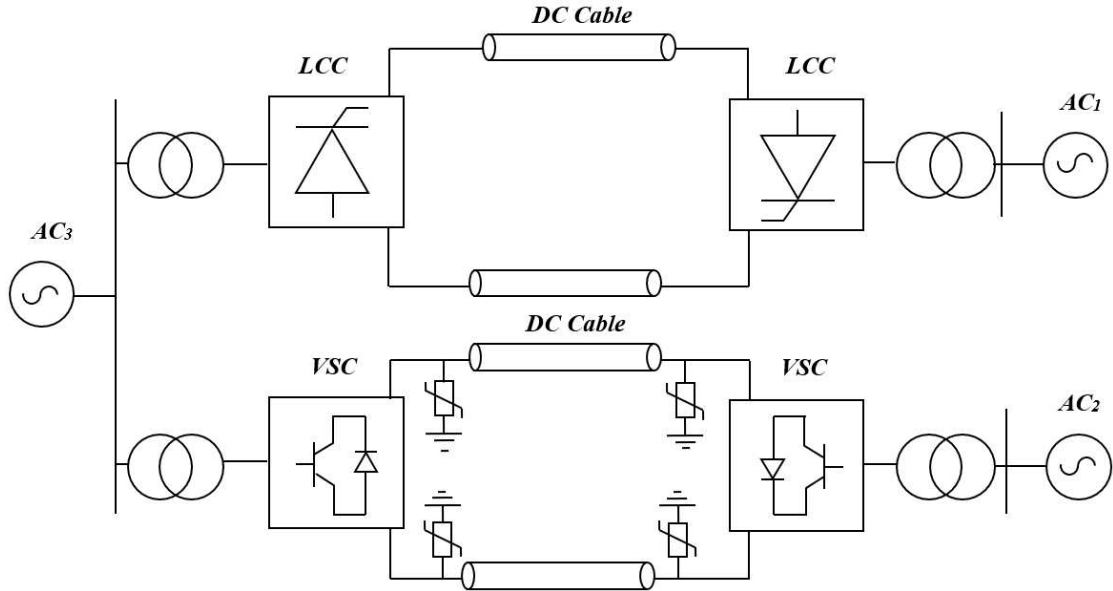
Figure 2.50: HVDC Multi-Infeed configuration

The analysed system is the HVDC multi-infeed configuration shown in 2.50. The whole system is composed of two HVDC links, which exploit the LCC and VSC technologies. The main characteristics of the AC grids and of the HVDC configurations are summarized in Table 2.5 and 2.6 respectively. The EMT investigation is performed by analysing the HVDC multi-infeed system for different fault position in the HVDC-VSC link and by observing the overvoltage response at both the HVDC LCC and VSC links as shown in Figure 2.51 and summarized in table 2.7. At first, the multi-infeed HVDC system is analysed without using the surge arresters on the HVDC-LCC link. Thereafter, the surge arresters are adopted in the whole system in order to reduce the transient overvoltages also at the HVDC-LCC side.
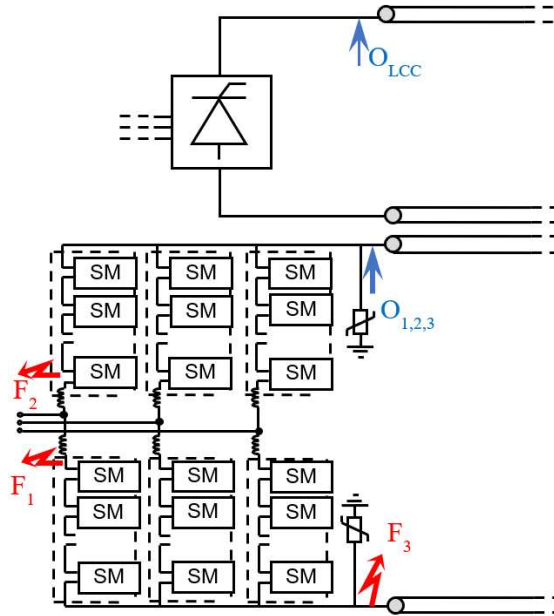
Figure 2.51: HVDC Multi-Infeed faults and observation points

Table 2.5: Main AC Grids Parameters

	AC Grid 1	**AC Grid 2**	**AC Grid 3**
Rated Voltage	345 kV	400 kV	500 kV
Frequency	50 Hz	50 Hz	50 Hz
Short-Circuit Power	5 GVA	10 GVA	5 GVA

Table 2.6: Main AC Grids Parameters

	HVDC-LCC	**HVDC-VSC**
Rated power of whole interconnection	345 kV	400 kV
Configuration	50 Hz	50 Hz
Rated pole voltage (pole to ground)	5 GVA	10 GVA
Surge Arrester	Not applied	Zinc oxide
Power Cable Type	MI-PPL	XLPE

Table 2.7: Main AC Grids Parameters

F_1	Phase-to-ground fault of negative MMC converter leg
F_2	Phase-to-ground fault of positive MMC converter leg
F_3	Phase-to-ground fault of negative DC power cable of VSC link
$O_{1,2,3}$	Observation point related to F1, F2, F3 fault positions
O_{LCC}	Observation point related to F1, F2, F3 fault positions on LCC side

2.4.3 EMT analysis

The transient overvoltage due to the F1 fault is shown in Figure 2.52.a and 2.52.b. In particular, Figure 2.52.a shows the transient overvoltage dynamic for the HVDC-LCC power cable in the O_{LCC} observation point, whereas Figure 2.52.b shows the transient overvoltage in the O1 observation point. As it can be noted, the maximum voltage peak reached on the LCC side is 671.8 kV and on the VSC side is 382.5 kV. With reference to Figure 2.52.c, the transient due to the F2 fault results in an overvoltage on the LCC side up to 673.7 kV, whereas for the VSC side the transient generates an overvoltage with a voltage peak of 386 kV (see Figure 2.52.d). As it can be noted from Figure 2.53, the transient due to F3 fault on the VSC power cable generates an overvoltage on the VSC side up to 531.7 kV (see Figure 2.53.a) and on the LCC side with a peak of 670.7 kV (see Figure 2.53.b).
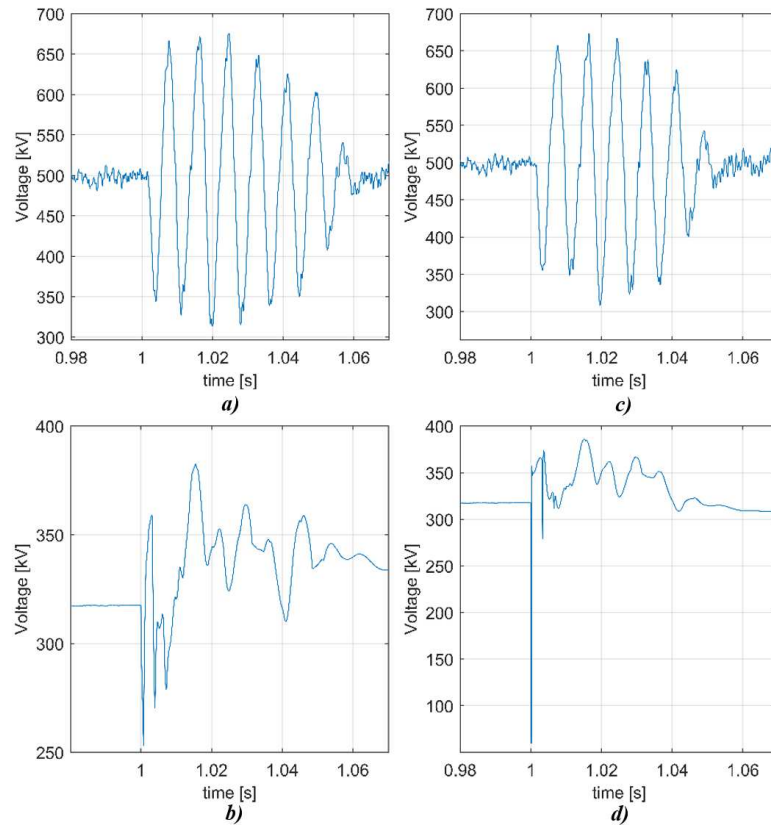
Figure 2.52: TOV behaviours: a) voltage dynamics at the O_{LCC} observation point when F_1 fault condition occurs; b) voltage dynamics at the O_1 observation point when F_1 fault condition occurs; c) voltage dynamics at the O_{LCC} observation point when F_2 fault condition occurs; d) voltage dynamics at the O_2 observation point when F_2 fault condition occurs.
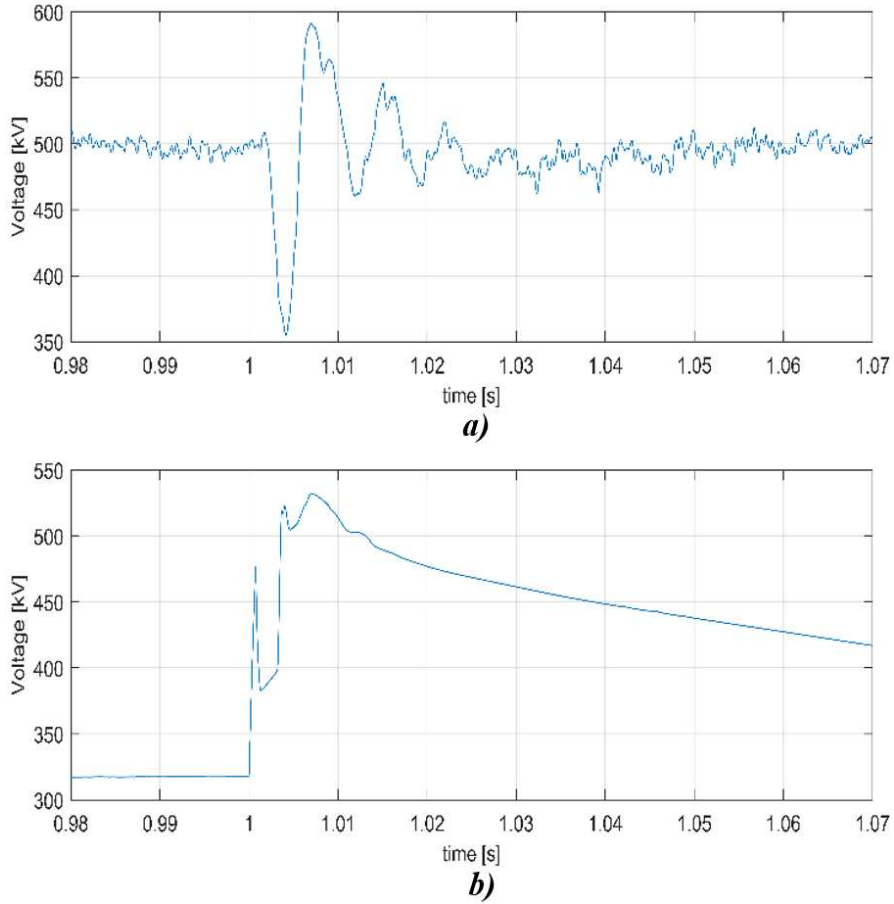
Figure 2.53: TOV behaviours: a) voltage dynamics at the O_{LCC} observation point when F_3 fault condition occurs; b) voltage dynamics at the O_3 observation point when F_3 fault condition occurs

Such a system includes deep voltage and overcurrent detectors and they are activated when the DC current is higher than the maximum current limit set. After the DC protection intervention, the MMC station is tripped, the converter is blocked and the ac breakers are opened.

2.4.4 EMT Analysis: Surge Arrester Solution

In order to preserve the DC power cables and to reduce the transient overvoltage on the HVDC-LCC link, zinc oxide surge arresters are adopted. In particular, Figure 2.54.a clearly shows the voltage reduction with an overvoltage up to 587 kV for the HVDC-LCC link, whereas the overvoltage at the O1 observation point reaches a voltage peak of 378.5 kV (see Figure 2.54.b).

127
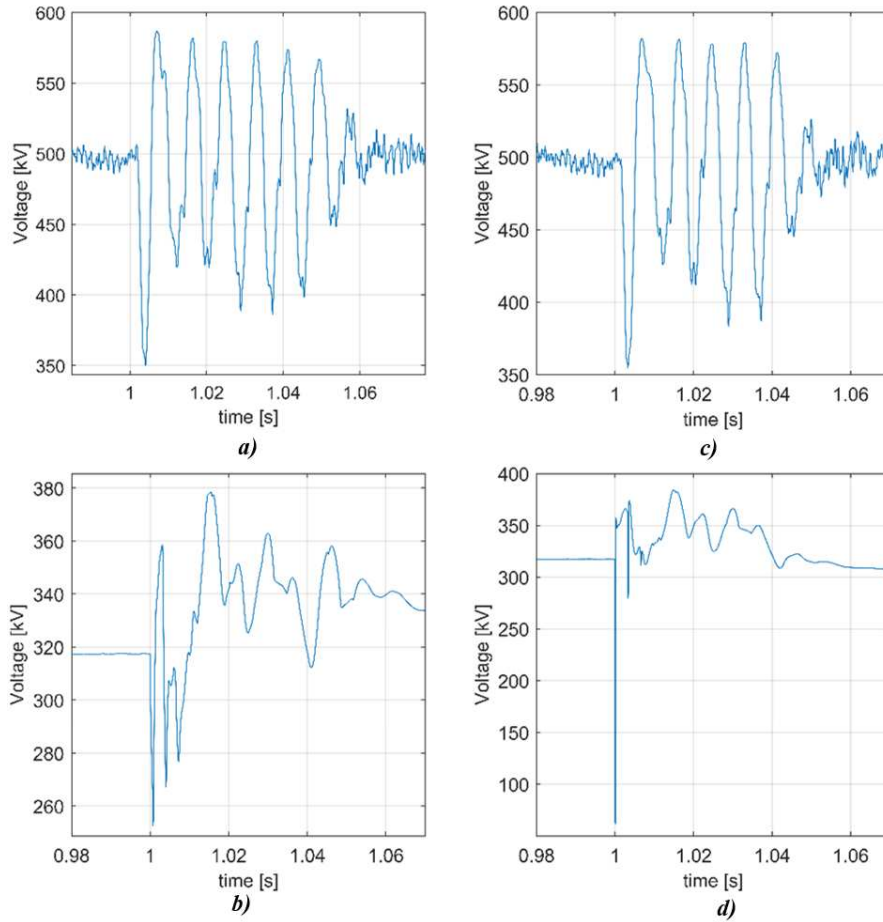
Figure 2.54: TOV behaviours with surge arresters on the HVDC-LCC link: a) voltage dynamics at the O_{LCC} observation point when F_3 fault condition occurs; b) voltage dynamics at the O_3 observation point when F_3 fault condition occurs

Such a system includes deep voltage and overcurrent detectors and they are activated when the DC current is higher than the maximum current limit set. After the DC protection intervention, the MMC station is tripped, the converter is blocked and the ac breakers are opened.

With reference to Figure 2.54.c the voltage reduction results in an overvoltage up to 582.3 kV for the LCC side, whereas for the VSC link the overvoltage peak is of 384.1 kV (Figure 2.54.d).

The transient overvoltage on the DC power cable for the HVDC-LCC system reaches a peak voltage value of 591.1 kV (see Figure 2.55.a) and of 531.8 kV for the HVDC-VSC link (see Figure 2.55.b).

The peak overvoltage values for the HVDC-LCC link before and after the surge arrester adoption are reported in Table 2.8. As it is possible to note, the adoption of surge arresters on the HVDC-LCC link allows a transient overvoltage reduction of about 12.5 %.
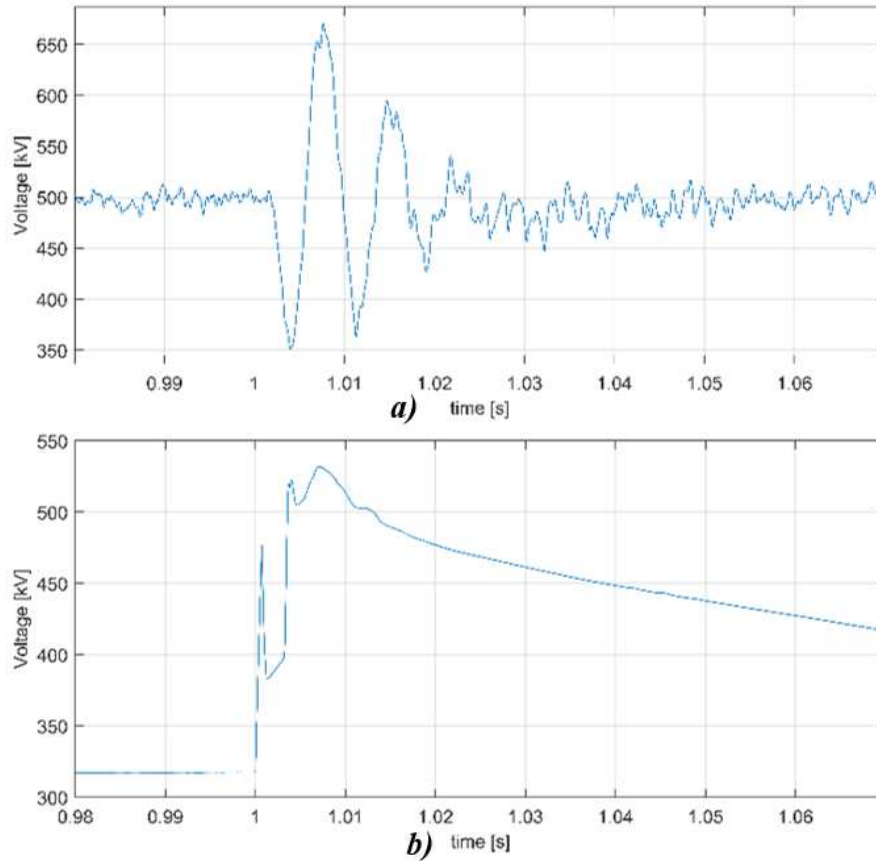
Figure 2.55: TOV behaviours with surge arresters on the HVDC-LCC link: a) voltage dynamics at the O_{LCC} observation point when F_3 fault condition occurs; b) voltage dynamics at the O_3 observation point when F_3 fault condition occurs

129

Table 2.8: TOV reduction with surge arresters adoption on HVDC-LCC system

Type of Fault	TOV [kV] (w/o surge arrester)	TOV [kV] (with surge arrester)	TOV Reduction [%]
F1	671.8	587	12.62
F2	673.7	582.3	13.57
F3	670.7	591.1	11.87

2.4.5   Conclusions

In this section, the EMT analysis of a multi-infeed HVDC system is performed. In particular, the paper focuses on the voltage perturbations that result on the HVDC-LCC DC power cable when different faults occur on the HVDC-VSC link. This type of cable stress is not dangerous for the LCC cable insulator [78], but continued exposure to these types of stresses could lead to premature cable system aging. The use of surge arresters to protect the cable system of the HVDC-LCC connection allows obtaining a reduction in overvoltage of about 12%. To avoid overvoltages on the HVDC links, in the multi-infeed configuration, the surge arrester solution could be adopted in both the VSC and LCC systems. This arrester configuration can be used for further studying the overvoltages, insulation coordination, as well as for improving the reliability index [85–92] and the security of the power transmission system.

Chapter 3

Reliability assessment of the HVDC transmission systems

This chapter describes a general analytical procedure for the availability assessment of HVDC systems. In the introduction of this chapter a review of the main terminologies typically used in the reliability field is presented. Furthermore, different approaches for the estimation of the reliability of HVDC systems are examined to understand the advantages and disadvantages that each method can offer. Moreover, the reliability of the MMC converter is performed by taking into account different redundancies management in order to assess the overall availability of an HVDC-VSC system. Subsequently, by combining the Markov Chain theory and the matrix-based reliability method the availability of multi-terminal HVDC systems is evaluated by taking into account the real spare management of the HVDC components focusing on the cable system.

3.1 Definitions

Below a description of the main parameters that will enter in the availability calculation procedure is presented. These definitions are essential for a complete understanding of the results[91, 93].

Assumptions for the following definitions are that:

- the component under analysis admits only two possible operating states: operational or fault;

- the environmental and operating conditions of the component under analysis are established and that these conditions remain constant over the evaluation time period.

3.1.1 Failure Rate

The failure rate $\lambda(t)$ can be expressed as the "number of failures in the unit of time (typically one year)", i.e. as a measure of the speed at which the failure occurs and its progress is shown in Figure 3.1.
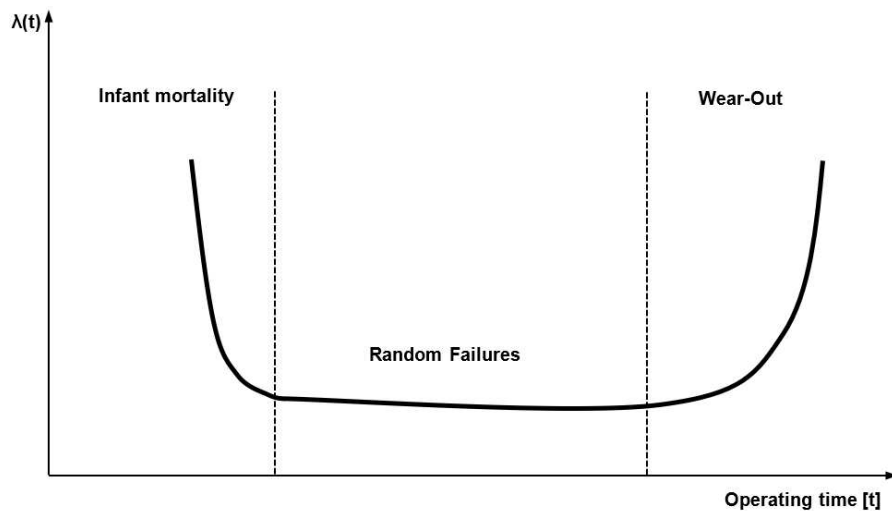
Figure 3.1: Bathtub failure rate curve

This curve is valid for the entire life of a component and three operating zones can be observed:

- Infant mortality zone, which represents the initial period of life of the component that could be defective and therefore fail in a short time. The failure rate, however, drops rapidly to the next zone;

133

- random failures zone, which represents the component's full operation and the failure rate is constant;

- wear-out zone, which represents the period when the component is aging and the failure rate increases until the component fails permanently.

Referring to figure 3.1 the life of the components under analysis can be described through the Weibull distribution, a distribution that belongs to the class of exponential distributions and is a function with two parameters (α and β):

$$y(t) = e^{-(\frac{t}{\alpha})^{\beta}} \tag{3.1}$$

This distribution is used to express the reliability function both during the infantile failure phase and during the useful life and in particular the parameter α expresses the characteristic life of the component while β is a characteristic shape parameter of the distribution. The Weibull probability density function is expressed as:

$$y(t|\alpha, \beta) = \frac{\beta}{\alpha^{\beta}} \cdot t^{\beta-1} \cdot e^{-(\frac{t}{\lambda})^{\beta}} \tag{3.2}$$

Figure 3.2 shows the development of Weibull's probability density as the form factor β changes.

Figure 3.2: Weibull's probability density function as the form factor changes

3.1.2 Repair Rate

The failure rate μ can be expressed as the average number of hours required to make a repair with reference to the component in question.

3.1.3 Reinstallation Time

The reinstallation rate γ can be expressed as the average number of hours required to reinstall the component in question.

3.1.4 Mean Time To Repair

Expresses the average time the component is in a state of failure before it is repaired.

3.1.5 Mean Time To Failure

Mean time to failure (MTTF) is a maintenance metric that measures the average amount of time a non-repairable asset operates before it fails.

$$MTTF = \int_0^\infty R(t)dt \tag{3.3}$$

where R(t) is the reliability function of the component.

3.1.6 Reliability

It is defined as the probability R(t) that a certain component or system will work continuously for a certain time t.

The failure probability density function f(t) is defined as the probability that the component under analysis at time t=0, will fail exactly between time t and t+dt. Thus, the cumulative distribution function (CDF) results to be:

$$F(t) = \int_0^t f(t)dt \tag{3.4}$$

As the cumulative probability density of failure F(t) increases, the R(t) function decreases, in fact the two functions are complementary, the following relationship is valid:

$$R(t) = 1 - F(t) = 1 - \int_0^t f(t)dt \tag{3.5}$$

With reference to (3.1), assuming to be in the trait of useful life (see Figure 3.1) it is possible to express the function R(t) as:

$$y(t) = e^{-(\frac{t}{\alpha})^{\beta}} \tag{3.6}$$

by assuming:

$$\alpha = \tfrac{1}{\lambda} \quad \beta = 1$$

turns out to be:

$$
\begin{cases}
R(t) = e^{\lambda \cdot t} \\
F(t) = 1 - R(t) = 1 - e^{\lambda \cdot t} \\
MTTF = \tfrac{1}{\lambda} \\
MTTR = \tfrac{1}{\mu}
\end{cases}
\tag{3.7}
$$

3.1.7 Availability

It is defined as the probability that at time t the component is in good working order. It can be expressed as the ratio between the operating time in healthy condition and the total time in which operation is required. It is often also expressed as the probability that the system will remain in acceptable operating conditions for a given period of time (typically one year).

3.2 Analysis of HVDC transmission system availability calculation methods

The evaluation of availability and reliability in power transmission systems is becoming increasingly important due to the continuous increase in complexity and number of systems[94, 95]. Today, the continuous increase in distributed generation and the increase in power installed by users leads to less and less predictable power flows. Adapting the system to the new structure, therefore, requires not only a "robust" network but also more flexible, intelligent, and efficient than the current one. HVDC has proven over the years to respond well to the needs of the electrical system, in particular, the development of impressed voltage converters (VSC) has brought countless advantages and with the development of multilevel impressed voltage converters (MMC) there has been a further improvement both in terms of control of transmitted power and a decrease in switching losses with a relative decrease in harmonic content[15, 16, 65, 96–99]. The HVDC-VSC systems, widely described in chapter 1, also allow the use of cables with extruded polyethylene insulation (XLPE), which is not negligible given the wide market for this type of cables. However, technological development has led to the adoption of more and more complex systems and therefore there has been a considerable increase in the number of components that must interact in a coordinated and uninterrupted way to make the service availability constant. In particular, the HVDC-MMC systems that adopt multilevel converters must guarantee certain standards of reliability, and typically a design of the conversion systems is carried out, using different redundancy strategies, so that the level of reliability is reached coincides with or exceeds the maintenance period programmed for the converter. As regards the evaluation of the availability of HVDC-VSC systems (but it can be extended to a large number of electrical systems) it is possible to state how a preventive evaluation of the availability can allow making a better choice on the number of reserve components that a system requires to maintain a certain level of total availability. Moreover, it provides a necessary analysis tool during the feasibility analysis of the plant because it allows studying in an average period (typically one year) how much power will be transmitted. It is therefore immediate to observe that:

- the procedural evaluation of reliability is not unrelated to the design of the conversion system, on the contrary, it becomes support in the design phase;

- a preventive evaluation of the availability allows knowing the average power transmitted in a period of considered time and optimal management of the warehouse thanks to the knowledge of the necessary minimum reserves in order to maintain that degree of chosen availability.

3.2.1 Basic concepts on the evaluation of availability

With reference to the generic scheme of a multi-terminal HVDC system:
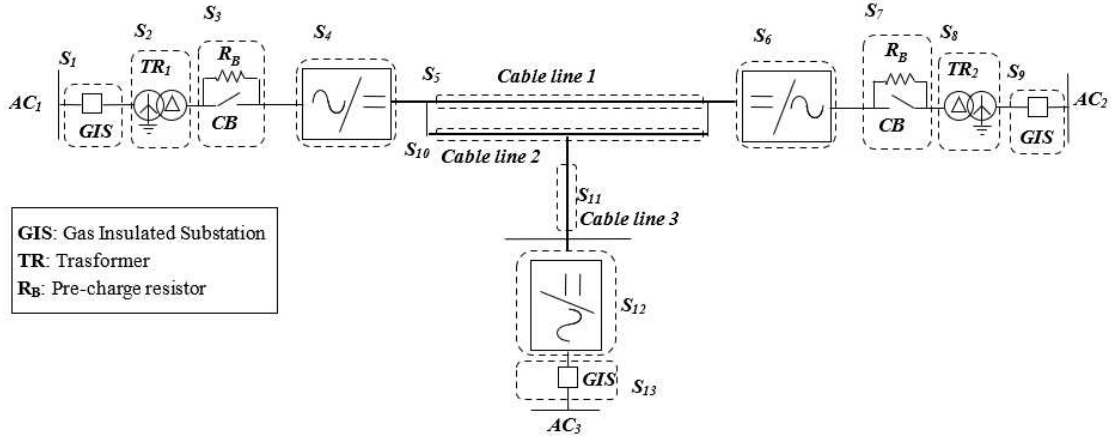
Figure 3.3: diagram of a multiterminal HVDC system divided into subsystems

The total A_s availability of the HVDC system derives from knowledge of the availability of the individual A_i subsystems[91, 93]. The A_i availability calculation is based on knowledge of the failure rates i [occurrences/year] and repair rates i [number of repairs/maintenance time] of each component. The simplest method for the calculation of availability for individual components results from the following expression:

$$\mathbf{A_i} = \frac{MTTF_i}{MTTF_i + MTTR_i} \tag{3.8}$$

and the availability of the complete system is the product of the availability of the individual components:

$$\mathbf{A_s} = \prod_{i=1}^{n} \mathbf{A_i} \tag{3.9}$$

It has to be noted that (3.9) can be applies only to systems without redundancy (the loss of a component puts the entire system out of service).

Starting from the expression (3.8) several methods have been developed in the technical literature. These methods can be classified by the way in which A_i and A_s availabilities are assessed.

3.2.2   Availability assessment methods for HVDC systems

The availability assessment methods for HVDC systems can be divided into two categories:

- analytical methods;
- simulative methods.

The analytical methods are mainly the following:

- Markov models;
- multi-state reliability (MSR);
- Bayesian networks.

The simulative methods are mainly the following:

- Montecarlo.

A requirement, which applies to all methods of availability assessment, is that each individual component can have two possible states:

- healthy component (ON);
- faulty component (OFF).

The main difference between these two approaches lies in the information they provide as a result. Analytical methods provide a single value as a result that only takes into account the events that the user believes are possible for that particular configuration, associating to these events also a certain transmitted power capacity if the evaluation of the probability of transmission of a certain percentage of the total transmitted power is required. The analytical methods also have the considerable advantage of having an extremely limited computation time (a few seconds). The disadvantage of the analytical methods lies in the fact that they do not provide any information regarding the temporal evolution of the component state and therefore it is not possible to evaluate the probability that a component (or system) has a certain availability value, which instead can be observed through the probability distributions of availability that can be evaluated with the simulative methods. It can be inferred, therefore, how the simulative methods offer a greater amount of information but with the disadvantage of having long computational times (hours).

3.2.3 Markov state diagrams

The great advantage of using Markov state diagrams lies in the possibility of optimising the management of spare parts to maintain a certain degree of availability chosen as a target[62, 89, 91, 93–95, 100]. The set of probabilities of residing in states that put a component (or system) in ON or OFF state are enclosed in a Ω probability space called "Markov state diagram". Following the construction of the Markov state diagram relative to the component under consideration, we extract through a matrix approach and in the system condition at regime, what is called "transition matrix" P_i relative to component i. This matrix has as unknowns the probabilities P_x (with x=1, ..., number of states) to reside in state x (state that can be ON or OFF). Then, taking into account that the sum of the probabilities contained in a state diagram is equivalent:

$$\sum_{x=1}^{n_{states}} p_x = 1 \tag{3.10}$$

the availability A_i relative to the single component is determined through the following relationship:

$$\mathbf{A_i} = \sum_{x=1}^{n_{upstates}} p_{i,x_{up}} = 1 \tag{3.11}$$

Thus, adding up all the probabilities of the states present in the Markov states diagram in which the component was healthy.

Take for example the GIS (Gas Insulated System) component, one of the possible diagrams of the states associated with this component is as follows:

the matrix of the P_{GIS} states associated with the diagram of the states in Figure 3.4 results to be:

$$\begin{bmatrix} -\lambda_{GIS} & 0 & 0 & 0 & \tau_{restock} \\ \lambda_{GIS} & -\mu_{GIS} & 0 & \tau_{refill} & a\lambda_{GIS} \\ 0 & \mu_{GIS} & -\gamma & 0 & 0 \\ 0 & 0 & 0 & -\tau_{refill} & u\lambda_{GIS} \\ 1 & 1 & 1 & 1 & 1 \end{bmatrix} \begin{bmatrix} p_1 \\ p_2 \\ p_3 \\ p_4 \\ p_5 \end{bmatrix} = \begin{bmatrix} 0 \\ 0 \\ 0 \\ 0 \\ 1 \end{bmatrix} \tag{3.12}$$

By solving the system of equations (3.12) all the probabilities (five in this case) of residing in each of the states shown in 3.4 are determined. Applying the (3.11) one
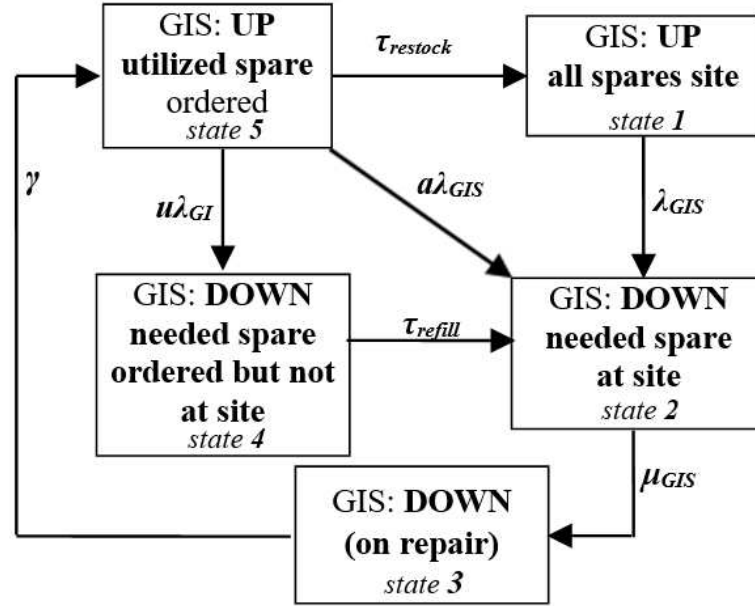
Figure 3.4: Markov state space diagram of the GIS subsystem

has:

$$\mathbf{A_i} = p1 + p5 \qquad (3.13)$$

Where p_1 and p_5 are the only two states in which the component is healthy and therefore the only two probabilities to be taken into account when assessing availability.

It is therefore possible to make some fundamental considerations:

- the method is applicable starting from the knowledge of failure, repair and reinstallation rates, therefore, it does not need other algorithms for the application of the method;

- the construction of Markov's state diagrams is strongly dependent on the designer's technical knowledge, since it is necessary to insert in the diagram the states that are really possible to happen;

- the custom construction of Markov's diagrams with the states that the system could actually assume allows to eliminate the states that surely won't happen, particularly very important that other methods (especially those that use a simulative approach) neglect.

142

It should be noted that, strictly speaking, if one were interested in assessing availability no longer in a regime situation but dependent on time, it is possible to use the Markov diagrams approach, but the system of algebraic equations (3.13) becomes a system of differential equations whose resolution is of little practicality. This complication would lead to the logical choice of simulative methods as we shall see below.

3.2.4 Multi-State Reliability Method

The Multi-State Reliability (MSR) method is very effective when assessing the availability of a very complex HVDC system such as a multi-terminal direct current connection (MTDC)[90, 92, 100–102]. When a system with components (with i=1, ..., n) is taken, all states in which the overall system can reside are represented by the $C_{[i]}$ matrix whose construction is shown in (3.14).

$$
\mathbf{C_{[1]}} = \begin{array}{cc} \mathbf{c}^{E_1(1)} & \mathbf{c}^{E_1(2)} \\ \begin{bmatrix} 1 & 0 \\ 0 & 1 \end{bmatrix} \end{array}
\quad
\mathbf{C_{[2]}} = \begin{array}{cccc} \mathbf{c}^{E_1(1)} & \mathbf{c}^{E_1(2)} & \mathbf{c}^{E_2(1)} & \mathbf{c}^{E_2(2)} \\ \begin{bmatrix} 1 & 0 & 1 & 0 \\ 0 & 1 & 1 & 0 \\ 1 & 0 & 0 & 1 \\ 0 & 1 & 0 & 1 \end{bmatrix} \end{array}
$$

$$
\mathbf{C_{[3]}} = \begin{array}{cccccc} \mathbf{c}^{E_1(1)} & \mathbf{c}^{E_1(2)} & \mathbf{c}^{E_2(1)} & \mathbf{c}^{E_2(2)} & \mathbf{c}^{E_3(1)} & \mathbf{c}^{E_3(2)} \\ \begin{bmatrix} 1 & 0 & 1 & 0 & 1 & 0 \\ 0 & 1 & 1 & 0 & 1 & 0 \\ 1 & 0 & 0 & 1 & 1 & 0 \\ 0 & 1 & 0 & 1 & 1 & 0 \\ 1 & 0 & 1 & 0 & 0 & 1 \\ 0 & 1 & 1 & 0 & 0 & 1 \\ 1 & 0 & 0 & 1 & 0 & 1 \\ 0 & 1 & 0 & 1 & 0 & 1 \end{bmatrix} \end{array}
\tag{3.14}
$$

$$
\mathbf{C_{[i]}} = \begin{bmatrix} \mathbf{C_{[i-1]}} & 1 & 0 & \ldots & 0 & 0 \\ \mathbf{C_{[i-1]}} & 0 & 1 & \ldots & 0 & 0 \\ \vdots & \ldots & \ldots & \ldots & \ldots & \ldots \\ \mathbf{C_{[i-1]}} & 0 & 0 & \ldots & 1 & 0 \\ \mathbf{C_{[i-1]}} & 0 & 0 & \ldots & 0 & 1 \end{bmatrix}
$$

It can be noted that the columns of the matrix $C_{[i]}$ represent the event vectors $C^{Ei(k)}$, i.e. all the independent events that can occur for each single component, in which the component was healthy (k = 1) or was broken (k = 2) respectively. On

144

the other hand, the rows of the matrix $C_{[i]}$ represent the $s_i = 2^i$ MECE (mutually exclusive and collectively exhaustive) events. Once the matrix X has been identified, it is necessary to identify, for each component, what is the probability that the event $E_{i(k)}$ will occur. Therefore, the generic vector $P_{[i]}$ that identifies the probability that the i-th component resides in the j-th state (for i=1, ..., n and j=1, ..., s_i) is equivalent to:

$$\mathbf{P_{[i]}} = \begin{bmatrix} p_{[i-1]} \cdot p_1 \\ p_{[i-1]} \cdot p_1 \\ \vdots \\ p_{[i-1]} \cdot p_j \\ \vdots \\ p_{[i-1]} \cdot p_s i \end{bmatrix} \tag{3.15}$$

For a system consisting of 3 components, the matrices $C_{[3]}$ and $P_{[3]}$ are:

$$
\mathbf{C_{[3]}} =
\begin{array}{cccccc}
\mathbf{c}^{E_{1(1)}} & \mathbf{c}^{E_{1(2)}} & \mathbf{c}^{E_{2(1)}} & \mathbf{c}^{E_{2(2)}} & \mathbf{c}^{E_{3(1)}} & \mathbf{c}^{E_{3(2)}}
\end{array}
\begin{bmatrix}
1 & 0 & 1 & 0 & 1 & 0 \\
0 & 1 & 1 & 0 & 1 & 0 \\
1 & 0 & 0 & 1 & 1 & 0 \\
0 & 1 & 0 & 1 & 1 & 0 \\
1 & 0 & 1 & 0 & 0 & 1 \\
0 & 1 & 1 & 0 & 0 & 1 \\
1 & 0 & 0 & 1 & 0 & 1 \\
0 & 1 & 0 & 1 & 0 & 1
\end{bmatrix}
$$

$$
\mathbf{C_{[3]}} =
\begin{array}{ccc}
\mathbf{c}^{E_{1(1)}} & \mathbf{c}^{E_{2(1)}} & \mathbf{c}^{E_{3(1)}}
\end{array}
\begin{bmatrix}
1 & 1 & 1 \\
0 & 1 & 1 \\
1 & 0 & 1 \\
0 & 0 & 1 \\
1 & 1 & 0 \\
0 & 1 & 0 \\
1 & 0 & 0 \\
0 & 0 & 0
\end{bmatrix}
\tag{3.16}
$$

$$
\mathbf{P_{[3]}} =
\begin{bmatrix}
p_{1(1)} \cdot p_{2(1)} \cdot p_{3(1)} \\
p_{1(2)} \cdot p_{2(1)} \cdot p_{3(1)} \\
p_{1(1)} \cdot p_{2(2)} \cdot p_{3(1)} \\
p_{1(2)} \cdot p_{2(2)} \cdot p_{3(1)} \\
p_{1(1)} \cdot p_{2(1)} \cdot p_{3(2)} \\
p_{1(2)} \cdot p_{2(1)} \cdot p_{3(2)} \\
p_{1(1)} \cdot p_{2(2)} \cdot p_{3(2)} \\
p_{1(2)} \cdot p_{2(2)} \cdot p_{3(2)}
\end{bmatrix}
=
\begin{bmatrix}
A_1 \cdot A_2 \cdot A_3 \\
U_1 \cdot A_2 \cdot A_3 \\
A_1 \cdot U_2 \cdot A_3 \\
U_1 \cdot U_2 \cdot A_3 \\
A_1 \cdot A_2 \cdot U_3 \\
U_1 \cdot A_2 \cdot U_3 \\
A_1 \cdot U_2 \cdot U_3 \\
U_1 \cdot U_2 \cdot U_3
\end{bmatrix}
$$

It can be seen how the matrix $C_{[3]}$ can be reduced since the even columns represent the complement of the odd columns, while the probabilities $P_{i(k)}$ that make up the matrix $P_{[3]}$ are the availability for the component that is healthy (k = 1) and the unavailability for the component that is faulty (k = 2).

It is now necessary to create the system event vector C_{sys_3} that characterizes a certain situation of the overall system. This is possible by combining the event vectors $C^{[E_i(k)]}$ that make up the matrix $C_{[3]}$ using the Boolean operators.

For example, to calculate the overall availability of the system composed of 3 components, it is necessary to determine the event vector that takes into account only the states in which the system is always healthy:

$$\mathbf{C_{sys_{[3]}}} = \mathbf{C^{E_1(1)}} \ \& \ \mathbf{C^{E_2(1)}} \ \& \ \mathbf{C^{E_3(1)}} \tag{3.17}$$

The total availability of the system can therefore be evaluated as:

$$\mathbf{P(E_{sys})} = \mathbf{C_{sys[3]}} \cdot \mathbf{P_{[3]}} \tag{3.18}$$

in matrix form then:

$$\mathbf{P(E_{sys})} = \begin{bmatrix} 1 & 0 & 0 & 0 & 0 & 0 & 0 & 0 \end{bmatrix} \cdot \begin{bmatrix} A_1 \cdot A_2 \cdot A_3 \\ U_1 \cdot A_2 \cdot A_3 \\ A_1 \cdot U_2 \cdot A_3 \\ U_1 \cdot U_2 \cdot A_3 \\ A_1 \cdot A_2 \cdot U_3 \\ U_1 \cdot A_2 \cdot U_3 \\ A_1 \cdot U_2 \cdot U_3 \\ U_1 \cdot U_2 \cdot U_3 \end{bmatrix} = A_1 A_2 A_3 \tag{3.19}$$

All possible system configurations can be obtained by suitably combining the event vectors using the logical operators AND, OR, NOR and EXOR.

3.2.5 Bayesian network

The definition of a Bayesian network is as follows[103–105]: "A Bayesian network is a graph made up of nodes and arrows with the property of being oriented and acyclic (ie once a node is chosen, it is not possible to go back to the same node by traveling the network)". The nodes represent random variables that affect the system, while the arrows represent the dependence between the aforementioned variables. The application of Bayesian networks in assessing the availability of HVDC links makes it possible to identify the events that are most likely to lead to the failure of the overall system. This method is based on Bayes' theorem:

$$\mathbf{P(A|B)} = \frac{\mathbf{P(B|A) \cdot P(A)}}{\mathbf{P(B)}} \tag{3.20}$$

where (see Figure 3.5):

- P(A) represents the probability that the main event associated with component A occurs;

- P(B) represents the probability that the event associated with component B that influences the main event A occurs;

- P(A|B) represents the probability conditional on the fact that the main event associated with component A occurs, once event B has already occurred;
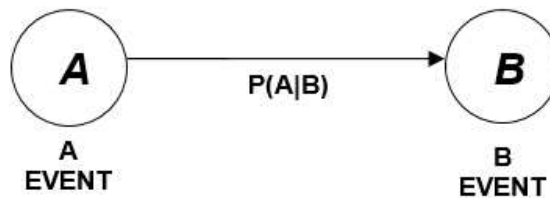
Figure 3.5: Bayesian network consisting of two components A and B

The representation of connections in series and parallel configuration of the components is of particular interest since these are carried out through the use of logic gates.

- Series connection The connections in series configuration are represented by using the AND logic gate (see Figure 3.6);

- Parallel connection Connections in parallel configuration are represented by using the OR logic gate (see Figure 3.7);

As previously mentioned, the objective of this method is to identify which event leads the overall system to failure, therefore, in other words our objective function
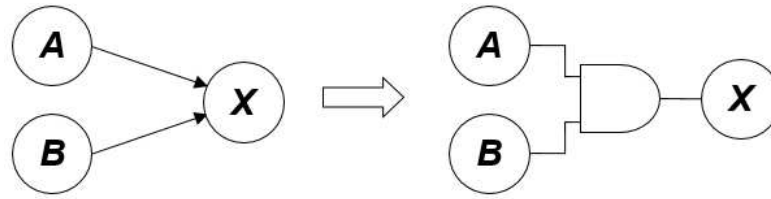
Figure 3.6: Bayesian network consisting of two components A and B connected in series configuration
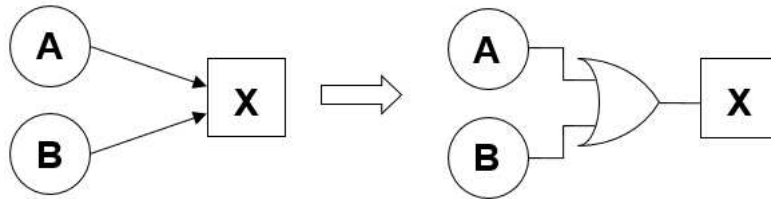
Figure 3.7: Bayesian network consisting of two components A and B connected in parallel configuration

TE (Target Event) is the "system failure". It is necessary to have in mind the table of the truth of the two logic gates AND and OR, which is recalled in the following:

We can therefore deduce, bearing in mind our objective function TE (which corresponds to the logic value 1) and the truth tables, that for a series connection the AND logic gate will give a positive output only when the condition P (X = 1 | A = 1, B = 1), that is, both failure events of components A and B are verified, while, in the case of parallel connections we will have a positive output only when at least one of the failure events of A or B occurs is verified. Let us now take as an example a generic system (see Figure 3.7) consisting of four components (A, B, C, D), in which A and B are connected in parallel while C and D are connected in series and the result of the two groups (X1, X2) is in turn connected in series.

Applying Table 3.1 it can be deduced that the probability of reaching the TE is equivalent to:

$$\mathbf{TE} = P(C) \cdot P(D) \cdot P(A) + P(C) \cdot P(D) \cdot P(B) \tag{3.21}$$

where P(Y) with Y generic component is equivalent to:

$$\mathbf{P(Y)} = 1 - e^{-\lambda_Y t} \tag{3.22}$$

149

Table 3.1: Truth tables for AND and OR logic gates

LOGIC GATES			
AND	**OUTPUT**	**OR**	**OUTPUT**
P(X=1|A=0, B=0)	0	P(X=1|A=0, B=0)	0
P(X=1|A=0, B=1)	0	P(X=1|A=0, B=1)	1
P(X=1|A=1, B=0)	0	P(X=1|A=1, B=0)	1
P(X=1|A=1, B=1)	1	P(X=1|A=1, B=1)	1
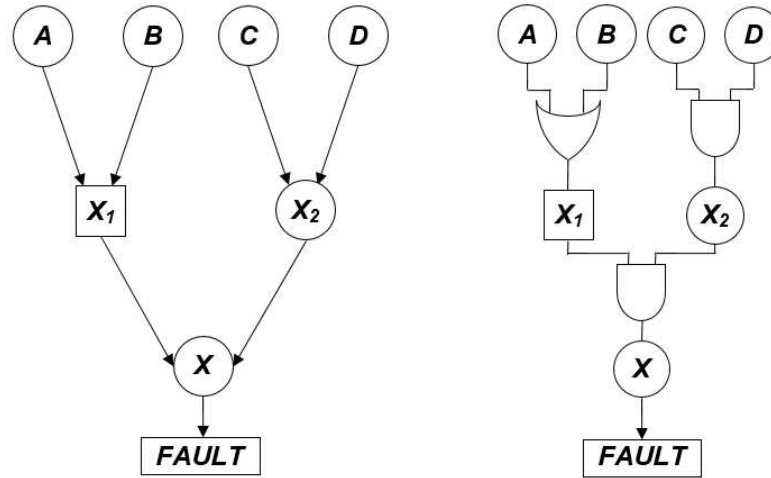
Figure 3.8: Bayesian network consisting of four components (A, B, C, D) connected in series/parallel configuration

Therefore, the availability of the total system is:

$$\textbf{Availability} = \textbf{1} - \textbf{TE} \tag{3.23}$$

If we wanted to evaluate the probability that, once the system is broken, the cause was a failure of component A, for example, this can be evaluated by applying (3.20):

$$\mathbf{P(TE|A = 1)} = \frac{\mathbf{P(A = 1|TE) \cdot P(TE)}}{\mathbf{P(A = 1)}} \tag{3.24}$$

this relationship can obviously be applied to any component of the system.

3.2.6 Montecarlo

The Montecarlo method is the simulation approach that generally provides more information about the system under analysis[106–108]. It allows to evaluate MTTF and MTTR no longer only in a steady state condition but dependent on time. A necessary condition for using the method is that the MTTF and MTTR follow an exponential distribution of the type:

$$
\begin{aligned}
MTTF &= -\frac{1}{\lambda_i} \cdot \ln N_i \\
MTTR &= -\frac{1}{\mu_i} \cdot \ln N_i
\end{aligned}
\tag{3.25}
$$

where Ni are numbers between 0 and 1, taken randomly from a uniform distribution for each component i. We can therefore deduce how we will have a distribution that defines as time t varies what is the probability of having a certain value of MTTF and MTTR (see Figure 3.9):
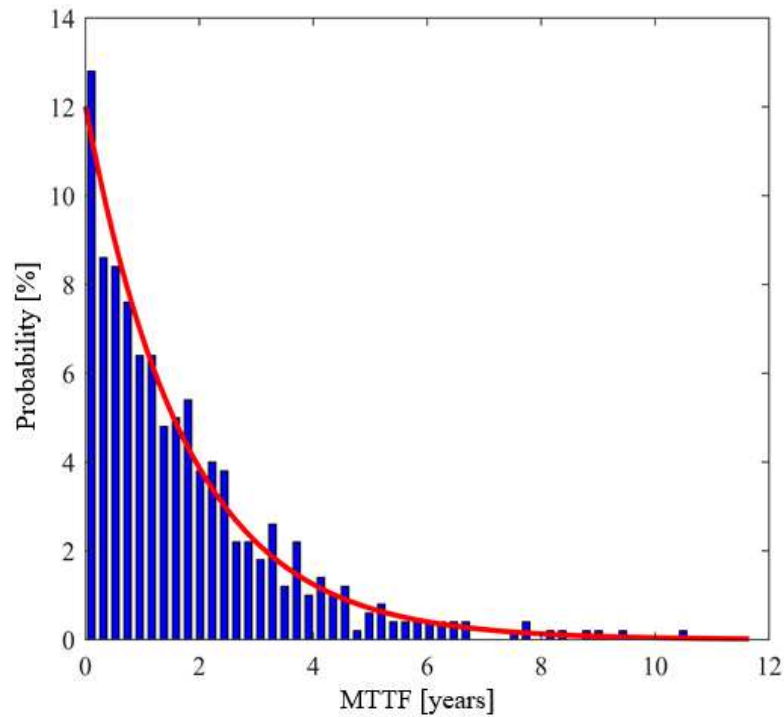
Figure 3.9: Probability distribution of the MTTF parameter over time

The concept on which the Montecarlo method is based lies in combining the "life" of each component, created by generating the distributions of MTTF and MTTR

according to (3.25), appropriately evaluating all the combinations that take the system out of service.

Let us observe a system composed of two components:
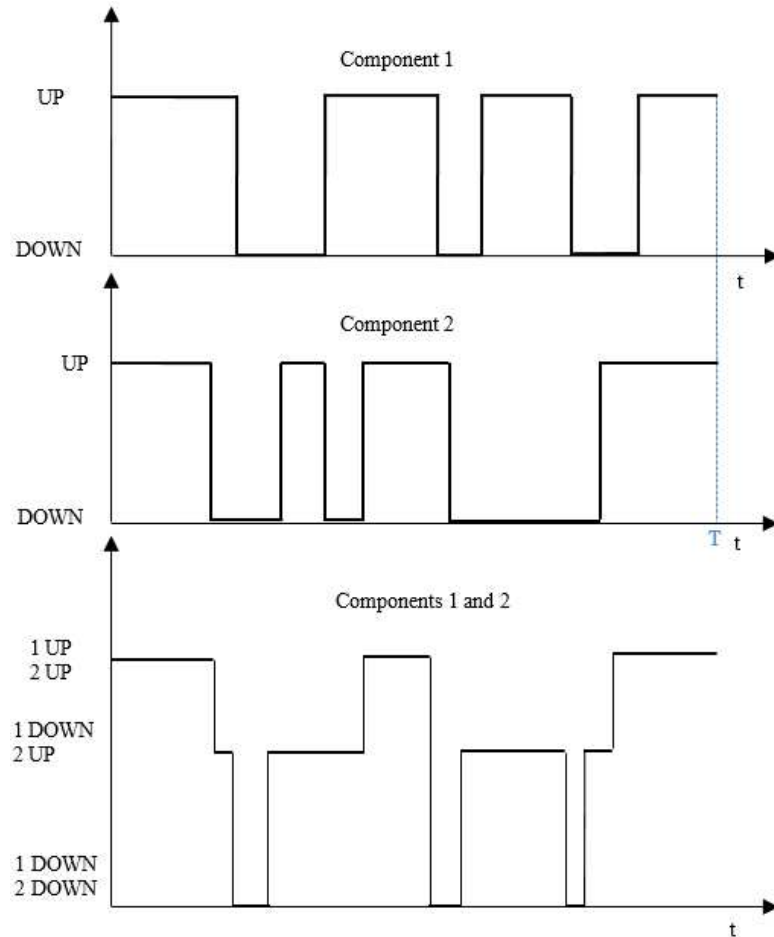
Figure 3.10: life generation of the two-component system with the Montecarlo method

It is possible to observe from Figure 3.10 how the Montecarlo method constructs a life profile of the total system to which it is possible to associate a transmitted capacity. It is therefore possible, once the load diagram of the system to be powered is known, to analyze the instants in time in which the demand for power required by the load is not matched by a transmitted capacity due to a failure of a component of the system (see Figure 3.11), thus defining the ENS (Energy Not Supplied) parameter which therefore allows to quantify the hours of energy not supplied in the time span t being analyzed.
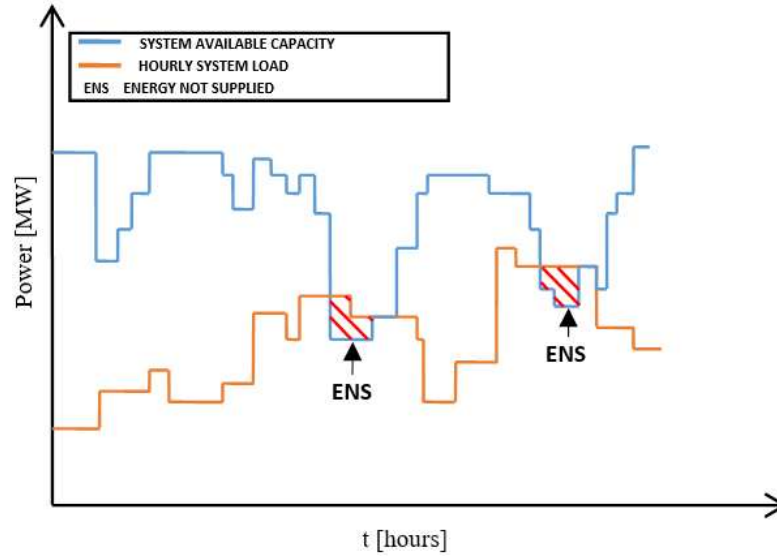
Figure 3.11: Energy not supplied for an HVDC system as a function of load profile variations

The total availability of the system over the period of time considered can therefore be determined as:

$$\mathbf{A} = \frac{\sum_{i=1}^{n_{up}} T_{i,up}}{\sum_{i=1}^{n_{up}} T_{i,up} + \sum_{i=1}^{n_{down}} T_{i,down}} \tag{3.26}$$

with $T_{i,up}$ and $T_{i,down}$ the durations of the respective UP and DOWN states of the system.

It is of fundamental importance to note that:

- The Montecarlo method provides a probability distribution of availability and not a single average value;

- The Montecarlo method will always have a higher probability density in the availability value calculated with the expression (3.8), since at steady state the method must tend to the average value of availability at steady state (see Figure 3.12).

It is possible to observe how (3.26) is also applicable to the single components of the system, therefore, this method can also be applied only if one is interested in evaluating the availability of the single components. Since this is a simulation method that creates a fictitious life for each component and for the entire system, it can be easily deduced that the computational weight is not indifferent. In fact,
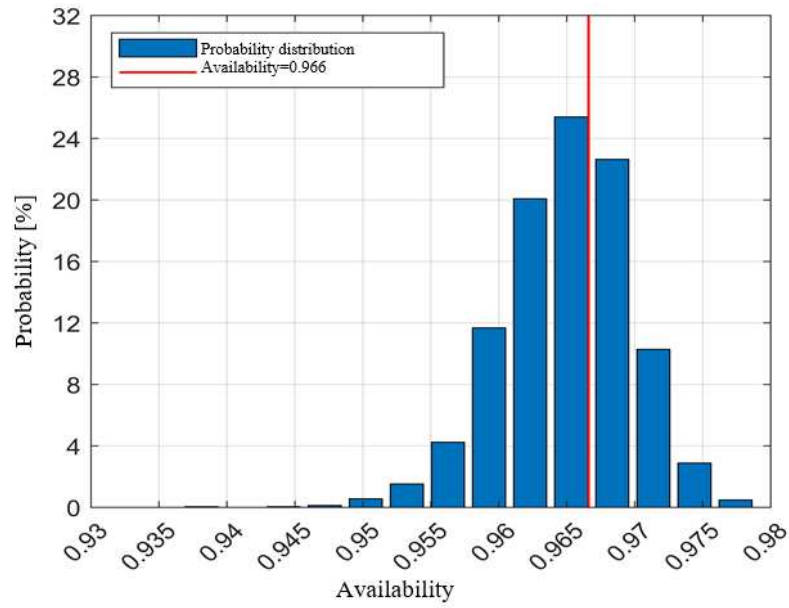
Figure 3.12: Typical output of the Montecarlo approach: the probability distribution of the availability of a given system

typically the calculation times can range from minutes to several hours depending on whether one is interested in evaluating the availability of single components or complex systems.

3.2.7 Summary of the main peculiarities of each computation method

In Table 3.2, the main influence variables which can be considered with each of the described methods have been briefly summarized.

Table 3.2: Summary of the chief influence variables which each method is able to take into account in the availability computation

Influence Variables	Methods			
	Markov models	Multi-State Matrix	Montecarlo	Bayesian network
Spare Management	X	X		
Multi-terminal connection		X	X	X
Topology of the system		X	X	X
Availability of the system over the time	X		X	
Transmittable power estimation		X	X	

3.3 HVDC-VSC XLPE Cable Availability Assessment Through Markov Modelling

This section proposes a modus operandi, based on analytical methods, for availability assessment of HVDC-VSC point-to-point connections. In particular, cross-linked-polyethylene-extruded cable links are investigated with focus on symmetrical monopoles, the most common configuration in recent high-capacity land projects: availability estimation of a typical layout is carried out. Key reliability features of state-of-the-art modular multilevel converter are highlighted: modularity and easy assembly of redundant IGBT sub-modules for long-lasting fault tolerant operation. Different redundancy strategies are evaluated: cold standby and active redundant conventional mode with constant sub-module failure rates, warm standby and load-sharing active redundant mode with sub-module failure rates changing upon successive sub-module failures. Closed-form equations for reliability function calculation are used for all strategies in this work. Fulfilling results are obtained also for warm standby and load sharing active schemes in realistic functioning conditions. Steady-state availability of the subsystems, in which the whole link is partitioned for ease of calculation, is estimated by means of Markov models. The converter planned availability is also included by considering a converter redundant design assuring high probability of fault-tolerant operation through the time interval between scheduled maintenances usually chosen by utilities. Basic policy for reaching target levels of availability in critical connections of this kind is expounded.

3.3.1 Introduction

HVDC VSC (voltage-source-converter) transmission gains growing interest for its capability of providing multiple vital services within electrical power networks. By making bulk power transfer over long distances more economic and links between non-synchronous grids feasible, it facilitates power exchanges between zones with different production/load and seasonal patterns, so enabling efficient electricity markets and improving security of supply. The HVDC VSC operational flexibility and favourable technical characteristics make it possible to foresee an ever increasing utilization of VSC technology in combination with cross-linked-polyethylene-extruded (XLPE) cables. These systems look like the most suitable way for grid-integration of isolated sources of renewable energy. At the same time, the presence of VSC-based links provides valuable benefits to the grid in the form of supply of reactive power and other ancillary services, which can be secured even if an outage interrupts the transmission function itself. this work focuses on the employment of analytical methods for reliability/availability assessment of HVDC VSC point-to-point connections; in particular, symmetrical monopoles made of underground spans of XLPE cable will be investigated and an exemplificative

calculation for a typical layout carried out. Key reliability features of modular multilevel converters (MMC) are highlighted and closed-form reliability equations, fitting to the operative features of the two most widespread converter alternative structures for HVDC transmission, are applied. It is worth noting that, with respect to specific components only recently installed in commercial plants, the input values relating to their performance characteristics being used in reliability estimations originate from both accelerated lifetime tests and rational interpretation of the scarce, often incoherent, on-field statistics available. On the other hand, VSC transmission systems also include conventional industrial equipment for which large statistical collections exist. The state-of-the-art of modular multilevel converters technology [2, 34, 69, 109–111], selected for the most recent VSC transmission projects, shows many advantages from a reliability standpoint. Converters with high number of voltage steps generate the requested output voltage waveform with a low harmonic content. A MMC consists of three phase legs (pl), each of them composed of an upper and a lower arm. Each arm includes a high number of sub-modules (SM). The two most common SM architectures for HVDC VSC cable applications consist of:

- single-IGBT valves configuration, wire-bonded, base-insulated package Hi pack SMs: (I-SM in the following);

- multiple IGBT valves configuration, presspack modules in series, namely Stak Pak (SP: S-SM in the following) [69, 110].

The SMs are connected in series with one converter reactor (CR), whose function is both to limit short-circuit currents through the valves in the event of a fault and to reduce the balancing currents between individual phases to very low values. Each sub-module basically contains:

- an IGBT-based half bridge (HB) converter;

- a DC capacitor module for energy storage.

Basic and efficient half-bridge based MMCs find optimal utilization in HVDC VSC point-to-point symmetrical monopoles with XLPE cables. Inherently permanent cable faults are usually cleared by opening AC circuit breakers to permit repair of the affected section with de-energized circuit. In contrast to overhead lines, no full-bridge SMs (which, in case of temporary faults, contrast the short circuit current by generating an opposite voltage) are needed: the MMCs for cable systems contain the minimal number of IGBTs, requiring reduced investment costs and operating with lower losses and failure probabilities. Some significant contributions in literature highlight the main aspects to estimate HVDC VSC systems availability and reliability. In particular, Wang et al [112] clearly expounds the main reliability

157

issues related to HVDC VSC converters and shows the analytical procedure to determine the reliability function of the converter. Guo et al [113] found that the use of closed form equations for reliability estimation applied to real size HVDC VSC converters (i.e. characterized by a great number of SMs) fails because of round-off errors giving instability in the procedure. Tourgoutian et al [114] proposes an availability assessment of HVDC VSC links by means of Bayesian Network models, by considering system components with only two possible states. In the present work the authors present a procedural approach for overall availability assessment of a point-to-point HVDC VSC symmetrical monopole by making use of Markov models, able to thoroughly represent repair and maintenance processes of system components. To this purpose, as first and essential step, analytical procedures to evaluate the reliability function of HVDC VSC converters of any size, both considering single/multiple IGBT valve configurations and different redundancy strategies, are carried out. These analyses aim at identifying converter redundant configurations which guarantee, from a statistical standpoint, uninterrupted operation along the interval between scheduled maintenances. Then unavailability figures of each sub-system of the link can be estimated by means of Markov models, whereas the converter unavailability due to planned outages is also computed by considering periodic down times for maintenance, external causes of converter failures neglected.

3.3.2 Overview of HVDC-VSC symmetrical monopolar configuration

The symmetrical monopole is the preferred operating configuration for land cable projects. It requires two fully insulated cables at the rated voltage $\pm$ Vdc; ground return current is zero. Interface transformers in symmetrical monopoles are exposed to negligible DC stresses, hence regular equipment (usually, three mono-phase units with tap changer) is used. No redundancy of transmission capability is provided by the symmetrical monopole arrangement: the two cables cannot be operated independently. On the other hand, two asymmetric monopoles can be coupled together into a bipolar arrangement, fulfilling more stringent availability requirements against symmetric monopoles of the same rating. In the event of a single pole outage (ground fault, loss of one of the two converters) the bipole can still be operated as asymmetric monopole at reduced capacity allowing uninterrupted power transfer at 50% of link rated capacity (half-redundant system). Repair of faulted items can be carried out while the sound pole operates. The bipolar arrangement is more expensive with respect to the corresponding symmetric monopole as it requires a third low-voltage insulated DC neutral cable (metallic return) and because of the specially designed interface transformers. Owing to the asymmetrical configuration, the transformer is exposed to the DC offset in

the valve side. Contrary to the symmetric case, the tap changer is located on the network side to avoid troubles arising with handling the DC offset. However, the bipole option shows economic benefits in specific conditions like: - projects foreseeing staged increase of transmitted power in the future and operating at the initial stage as asymmetric monopole; - locations where emergency operation with ground or sea electrodes is tolerated, because the investment cost for the third cable is eliminated. Construction of two independent identical parallel symmetrical monopoles is common practice for high capacity projects. Considering both circuits forming a joint transmission system, the transmission capability of this system is 50% (or more for short periods) of the link full rated capacity in case of outage of one single monopole. Hence, the joint system is half redundant from a reliability standpoint. It's straightforward to estimate the availability of the full-rating and the half-rating power transmission function, once the availability of a single monopole has been calculated. Moreover, the configuration with two independent monopoles shows the highest flexibility in case of faults, contributing to the security of supply of the network in which the HVDC link is embedded.

3.3.3 Converter reliability requirements: technological solutions

From a reliability standpoint, the two SM types show different failure modes and mechanisms. A basic reliability requirement for transmission systems is no interruption of operation following a single component failure. Though proven high reliability of factory- tested and assembled SMs, random failures of individual units in operation may not be excluded. Even upon failure of a pre-set SM percentage, the forced outage of the whole converter system must be avoided. This target can be reached by integrating redundancies either at valve level (in the case of S-SM assembly: redundant SPs) or at arm level (in both I-SM and S-SM MMC configurations: redundant SMs). The addition of redundant I-SMs in each converter arm builds-in higher reliability ensuring fault-tolerant operation after individual SM failures, if the faulty component is promptly disconnected and bypassed. To this purpose a high reliable, high speed, mechanical bypass switch along with a protection thyristor (for shunting high fault currents) is mounted inside I-SMs. Hence, the load current continues to flow, while the control turns an idle stand-by redundant SM into operation. On the other hand, the intrinsic SP short circuit failure mode (SCFM) allows the load current continuing to flow through the faulted SP. SP units, stacked in series connection inside each S-SM valve, are not allowed to fail open in order to ensure continuing converter operation: they must fail-safe into a stable short-circuit in every possible failure case [110]. Subsequent open failures of the same SP are instantaneously turned into safe shorts owing to SCFM property, characteristic of the SP structure, till all available chips in the structure

are exploited. In both configurations, each SM IGBT valve is able to work at the nominal SM voltage, though, usually, a safety voltage margin is foreseen. This is necessary for both voltage harmonic reduction and lifetime increase of single SMs (though, beyond voltage stress, other factors, like thermal stress and load profile, influence IGBTs and SM lifetime). The de-rating factor $\eta = \frac{V_i}{V_w}$ usually ranges in the interval (0.5÷0.7), where V_i is the actual operating voltage of the ith SM and V_w is its withstanding voltage. In general, the nominal voltage of each SM is $V_{SM} = s\eta V_w$, where z is the minimal number of IGBTs in series inside the SM valve (z=1 in the case of I-SM; z>1 for S-SM). Each arm consists of $k = \frac{V_{DC}}{V_{SM}}$ SMs at least and it is able to generate k+1 output voltage levels. n-k redundant SMs, with n=k+m where m is the number of redundant SMs, ensure uninterrupted converter operation till failure of (n-k+1) SMs. The arm voltage Varm is

$$V_{arm} = \frac{V_{pl}}{2} = V_{DC} \qquad (3.27)$$
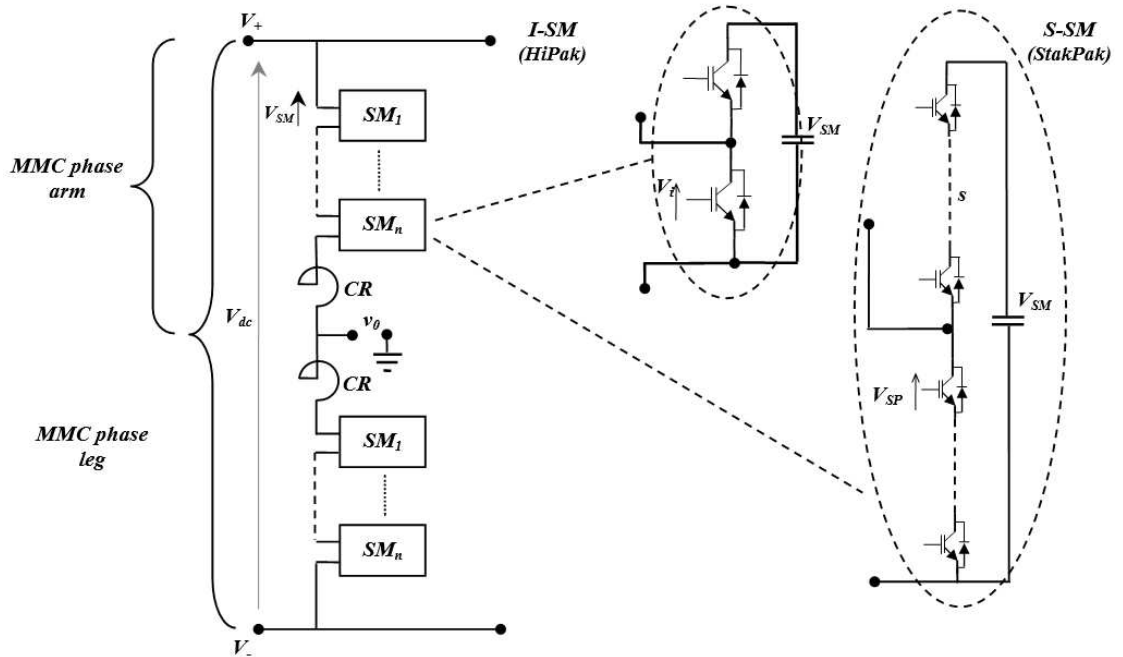
Figure 3.13: I-SM and S-SM MMC configurations converter typology

3.3.4 Availability assessment of HVDC links: analytical methods

For ease of analysis, the HVDC transmission system is split into 4 subsystems. The first step of our reliability study, is to illustrate the reliability block diagrams (RBD)

of each subsystem and of the whole link (see Figure 3.14) in order to define the logical connections among working components needed to fulfil the specified operative function. RBD is a suitable representation of the system as long as its components are statistically independent and non-reparable. The system works if there is an unbroken path from the beginning of the diagram to the end. Each block contains series/parallel connected items. Hence, it is a success-oriented network describing the system power transmission function. Two main performance measures have to be combined to estimate the expected availability of the transmission system object of the present investigation. The former is the reliability function R(t), which is in general of interest for systems observed from the moment they are initially put into service until they fail after uninterrupted operation: components are assumed non-repairable, scheduled outages are usually planned before the expected failure of the system with the purpose of replacing the faulted items. This characteristic fits well with the operation of the conversion system. The latter, the availability function A, is more significant for continuously operated systems, whose components are generally assumed repairable: it can be expressed by the average proportion between the system up time and the sum of system up and down times (steady-state availability, A_∞). Therefore, the availability analysis is of utmost interest for subsystems 1, 2, and 4 of Figure 3.14. In particular, in this work detailed Markov models [91, 93] have been used for availability evaluation. By means of Markov method it is possible to analyse each subsystem wholly and exclusively contained in one RBD block. Extended models allow including into the analysis the occurrence of dependent and common cause failures. Hence, with relation to the stated functions and the operating conditions, reliability is interpreted as the probability of a component/system staying in the operating state without failure, whereas availability is interpreted as the probability of finding it in the operating state at some time into the future [91, 93].
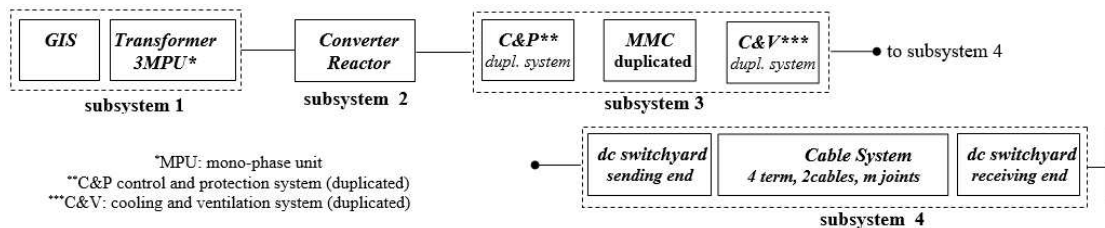
Figure 3.14: RBD of the whole transmission system: each item belonging to the link is shown exclusively in one block

3.3.5 MMC Redundant Configuration alternatives

It is possible to manage redundancies in two modes:

- passive redundant mode, with idle or partially-loaded standby redundant SMs;

- active redundant mode: all redundant and non-redundant SMs in the arm work.

Passive Redundant Mode

In passive redundant mode, the redundant SMs remain on standby in normal operation without bearing any load; zero failure rate is assumed for idle SMs in cold standby. Upon failure of one working SM, it is disconnected and bypassed by a high speed mechanical switch, while one redundant unit is switched into operation by the control to replace the faulted unit. The mean voltage applied to each working SM defined by the arm output voltage is constant, not depending on the number of surviving redundant SMs. The bypass of the faulted item and the passage to full operation of the standby SM actually need time: a transient interval, including SM charging, affects converter operation. The risk of switching failures should be taken into account. Differently, partly loaded redundant SMs (warm standby configuration), which are maintained under voltage but not in operation, show a dormant failure rate much smaller than the working failure rate. Moreover, transition into operation is fast, whereas probability of switching failures can be assumed lower.

Active Redundant Mode

Essentially, two different active redundancy strategies exist, generally referred to as conventional mode and load-sharing mode. The arm consists of n SMs of which m=n-k redundant: all SMs are in active operation and the converter control handles all SMs in the arm in the same way. In the conventional mode, the number of voltage levels, k+1, is constant and an optimization algorithm chooses at any time k SMs to be switched-on among all n SMs. The reference voltage of each SM remains constant upon failure of one SM at its initial nominal value. As a number of SMs larger than the minimum needed for converter operation is available, the mean SM switching frequency is lower and at any time a number of SMs bear zero voltage. With a greater number of working SMs per arm, the control and voltage-balancing algorithms have a larger set of SMs from which selecting the unit to connect or bypass in the next switching instant. The percent switching frequency reduction per SM, proportional to the number of active redundant SMs, is equal to (k/k+m)100. The SM lower average switching frequency has a beneficial effect on its reliability. In contrast, in the load sharing mode, all n SMs equally share the total arm voltage. In this case, all n=k+m SMs resist a voltage at any moment;

the instantaneous voltage blocked by each SM is initially lower than its nominal voltage, whereas the mean SM switching frequency is higher. The voltage applied to each SM increases upon failure of one SM in the arm; consequently, the SM failure rate λ_{SM} increases with direct proportion to the increasing voltage applied. The converter works until only k SMs survive, resisting the nominal arm voltage. This mode of operation exploits the presence of redundant components for improvement of normal operation performance. Individual SM failure rate is initially lower than either in standby and conventional active mode (thanks to reduced voltage stress on single items), but increases with succeeding failures of redundant items. The valve arm failure chance is proportional to the current number n-i, with $0 \leq i \leq k$, of surviving SMs. Higher conduction losses occur in load sharing active redundant mode, though the increase is less than proportional to the number of operating SMs. It is worth noting that the lower mean voltage stress imposed to SMs in load sharing mode versus conventional mode qualitatively implies a reduced failure rate, as explained in [113]. Here, the voltage stress law (normally used for accelerated life tests) was pointed as proper for evaluating the λ_{SM} reduction consequent to the lower voltage stress suffered. In the present work, authors prefer to ignore the benefits of the λ_{SM} reduction due to the lower voltage applied to SMs in load sharing mode, in a similar way as in the case of de-rating applied to components of any type, in line with a more stringent conservative criterion. However, it is easy to consider lower voltage stress as well as de-rating effects on IGBT module failure rates by applying [112, 115]:

$$\lambda_{SM}^{\star} = \lambda_{SM} \times v_s^{\eta} \tag{3.28}$$

where $\lambda_{SM}^{\star}$ is the reduced failure rate and $vs = \frac{V_i}{V_{SM}}$. Within this work only the load sharing active redundancy is considered in the calculations. In conclusion, for both active and passive redundant configurations, the converter reliability increases with the number of redundant SMs per arm though the marginal reliability improvement decreases as the level of redundancy increases.

3.3.6 MMC Reliability Function Calculation By Means Of Closed-Form equations

The reliability function of one SM can be expressed as the product of the reliabilities of its components. For example, by considering only the reliability functions of most vulnerable components like the IGBTs, the capacitor module and the gate unit, the SM reliability function can be expressed as:

$$\mathbf{R_{SM}(t)} = \mathbf{R_{IGBT_1}(t)} \cdot \mathbf{R_{IGBT_2}(t)} \cdot \mathbf{R_{Cm}(t)} \cdot \mathbf{R_{gu}(t)} \qquad (3.29)$$

where:

$$\mathbf{R_{IGBT_1}(t)} = \mathbf{R_{IGBT_2}(t)} = e^{-\int_0^t \lambda_{IGBT}(t)}$$
$$\mathbf{R_{Cm}(t)} = e^{-\int_0^t \lambda_{Cm}(t)} \qquad (3.30)$$
$$\mathbf{R_{gu}(t)} = e^{-\int_0^t \lambda_{gu}(t)}$$

are the reliability functions of the IGBTs, of the capacitor module, and of the gate unit respectively. λ_{IGBT}, λ_{Cm} and λ_{gu} are the corresponding failure rates. The validity of the bathtub failure pattern for electronic components is universally recognized. Hence, by assuming each module operating in the incidental failure period with all its components following exponential lifetime distributions, with:

- cumulative distributed function (CDF) in the form:

$$\mathbf{F(t)} = 1 - e^{-\lambda t} \qquad (3.31)$$

- probability density function (PDF): f(t)=λ_e-λ_t with t>0, $\lambda > 0$, characterized by constant hazard rate z(t)=f(t)/[1-F(t)]=$\lambda > 0$, (i.e. components as good as new as long as they are working) the reliability function RSM(t) of a SM may be written in exponential form as:

$$\mathbf{R_{SM}(t)} = e^{-2\lambda_{IGBT}t} \cdot e^{-\lambda_{Cm}t} \cdot e^{-\lambda_{gu}t} = e^{-(2\lambda_{IGBT}+\lambda_{Cm}+\lambda_{gu})t} \qquad (3.32)$$

The converter phase leg consists of one upper valve arm (at positive potential) and one lower valve arm (at negative potential) with a converter reactor connected in series to each valve arm (see Figure 3.13). Both valve arms contain n statistically identical independent distributed (i.i.d.) series connected SMs. k of them are sufficient to withstand the arm voltage, n-k are redundant (either standby or active). The reliability function $R_{va}(t)$ of the valve-arm k-out-of-n:G redundant system is the sum probability of having at time t a number of surviving SMs greater

than or equal to k; it can be expressed by means of the binomial distribution [34]:

$$\mathbf{R_{va}(t)} = \sum_{i=k}^{n} \binom{n}{i} (e^{-(\lambda_{SM}t)^i})(1 - e^{-(\lambda_{SM}t)^{n-i}}) \tag{3.33}$$

and its mean time to failure (MTTF) is:

$$\mathbf{MTTF} = \sum_{i=k}^{n} \binom{n}{i} \int_{0}^{\infty} (e^{-(\lambda_{SM}t)^i})(1 - e^{-(\lambda_{SM}t)^{n-i}}) dt = \frac{1}{\lambda_{SM}} \sum_{i=k}^{n} (\frac{1}{i}) \tag{3.34}$$

Hence, the reliability functions of upper $R_{ua}(t)$ and lower $R_{la}(t)$ arm are given by:

$$\mathbf{R_{ua}(t)} = \mathbf{R_{la}(t)} = \mathbf{R_{va}(t)} \cdot \mathbf{R_{CR}(t)} \tag{3.35}$$

where R_{CR} is the reliability of the converter reactor. Since one phase leg works only if both its upper and lower arms work, the phase leg reliability $R_{pl}(t)$ is:

$$\mathbf{R_{pl}(t)} = \mathbf{R_{ua}(t)} \cdot \mathbf{R_{la}(t)} \tag{3.36}$$

The whole converter only works if all the three phases simultaneously operate. Its reliability function $R_{Conv}(t)$ is therefore:

$$\mathbf{R_{Conv}(t)} = (\mathbf{R_{pl}(t)})^3 \tag{3.37}$$

In this section, for the I-SM converter, although active redundancy is usually preferred for simpler SM construction (no need of switch-on devices), also the cold standby and the warm standby cases are developed. Cold standby is a theoretical, limit case, whereas the warm standby operation mode is applied in real installations. These analyses are useful for comparison with the active redundant case. For the S-SM converter the analysis of the active redundant mode is carried out: at S-SM level it is imposed by the constructive features of this technology, whereas at arm level both active and standby operation modes of redundant S-SMs are feasible. The Markov chain model is of conventional use for representing system behaviour with transitions between states upon failure of single SMs, for both the load-sharing active redundant and the warm standby redundant systems [93]. The change of SMs failure rate under varying stress conditions is explicitly shown. The calculation of the time-dependent state probabilities implies the solution of the corresponding set of differential equations, whose numerical computation is time-consuming. On the opposite, use of closed-form equations, exploiting the properties of exponential

distributions, simplifies computations still providing accurate solutions in practical conditions.

I-SM Cold standby Redundant Mode

The converter valve arm is assumed operating as k-out-of-n:G cold standby redundant system of i.i.d. SMs with perfect monitoring and switching. (n-k) SMs are assumed initially idle with zero failure rate (no SM failure possible in standby mode). At any time, k identical SMs work in series with individual failure rate λ_{SM}: the series working failure rate is equal to the sum of components failure rates. Hence, the valve arm series subsystem shows failure rate k·λ_{SM}. Whenever one SM fails, it is short-circuited by the local control and instantly replaced by switching-on one standby item. The new subseries follows the exponential distribution with the same failure rate k·λ_{SM} (because of the memory-less property of the exponential distribution: each one of the k SMs included in a new subseries is assumed as good as new). As soon as the subsystem consisting of the last k surviving SMs fails, the valve arm and the whole converter fail. Valve arm lifetime is expressed as:

$$\mathbf{T_{va}} = T_1 + T_2 + ... + T_i + ... + T_{n-k+1} \tag{3.38}$$

where each of the n-k i.i.d. random variables (rv) Ti, represents the exponential distributed lifetime of the i_{th} subsystem consisting of k working SMs. The sum T_{va} of the exponential i.i.d. rv T_i follows the gamma distribution:

$$\mathbf{\Gamma}(k \cdot \lambda_{SM}, n - k + 1) \tag{3.39}$$

with scale parameter $k \cdot \lambda_m$ and shape parameter n-k+1. The probability density function (PDF) is therefore given by:

$$\mathbf{f_{va}}(t) = k \cdot \lambda_{SM} \cdot e^{-k \cdot \lambda_{SM} t} \frac{(k \cdot \lambda_{SM} t)^{n-k}}{(n-k)}, \quad t \geq 0 \tag{3.40}$$

Hence, in case of cold standby redundant mode, the general expression for the k-out-of-n:G valve-arm system reliability, $R_{va}(t)$, turns into:

$$\mathbf{R_{va}}(t) = e^{-k \cdot \lambda_{SM} t} \sum_{j=0}^{n-k} \frac{(k \cdot \lambda_{SM} t)^j}{j!} \tag{3.41}$$

I-SM Warm Standby Redundant Mode

In reality, redundant standby SMs are initially energized (capacitor charge) and often cyclically switched by the control function from standby to active operation to the purpose of uniform exploitation of all SMs in the arm. Warm standby SMs may fail in dormant state, whereas active SMs may fail in operation; all identical SMs show exponential distributed lifetimes with parameter λ_d in the dormant state and λ_o in the active state, respectively(normally, $\lambda_d \ll \lambda_o$). By hypothesizing perfect sensing and switching and by excluding occurrence of simultaneous SMs failures, a closed form equation for the valve arm k-out-of-n:G warm standby redundant system reliability can be obtained. From the reliability expression of the k-out-of-n system, by taking into account the first operating SM failure at instant t1 and expanding the pdf in recursive way, the bound (t-tn-k;k,k) is finally reached. Integrating recursively the n-k terms and rearranging, the reliability of the valve-arm k-out-of-n warm standby redundant system, taking into account the consecutive failures of all redundant (n-k) SMs, can be written as [116]:

$$\mathbf{R_{va}}(t) = \frac{1}{(n-k)!\lambda_d^{n-k}} \sum_{i=0}^{n-k} (-1)^i \binom{n-k}{i} \cdot \left[\prod_{j=0, j \neq i}^{n-k} (k \cdot \lambda_o + j \cdot \lambda_d) \right] \cdot e^{-(k \cdot \lambda_o + i \cdot \lambda_d)t} \tag{3.42}$$

When $\lambda_d=0$, the equation gives the reliability of the k out of n cold standby redundant valve-arm system. Amari et al. [117] find that the k-out-of-n warm standby redundant system with dormant failure rate λ_d behaves like a k_d-out-of-n_d active redundant system for which the failure (hazard) rate of each component is λ_d, while $k_d = k\lambda_o/\lambda_d$ and n_d=n-k+k_d. Consequently, the valve arm warm standby redundant system can be viewed as an active redundant system with modified parameters. Hence, the reliability of the valve arm system can be expressed as:

$$\mathbf{R_{va}}(t) = \sum_{i=0}^{n-k} \binom{n_d}{i} (e^{-\lambda_d t})^{n_d-i} (1 - e^{-\lambda_d t})^i \tag{3.43}$$

The problem of round-off errors which may occur by applying (9), especially in case of a great number of SMs per valve arm is completely removed.

I-SM k-out-of-n Active Redundant System with Load Sharing

From the beginning, all the n identical I-SMs share the arm nominal voltage. Each converter arm is modelled as k-out-of-n:G active redundant system of i.i.d. SMs. In the event of one SM failure, the surviving SMs go on working, equally sharing the constant arm nominal voltage. Consequently, as verified in real working

167

circumstances, the individual SM failure rate increases with direct proportionality to the increasing voltage resisted. Upon i_{th} failure, the individual SM failure rate of each of the n-i surviving SMs is:

$$\lambda_{SM}^0 \leq ... \leq \lambda_{SM}^i \leq ... \leq \lambda_{SM}^{n-k} \quad 0 \leq i \leq n-k. \tag{3.44}$$

The arm and the whole converter fail as soon as n-k+1 SMs fail. Since all i.i.d. I-SMs follow the exponential distribution, the interarrival times to failure (i.e. the time between the i-1th and the ith failure) are independent random variables $X_i = T_i \check{\ } T_{i-1}$, where Ti is the time to the ith failure, assuming $T_0 \equiv 0$, i=1,2,...,n-k+1 and following the same exponential distribution with parameter $\theta = \theta_i = (n-i)\lambda_{SM}^{i-1}$, with i=1,2,..., n-k+1. It is worth considering that as:

- direct proportionality of SM failure rate increase with the increase of the voltage applied to it upon failure of one redundant SM is assumed within this work;

- the number n-i of surviving SMs in the valve arm is inversely proportional to the voltage increase;

the valve arm total failure rate remains constant with i. The lifetime of the I-SM valve arm $T_{va} = X_1 + X_2 + \ldots + X_{n-k+1}$, sum of n-k+1 i.i.d. r.v., follows the gamma distribution $\Gamma(\theta, n-k+1)$ with pdf:

$$\mathbf{R_{va}} = \frac{\theta(\theta t)^{n-k}}{(n-k)!}e^{-\theta t} \tag{3.45}$$

Therefore, the k-out-of-n:G active redundant valve arm system reliability function and MTTF can be expressed as

$$\mathbf{R_{va}} = e^{-\theta t} \sum_{j=0}^{n-k} \frac{(\theta t)^j}{j!} \tag{3.46}$$

S-SM MMC Reliability Calculation

One S-SM consists of two multiple-IGBT valves and one storage capacitor in logical series. The whole S-SM fails if any of the component subassemblies fails. IGBTs in the same valve must switch simultaneously. Each valve contains several identical SP devices stacked in series. Thanks to the SCFM property of series assembled SPs, an effective way to extend S-SM lifetime is to include redundant SPs in each valve. Given that l is the minimal number of SPs able to withstand the S-SM blocking voltage, the addition of a suitable number m of active redundant SPs

allows fault-tolerant operation of the S-SM upon failure of individual redundant SPs. The S-SM valve represents a l-out-of-m:G redundant system, whose reliability function $R_{S-SMv}(t)$ is:

$$\mathbf{R_{S_{SMv}}} = \sum_{i=1}^{m} \binom{m}{i} \mathbf{R_{SP}(t)^i}(1 - \mathbf{R_{SP}(t)})^{\mathbf{m-i}} \tag{3.47}$$

where $R_{SP}(t)$ is the reliability of one SP. It is assumed that all SPs follow i.i.d. exponential lifetime distributions as long as they work in the bathtub random failure period. One converter phase leg consists of identical upper and lower arm. Each arm comprises n identical, stochastically independent S-SMs, n-k of which redundant, and one converter reactor all in series. The reliability function of the valve arm k out of n:G active redundant system can be written as:

$$\mathbf{R_{va}} = \sum_{i=k}^{n} \binom{n}{i} \mathbf{R_{S_{SM}}}(t)^i(1 - \mathbf{R_{S_{SM}}}(t))^{n-1} = \sum_{i=k}^{n} \binom{n}{i} (e^{-\lambda_{S_{SM}}t})^{n-1} \tag{3.48}$$

by assuming that all the S-SMs follow identical exponential distributions of times to failure with constant failure rate, λ_{S-SM}, (random failures). Hence, similarly to the I-SM MMC case, the upper arm, the lower arm, the phase leg and the whole converter reliability expressions for the S-SM configuration can be obtained by substituting the expression of R_{va} in equations (3.35)-(3.37).

S-SM Valve z-out-of-s Active Redundant System: SPs Equally Sharing the S-SM Blocking Voltage

At the beginning all SPs are good and their initial constant failure rate is $\lambda_{0,SP}$. When the first SP fails safe in SCFM, the s-1 surviving units (with s total number of IGBTs per valve) continue to operate sharing in equal proportion the nominal S-SM voltage, thereby they withstand an increased voltage. The individual SP failure rate also increases with direct proportion to the voltage resisted by the SP to a value $\lambda_{1,SP} \geq \lambda_{0,SP}$ and, for this reason, the valve failure rates remain constant for all the following failures. The second failure occurs at the valve failure rate $\theta = (s-1)\lambda_{1,SP}$. With i failed units, the failure rate of the remaining (s-i) working units is $\lambda_{i,SP}$ where: $\lambda_{0,SP} \leq ... \leq \lambda_{i,SP} \leq ... \leq \lambda_{s-z,SP}$ with $0 \leq i \leq s - z$. The valve voltage $V_{S,SM}$ is equally distributed over all surviving SPs. Being $V_{S,SM}$ the nominal S-SM voltage, the initial voltage applied to each single SP is

$$\mathbf{V_0^{SP}} = \frac{V_{SM}}{s} \tag{3.49}$$

and as consecutive SP failures occur:

$$\mathbf{V_i^{SP}} = \frac{\mathbf{V_{S,SM}}}{s-i} = \frac{s}{s-i}\mathbf{V_0^{SP}}.$$
(3.50)

Owning to the properties of exponential distributions, the S-SM lifetime, TS-SM, follows the gamma distribution $\Gamma(\theta, m-l+1)$ and the reliability function of the S-SM valve (whose failure rate θ remains constant with the number i≤(m-l) of failed SPs), can be written as:

$$\mathbf{R_{S,SMv}}(t) = e^{-\theta t} \sum_{j=0}^{s-z} \frac{(\theta t)^j}{j!}$$
(3.51)

S-SMC converter Arm k-out-of-n:G System: S-SMs Equally Sharing the Converter Valve Arm Voltage

Each converter arm is modelled as k out of n:G active redundant system of i.i.d. S-SMs, equally sharing the converter arm voltage. Hence, the analysis is similar to that developed in the I-SM active redundant system.

3.3.7   Common Cause Failure

In the above formulation all SMs were assumed identical and independent from each other. Each one fails independently from all others, i.e. the failure of any SM does not affect the state of the other ones in the arm: $Pr\{F_{SMi}/F_{SMj}\} = Pr\{F_{SMi}\}$, for all $i \neq j$, F_{SMi} representing the failure event of one single SM. The independent failure assumption may not be verified in practice: a single or common cause can affect more than one component and cause several components to fail simultaneously. Common cause failures (CCFs) may limit the reliability improvements gained by adding redundancies to the system: thereby, they are relevant for converters, whose fault tolerant behaviour is reliant on the presence of redundant SMs. The model should be modified to evaluate the impact of CCF. The correct quantitative evaluation of CCFs would require a large set of parameters (the failure probabilities of specific groups of units) fast growing with the number of redundant units. Parametric models requiring all this information, not supplied by statistical records, are of impossible implementation. The Basic Parametric Model (BPM) introduces simplifying assumptions (above all, the symmetry assumption) which significantly reduce the total number of parameters required. In spite of its simplifications, the BPM too is not a feasible method in the majority of practical situations, characterized by severe lack of operational statistics. These constraints have imposed the β-factor model which puts the least stringent requirements. The

β-factor model is the most commonly used in reliability analysis [91, 93]: it is easy to handle and provides reasonably correct, conservative (for high levels of redundancy) results. It needs only two parameters as only two failure types are modelled: the individual unit independent failure and the simultaneous failure of all units as consequence of a common cause. The simultaneous failure of all SMs of one arm is represented in the RBD by a virtual component in series with the initial (parallel) system RBD. Its failure rate is λ_{cc}. All common-cause failures result in the failure of all the redundant SMs. This simplification permits to introduce only one additional parameter in the independent failure model. The total failure rate λ_T is defined as: $\lambda_T = \lambda_{SM} + \lambda_{cc}$, λ_{SM} being the SM independent failure rate. Hence, by defining the parameter β as:

$$\beta = \frac{\lambda_{cc}}{\lambda_T} \tag{3.52}$$

the valve arm reliability in presence of CCFs is:

$$\mathbf{R}(t) = \mathbf{R_{va}} \cdot e^{-\frac{\beta}{1-\beta}\lambda_{SM}t} \tag{3.53}$$

3.3.8 Converter Reliability as a Function of The Redundancy Configuration

In this section, the reliability of a hypothetic $\pm$ 320 kV HVDC VSC converter, composed of 4.5 kV SMs, has been calculated as a function of:

- SMs typology: either I-SMs composed of two 4.5 kV IGBTs or S-SMs composed of s 4.5 kV IGBTs in series per valve;

- redundancy strategy: cold standby, warm standby, active load sharing redundancy for I-SM MMC; active load sharing redundancy for S-SM MMC;

- minimum SM number (k) per valve arm, resulting from the nominal arm voltage and the applied de-rating factor;

- Percentage r of redundant SMs.

The purpose of this reliability analysis is to identify, by means of the above described analytical formulae, the converter redundancy architecture for which its reliability function R(t) remains at a value ≥ 0.995 at least for five years from the start of operation. This constraint implies an extremely high probability of uninterrupted operation of the MMC during the scheduled maintenance interval (two years). The number of IGBTs is the same for each analysed converter configuration, with λ_{SM}=0.004 and λ_d=0.001 [118–122] (for the warm standby configuration).
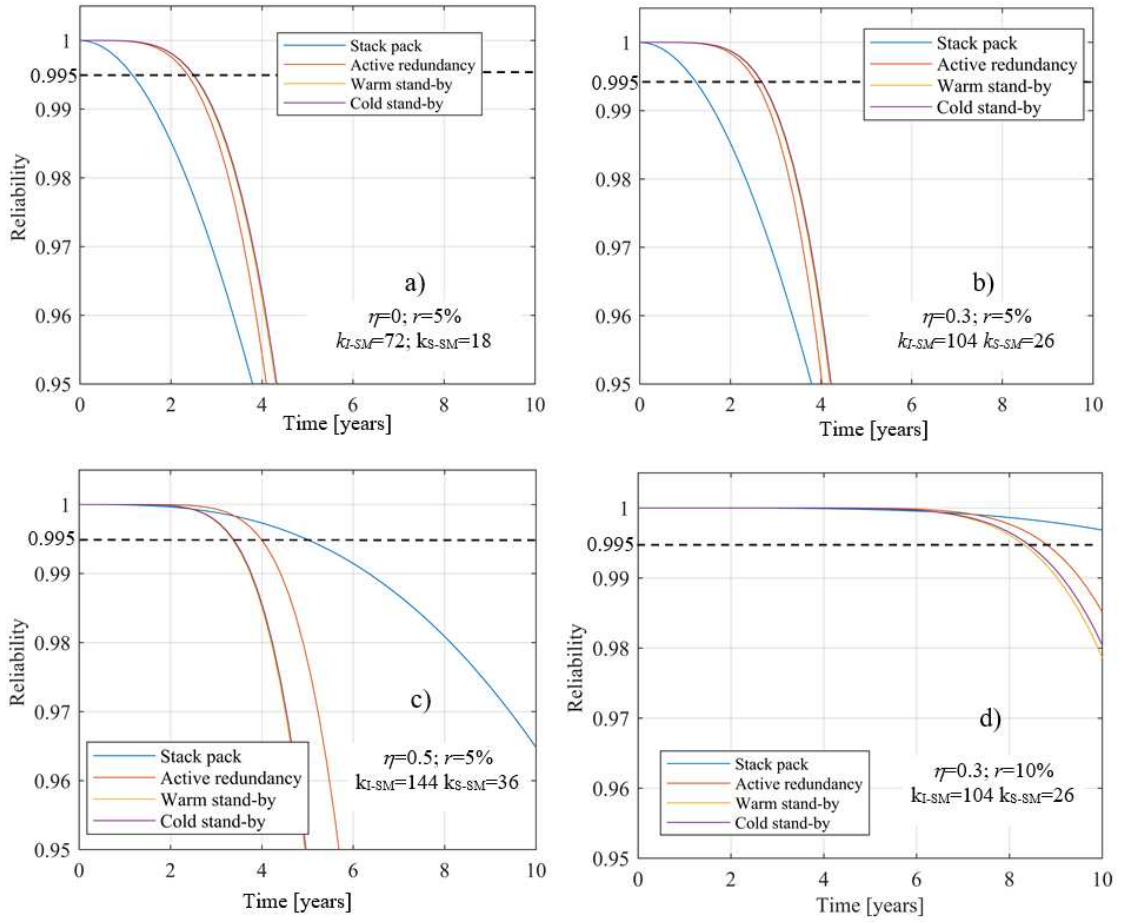
Figure 3.15: R(t) of the converter as a function of k_{I-SM}, k_{S-SM} and η

Figure 3.15 a) shows the converter R(t) behaviour with r=5%, k_{I-SM}=72, k_{S-SM}=18 and $\eta = 0$, for the different redundancy strategies. Obviously this is only a theoretical configuration, not used in practice but useful to understand the influence of the redundancy and derating choices on the R(t) behaviour. In Figure 3.15 b) the redundancy has been increased to 10%, with k_{I-SM}=104, k_{S-SM}=26 and η=0.3. In Figure 3.15 c) the behaviour of the converter for k_{I-SM}=144, k_{S-SM}=36 and η=0.5 with a redundancy of 5% is shown, whereas in 3.15 d) the parameters are k_{I-SM}=104, k_{S-SM}=26, η=0.3 and r=10%. As it is possible to see in Figure 3.15, the constrain R(t)≥0.995 for the first five years is verified for the curves 3.15 c) and 3.15 d). In fact, the parameters k_{I-SM}, k_{S-SM}, η and the percentage redundancy of Figure 3.15 c) are very similar to the ones typically applied to real converter installations.

It is interesting that the reliability of S-SM configuration increases more than the

other ones as the number of redundant SMs is increased. The reason why S-SM configuration shows a lower reliability in Figure 3.15 a) can be imputed to the fact that redundant SMs are present only at the arm level and not at the valve one. This choice has been adopted to perform the comparisons of Figure 3.15 maintaining constant the IGBT number, even if commercial S-SM converters typically use redundancy at valve level with consequent reliability grow. The difference between the reliability of the active redundant mode and the warm standby one is negligible and it becomes apparent above 10% of SMs redundancy.

3.3.9   Availability assessment through Markov models

Steady-state availability A_∞ is the most significant reliability measure for repairable systems. In the following, the procedural approach to estimate the overall availability of an exemplificative HVDC VSC symmetrical monopole is described. In particular, Markov models for the subsystems portrayed in the RBD of 3.14, making up the 105 km long XLPE cable HVDC VSC symmetrical monopole, are built. Values for failure/repair rates are selected with reference to the most recent published statistical collections [118–122]. Markov methods allow efficiently representing systems with more than two states (in contrast to static two-states RBD portrayals); in this context, they help analysing the transmission system going through repair and maintenance processes.

Description of Markov State Space Models

In general, a Markov chain is a special type of stochastic process, whose state at time t is expressed by the random variable {X(t), t > 0}. The set of all possible states is called the state space Ω; it can be either finite or countable infinite. The system may behave either discretely or continuously with respect to time and space. The continuous-time Markov chain is also called Markov process which owns the Markov property. Through Markov chains, systems with several sojourn states and jump transitions between them may be m. The Markov property requires the system behaviour to be characterized by lack of memory (i.e., the system future state only depends on its present state). If the process also shows stationary transition probabilities (i.e., the probability of making a transition from one given state to another in Ω is the same at all times), then {X(t), t≥0} is a time-homogeneous Markov process. In the present application, Ω is assumed finite (states $\in \Omega$ correspond to the concrete states wherein the transmission link can reside) whereas time continuous. Stochastic processes with i.i.d. interarrival times, like those modelled by exponential or Poisson distributions with constant hazard rates, correspond to time-homogeneous Markov processes. For the time-homogeneous Markov process {X(t), t≥ 0}, its time-independent transition probabilities may be

173

written as:

$$\mathbf{p_{ij}}(s) = \mathbf{Pr}[X(t + s) = j | X(t) = i] \tag{3.54}$$

for i,j $\in \Omega$ and s>0. If P(s) is the transitional probability matrix and P(0) the identity matrix, the Chapman-Kolmogorov equation:

$$\mathbf{P}(t + s) = \mathbf{P}(t) \cdot \mathbf{P}(s) \quad for \quad t, s \geq 0 \tag{3.55}$$

is valid. By symbolizing with $\pi(t)$ the probability distribution {X(t), t$\geq$ 0} at time t and fixing the initial distribution $\pi(0)$ at time 0, it follows:

$$\pi(t) = \pi(0) \cdot \mathbf{P}(t). \tag{3.56}$$

By identifying the transitional matrix Q, whose elements q_{ij} for i,j $\in \Omega$ are the transition rates, as:

$$\mathbf{Q} = \lim_{s \to 0} \frac{1}{s}[\mathbf{P}(s) - \mathbf{P}(0)] = \frac{d}{dt}\mathbf{P}(t)|_{t=0} \tag{3.57}$$

Q has the following properties:

- for an infinitesimal time interval (t, t+s) and i,j $\in \Omega$ with i$\neq$j:

$$\mathbf{Pr}[X(t + s) = j | X(t) = i] = q_{ij} \cdot s$$
$$\mathbf{Pr}[X(t + s) = j | X(t) = i] = 1 - \sum_{j \neq i} q_{ij} \cdot s \tag{3.58}$$

- the row-sums of $\mathbf{Q}$ are equal to zero and its diagonal elements non-positive:

$$0 \geq q_{ii} = - \sum_{j \neq i} q_{ij} \quad for \quad i, j \in \Omega. \tag{3.59}$$

Hence, combining the Chapman-Kolmogorov equation (3.55) with (3.57) the Kolmogorov forward and backward equations yield:

$$\frac{d}{dt}\mathbf{P}(t) = \mathbf{P}(t) \cdot \mathbf{Q}$$
$$\frac{d}{dt}\mathbf{P}(t) = \mathbf{Q} \cdot \mathbf{P}(t) \tag{3.60}$$

which can be solved, by setting the initial condition P(0)=I (where I is the identity matrix):

$$\mathbf{P}(t) = e^{Qt} = \sum_{k=0}^{\infty} \frac{t^k}{k!}\mathbf{Q}^k \tag{3.61}$$

Hence, the transition probabilities may be obtained from matrix Q; the probability distribution of the process is:

$$\pi = \pi(0) \cdot \mathbf{P}(t) = \pi(0) \cdot e^{Qt}. \tag{3.62}$$

For the finite, continuous-time Markov process $\{X(t), t \geq 0\}$, a limiting distribution of the probabilities, $\mathbf{p}_i$, of the system being in each ith state in the long run, $\pi^{\star}$, always exists:

$$\pi^{\star} = \lim_{t \to \infty} \pi(t) \tag{3.63}$$

where: $\pi^{\star}$ is a row vector, whose ith element is the steady-state probability $\mathbf{p}_i$ of being in state i. If $\{X(t), t \geq 0\}$ is ergodic, for all $t \geq 0$:, $\pi^{\star} \cdot T(t) = \pi^{\star}$, $\pi^{\star}$ is the unique solution of the linear equation system (called global balance equations):

$$\begin{aligned} \pi \cdot \mathbf{Q} &= 0 \\ \sum_i \pi_i &= 1 \end{aligned} \tag{3.64}$$

$\pi^{\star}$ is often referred to as steady-state distribution, because $\pi^{\star}$ is independent of $\pi(0)$. Hence, on this notional basis, in order to estimate the availability of each subsystem of Figure 3.14, the state space diagram, illustrating all conceivable states of the transmission system along with the transitions between them, is firstly constructed. From the solution of the global balance equations written for the represented system, the long-run probabilities of residing in each identified state can be obtained. Hence, the steady-state availability is expressed as sum of the up-state long run probabilities $\mathbf{p}_i$.

$$\mathbf{A_x} = \sum_{x=i}^{n_{sub}} p_{ix,up} \tag{3.65}$$

where x is the analysed subsystem.

The overall availability of the whole HVDC VSC system is given by:

$$\mathbf{A} = \prod_{x=1}^{n_{sub}} \mathbf{A_x} \tag{3.66}$$

where n_{sub} is the number of submodules which composes the whole HVDC system.

MMC Availability

The converter was assumed operating without interruptions in the time interval between two consecutive scheduled maintenances, performed to replace the faulted components. Uninterrupted fault-tolerant operation of the MMC through this time (usually 2 years, or less only in occasion of outages due to faults in other sections of the link) is statistically guaranteed by designing the converter with compliance to the condition set for its reliability value through at least five years from operation start. Hence, the availability A_{MMC} of the MMC subsystem is synthetically expressed as:

$$\mathbf{A_{MMC}} = \frac{MTSM}{MTSM + MTTR} \tag{3.67}$$

where MTSM (Mean Time To Scheduled Maintenance) is the expected up time (usually 2 years), whereas MTTR (Mean Time To Repair) is the expected planned outage down time.

The control and protection system (C&P) and the cooling/ventilation system (C&V) are often included in the same subsystem of the converter. No alternative exists when only cumulated performance figures of the converter and of C&P and C&V are available from recorded statistics. Otherwise, their reliabilities may be separately evaluated and multiplied by the reliability of the converter. Since C&P and C&V systems are usually duplicated (hot standby systems), their reliability is approximated by the expression of the reliability function for parallel redundant systems: $R_{dsC\&P}(t) = [1 - (1 - R_{C\&P}(t))^2]$ and $R_{dsC\&V}(t) = [1 - (1 - R_{C\&V}(t))^2]$, respectively. Since this work focuses on the availability assessment of the whole transmission link, it was preferred to express the performance figures of C&P and C&V in terms of availability. Thereby the corresponding availability values shown in tab. 1, calculated by means of Markov models built for the C&P and C&V hot standby systems respectively, contribute to the total value of availability of subsystem 3.

Application of Markov Processes

For each repairable subsystem of Figure 3.14, the Markov state space diagram, illustrating all reasonable states in which the subsystem is likely to sojourn and the transitions between them (see Figure 3.16-3.17) is constructed in view of actual operation conditions and the assumed utility strategies. It is worth highlight that mean values of the system availability not only depend on the estimated values of failure, repair and reinstallation rates, but also on the number of spares assumed available for each type of component. Usually one set of insurance spare parts is purchased along with the equipment itself for all critical equipment, whenever the

176

lead time of procurement is long and the repair of the damaged part is not possible at site. Insurance-type spares are normally expensive items, failing randomly, not used for scheduled maintenance: if not promptly available, the consequent outage cost is usually high. When a failure of a critical unit occurs, it is replaced by the spare immediately available at site: the transmission system outage time is reduced to the item reinstallation time. If the faulted item is repairable, it is sent to a specialized workshop: the repair time is often long, as in the case of faulted transformers, and, once repaired, the item is stored at a central store. In the models built for this case study, it is assumed that a continuous review inventory policy is performed: immediately after the utilization of the spare, a resupply order is sent to either the manufacturer or the utility central store. On the receipt of the item, it is stored as spare at site. The base stock for a given item may be estimated by an analytic method assuming Poisson demand (that is, a constant demand rate, which can be approximated by the constant failure rate λ of the item), the item resupply/repair rate μ, the total number n of identical items employed in the system and by imposing a minimal level of item availability α at site. In practice, given n, λ, μ, α, the smallest integer msp is sought: that is, the number of spare items of one given type to be stocked at site in order to warrant that the probability of having this type of spare available at site in any moment is $\geq \alpha$. Economic optimization is neglected in this analysis. For the XLPE cable system, the availability of component spares at site is ≥ 0.999 provided that the base spare stock consists at least of: 1 spare cable span, 3 joints, 1 termination. Figure 3.16, 3.18, 3.20 and 3.22 show the Markov state space diagrams of the following subsystems: cable, GIS, converter reactor, and transformer (C&P and C&V state space diagrams are omitted because they are trivial) where:

- τ_x time rate to resupply the component x;

- T one spare cable termination;

- CS one spare cable span;

- J one spare joint;

- μ_x mean time rate to repair of component x;

- n number of spans of 1 cable;

- n_{jtot} =2(n-1) total number of joints;

- l_{span} length of one cable span;

- $L = n \cdot l_{span}$ length of each cable;

- n_T=4 total number of terminations.

177
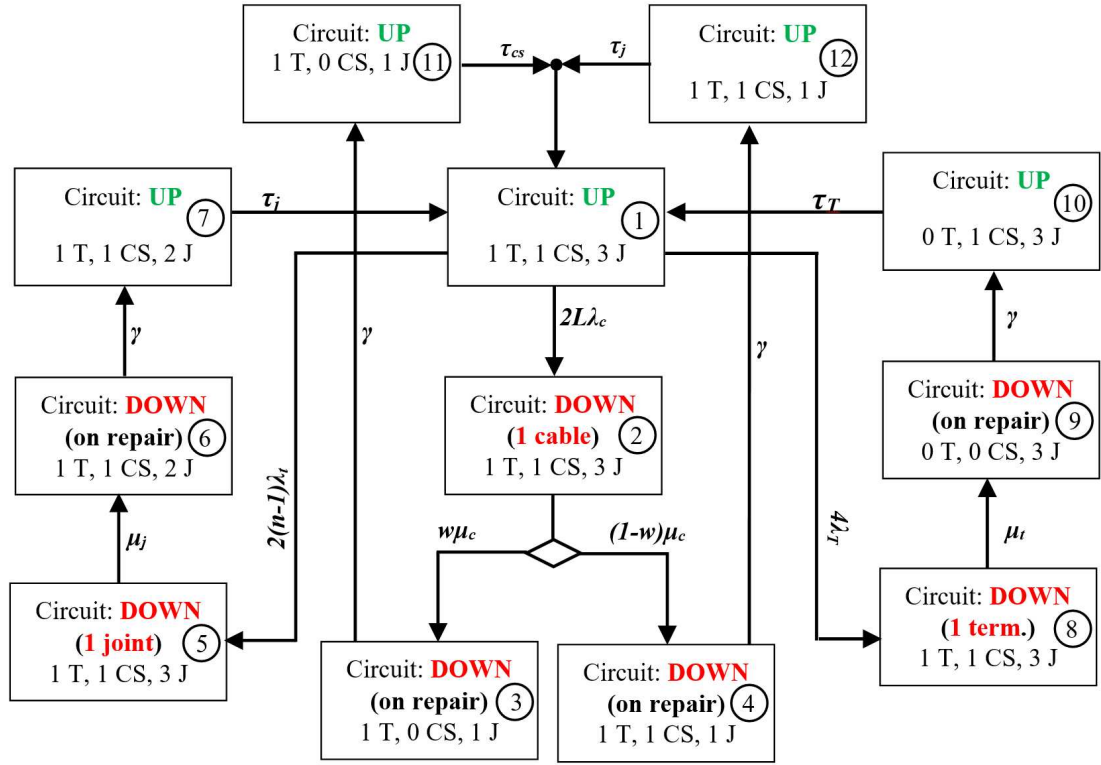
Figure 3.16: Markov state space diagram of the cable subsystem (faulted component highlighted in red in brackets)

$$
\begin{bmatrix}
-2\lambda_c L - 4\lambda_t - 2\lambda_j(n-1) & 0 & 0 & 0 & 0 & 0 & \tau & 0 & 0 & \tau' & \tau & \tau \\
2\lambda_c L & -\mu_c w - \mu_c(1-w) & 0 & 0 & 0 & 0 & 0 & 0 & 0 & 0 & 0 & 0 \\
0 & \mu_c w & -\gamma & 0 & 0 & 0 & 0 & 0 & 0 & 0 & 0 & 0 \\
0 & \mu_c(1-w) & 0 & -\gamma & 0 & 0 & 0 & 0 & 0 & 0 & 0 & 0 \\
2(n-1)\lambda_j & 0 & 0 & 0 & -\mu_j & 0 & 0 & 0 & 0 & 0 & 0 & 0 \\
0 & 0 & 0 & 0 & 0 & \gamma & -\tau & 0 & 0 & 0 & 0 & 0 \\
4\lambda_t & 0 & 0 & 0 & 0 & 0 & 0 & -\mu_t & 0 & 0 & 0 & 0 \\
0 & 0 & 0 & 0 & 0 & 0 & 0 & \mu_t & -\gamma & 0 & 0 & 0 \\
0 & 0 & 0 & 0 & 0 & 0 & 0 & 0 & \gamma & -\tau & 0 & 0 \\
0 & 0 & \gamma & 0 & 0 & 0 & 0 & 0 & 0 & 0 & -\tau' & 0 \\
0 & 0 & 0 & \gamma & 0 & 0 & 0 & 0 & 0 & 0 & 0 & -\tau \\
1 & 1 & 1 & 1 & 1 & 1 & 1 & 1 & 1 & 1 & 1 & 1
\end{bmatrix}
$$

Figure 3.17: State matrix associated with the state space diagram of figure 3.16

On the basis of the Markov state space diagrams, the solution of the corresponding sets of linear equations yields the steady–state availability of each subsystem, as sum of the up state probabilities; the availability of the whole HVDC-VSC symmetrical monopole system is computed through and further multiplying by the converter availability. Table 3.3 shows the results for the 105 km long cable. The cable section heavily influences the overall link availability, its weight increasing
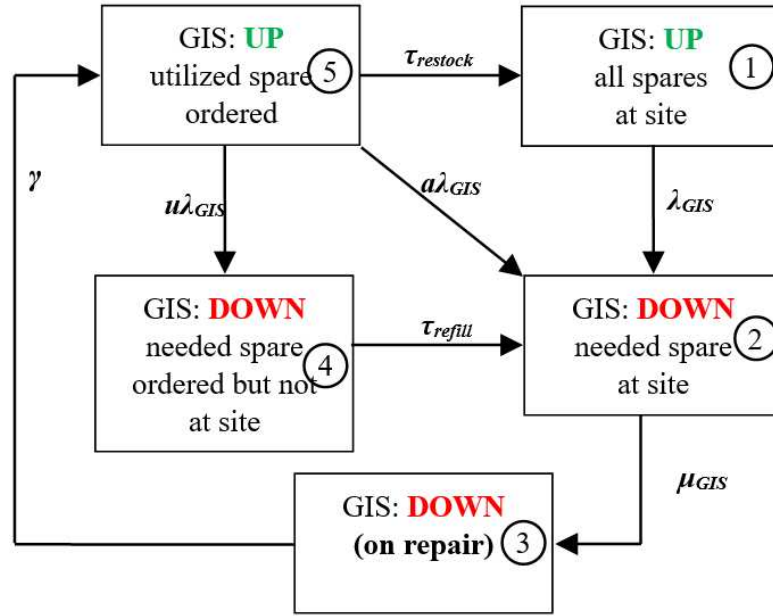
Figure 3.18: Markov state space diagram of the GIS subsystem (faulted component highlighted in red in brackets)

$$
\begin{bmatrix}
-\lambda_{GIS} & 0 & 0 & 0 & \tau_{restock} \\
\lambda_{GIS} & -\mu_{GIS} & 0 & \tau_{refill} & a\lambda_{GIS} \\
0 & \mu_{GIS} & -\gamma & 0 & 0 \\
0 & 0 & 0 & -\tau_{refill} & u\lambda_{GIS} \\
1 & 1 & 1 & 1 & 1
\end{bmatrix}
$$

Figure 3.19: State matrix associated with the state space diagram of figure 3.18

proportionally to the length of the link.

Being A_m the availability of one symmetrical monopole, in case of two identical parallel independent symmetrical monopoles the overall availability of the global system A_g is shown in Table 3.4:

It is worth noting that the cable failure probability is strongly influenced by its laying conditions; for cables placed inside tunnels statistics allows expecting failure probabilities reduced to an half of those expected for cables directly buried.
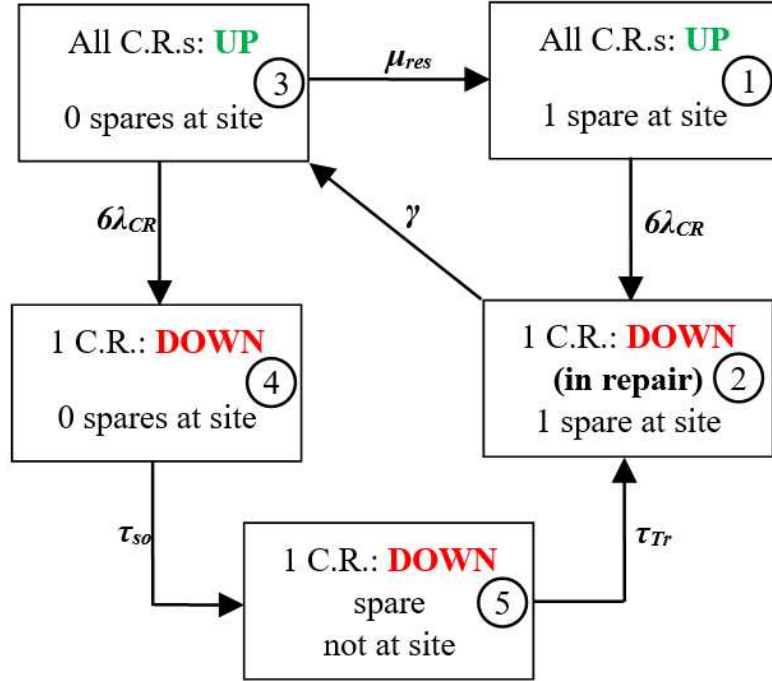
Figure 3.20: Markov state space diagram of the converter reactor (faulted component highlighted in red in brackets)

$$
\begin{bmatrix}
-6\lambda_{CR} & 0 & \mu_{restock} & 0 & 0 \\
6\lambda_{CR} & -\gamma & 0 & 0 & \tau tr \\
0 & \gamma & -(\mu_{restock} + 6\lambda_{CR}) & 0 & 0 \\
0 & 0 & 6\lambda_{CR} & -\tau_{so} & 0 \\
1 & 1 & 1 & 1 & 1
\end{bmatrix}
$$

Figure 3.21: State matrix associated with the state space diagram of figure 3.20
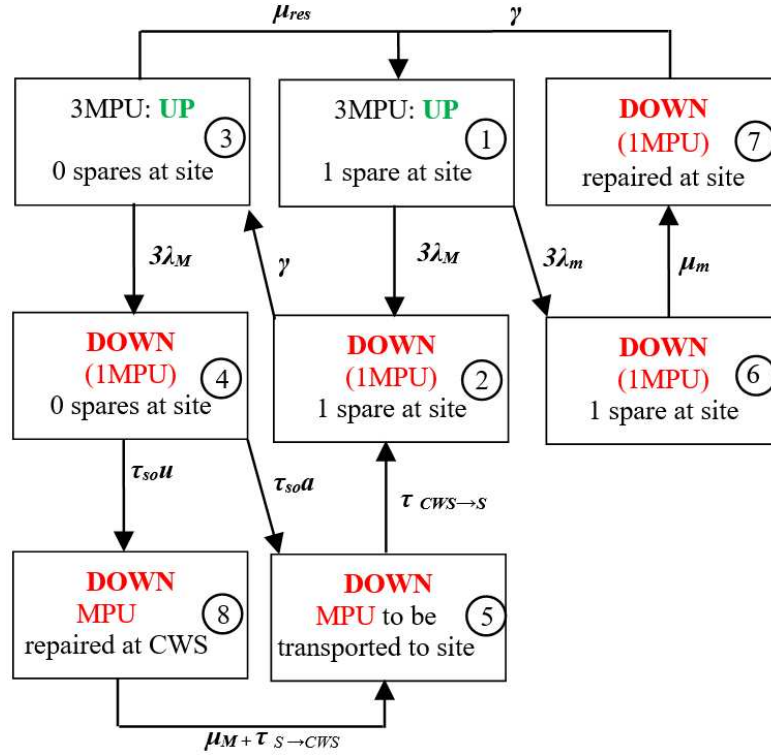
Figure 3.22: Markov state space diagram of the transformer: 3 mono-phase units; λ_M, λ_m: MPU major, minor failure rate; μ_M,μ_m: MPU major, minor repair rate (faulted component highlighted in red in brackets)

$$
\begin{bmatrix}
-3(\lambda_M + \lambda_m) & 0 & \mu_{restock} & 0 & 0 & 0 & \gamma & 0 \\
3\lambda_M & -\gamma & 0 & 0 & \tau_{CWS \to S} & 0 & 0 & 0 \\
0 & \gamma & -(\mu_{res} + 3\lambda_M) & 0 & 0 & 0 & 0 & 0 \\
0 & 0 & 3\lambda_M & -\tau_{so}(a+u) & 0 & 0 & 0 & 0 \\
0 & 0 & 0 & \tau_{so}a & -\tau_{CWS \to S} & 0 & 0 & (\mu_M + \tau_{S \to CWS}) \\
0 & 0 & 0 & 0 & 0 & \mu_m & -\gamma & 0 \\
3\lambda_m & 0 & 0 & 0 & 0 & 0 & -\mu_m & 0 \\
0 & 0 & 0 & \tau_{so}u & 0 & 0 & 0 & -(\mu_M + \tau_{S \to CWS}) \\
1 & 1 & 1 & 1 & 1 & 1 & 1 & 1
\end{bmatrix}
$$

Figure 3.23: State matrix associated with the state space diagram of figure 3.22

181

Table 3.3: Results of the overall availability analysis

Symmetrical monopole components	Availability	Unavailability	Mean Outage Time [hrs/year]
GIS	0.9997	$2.9303\cdot10^{-4}$	2.57
Transformer	0.9996	$3.1650\cdot10^{-4}$	2.77
Converter Reactor	0.9971	0.0029	25.4
Converter*(incl. C&P)	0.9986	0.0014	12**
Cooling system (C&V)	0.9999	$5.5\cdot10^{-7}$	0.0048
Control System	0.9999	$2.04\cdot10^{-7}$	0.0018
Cable Circuit (105 km)	0.9700	0.02991	262.01
DC Switchyard (Swy)	0.9993	0.0007	6.13
Cable Ct.+2 terminal Swys	0.9687	0.03131	274.28
Whole Link	**0.9637**	**0.0363**	**318.24**

*Fault tolerant operation assumed between scheduled outages.
Mean values calculated excluding forced outages of external origin as well as common cause failures.
**(24 hrs/every 2 years): in general, repair at scheduled maintenance.

Table 3.4: Availability of two identical parallel independent symmetrical monopoles

	100 % power transfer capability	50 % power transfer capability
A_g	$A_{gs}=A_m^2=0.9287$	$A_{gs}=A_m^2=0.9637$

3.3.10   Conclusions

this work shows a procedural approach which allows, by means of analytical formulations, assessing the overall average availability of HVDC VSC XLPE symmetrical monopoles. By designing the converter with enough redundancy to maintain its R(t) in excess of 0.995 beyond the 5th year of operation, it is possible to include the converter planned availability in the total availability figure of the HVDC VSC link. The cable system unavailability, proportional to the circuit length, represents the largest portion of the whole HVDC link expected unavailability in the case study of 105 km long monopole. Role of spares is of utmost importance in reducing down times and overall unavailability: provision of one spare transformer at both terminal stations is economically feasible thanks to power partition among three mono-phase units. It is worth considering that the presented method can be applied also for S-SM converter configuration with redundant SMs at valve level (not presented in the paragraph for the sake of brevity).

3.4 Reliability assessment of different HVDC technologies by means of Multi-State Matrix approach

The purpose of this section is to assess the availability of different HVDC transmission system technologies (LCC and VSC) for different transmitted power capacities in order to compare the strengths and weaknesses of each configuration. The matrix-based system reliability (MSR) method has been used since it turns out to be one of the best methods for reliability assessment of multi-terminal HVDC (MTDC) transmission systems taking into account multiple derated states. The results of this study can be useful in the planning and designing stage of HVDC systems.

3.4.1 Introduction

The ever-increasing production of energy from renewable sources and the progressive increase of interties between different countries see the high voltage direct current (HVDC) transmission lines as the present and future protagonist of the electrical power transmission. Basically, there are two types of HVDC technologies, line-commutated converters (LCC) and voltage source converters (VSC) exhaustively described in [87]: the use of overhead lines or undersea/underground cables, or a combination of them, depends on the type of application [10, 70, 85]. HVDC systems allow transmitting bulk power over distances longer than an alternating current (AC) transmission system [15, 65, 96–99]. In addition, HVDC transmission can stabilize and interconnect AC power networks operating at different frequencies. Once installed, HVDC transmission systems become an integral part of the electrical power system, having a full installation compatibility with railway/highway infrastructures [16], so improving the overall reliability. In particular, HVDC installations based on VSC modular multi-level converters (MMCs) appear to be the most attractive technology at nowadays [2, 9, 34, 69, 109]. However, a significant penetration of HVDC links in the worldwide networks implies that the current scenario of electrical power systems is becoming more and more complex due to the several number of components that need to work together and the availability and reliability requirements are becoming very stringent. Effective reliability and availability assessment tools [62, 89, 91, 93, 94, 100, 106–108] are of paramount importance in order to safely manage a whole HVDC-VSC link and to minimize the system outage risk. Moreover, the availability of a HVDC link can be associated to its transmittable power capacity. In fact, the failure of a single component does not necessary lead the whole system to the failure but this event certainly reduce the transmitted power capacity. This is particularly meaningful

Table 3.5: Reliability data of the HVDC components

COMPONENT	Failure rate (occ/yr)	Mean time to Repair (h)	Mean time to Reinstall (h)	Availability
ACF	0.54	6	0	0.999630274
CAP	0.002	6	0	0.999998630
VSC CAP	0.0015	10	0	0.999998288
DCF	0.4	12	0	0.999452355
VSC DCF	0.001	5	0	0.999999429
SR	0.05	300	0	0.998290598
PR	0.14	24	0	0.999616585
LCC CONVERTER	1	5	0	0.999429549
VSC CONVERTER	0.5	4	0	0.999771742
AC BREAKER	0.015	50	0	0.999914391
VSC AC BREAKER	0.001	40	0	0.999995434
DC BREAKER	0.033	50	0	0.999811679
DC SWITCH	1	4	0	0.999543587
DC CABLE (250 km)	3e-05	5	0	0.999999983
DC CABLE (200 km)	2.4e-05	5	0	0.999999986
LCC TRANSFORMER	0.07	1200	72	0.999424988
VSC TRANSFORMER	0.05	1000	48	0.999726102
CENTRAL BUS	0.11	50	0	0.999372540
PROTECTION DEVICES	0.003	20	0	0.999993151

in case of multi-terminal HVDC systems due to the huge amount of components connected together. A reliability computation method that fits well with HVDC multi-terminal connections is the multi-state matrix approach (MSR) [90, 101, 102] which, starting from the failure rates of the HVDC system components, allows correlating the reliability of the system with the transmitted power capacity. In the following sections, such a method is applied to compare the reliabilities of different HVDC multi-terminal links. In particular, the HVDC LCC-based and VSC-MMC-based technologies are compared and the influence of MMC technology on the reliability evaluation is investigated.

3.4.2 Case studies

In this section, the MSR method is applied to several three terminal HVDC configurations, summarized in Table 3.6 and schematized in Figure 3.24, 3.25 and 3.26. It is worth highlighting that the data in this section do not consider the real installation management of the components. The data used [90] as input for the MSR approach are summarized in Table 3.5. For the connection between the terminals 1 and 2 a double circuit 250 km long cable line is chosen, whereas the

Table 3.6: Analyzed cases

Case	1st **Terminal**	2nd **Terminal**	3nd **Terminal**
1	LCC	LCC	LCC
2	VSC	VSC	VSC
3	LCC	LCC	VSC
4	MMC	MMC	MMC

Table 3.7: Analyzed cases

State	Component out	Capacity [p.u.]
1	All in	1.0
2	Only one cap	0.9
3	Only one DCF with could be combined or not with the failure of one Cap	0.75
4	Only one ACF which could be combined or not with the failure of one DCF	0.65
5	Two Caps which could be combined or not with the failure of one DCF	0.62
6	One Cap and one ACF which could be combined or not with the failure of one DCF	0.6
7	One or more components affecting a branch formed by AC-Brk, Trn, Vlvs and/or a Cable line which could be combined or not with the failure of one Cap and/or the failure of One Cap and one ACF	0.5
8	Two Caps and one ACF which could be combined or not with the failure of one DCF and/or with the failure of one or more components affecting a branch formed by AC-Brk, Trn, Vlvs and/or Cable line	0.3
9	Other combinations	0

terminal 3 is connected by means of a 200 km long cable line. For each case study, the capacity states condition is summarized in Table 3.7 and by estimating the related power transmitted capacity. The capacity states condition are summarized in Table3 which shows how the power transmitted capacity change when the fault condition of one or more components occur [100]. In order to cover the typical HVDC configuration that are nowadays installed four case studies have been analyzed taking into account the LCC configuration for two terminals with a derived VSC tapping station as well.
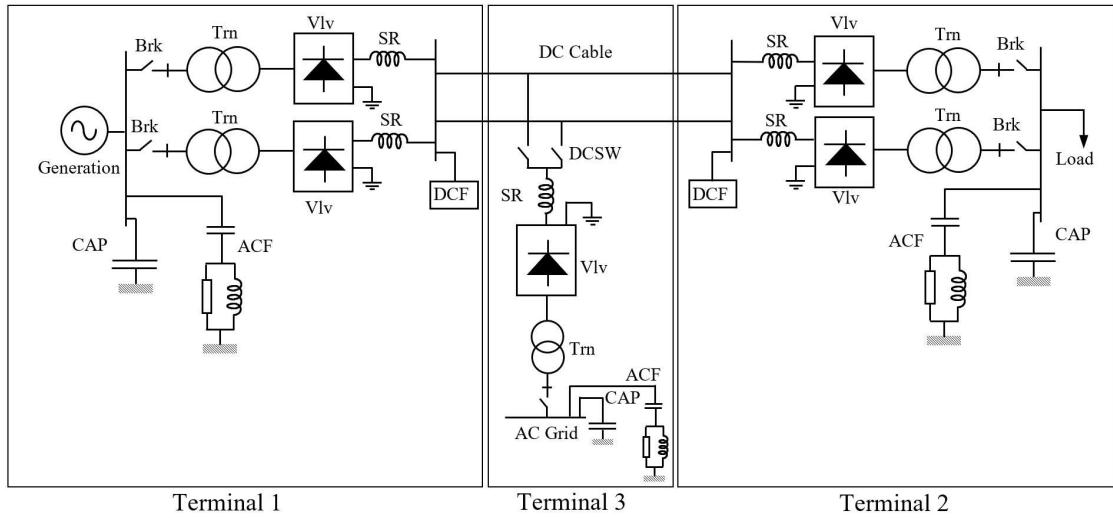
Figure 3.24: Electrical scheme of a HVDC-LCC multi-terminal connection

3.4.3 LCC-MTDC Analysis (Case study 1)

With reference to Figure 3.24, the LCC-MTDC configuration consists of a bipolar LCC for the first and second terminal, whereas the third terminal, which is derived from the middle of the cable line, consists of a LCC monopolar system. By using the MSR approach, the estimated reliability for different power transmitted capacity is shown in Table 3.8. It can be noted how the capacity states for the whole system are more than the capacity states of Table 3.7. This effect is due to the combination of the three terminals, which determines 15 possible fault conditions for the overall system. From Table 3.8 it can be observed how the probability $A_{100\%}$ that the whole system transmits the 100% of its power capacity is $A_{100\%}$=0.984676368. This means that the unavailability of the overall system results $U_{100\%}$=134.235 [h/yr].

Table 3.8: Availability Assessment For Case 1

Transferred Power Capacity [p u]	Estimated Availability For Capacity States
1	0.984676368
0.95	0.001074447
0.9	2.712585212e-06
0.85	7.260467866e-04
0.82	1.842198160e-12
0.8	1.989370920e-09
0.75	0.001085727
0.7	0.005793188
0.65	7.379580335e-04
0.62	1.872426464e-12
0.6	2.022014156e-09
0.5	0.005881950
0.3	1.393317875e-15
0.2	1.075114019e-05
0	1.084429917e-05
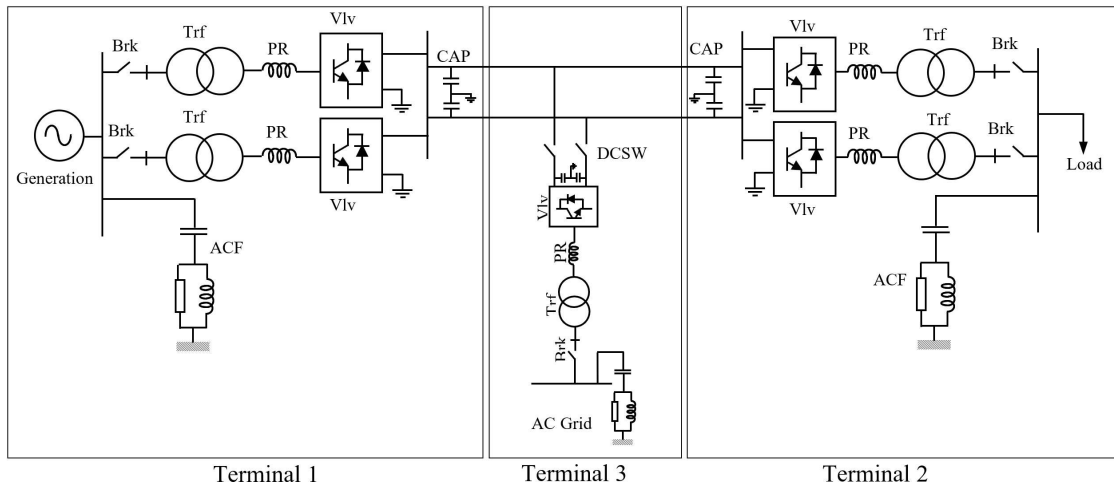
Figure 3.25: Electrical scheme of a HVDC-VSC multi-terminal connection divided for each terminal

3.4.4   VSC-MTDC Analysis (Case study 2)

With reference to 3.25, the VSC-MTDC topology is based on a bipolar configuration for the terminals 1 e 2, while for the terminal 3 a VSC monopolar tapping station has been included. Since VSC converters at terminal 1 and 2 are not MMC type, it is not possible to avoid the use of AC filters. A phase reactor is required for voltage source HVDC schemes in order to allow the control of the active and reactive powers from the VSC. Moreover, the phase reactor reduces the high frequency harmonic contents and limits AC side short circuit currents. By using MSR method, the estimated reliability for different power transmitted capacity is shown in Table 3.9. It is interesting to note that the capacity states the case study 2 can assume are less compared to the ones of case study 1. This is due to the lower number of components. From Table 3.9 it can be observed how the probability $A_{100\%}$ that the whole system transmits the $A_{100\%}$ of its power capacity is $A_{100\%}=0.99496892$. This means that the unavailability of the overall system results $U_{100\%}=$ 44.1 h/yr.

Table 3.9: Availability Assessment For Case 2

Transferred Power Capacity [p u]	Estimated Availability For Capacity States
1	0.99496892
0.9	3.412627156e-06
0.85	7.347405400e-04
0.82	2.911202551e-12
0.8	2.515755916e-09
0.7	0.001769480
0.65	7.391206002e-04
0.62	2.92856101e-12
0.6	2.530756467e-09
0.5	0.001780037
0.3	2.170203750e-15
0.2	2.134508275e-06
0	2.141853191e-06
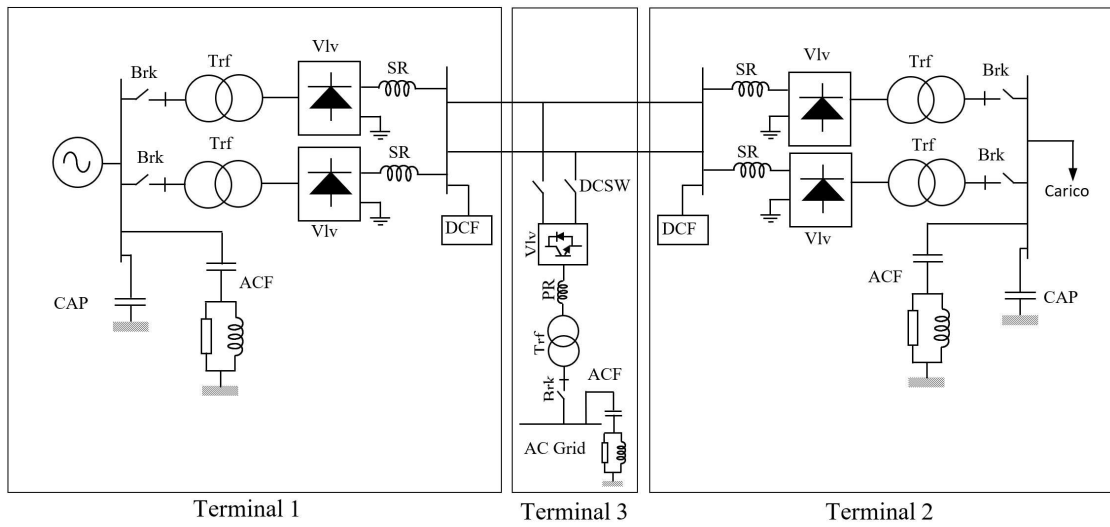
Figure 3.26: Electrical scheme of a mixed (VSC and LCC) HVDC multi-terminal connection divided for each terminal

3.4.5   Mixed-MTDC Analysis (Case study 3)

With reference to figure 3.26, it is proposed a mixed HVDC-MTDC configuration. In this case, terminal 1 and 2 are based on LCC technology and the terminal 3 on the VSC one. By applying the MSR method, the estimated reliability for different power transmitted capacity is shown in Table 3.10. It is possible to observe that the probability of transmitting the 100% of the system power capacity is $A_{100\%}$=0.984676375, and that the unavailability of the overall system results $U_{100\%}$=134.234 h/yr.

Table 3.10: Availability Assessment For Case 3

Transferred Power Capacity [p u]	Estimated Availability For Capacity States
1	0.984676375
0.95	0.001077244
0.9	2.705599753e-06
0.85	7.279368111e-04
0.82	1.846993719e-12
0.8	1.994549595e-09
0.75	0.001082932
0.7	0.005808269
0.65	7.360770932e-04
0.62	1.867650404e-12
0.6	2.016856538e-09
0.5	0.005866858
0.3	1.389721949e-15
0.2	1.077912726e-05
0	1.081631211e-05

3.4.6 MMC Effect (Case study 4)

In this case study, the MMC technology is taken into account. If a high number of levels is assumed for the converters, it is possible to avoid the use of AC filters. In addition, the shunt capacitor banks are not necessary for MMC installations. By using the MSR method, the estimated reliability for different power transmitted capacity is shown in Table 3.11. As above mentioned, the VSC technology requires a lower number of components compared to the LCC ones. Hence, the case study 4 presents the lower number of capacity states among the considered case studies since all the HVDC terminals are based on the VSC technology. From Table 3.11 it is possible to note that for case study 4 the probability of transmitting the 100% of the system power capacity is $A_{100\%}$=0.996445169 and the related unavailability is $U_{100\%}$=31.140 h/yr.

Table 3.11: Availability Assessment For Case 4

Transferred Power Capacity [p u]	Estimated Availability For Capacity States
1	0.996445169
0.7	0.001772764
0.5	0.001780704
0.2	6.799950703e-07
0	6.818284098e-07

3.4.7 Conclusions

In this section, the availability assessment of a multi-terminal (MTDC) configuration for different HVDC technologies by using the MSR approach has been investigated. In particular, line-commutated converters (LCC), voltage source converters (VSC) and the effect of multi-levels modular converter are analyzed and the main results are summarized in Table 3.12. It is worth noting that the configuration where each terminal uses the VSC technology seems to be the most effective one from the availability standpoint, with an availability of 65% more than a pure LCC MTDC configuration. Moreover, if MMC are used it is possible to observe from Table 3.12 that system availability can be further increased by an additional 10%. The mixed HVDC configuration does not seem to increase significantly the availability respect to the first configuration. It should be noted that the comparison is made only in terms of availability and it is not possible to state that in general the VSC configuration results to be the most effective one. It is well-known how the choice between LCC or VSC depends on different system requirements (e.g. rated power, rated voltage, etc.) and the design choices have to consider different installation factors. In other words, each installation has different needs and the choice of the kind of technology has to be evaluated on a case-by-case basis. In addition, the MSR method is used without taking into account the spare management or cable accessories but the analysis was made by using only literature data.

Table 3.12: Results of the availability assessment

Technology	Availability	Unavailability [h/yr]
HVDC-LCC	0.984676368	134.235
HVDC-VSC	0.99496892	44.1
HVDC-MMC	0.996445169	31.140
MIXED HVDC	0.984676375	134.234

3.5 Reliability Assessment of a Multi-State HVDC System by Combining Markov and Matrix-Based Methods

The following sections show how reliability analysis requires a more detailed characterization of the cable management significantly affects the availability estimation since the cable represents one of the most critical elements of such systems. The analyzed case study consists of a multi-terminal direct current system based on both line commutated converter and voltage source converter technologies in different con-figurations, whose availability is computed for different transmitted power capacities. For these analyses, the matrix-based reliability estimation method is exploited together with the Montecarlo approach and the Markov state space one. this work shows how reliability analysis requires a deep knowledge of the real installation conditions. The impact of these conditions on the reli-ability evaluation and the involved benefits are also presented.

3.5.1 Introduction

High Voltage Direct Current (HVDC) systems represent a key technology for strengthening the electrical network, as it is confirmed by several contributions in scien-tific literature. They are able to connect grids that operate at different frequencies and allow installing very long interties by involving fewer power losses than HVAC systems. In the energy transition scenario, characterized by the increasing penetration of renewable energy sources in the electrical network, HVDC interconnections are an effective support for the grid to counteract the stability problems that a massive installation of RESs im-plies, thereby making the electrical grid more reliable and safer[65, 96–99]. It is also worth noting that the fewer power cables required for the DC transmission lines compared with the AC ones and the negligible electromagnetic field emission make the HVDC systems fully compatible with the installation in railway/highway infrastructures[15]. However, a significant penetration of HVDC links in the worldwide networks implies that the current scenario of electrical power systems is becoming more and more complex due to the number of components that need to work together, and their availability and reliability requirements are becoming very stringent. There are two types of HVDC technologies, Line Commutated Converter (LCC) based and Voltage Source Converters (VSC) based, exhaustively described in[2, 9, 69, 87, 109]. Regarding the VSC systems, the modular multi-level converter (MMC) configuration is the most used. In particular, the VSC-based HVDC links currently are living a continuous boost due to their key features: in combination with cross-linked-polyethylene-extruded (XLPE) cables, VSC-HVDC technologies are able to provide vital services

for the electrical grids, such as the frequency or the voltage regulation ones [16]. The use of overhead lines or submarine/underground cables, or a combination of them, generates different issues and have pros and cons depending on the type of application [10, 70, 85]. Effective reliability and availability assessment tools [89, 91, 93, 100, 106–108, 123, 124] are of paramount importance in order to safely manage a whole HVDC-VSC link and to minimize the system outage risk. The availability of an HVDC link can be associated with its transmittable power ca-pacity. In fact, the failure of a single component does not necessarily lead the whole sys-tem to fail, but this event certainly reduces the transmitted power capacity. This is partic-ularly meaningful in the case of multi-terminal HVDC systems due to the huge amount of components connected together. A reliability computation method that fits well with HVDC multi-terminal connec-tions is the multi-state matrix approach (MSR) [90, 101, 102, 125] which, starting from the availabili-ties of the HVDC system components, allows correlating the reliability of the system with the transmitted power capacity. The authors applied the MSR technique to compare the reliabilities of different HVDC multi-terminal systems based on both HVDC-LCC and VSC-MMC technologies in the conference paper [125]. Since the MSR approach foresees the component availabilities of the whole HVDC system as input data, the present work is an extended and enriched version of [125], where different techniques are adopted to estimate the availability of the cable systems. The aim of the following sections is to evaluate how different availability computation methods can affect the overall availability estimation of an HVDC system by applying the MSR and Markov approaches. Typically, the use of the MSR method does not take into account the real management of the cable system. Differently, in the following sections, the reliability assessment is addressed by combining the matrix-based reliability method with the Markov state dia-gram approach. In particular, the Markov models are exploited in order to analyze the impact of the cable spare management on the overall availability of the MTDC systems, thus a much more realistic approach to the reliability evaluation problem.

3.5.2   Materials and Methods

Case Studies and Availability Estimation Methods

The availability analysis of different Multi-Terminal DC (MTDC) configurations is performed for different transferred power capacities. The data used as input for the avail-ability estimations are reported in Table 3.13 and they are taken from the technical literature [90, 101, 102, 125]. In particular, for the cable system failure rates and mean time to repairs (MTTRs), the Cigrè TB [35] is considered whereas, for the other components of the system, the input data are based on the paper [90].

The different MTDC configurations considered in this study are summarized in

Table 3.13: Reliability data of the HVDC components

COMPONENT	Failure rate (occ/yr)	Mean time to Repair (h)	Mean time to Reinstall (h)	Availability Montecarlo
ACF	0.54	6	0	0.999630274
CAP	0.002	6	0	0.999998630
VSC CAP	0.0015	10	0	0.999998288
DCF	0.4	12	0	0.999452355
VSC DCF	0.001	5	0	0.999999429
SR	0.05	300	0	0.998290598
PR	0.14	24	0	0.999616585
LCC CONVERTER	1	5	0	0.999429549
VSC CONVERTER	0.5	4	0	0.999771742
AC BREAKER	0.015	50	0	0.999914391
VSC AC BREAKER	0.001	40	0	0.999995434
DC BREAKER	0.033	50	0	0.999811679
DC SWITCH	1	4	0	0.999543587
DC CABLE (250 km)	0.2495	720	0	by considering only the cable failure rate: 0.979905231 by considering the failure rates of cable spans, terminations, and joints and their management: 0.960061242
DC CABLE (200 km)	0.1996	720	0	by considering only the cable failure rate: 0.983859316 by considering the failure rates of cable spans, terminations, and joints, and their management: 0.967727545
LCC TRANSFORMER	0.07	1200	72	0.999424988
VSC TRANSFORMER	0.05	1000	48	0.999726102
CENTRAL BUS	0.11	50	0	0.999372540
PROTECTION DEVICES	0.003	20	0	0.999993151

Table 23.14. The connection between terminals 1 and 2 consists of a 250 km long double-circuit submarine cable, whereas terminal 3 is connected by means of a 200 km long submarine cable. In order to cover the typical HVDC configurations that are installed nowadays, four case studies are analyzed by taking into account the LCC configuration for two terminals with a derived VSC tapping station.

Table 3.15 shows the difference in the availability estimation of the cable systems by considering different spare quantities and times to resupply τ_x for a given failure rate, λ_x, in order to have an idea of their impact on the cable availability. It is possible to note that a more detailed characterization of the cable systems performed by means of the Markov chains significantly affects the availability estimation of the overall HVDC multi-terminal interconnection. For each case study, the availability analysis is carried out by exploiting the MSR method for different fault conditions [90, 101, 102, 125], which determines different power transmission capacities (capacity states) which are summarized in Table 3.16.

At first, the availability of the cable systems, which is necessary as input for MSR, is computed by means of the Montecarlo approach, with and without considering the in-fluence of joints and terminations. Subsequently, the cable system availability is estimated by means of the Markov chains by exploiting the state space diagram of Figure 3.27 as an example of management for the cable system by assuming one spare available for each component (10 states required) and time to resupply the cable spare of 5 months. Hence, the overall availability of the HVDC system

197

Table 3.14: Analyzed cases

Case	1st **Terminal**	2st **Terminal**	3st **Terminal**
1	HVDC-LCC	HVDC-LCC	HVDC-LCC
2	HVDC-VSC	HVDC-VSC	HVDC-VSC
3	HVDC-LCC	HVDC-LCC	HVDC-VSC
4	HVDC-MMC	HVDC-MMC	HVDC-MMC

Table 3.15: Sensitivity Analysis of the 250 km cable system

	Montecarlo (By Considering Joints and Terminations)	**Markov** (1 Spare) τ_{cs}= 5 Months	**Markov** (3 Spares) τ_{cs}= 5 Months	**Markov** (1 Spares) τ_{cs}= 3 Months	**Markov** (3 Spares) τ_{cs}= 3 Months	**Markov** (1 Spare) τ_{cs}= 7 Months	**Markov** (3 Spare) τ_{cs}= 7 Months
Availability	.960169250	0.929307760	0.959131820	0.948094450	0.960220020	0.904892290	0.955983320
Unavailability [h/year]	348.9	619.2	358	454.7	348.5	833.1	385.6

Table 3.16: Availability assessment for different fault conditions for Case 1

State	Component out	Capacity [p.u.]
1	All in	1.0
2	Only one cap	0.9
3	Only one DCF with could be combined or not with the failure of one Cap	0.75
4	Only one ACF which could be combined or not with the failure of one DCF	0.65
5	Two Caps which could be combined or not with the failure of one DCF	0.62
6	One Cap and one ACF which could be combined or not with the failure of one DCF	0.6
7	One or more components affecting a branch formed by AC-Brk, Trn, Vlvs and/or a Cable line which could be combined or not with the failure of one Cap and/or the failure of One Cap and one ACF	0.5
8	Two Caps and one ACF which could be combined or not with the failure of one DCF and/or with the failure of one or more components affecting a branch formed by AC-Brk, Trn, Vlvs and/or Cable line	0.3
9	Other combinations	0

has been assessed once again. The cable spans are supposed 20 km long [126]. Regarding the mathematical steps to pass from the Markov diagram of a given system to its availability and to characterize different spare quantities with the Markov chain, refer to [93]. The significant digits used in the simulations are kept at nine in order to achieve greater computational accuracy.
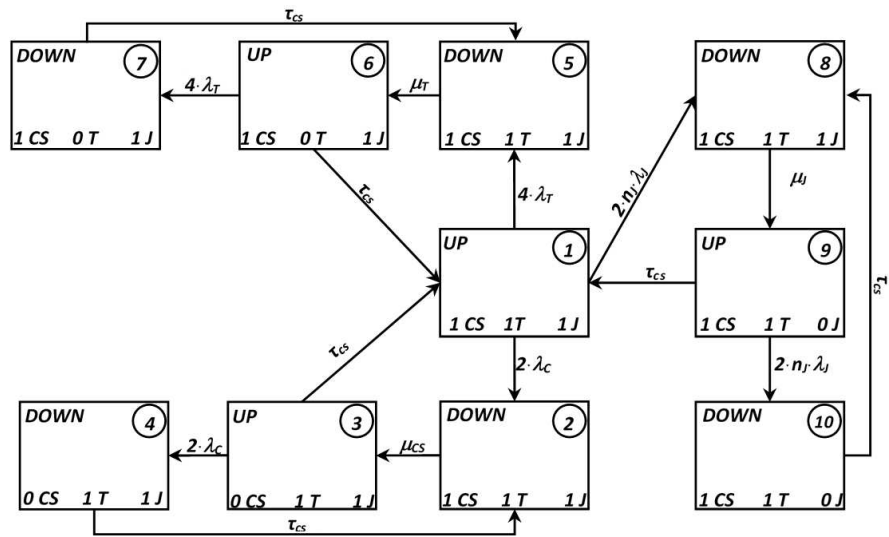
Figure 3.27: Markov state space diagram of the cable subsystem

3.5.3 Results

LCC-MTDC Analysis (Case Study 1)
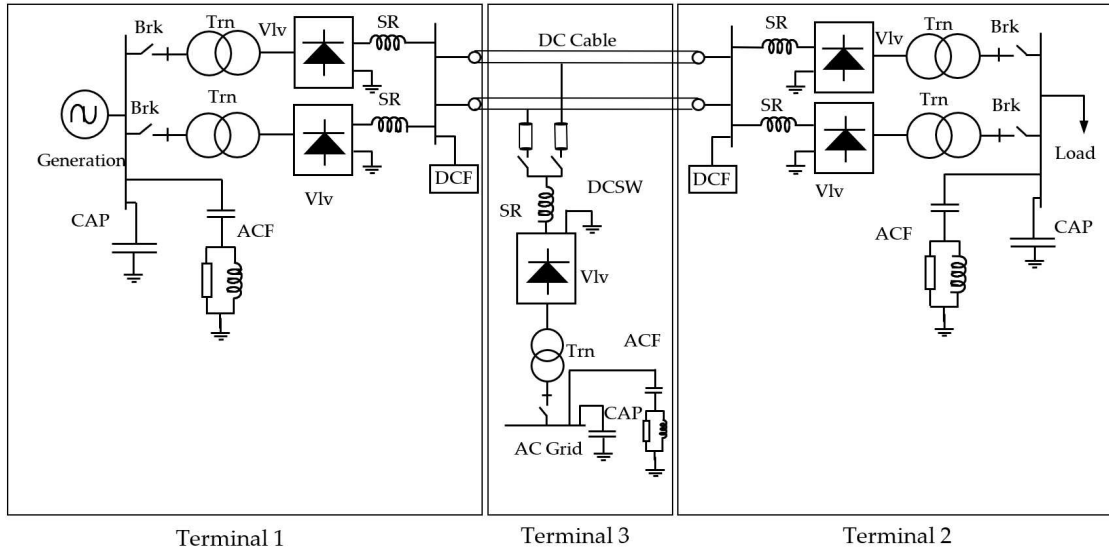
Figure 3.28: Markov state space diagram of the cable subsystem

With reference to Figure 3.28, the LCC-MTDC configuration consists of a bipolar LCC for the first and second terminal, whereas the third terminal, which is derived from the mid-dle of the cable line, consists of an LCC monopolar system. By using the MSR approach, the estimated reliability for different power transmitted capacities are shown in Table 3.17. It can be noted how the capacity states for the whole system are more than the capacity states of Table 3.16. This effect is due to the combination of the three terminals, which determines 15 possible fault conditions for the overall system.

Table 3.17: Availability Assessment for Case 1

Transferred Power Capacity [p u]	Availability MSR (By Considering Joints and Terminations)	Availability MSR (By Considering Joints and Terminations)	Availability MSR & Markov (1 Spare) τ_{cs}= 5 Months
1	0.838431777	0.836921414	0.734398449
0.95	0.000885806351	0.000883893503	0.000758777026
0.9	0.00000238229892	0.00000237879947	0.00000212945309
0.85	0.000598574247	0.000597281661	0.000512735529
0.82	1.51876215e-12	1.51548247e-12	1.30096361e-12
0.8	0.00000000164009568	0.00000000163655399	0.00000000140489727
0.75	0.000953517617	0.000952116848	0.000852309524
0.7	0.0716220665	0.0722307951	0.11030195
0.65	0.000697349156	0.000696853214	0.000657587622
0.62	1.76942560e-12	1.76816758e-12	1.66855522e-12
0.6	0.00000000191078458	0.00000000190942606	0.00000000180185568
0.5	0.0835876285	0.0844250210	0.142377211
0.3	1.43267368e-15	1.43305281e-15	1.45197815e-15
0.2	0.00155131567	0.00158412007	0.00476723031
0	0.00166957954	0.00170612214	0.00537161837

VSC-MTDC Analysis (Case Study 2)
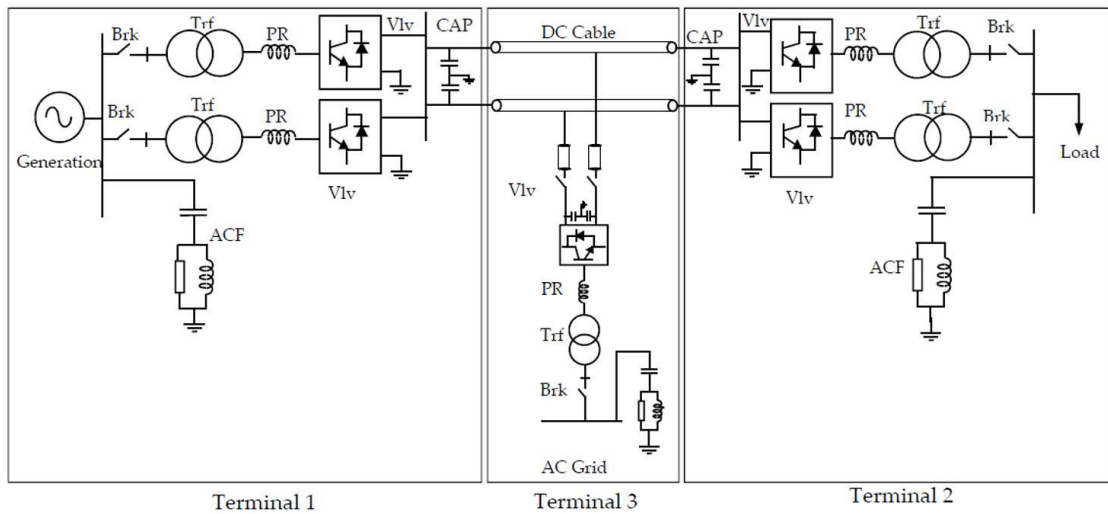
Figure 3.29: Markov state space diagram of the cable subsystem

With reference to Figure 3.29, the VSC-MTDC topology is based on a bipolar configura-tion for terminals 1 and 2, while for terminal 3, a VSC monopolar tapping station has been included. Since VSC converters at terminals 1 and 2 are not MMC type, it is not possible to avoid the use of AC filters. A phase reactor is required for voltage source HVDC schemes in order to allow the control of the active and reactive powers from the VSC.

Moreover, the phase reactor reduces the high-frequency harmonic content and limits AC side short circuit currents. By combining the MSR method with different availability estimation approaches for the cable system as described in Section 4, the estimated reliability for different power transmitted capacities is shown in Table 3.18. It is interesting to note that the capacity states that case study two can assume is less compared to the ones of case study one. This is due to the lower number of components.

Table 3.18: Availability Assessment for Case 2

Transferred Power Capacity [p u]	Availability MSR (By Considering Joints and Terminations)	Availability MSR (By Considering Joints and Terminations)	Availability MSR & Markov (1 Spare) τ_{cs}= 5 Months
1	0.847195666	0.845669511	0.742074892
0.9	0.00000299777836	0.00000299338197	0.00000267999401
0.85	0.000605741633	0.000604433569	0.000518875073
0.82	2.40008070e-12	2.39489786e-12	2.05589641e-12
0.8	0.00000000207406290	0.00000000206958408	0.00000000177663129
0.7	0.0687501958	0.0693701595	0.108161849
0.65	0.000698962649	0.000698470616	0.000659404429
0.62	2.76950414e-12	2.76755512e-12	2.61279252e-12
0.6	0.00000000239330527	0.00000000239162100	0.00000000225788076
0.5	0.0795319491	0.08037035862	0.138426587
0.3	2.23184555e-15	2.23243965e-15	2.26212113e-15
0.2	0.00155226264	0.00158526662	0.00478756778
0	0.00166222565	0.00169880291	0.00536814065

MIXED-MTDC Analysis (Case Study 3)
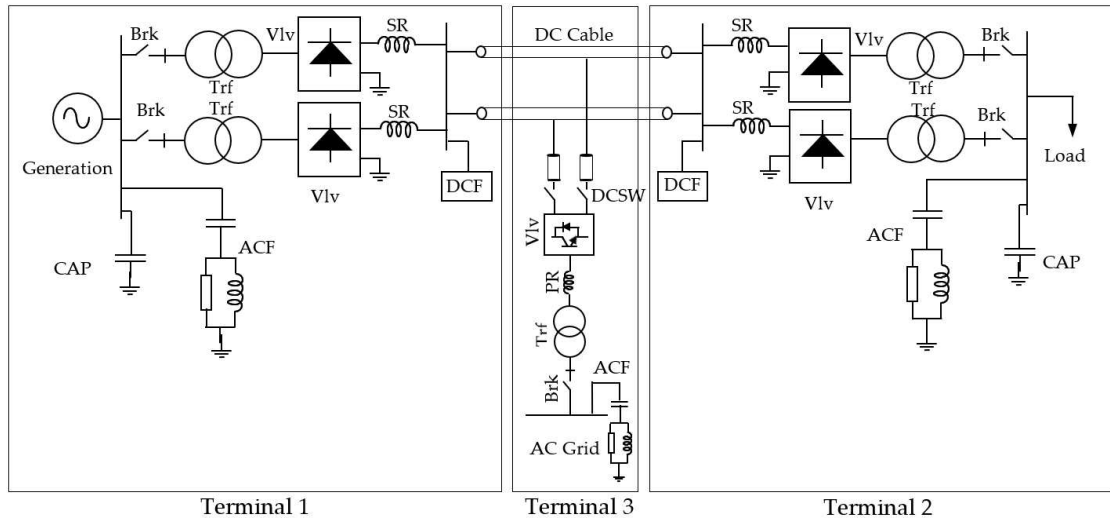
Figure 3.30: Electrical scheme of a mixed (VSC and LCC) HVDC multi-terminal link

With reference to Figure 3.30, it is proposed a mixed HVDC-MTDC configuration. In this case, terminal 1 and 2 are based on LCC technology and terminal 3 on the VSC one. The estimated reliability for different power transmitted capacities is shown in Table 3.19.

Table 3.19: Availability Assessment for Case 3

Transferred Power Capacity [p u]	Availability MSR (By Considering Joints and Terminations)	Availability MSR (By Considering Joints and Terminations)	Availability MSR & Markov (1 Spare) τ_{cs}= 5 Months
1	0.838431782	0.836921421	0.734398454
0.95	8.88112251e-4	8.86194492e-4	7.60752255e-4
0.9	2.37653982e-6	2.37305280e-6	2.12451990e-6
0.85	6.00132430e-4	5.98836481e-4	5.14070262e-4
0.82	1.5227151e-12	1.5194272e-12	1.3043501e-12
0.8	1.64436514e-9	1.64081428e-9	1.40855445e-9
0.75	9.51213417e-4	9.49817615e-4	8.50335757e-4
0.7	0.0718085110	0.0724188242	0.1105890851
0.65	6.95927172e-4	6.95435771e-4	6.56463821e-4
0.62	1.76581445e-12	1.76456873e-12	1.66570124e-12
0.6	1.906885143e-9	1.905539101e-9	1.798773712e-9
0.5	0.0834010460	0.0842368528	0.142089863
0.3	1.42920245e-15	1.42958323e-15	1.44860712e-15
0.2	0.0015553540	0.0015882438	0.00477964020
0	0.00166554121	0.00170199841	0.00535920841

MMC Effect (Case Study 4) and Summary

In this case study, the MMC technology is taken into account. If a high number of lev-els is assumed for the converters, it is possible to avoid the use of AC filters. In addition, the shunt capacitor banks are not necessary for MMC installations. By using the MSR method, the estimated reliability for different power transmitted capacities is shown in Table 3.20. As above mentioned, the VSC technology requires a lower number of components compared to the LCC one. Hence, case study four presents the lower number of capacity states among the considered case studies since all the HVDC terminals are based on the VSC technology. The summary of the estimated availabilities for the analyzed case studies is reported in Table 3.21. It is possible to see that different characterization of the cable systems deter-mine very different values of unavailability for the HVDC link, up to 908 h/year. Hence, it is necessary to correctly represent the cable systems in order to have reliable availability estimations. Moreover, it must be observed that in [90] for 1 p.u. transferred power capaci-ty state which corresponds to case study three of this work, the computed availability value is equal to 0.9846596. By comparing this value with respect to the reliability assess-ment which takes into account the real installation conditions of the cable system (in-cluding joints and terminations), an availability decrease of about 15% arises. In addition, if also spare management is taken into account, the availability decreases by about 25%.

Table 3.20: Availability assessment for Case 4

Transferred Power Capacity [p u]	Availability MSR (By Considering Joints and Terminations)	Availability MSR (By Considering Joints and Terminations)	Availability MSR & Markov (1 Spare) τ_{cs}= 5 Months
1	0.848452743	0.846924329	0.743176049
0.7	0.0688777605	0.0694988746	0.108362541
0.5	0.0795699558	0.0804088501	0.138502406
0.2	0.00149735393	0.00152982457	0.00469681485

Table 3.21: Results of the availability assessment

Technology	Availability MSR (By Not Considering Joints and Terminations)	Availability MSR (By Considering Joints and Terminations)	Availability MSR & Markov (1 Spares) τ_{cs}= 5 Months	Unavailability MSR (By Not Considering Joints and Terminations)	Unavailability MSR (By Considering Joints and Terminations)	Unavailability MSR & Markov [h/year]
HVDC-LCC	0.838431777	0.836921414	0.734398449	1415.3	1428.5	2326.6
HVDC-VSC	0.847195666	0.845669511	0.742074892	1338.6	1351.9	2259.4
HVDC-MMC	0.848452743	0.846924329	0.743176049	1327.5	1340.9	2249.8
MIXED HVDC	0.838431782	0.836921420	0.734398454	1415.3	1428.6	2326.7

3.5.4 Conclusions

In this work, the availability assessment of MTDC configurations for different HVDC technologies has been carried out by using the MSR approach. From the performed analyses, it emerges that the spare management of the cable systems strongly affects the availability estimation of the overall HVDC link. It has been demonstrated that the MSR approach combined with the Markov chain is an effective tool to support the planning and design phase of HVDC installations and to optimize the scheduled maintenance of the system. Moreover, it has been highlighted that the joint use of MSR and Markov's chains can be proposed as a way to be considered towards a single and analytical tool: by means of it, it is possible to represent all the HVDC configurations and installation conditions. The analysis carried out allows concluding that the reliability of each installation depends not only on the performance of the components but also on how the different components are managed.

Chapter 4

Ph.D. Thesis Conclusions

The first part of the PhD research dealt with the study of the new HVDC connection technology with multilevel VSC converters. In particular, all the components and configurations in which this technology is adopted were analyzed. The control system of multilevel converters is a more complicated system than VSC converters with two or three levels, this is because the performances and ancillary services that the connection with this type of technology provides are many and of different types. For this reason, it was necessary to analyze in detail how the MMC control system worked by analyzing the scientific literature, material provided by research centers and technical references provided by some of the most important electromagnetic simulation programs. Subsequently, an HVDC-MMC connection model with a symmetrical monopolar configuration was developed through an electromagnetic transient program. This EMT model was implemented by modeling a real HVDC cable with XLPE insulation and all the control systems necessary for the operation of the HVDC-VSC connection with multilevel converters.

Subsequently, with the participation in conferences, in which I had the opportunity to discuss with some of the largest international cable companies and with the comparisons with the Italian transmission system operator during a research project, it was decided to investigate the problem of transient overvoltages typically found in HVDC-VSC monopolar configurations with multilevel converters. The model was therefore used in a first step to verify the normal operation of the connection, and then, the compliance by the system with the requirements of the network code was analyzed. Furthermore, the start-up procedure of the HVDC-VSC connections with multilevel converters was verified, studying and observing the associated dynamics.

The next step was to analyze the dynamics of the connection in the event of transient overvoltages due to faults on the converter arms and on the DC power

cable. This problem has been highlighted throughout the scientific literature and is a current problem for all these types of HVDC-VSC links. For this reason, the factory test relating to power cable tests has also been modified. To solve or at least mitigate the problem, thus making it acceptable, it has been modeled zinc oxide surge arresters.

The arresters consist of a number of metal oxide resistors, in this case oxide zinc, connected in series and/or parallel. These resistors are characterized by a characteristic non-linear voltage/current behavior. This feature constitutes a low resistance path for overvoltages while one with high resistance for industrial frequency voltage. This implies that in normal operation they can be considered as open sides.

The adoption of these arresters has led to an overvoltage reduction of about 12of the results obtained was then verified during the training period at the research center of the French electricity operator Le réseau de transport de l'électricité (RTE). The system modeled in EMTP-RV was subsequently compared to a PowerFactor DigSilent model.

This comparison has shown how the two models lead to practically identical behavior in the steady state phases (transient extinct) whereas in the dynamic phase they show differences in the different control approach adopted by the two EMT programs. The study of HVDC systems continued with the analysis of recent HVDC multi-infeed configurations.

In particular, the interaction of the LCC technology with respect to the VSC technology when a transient overvoltage event occurs on the VSC side was analyzed. In addition, arresters for the LCC system were modeled in order to limit the disturbance on the DC power cable.

Another key point of my PhD was the analysis of the reliability and availability of HVDC-VSC point-to-point and multi-terminal systems with multi-level converts. The first approach used was the Markov models. With this method, all the elements of the HVDC connection are represented through diagrams defined in the state space that represent the subsystem.

In turn, each diagram is then translated into a state matrix whose resolution makes it possible to calculate the probability that the component lies in a certain state. Once the states of the spaces are created for each subsystem, they are combined analytically in order to define the total availability of the system. Markov approach is particularly useful for point-to-point HVDC connections and it also allows to take into account any spare parts of each subsystem. Theoretically, it is possible to extend the Markov approach to time dependent models, but this implies a considerable complication of the matrix modelling, therefore this solution is rarely

209

applied. The calculation of the availability of a symmetrical monopolar HVDC-VSC system was carried out in collaboration with Terna.

The converter reliability, as a function of the redundancy configuration, was also evaluated taking into account the sub-modules technology (I-SM: single IGBT valve sub-module, S-SM: Multiple IGBT valve sub-module), the Percentage of redundant SMs, a De-rating factor and the minimum number of sub-modules per arm.

For multi-terminal configurations, it was preferred to develop a more flexible approach given the number of components that make up the system. The developed method is the matrix-based reliability method. This method was used for the reliability analysis of multi-terminal systems based on both VSC and LCC technology.

4.0.1   Future developments

The work done in these years has been focused on the HVDC transmission systems with voltage source converter (VSC) technology. In particular, HVDC-VSC systems with multilevel converters were analyzed. The modeling and dynamic analysis of these systems was fundamental to understand their behavior and the advantages and disadvantages that this type of technology brings.

Furthermore, the collaboration with the Italian transmission system operator (Terna) and with the Italian energy research center (RSE) offered opportunities for comparison and growth concerning both HVDC systems and scientific research. The analytical study of the reliability and the analysis of the control systems of VSC converters were a challenging moment since these topics were not covered during my studies, but it was an outstanding opportunity to learn and grow as well.

Future works will focus on the extension of the EMT models developed to mesh-type DC networks. In particular, this approach will give the possibility of evaluating HVDC systems as meshed power system i.e. the "SuperGrids" DC network.

Appendix A

EMTP model for the Symmetrical Monopolar HVDC-VSC System analysis
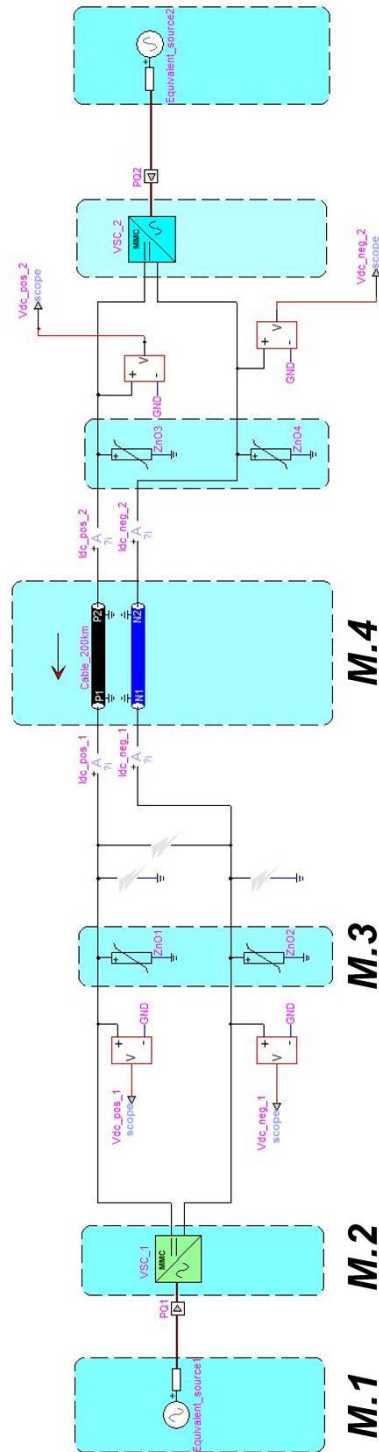
Figure A.1: General block diagram of the model
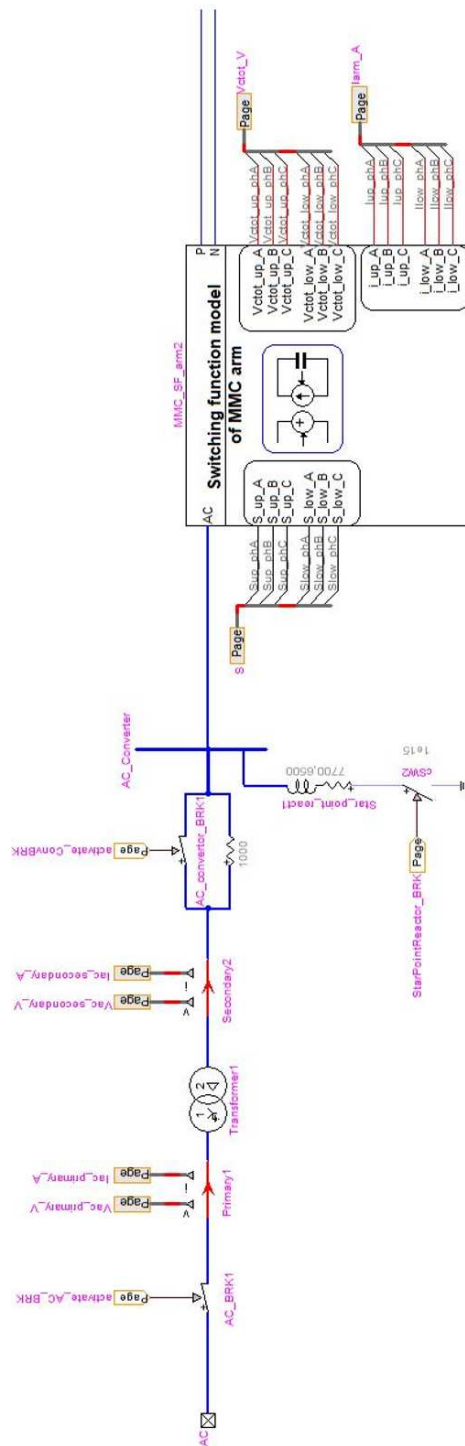
Figure A.2: Converter station

Bibliography

[1] V. K. Sood, *HVDC and FACTS controllers: applications of static converters in power systems.* Springer Science & Business Media, 2006 (cit. on p. 2).

[2] D. Westermann, D. Van Hertem, G. Real, *et al.*, *Voltage source converter (VSC) HVDC for power transmission–economic aspects and comparison with other AC and DC technologies.* Cigré; Paris, 2012 (cit. on pp. 2, 157, 184, 195).

[3] W. B4.60, *Designing HVDC grids for optimal reliability and availability performance.* Cigré; Paris, 2017 (cit. on p. 5).

[4] C. Franck, R. Smeets, and M. A. 34, «Technical requirements and specifications of state-of-the-art HVDC switching equipment», *CIGRE WG A3/B4. 34, Report No. 683*, 2017 (cit. on pp. 9, 10).

[5] D. Jovcic, *High voltage direct current transmission: converters, systems and DC grids.* John Wiley & Sons, 2019 (cit. on p. 16).

[6] N. Mohan, T. M. Undeland, and W. P. Robbins, *Power electronics: converters, applications, and design.* John wiley & sons, 2003 (cit. on p. 21).

[7] S. Malgarotti and A. Ardito, «Technical requirements and specification of large HVDC transmission systems», in *HVDC International Workshop Venice*, AEIT, 2017, pp. 1–31 (cit. on p. 22).

[8] W. B4.37, *VSC Transmission.* Cigré; Paris, 2005 (cit. on p. 24).

[9] A. Nami, J. Liang, F. Dijkhuizen, and G. D. Demetriades, «Modular multilevel converters for HVDC applications: Review on converter cells and functionalities», *IEEE Transactions on Power Electronics*, vol. 30, no. 1, pp. 18–36, 2014 (cit. on pp. 27, 184, 195).

[10] G. Rinzo, G. Pedrazzoli, and A. Chiarelli, «HVDC Unsolved Issues: A Review», in *2018 IEEE International Conference on Environment and Electrical Engineering and 2018 IEEE Industrial and Commercial Power Systems Europe (EEEIC/I&CPS Europe)*, IEEE, 2018, pp. 1–6 (cit. on pp. 34, 67, 121, 184, 196).

[11] S. Cui and S.-K. Sul, «A comprehensive DC short-circuit fault ride through strategy of hybrid modular multilevel converters (MMCs) for overhead line

transmission», *IEEE Transactions on Power Electronics*, vol. 31, no. 11, pp. 7780–7796, 2015 (cit. on p. 35).

[12] S. Ruihua, Z. Chao, L. Ruomei, and Z. Xiaoxin, «VSCs based HVDC and its control strategy», in *2005 IEEE/PES Transmission & Distribution Conference & Exposition: Asia and Pacific*, IEEE, 2005, pp. 1–6 (cit. on p. 39).

[13] N. Iwamuro and T. Laska, «IGBT history, state-of-the-art, and future prospects», *IEEE Transactions on Electron Devices*, vol. 64, no. 3, pp. 741–752, 2017 (cit. on p. 42).

[14] S. Bolik, G. Ebner, *et al.*, «HVDC connection of offshore wind power plants», *Cigré WG B*, vol. 4, 2015 (cit. on p. 49).

[15] R. Benato, M. Forzan, M. Marelli, A. Orini, and E. Zaccone, «Harmonic behaviour of HVDC cables», *Electric power systems research*, vol. 89, pp. 215–222, 2012 (cit. on pp. 53, 73, 121, 138, 184, 195).

[16] R. Benato, S. D. Sessa, L. Guizzo, and M. Rebolini, «Synergy of the future: High voltage insulated power cables and railway-highway structures», *IET Generation, Transmission & Distribution*, vol. 11, no. 10, pp. 2712–2720, 2017 (cit. on pp. 53, 67, 121, 138, 184, 196).

[17] R. Benato, S. D. Sessa, F. Guglielmi, R. De Zan, A. Gualano, L. Guizzo, and M. Rebolini, «Linee elettriche in infrastrutture stradali/ferroviarie: un utilizzo affidabile delle sinergie», *L'Energia Elettrica*, vol. 91, pp. 49–62, 2014 (cit. on pp. 53, 67, 121).

[18] R. Benato, P. Brunello, and L. Fellin, «Thermal behavior of EHV gas-insulated lines in Brenner pass pilot tunnel», *IEEE transactions on power delivery*, vol. 25, no. 4, pp. 2717–2725, 2010 (cit. on p. 53).

[19] R. Benato, P. Brunello, E. Carlini, *et al.*, «Italy–Austria GIL in the new planned railway galleries Fortezza–Innsbruck under Brenner Pass», *e & i Elektrotechnik und Informationstechnik*, vol. 123, no. 12, pp. 551–558, 2006 (cit. on p. 53).

[20] R. Benato, C. Di Mario, and H. Koch, «High-capability applications of long gas-insulated lines in structures», *IEEE transactions on power delivery*, vol. 22, no. 1, pp. 619–626, 2006 (cit. on p. 53).

[21] R. Granadino, M. Portillo, J. Planas, and F. Schell, «Undergrounding the first 400 kV transmission line in Spain using 2 500 mm2 XLPE cables in a ventilated tunnel: the Madrid "Barajas" airport project», in *Proc. of Jicable*, 2003 (cit. on p. 53).

[22] S. Sadler, S. Sutton, H. Memmer, *et al.*, «1600 MW electrical power transmission with an EHV XLPE cable system in the underground of London», *Proc. of Cigré, Paper B1-108*, 2004 (cit. on p. 53).

[23] J. C. del Pino Lopez and P. C. Romero, «Influence of different types of magnetic shields on the thermal behavior and ampacity of underground power

cables», *IEEE Transactions on Power Delivery*, vol. 26, no. 4, pp. 2659–2667, 2011 (cit. on p. 53).

[24] E. Salinas, O. Bottauscio, M. Chiampi, *et al.*, «Mitigation techniques of power frequency magnetic fields originated from electric power systems», 2009 (cit. on p. 53).

[25] R. Benato, D. Capra, R. Conti, M. Gatto, A. Lorenzoni, M. Marazzi, G. Paris, and F. Sala, «Methodologies to assess the interaction of network, environment and territory in planning transmission lines», *Proc. of CIGRÉ*, 2006 (cit. on p. 53).

[26] R. Benato, M. Del Brenna, C. Di Mario, A. Lorenzoni, and E. Zaccone, «A New procedure to compare the social costs of EHV-HV overhead lines and underground XLPE cables», in *Proc. CIGRE*, 2006 (cit. on p. 53).

[27] R. Benato, M. Bernocchi, L. Camilli, C. Di Mario, C. Fourment, G. Roinel, and F. Lesur, «Compatibility between electrical energy transmission lines and new railway infrastructures», in *Proc. of CIGRÉ 2008*, 2008, pp. 1–308 (cit. on pp. 53, 67).

[28] G. Armani, R. Benato, C. Di Mario, A. Lorenzoni, M. Rebolini, and F. Renaud, «Application of multi-criteria methodology for planning an electric transmission line», in *Proc. of CIGRÉ 2008*, 2008, pp. 24–29 (cit. on p. 53).

[29] R. Benato, S. Lauria, F. Gatta, L. Colla, M. Rebolini, and F. Renaud, «Steady-state and transient EHV AC cable shunt reactive compensation assessment», in *CIGRE C4_109 Conf*, 2010 (cit. on p. 53).

[30] R. Awad, C. Peacock, R. Benato, *et al.*, «Cable systems in multi-purpose or shared structures», *Cigré Technical Brochure*, no. 403, 2010 (cit. on p. 53).

[31] H. Koch, R. Benato, M. Laußegger, *et al.*, «Application of long high capacity gas-insulated lines in structures», *CIGRE Technical Brochure*, no. 351, 2008 (cit. on p. 53).

[32] G. Mazzanti and M. Marzinotto, *Extruded cables for high-voltage direct-current transmission: advances in research and development.* John Wiley & Sons, 2013, vol. 93 (cit. on pp. 55, 121).

[33] M. Marzinotto, M. Albertini, L. Benard, F. Charles, and P. Hondaâ, «Cable system qualification process for the Italy-France HVDC intertie», in *Proc. Of 41 th International Conference on Large High Voltage Electric Systems, CIGRE*, 2016, B–1 (cit. on p. 55).

[34] J. Guo, J. Liang, X. Zhang, P. D. Judge, X. Wang, and T. C. Green, «Reliability analysis of MMCs considering submodule designs with individual or series-operated IGBTs», *IEEE Transactions on Power delivery*, vol. 32, no. 2, pp. 666–677, 2016 (cit. on pp. 67, 157, 165, 184).

[35] R. Rosevear, M. Choquette, M. Fairhurst, H. Jorgensen, J. Larsen, B. Mampeay, A. Rakowska, S. Tricoli, and V. Waschk, «Update of service experience

of HV underground and submarine cable systems», *CIGRE TB*, vol. 379, pp. 1–84, 2009 (cit. on pp. 67, 196).

[36] R. Benato, S. D. Sessa, L. Guizzo, and M. Rebolini, «Saving environmental impact of electrical energy transmission by employing existing/planned transport corridors», in *2017 IEEE International Conference on Environment and Electrical Engineering and 2017 IEEE Industrial and Commercial Power Systems Europe (EEEIC/I&CPS Europe)*, IEEE, 2017, pp. 1–6 (cit. on p. 67).

[37] F. Venter, J. Grant, and C. Joannides, «A distributed sequential control system for the Apollo HVDC substation», in *Proceedings of IEEE. AFRICON'96*, IEEE, vol. 2, 1996, pp. 869–873 (cit. on p. 67).

[38] R. Moore, «Cahorabassa-Apollo HVDC link», in *Proceedings of IEEE. AFRICON'96*, IEEE, vol. 2, 1996, pp. 699–704 (cit. on p. 67).

[39] R. Sundararajan and R. Gorur, «Effect of insulator profiles on DC flashover voltage under polluted conditions. A study using a dynamic arc model», *IEEE Transactions on Dielectrics and Electrical Insulation*, vol. 1, no. 1, pp. 124–132, 1994 (cit. on p. 68).

[40] D. Zhang, Z. Zhang, X. Jiang, W. Zhang, J. Zhao, and M. Bi, «Influence of fan-shaped non-uniform pollution on the electrical property of typical type HVDC insulator and insulation selection», *IET Generation, Transmission & Distribution*, vol. 10, no. 14, pp. 3555–3562, 2016 (cit. on p. 68).

[41] X. Jiang, S. Wang, Z. Zhang, J. Hu, and Q. Hu, «Investigation of flashover voltage and non-uniform pollution correction coefficient of short samples of composite insulator intended for±800kV UHVDC», *IEEE Transactions on Dielectrics and Electrical Insulation*, vol. 17, no. 1, pp. 71–80, 2010 (cit. on p. 68).

[42] W. Lampe, T. Hoglund, C. Nellis, P. Renner, and R. Stearns, «Long-term tests of HVDC insulators under natural pollution conditions at the Big Eddy Test Center», *IEEE transactions on power delivery*, vol. 4, no. 1, pp. 248–259, 1989 (cit. on p. 68).

[43] A. Abbasi, A. Shayegani, and K. Niayesh, «Pollution performance of HVDC SiR insulators at extra heavy pollution conditions», *IEEE Transactions on Dielectrics and Electrical Insulation*, vol. 21, no. 2, pp. 721–728, 2014 (cit. on p. 68).

[44] H. Ye, J. Zhang, Y. Ji, W. Sun, K. Kondo, and T. Imakoma, «Contamination accumulation and withstand voltage characteristics of various types of insulators», in *Proceedings of the 7th International Conference on Properties and Applications of Dielectric Materials (Cat. No. 03CH37417)*, IEEE, vol. 3, 2003, pp. 1019–1023 (cit. on p. 68).

[45] X. Jiang, J. Yuan, L. Shu, Z. Zhang, J. Hu, and F. Mao, «Comparison of DC pollution flashover performances of various types of porcelain, glass, and

composite insulators», *IEEE Transactions on Power Delivery*, vol. 23, no. 2, pp. 1183–1190, 2008 (cit. on p. 68).

[46] C. Engelbrecht, J. Reynders, I. Gutman, K. Kondo, C. Lumb, A. Pigini, V. Sklenicka, and D. Wu, «Outdoor insulation in polluted conditions: guidelines for selection and dimensioning Part 2: The DC Case», *CIGRE Technical Brochure*, vol. 518, 2012 (cit. on p. 68).

[47] B. S. Reddy and A. R. Verma, «Pollution performance of HVDC insulator strings under normal and faulted conditions», in *2014 6th IEEE Power India International Conference (PIICON)*, IEEE, 2014, pp. 1–6 (cit. on pp. 68, 69).

[48] C. Townsend, R. Aguilera, P. Acuna, G. Konstantinou, J. Pou, G. Mirzaeva, and G. Goodwin, «Capacitance minimization in modular multilevel converters: Using model predictive control to inject optimal circulating currents and zero-sequence voltage», in *2016 IEEE 2nd Annual Southern Power Electronics Conference (SPEC)*, IEEE, 2016, pp. 1–6 (cit. on pp. 71, 72).

[49] L. Van der Sluis, *Transients in power systems.* John Wiley & Sons Ltd, 2001 (cit. on p. 71).

[50] N. G. Hingorani, «Transient overvoltage on a bipolar HVDC overhead line caused by DC line faults», *IEEE Transactions on Power Apparatus and systems*, no. 4, pp. 592–610, 1970 (cit. on p. 71).

[51] E. W. Kimbark, «Transient overvoltages caused by monopolar ground fault on bipolar DC line: Theory and simulation», *IEEE Transactions on Power Apparatus and Systems*, no. 4, pp. 584–592, 1970 (cit. on p. 72).

[52] G. Wrate, I. Tasinga, S. Low, D. Melvold, R. Thallam, D. Gerlach, and J. Chang, «Transient overvoltages on a three terminal dc transmission system due to monopolar ground faults», *IEEE transactions on power delivery*, vol. 5, no. 2, pp. 1047–1053, 1990 (cit. on p. 72).

[53] M. Heindl, M. Beltle, M. Reuter, D. Schneider, S. Tenbohlen, D. Oyedokun, and C. Gaunt, «„Investigation of GIC related Effects on Power Transformers using Modern Diagnostic Methods,"» in *International Symposium on High Voltage Engineering*, 2011 (cit. on p. 72).

[54] S. Arabi, M. Komaragiri, and M. Tarnawecky, «Effects of geomagnetically-induced currents in power transformers from power systems point of view», *Canadian Electrical Engineering Journal*, vol. 12, no. 4, pp. 165–170, 1987 (cit. on p. 72).

[55] D. Boteler, Q. Bui-Van, and J. Lemay, «Directional sensitivity to geomagnetically induced currents of the Hydro-Quebec 735 kV power system», *IEEE transactions on power delivery*, vol. 9, no. 4, pp. 1963–1971, 1994 (cit. on p. 72).

[56] Y. Li, L. Luo, D. He, C. Rehtanz, D. Yang, and S. Ruberg, «Study on the Effects of the DC Bias on the Harmonic Characteristics of the New

Converter Transformer», in *2010 Asia-Pacific Power and Energy Engineering Conference*, IEEE, 2010, pp. 1–4 (cit. on p. 73).

[57]   S. S. Londhe and M. R. Bachawad, «Review of harmonic losses in HVDC converter transformer: Its causes and mitigation techniques», in *2017 Innovations in Power and Advanced Computing Technologies (i-PACT)*, IEEE, 2017, pp. 1–5 (cit. on p. 73).

[58]   S. Srivastava, R. Kumar, S. P. Singh, and N. Singh, «Harmonic compensation of HVDC rectifier using shunt active filter», in *2013 International Conference on Energy Efficient Technologies for Sustainability*, IEEE, 2013, pp. 1041–1045 (cit. on p. 73).

[59]   S. Farnesi, M. Marchesoni, and L. Vaccaro, «Reliability improvement of Modular Multilevel Converter in HVDC systems», in *2016 Power Systems Computation Conference (PSCC)*, IEEE, 2016, pp. 1–7 (cit. on p. 73).

[60]   S. Fu, Y. Xu, L. Chen, X. Chen, M. Liu, L. Zhang, Y. Gao, and S. Liu, «The status and prospects of VSC-HVDC reliability research», in *2016 China International Conference on Electricity Distribution (CICED)*, IEEE, 2016, pp. 1–6 (cit. on p. 73).

[61]   H. Xie, Z. Bie, P. Dong, and C. Zheng, «The influence of commutation failures on the reliability of HVDC transmission systems», in *TENCON 2015-2015 IEEE Region 10 Conference*, IEEE, 2015, pp. 1–4 (cit. on p. 73).

[62]   R. Benato, A. Chiarelli, S. D. Sessa, and D. Napolitano, «Overall availability assessment of HVDC VSC XLPE cable symmetrical monopolar configuration», in *2017 AEIT International Annual Conference*, IEEE, 2017, pp. 1–6 (cit. on pp. 73, 141, 184).

[63]   S. Cui, S. Kim, J.-J. Jung, and S.-K. Sul, «Principle, control and comparison of modular multilevel converters (MMCs) with DC short circuit fault ride-through capability», in *2014 IEEE Applied Power Electronics Conference and Exposition-APEC 2014*, IEEE, 2014, pp. 610–616 (cit. on p. 74).

[64]   T. Blank, J. Badeda, J. Kowal, and D. U. Sauer, «Deep discharge behavior of lead-acid batteries and modeling of stationary battery energy storage systems», in *Intelec 2012*, IEEE, 2012, pp. 1–4 (cit. on p. 76).

[65]   Y. Rink, L. Held, S. Wenig, M. Suriyah, and T. Leibfried, «Utilization of MMC-HVDC for Primary and Secondary Control in Hybrid ACDC Power Systems», in *2018 53rd International Universities Power Engineering Conference (UPEC)*, IEEE, 2018, pp. 1–6 (cit. on pp. 121, 138, 184, 195).

[66]   L. Abrahamsson, T. Kjellkvist, and S. Östlund, «HVDC Feeder Solution forr Electrical Railways», *IET Power Electronics*, 2012 (cit. on p. 121).

[67]   T. Kjellqvist, «On design of a compact primary switched conversion system for electric railway propulsion», Ph.D. dissertation, KTH, 2009 (cit. on p. 121).

[68] R. Benato, A. Chiarelli, S. D. Sessa, R. De Zan, M. Rebolini, and M. Pazienza, «HVDC Cables Along with Highway Infrastructures: the "Piedmont-Savoy" Italy-France Intertie», in *2018 AEIT International Annual Conference*, IEEE, 2018, pp. 1–6 (cit. on p. 121).

[69] B. Jacobson, P. Karlsson, G. Asplund, L. Harnefors, and T. Jonsson, «VSC-HVDC transmission with cascaded two-level converters», in *Cigré session*, 2010, B4–B110 (cit. on pp. 121, 122, 157, 184, 195).

[70] W. B1.32, «Recommendations for testing DC extruded cable systems for power transmission at a rated voltage up to 500 kV», *CIGRE Technical Brochure*, vol. 496, 2012 (cit. on pp. 122, 184, 196).

[71] C. Guo, Y. Zhang, A. M. Gole, and C. Zhao, «Analysis of dual-infeed HVDC with LCC–HVDC and VSC–HVDC», *IEEE Transactions on Power Delivery*, vol. 27, no. 3, pp. 1529–1537, 2012 (cit. on p. 122).

[72] Y. Liu and Z. Chen, «A flexible power control method of VSC-HVDC link for the enhancement of effective short-circuit ratio in a hybrid multi-infeed HVDC system», *IEEE Transactions on Power Systems*, vol. 28, no. 2, pp. 1568–1581, 2012 (cit. on p. 122).

[73] P. Fischer, J. Pan, K. Srivastava, W. Wang, and C. Hong, «Case study of a multi-infeed HVDC system», in *presented at Powercon*, 2008, pp. 12–15 (cit. on p. 122).

[74] D. L. H. Aik and G. Andersson, «Voltage stability analysis of multi-infeed HVDC systems», *IEEE Transactions on Power Delivery*, vol. 12, no. 3, pp. 1309–1318, 1997 (cit. on p. 122).

[75] H. Lips, «Aspects of multiple infeed of HVDC inverter stations into a common AC system», *IEEE Transactions on Power Apparatus and Systems*, no. 2, pp. 775–779, 1973 (cit. on p. 122).

[76] E. Rahimi, A. Gole, J. Davies, I. Fernando, and K. Kent, «Commutation failure in single-and multi-infeed HVDC systems», 2006 (cit. on p. 122).

[77] C. Thio, J. Davies, and K. Kent, «Commutation failures in HVDC transmission systems», *IEEE transactions on power delivery*, vol. 11, no. 2, pp. 946–957, 1996 (cit. on p. 122).

[78] C. Guo and C. Zhao, «Supply of an entirely passive AC network through a double-infeed HVDC system», *IEEE Transactions on Power Electronics*, vol. 25, no. 11, pp. 2835–2841, 2010 (cit. on pp. 122, 131).

[79] P. F. de Toledo, B. Bergdahl, and G. Asplund, «Multiple infeed short circuit ratio-aspects related to multiple HVDC into one AC network», in *2005 IEEE/PES Transmission & Distribution Conference & Exposition: Asia and Pacific*, IEEE, 2005, pp. 1–6 (cit. on p. 122).

[80] K. Dipti, C. Prabhakar, K. Meera, P. Balasubramanyam, S. Sujatha, and A. Tripathy, «Rtds simulation studies on the upcoming multi-infeed HVDC systems in India», *presented in B4–106, CIGRE*, 2008 (cit. on p. 122).

[81] H. Saad, P. Rault, S. Dennetière, and K. Dudas, «Study on Transient overvoltages in the Converter Station of HVDC-MMC links», in *International Conference on Power Systems Transients (IPST2017)*, 2017 (cit. on p. 122).

[82] F. B. Ajaei and R. Iravani, «Cable surge arrester operation due to transient overvoltages under DC-side faults in the MMC–HVDC link», *IEEE Transactions on Power Delivery*, vol. 31, no. 3, pp. 1213–1222, 2015 (cit. on p. 122).

[83] M. Goertz, S. Wenig, M. Suriyah, and T. Leibfried, «Determination of transient overvoltages in a bipolar MMC-HVDC link with metallic return», in *2018 Power Systems Computation Conference (PSCC)*, IEEE, 2018, pp. 1–7 (cit. on p. 122).

[84] C. Freye, S. Wenig, M. Goertz, T. Leibfried, and F. Jenau, «Transient voltage stresses in MMC–HVDC links–impulse analysis and novel proposals for synthetic laboratory generation», *High voltage*, vol. 3, no. 2, pp. 115–125, 2018 (cit. on p. 122).

[85] R. Benato, A. Chiarelli, and S. D. Sessa, «Transient overvoltage analysis in HVDC MMC power cables: Assessment of the critical points», in *2019 AEIT HVDC International Conference (AEIT HVDC)*, IEEE, 2019, pp. 1–6 (cit. on pp. 122, 131, 184, 196).

[86] D. Xu, X. Zhao, Y. Lu, K. Qin, and L. Guo, «Study on overvoltage of hybrid LCC-VSC-HVDC transmission», *The Journal of Engineering*, vol. 2019, no. 16, pp. 1906–1910, 2019 (cit. on pp. 122, 131).

[87] M. Daryabak, S. Filizadeh, J. Jatskevich, *et al.*, «Modeling of LCC-HVDC systems using dynamic phasors», *IEEE Transactions on Power Delivery*, vol. 29, no. 4, pp. 1989–1998, 2014 (cit. on pp. 131, 184, 195).

[88] G. Electra, *189 "Recommendations for tests of power transmission DC cables for a rated voltage up to 800 kV"*, 2000 (cit. on p. 131).

[89] R. Benato, A. Chiarelli, S. D. Sessa, D. Napolitano, and G. Rinzo, «Valutazione della disponibilità di sistemi HVDC VSC monopolari simmetrici in cavo», *L'Energia Elettrica*, vol. 95, no. 4-5, 2018 (cit. on pp. 131, 141, 184, 196).

[90] J. Contreras-Jiménez, F. Rivas-Dávalos, J. Song, and J. Guardado, «Multistate system reliability analysis of HVDC transmission systems using matrix-based system reliability method», *International Journal of Electrical Power & Energy Systems*, vol. 100, pp. 265–278, 2018 (cit. on pp. 131, 144, 185, 196, 197, 206).

[91] M. Rausand and A. Hoyland, *System reliability theory: models, statistical methods, and applications.* John Wiley & Sons, 2003, vol. 396 (cit. on pp. 131, 133, 139, 141, 161, 171, 184, 196).

[92] A. Chiarelli, «Reliability assessment of different HVDC technologies by means of Multi-State Matrix approach», in *2020 IEEE International Conference*

on Environment and Electrical Engineering and 2020 IEEE Industrial and Commercial Power Systems Europe (EEEIC/I&CPS Europe), IEEE, 2020, pp. 1–6 (cit. on pp. 131, 144).

[93] R. Billinton and R. N. Allan, *Reliability evaluation of engineering systems.* Springer, 1992 (cit. on pp. 133, 139, 141, 161, 165, 171, 184, 196, 198).

[94] S. D. Sessa, A. Chiarelli, A. L'Abbate, and R. Benato, «Availability Assessment Methods for HVDC Systems: a Review», in *2019 AEIT HVDC International Conference (AEIT HVDC)*, 2019, pp. 1–6. DOI: `10.1109/AEIT-HVDC.2019.8740550` (cit. on pp. 138, 141, 184).

[95] S. Dambone Sessa, A. Chiarelli, and R. Benato, «Availability Analysis of HVDC-VSC Systems: A Review», *Energies*, vol. 12, no. 14, 2019, ISSN: 1996-1073. DOI: `10.3390/en12142703`. [Online]. Available: `https://www.mdpi.com/1996-1073/12/14/2703` (cit. on pp. 138, 141).

[96] B. Silva, C. Moreira, L. Seca, Y. Phulpin, and J. P. Lopes, «Provision of inertial and primary frequency control services using offshore multiterminal HVDC networks», *IEEE Transactions on sustainable Energy*, vol. 3, no. 4, pp. 800–808, 2012 (cit. on pp. 138, 184, 195).

[97] E. Pierri, O. Binder, N. G. Hemdan, and M. Kurrat, «Challenges and opportunities for a European HVDC grid», *Renewable and Sustainable Energy Reviews*, vol. 70, pp. 427–456, 2017 (cit. on pp. 138, 184, 195).

[98] T. M. Haileselassie and K. Uhlen, «Primary frequency control of remote grids connected by multi-terminal HVDC», in *IEEE PES General Meeting*, IEEE, 2010, pp. 1–6 (cit. on pp. 138, 184, 195).

[99] M. Barnes, D. Van Hertem, S. P. Teeuwsen, and M. Callavik, «HVDC systems in smart grids», *Proceedings of the IEEE*, vol. 105, no. 11, pp. 2082–2098, 2017 (cit. on pp. 138, 184, 195).

[100] R. Benato, A. Chiarelli, and S. D. Sessa, «Reliability Assessment of a Multi-State HVDC System by Combining Markov and Matrix-Based Methods», *Energies*, vol. 14, no. 11, 2021, ISSN: 1996-1073. DOI: `10.3390/en14113097`. [Online]. Available: `https://www.mdpi.com/1996-1073/14/11/3097` (cit. on pp. 141, 144, 184, 186, 196).

[101] J. Song and W.-H. Kang, «System reliability and sensitivity under statistical dependence by matrix-based system reliability method», *Structural Safety*, vol. 31, no. 2, pp. 148–156, 2009 (cit. on pp. 144, 185, 196, 197).

[102] W.-H. Kang, J. Song, and P. Gardoni, «Matrix-based system reliability method and applications to bridge networks», *Reliability Engineering & System Safety*, vol. 93, no. 11, pp. 1584–1593, 2008 (cit. on pp. 144, 185, 196, 197).

[103] A. Bobbio, L. Portinale, M. Minichino, and E. Ciancamerla, «Improving the analysis of dependable systems by mapping fault trees into Bayesian

networks», *Reliability Engineering & System Safety*, vol. 71, no. 3, pp. 249–260, 2001 (cit. on p. 148).

[104] A. M. El Hassene, L. Radouane, and C. Alaa, «Bayesian networks for the evaluation of complex systems' availability», (cit. on p. 148).

[105] J. G. Torres-Toledano and L. E. Sucar, «Bayesian networks for reliability analysis of complex systems», in *Ibero-American Conference on Artificial Intelligence*, Springer, 1998, pp. 195–206 (cit. on p. 148).

[106] R. Billinton and A. Sankarakrishnan, «Adequacy assessment of composite power systems with HVDC links using Monte Carlo simulation», *IEEE transactions on power systems*, vol. 9, no. 3, pp. 1626–1633, 1994 (cit. on pp. 151, 184, 196).

[107] R. Y. Rubinstein and D. P. Kroese, *Simulation and the Monte Carlo method*. John Wiley & Sons, 2016, vol. 10 (cit. on pp. 151, 184, 196).

[108] R. Billinton and A. Sankarakrishnan, «A comparison of Monte Carlo simulation techniques for composite power system reliability assessment», in *IEEE WESCANEX 95. Communications, Power, and Computing. Conference Proceedings*, IEEE, vol. 1, 1995, pp. 145–150 (cit. on pp. 151, 184, 196).

[109] R. Marquardt and A. Lesnicar, «New concept for high voltage-modular multilevel converter», in *IEEE PESC*, 2004, pp. 1–5 (cit. on pp. 157, 184, 195).

[110] R. Schlegel, E. Herr, and F. Richter, «Reliability of non-hermetic pressure contact IGBT modules», *Microelectronics Reliability*, vol. 41, no. 9-10, pp. 1689–1694, 2001 (cit. on pp. 157, 159).

[111] M. Andriollo, R. Benato, M. Bressan, S. D. Sessa, F. Palone, and R. M. Polito, «Review of power conversion and conditioning systems for stationary electrochemical storage», *Energies*, vol. 8, no. 2, pp. 960–975, 2015 (cit. on p. 157).

[112] H. Wang and F. Blaabjerg, «Reliability of capacitors for DC-link applications in power electronic converters—An overview», *IEEE Transactions on Industry Applications*, vol. 50, no. 5, pp. 3569–3578, 2014 (cit. on pp. 157, 163).

[113] J. Guo, X. Wang, J. Liang, H. Pang, and J. Gonçalves, «Reliability modeling and evaluation of MMCs under different redundancy schemes», *IEEE Transactions on Power Delivery*, vol. 33, no. 5, pp. 2087–2096, 2017 (cit. on pp. 158, 163).

[114] B. Tourgoutian, A. Yanushkevich, and R. Marshall, «Reliability and availability model of offshore and onshore VSC-HVDC transmission systems», 2015 (cit. on p. 158).

[115] D.-U. Jeong, H.-S. Yun, E.-H. Lee, D.-S. Kwon, and S.-H. Lee, «Method of Estimating Environment Conversion Factor Analyzing Environment Factors

of MIL-HDBK-217F», *Journal of Applied Reliability*, vol. 11, no. 2, pp. 141–149, 2011 (cit. on p. 163).

[116] J. She and M. G. Pecht, «Reliability of a k-out-of-n warm-standby system», *IEEE Transactions on Reliability*, vol. 41, no. 1, pp. 72–75, 1992 (cit. on p. 167).

[117] S. V. Amari, H. Pham, and R. B. Misra, «Reliability characteristics of *k*-out-of-*n* warm standby systems», *IEEE Transactions on Reliability*, vol. 61, no. 4, pp. 1007–1018, 2012 (cit. on p. 167).

[118] A. Carvalho, M. Cormenzana, H. Furuta, *et al.*, «Final report of the 2004–2007 international enquiry on reliability of high voltage equipment», *Electra*, vol. 264, pp. 49–53, 2012 (cit. on pp. 171, 173).

[119] S. Tenbohlen, J. Jagers, F. Vahidi, *et al.*, «Transformer reliability survey», *Technical Brochure*, vol. 642, 2015 (cit. on pp. 171, 173).

[120] S. Dodds, «HVDC VSC (HVDC light) transmission-operating experiences», *CIGRE Session 2010*, 2010 (cit. on pp. 171, 173).

[121] A. Beddard and M. Barnes, «VSC-HVDC availability analysis», *The University of Manchester*, 2011 (cit. on pp. 171, 173).

[122] T. CIGRE, «379 Update of service experience of HV underground and submarine cable systems», *WG B1-10*, 2009 (cit. on pp. 171, 173).

[123] R. Benato and D. Napolitano, «Reliability assessment of EHV gas-insulated transmission lines: Effect of redundancies», *IEEE transactions on power delivery*, vol. 23, no. 4, pp. 2174–2181, 2008 (cit. on p. 196).

[124] ——, «Overall cost comparison between cable and overhead lines including the costs for repair after random failures», *IEEE transactions on Power Delivery*, vol. 27, no. 3, pp. 1213–1222, 2012 (cit. on p. 196).

[125] A. Chiarelli, «Reliability assessment of different HVDC technologies by means of Multi-State Matrix approach», in *2020 IEEE International Conference on Environment and Electrical Engineering and 2020 IEEE Industrial and Commercial Power Systems Europe (EEEIC / I CPS Europe)*, 2020, pp. 1–6. DOI: 10.1109/EEEIC/ICPSEurope49358.2020.9160766 (cit. on pp. 196, 197).

[126] T. Worzyk, *Submarine power cables: design, installation, repair, environmental aspects*. Springer Science & Business Media, 2009 (cit. on p. 198).